UNIVERSITY OF LONDON THESIS

Degree PhD Year 2005 Name of Author Lock, N. C.

Investigation into how mitotic spindle checkpoint function is compromised by SV40 large T antigen.

By

Rowena Lesley Lock

A thesis submitted to the University of London
for the degree of Doctor of Philosophy

Ludwig Institute for Cancer Research
University College Branch
91 Riding House Street
London W1W 7BS

Department of Biochemistry and Molecular Biology
University College London
Gower Street
London WC1E 6BT

2005

ProQuest LLC
789 East Eisenhower Parkway
P.O. Box 1346
Ann Arbor, MI 48106-1346

Abstract

The viral oncoprotein Simian virus 40 large T antigen (LT) efficiently immortalises primary rodent cells and occasionally transforms them to tumourigenicity. It has long been known that LT can cause genomic instability and induce aneuploidy, and that it disrupts the mitotic spindle checkpoint, involved in monitoring the segregation of sister chromatids.

LT has recently been shown to interact with the spindle checkpoint protein Bub1. This thesis describes research into the effects of LT on spindle checkpoint function and examines the possibility that interaction of LT with Bub1 is responsible.

Novel monoclonal antibodies against Bub1 were developed to aid this research.

The interaction site of Bub1 was mapped to amino acids 89-97 of LT using co-immunoprecipitation experiments in several cell lines, each expressing LT with a different mutation in the amino-terminal region. The non-Bub1-binding (dl89-97) mutant was capable of immortalising rat embryo fibroblasts as efficiently as wild-type LT, but was defective for focus formation, perhaps suggesting a role for Bub1 in the mechanism for transformation by LT.

In the presence of the microtubule-depolymerising drug nocodazole, the spindle checkpoint is activated and cells arrest in mitosis. LT was shown to compromise spindle checkpoint function, allowing some cells to pass through to the next cell cycle even in the presence of nocodazole. However, without Bub1 interaction, LT loses this ability and the spindle checkpoint is robust.

An investigation of the checkpoint proteins and complexes present during spindle checkpoint activation in cells expressing wild-type or dl89-97 LT was initiated to analyse possible mechanisms for perturbation of the spindle checkpoint by LT.

This study raises the possibility that LT induces genetic instability in mammalian cells by perturbation of spindle checkpoint function, and that this may be a critical component of the mechanism by which LT transforms cells.

Table of contents

List of figures

List of tables

Abbreviations

APC	Adenomatous Polyposis Coli
APC/C	Anaphase Promoting Complex or "Cyclosome"
APS	ammonium persulphate
ATM	Ataxia Telangiectasia Mutated
ATP	Adenosine triphosphate
ATR	Ataxia Telangiectasia and Rad3 related
Bax	Bcl2-associated X protein
bp	base pair
BKV	BK polyomavirus
BPV	bovine polyomavirus
BSA	Bovine Serum Albumin
Bub	Budding Uninhibited by Benomyl
CAK	CDK-activating kinase
CBP	CREB binding protein
CCD	Charge-coupled device
Cdc	Cell Division Cycle
CDK	Cyclin dependent kinase
cDNA	complementary deoxyribonucleic acid
CENP	Centromere protein
CHAPS	3-[(3-cholamidopropyl)dimethylamino]-1-propanesulphonate
Chk	Checkpoint kinase
CIN	Chromosomal Instability
CKI	Cyclin dependent kinase inhibitor
Cmt	Caught by Mad Two
CR	conserved region
CREB	cAMP responsive element binding protein
CREST	Calcinosis cutis, Raynaud's phenomenon, Esophageal dysmotility, Sclerodactyly and Telangiectasias
CT	carboxy-terminal

D-box	Destruction box
DCB	dihydrocytochalasin B
DCS	Donor calf serum
DMEM	Dulbecco's modified Eagle medium
DMSO	dimethyl sulphoxide
DNA	deoxyribonucleic acid
DNA-PK	DNA-dependent protein kinase
DSB	double-strand breaks
dsRNA	double-stranded RNA
Dup	Double park
ECL	Enhanced Chemiluminescence
EDTA	ethylenediaminetetraacetic acid
ELISA	Enzyme-Linked ImmunoSorbent Assay
ERK	extracellular signal-related protein kinase
FACS	Fluorescence-activated cell sorting
FCS	Foetal calf serum
FITC	Fluorescein
FRAP	Fluorescence recovery after photobleaching
GAP	GTPase activating protein
GLEBS	GLE2p-Binding Sequence
GSE	Genetic Suppressor Element
GST	Glutathione S-Transferase
GTP	Guanosine triphosphate
h	*Homo sapiens*
HA	influenza A virus haemagglutinin protein
Hec	Highly Expressed in Cancer
HEPES	N-[2-Hydroxyethyl]piperazine-N'-[2-ethanesulfonic acid]
HRP	Horseradish peroxidase
HTLV-1	Human T cell leukaemia virus type 1
IF	immunofluorescence
IgG	Immunoglobulin G

IgM	Immunoglobulin M
IP	immunoprecipitate/immunoprecipitation
IPTG	isopropyl-β-D-thiogalactopyranoside
JCV	JC polyomavirus
kb	kilobase
kDa	kilodalton
LB	Luria Broth
LT	SV40 large T antigen
LTR	Long Terminal Repeat
m	*Mus musculus*
M1	Mortality stage I
M2	Mortality stage II
Mad	Mitotic Arrest Defective
MAPK	Mitogen-activated protein kinase
MCC	Mitotic Checkpoint Complex
MDM	Mouse double minute
MIN	Microsatellite Instability
Mo MuLV	Moloney murine leukaemia virus
MOPS	3 - (N-morpholino) propanesulphonic acid
MPF	Maturation Promoting Factor
Mps	Monopolar Spindle
mRNA	messenger RNA
NBS	Nijmegen breakage syndrome
Ni-NTA	Nickel-nitrilotriacetic acid
NLS	Nuclear localisation signal
NMWL	nominal molecular weight unit
NP40	Nonidet P40
NT	amino-terminal
P2	Passage 2
PAGE	Polyacrylamide Gel Electrophoresis
PBS	phosphate buffered saline

PCNA	Proliferating cell nuclear antigen
PCR	Polymerase Chain Reaction
PI	propidium iodide
pRB	Retinoblastoma protein
PtK	Potoroo kidney epithelium
PTTG	pituitary tumour transforming gene
PyV	murine polyomavirus
rbs	ribosome binding site
RCC	Regulator of Chromosome Condensation
REF	Rat embryo fibroblast
RF-C	Replication factor C
RIPA	Radioimmunoprecipitation
RNA	ribonucleic acid
RNAi	RNA interference
RNase	ribonuclease
RPA	replication protein A
RPMI	Roswell Park Memorial Institute
SAC	Spindle Assembly Checkpoint
SDS	sodium dodecyl sulphate
Sgo	Shugoshin
siRNA	short interfering RNA
SOC	Spindle Orientation Checkpoint
SPB	Spindle Pole Body
SV40	Simian virus 40
TAE	Tris-Acetate-EDTA
TBP	TATA-binding protein
TEMED	N,N,N',N' tetraethylenemethyldiamine
TERT	Telomerase reverse transcriptase
TRITC	tetramethylrhodamine isothiocyanate
UV	ultra violet radiation
VP	viral protein

Enclosed unbound material

Publication:

Cotsiki, M., Lock, R.L., *et al.* (2004). Simian virus 40 large T antigen targets the spindle assembly checkpoint protein Bub1. *Proc Natl Acad Sci USA* **101**(4), 947-952.

Supplemental CD:

Contains time lapse movies of the data presented in Figures 5.7 and 5.8.

Statement concerning collaborations

The work presented in this thesis is the work of the author unless otherwise indicated.

Acknowledgements

It goes without saying that my most sincere thanks go to my supervisor, Parmjit Jat. Thank you for your endless support, patience and enthusiasm. I feel very lucky to have been given the opportunity to work with you.

The transformation group has been a very happy and relaxed environment to work in, and for that I also thank my colleagues in the lab, both past and present. I would like to thank Silvia Benvenuti, Kris Hardy, Kate Relph and Nunu Arora for all their help in teaching me new techniques and discussing my work, as well as our fun chats. In particular I would like to express my sincere gratitude to Marina Tarunina, Louise Mansfield and Tim Szeto for helping me through the writing up period via helpful discussions, willing proof-reading, and of course for putting up with me!

I shall be ever grateful to Ole Gjoerup and Tom Roberts, our collaborators at the Dana Farber Cancer Institute in Boston, MA. Thank you for sharing reagents with us, and for the useful discussions that we exchanged throughout my PhD. I also extend my thanks to our other collaborator, Raimundo Freire at the Hospital Universitario de Canarias in Tenerife, for kindly furnishing us with copious reagents whenever requested.

My thanks also go to Alan Entwistle for his ever-willing help with my cell biology questions, and for teaching me to use the light microscopy facility. Thank you also to Sabine Klischies for her collaboration on the immunofluorescence studies.

I would like to show my appreciation to Jerry Hyams, Mike O'Hare and Peter Shepherd for helpful discussions throughout the course of the project.

I am also grateful to Terry Jowett (UCL Monoclonal Antibody Facility), Derek Davies (CRUK FACS Laboratory) and Gary Mallinson (UCL Prion Unit, Institute of Neurology) for their practical help with different aspects of the project.

I would like to extend my thanks to the many friends that I have made both at the Ludwig Institute for Cancer Research, and at the UCL Biochemistry Department. I will never forget the fun parties that we enjoyed, and of course the free chocolate biscuits at tea time!

Huge thanks go to my family and close friends. Thank you all for supporting me through the good times and the bad. In particular, thank you Mum, Dad, Marisa and Andy for your care and never-ending words of encouragement. I shall never forget it.

That only leaves one very important person to thank, and that of course is my wonderful husband, Tim. I am constantly overwhelmed by your capacity to make me happy even when you yourself are stressed, and I will never forget the support and unending love that you have shown me during my PhD.

This research was supported by a Biotechnology and Biological Sciences Research Council PhD studentship. Additional funding was kindly provided by the Ludwig Institute for Cancer Research.

1. Introduction

Research in the Jat laboratory is focussed on elucidating the mechanisms by which the viral oncoprotein SV40 large T antigen (LT) carries out its immortalisation and transformation functions, and in studying the other known functions of LT. It has long been known that SV40 LT induces chromosome aberrations, and can disrupt mitotic checkpoints that are involved in maintaining genomic stability. However, the mechanism by which LT induces genetic instability in cells was not known. A previous graduate student in the laboratory, Marina Cotsiki, carried out a yeast two-hybrid screen to search for novel interacting proteins of LT, to identify previously unknown mechanisms by which LT could be carrying out its varied functions. Using the amino terminal 136 residues of LT as bait and a HeLa cDNA library as prey, the spindle checkpoint protein Bub1 was identified as a novel LT-interacting protein. Bub1 plays a critical role in the spindle checkpoint and mutations in the Bub1 gene have been associated with genetic instability in human cancers. It was hypothesised that interaction of LT with Bub1 could be responsible for induction of chromosome aberrations by LT. In addition, these aberrations may be important for the immortalisation and transformation functions of the LT protein.

A general background to the cell cycle, spindle checkpoint, genetic instability, and SV40 large T antigen will be provided in this introductory chapter.

1.1 THE CELL CYCLE

Cell division is fundamental for the growth of an organism and for the replacement of cells lost during normal wear and tear. This occurs via an orderly process known as the cell cycle (for recent reviews, see (Pardee, 2004; Tessema *et al.*, 2004)). Duplication of all molecules that comprise the cell is

required during the course of the cell cycle, and occurs at different stages of the cycle. For example, deoxyribonucleic acid (DNA), the heredity-carrying material in chromosomes, is duplicated specifically during a period that occurs for only a few hours mid-cycle, known as S phase, for (DNA) synthesis. The eukaryotic cell cycle is divided into four phases: gap 1 (G1 phase) during which the cell prepares for DNA synthesis, DNA synthesis (S phase), gap 2 (G2 phase) when the cell prepares for mitosis, and mitosis (M phase) during which the cell divides. Following M phase the two new daughter cells enter the next cycle. If a cell does not receive the necessary signals for proliferation or is terminally differentiated, it withdraws from the cell cycle at G1 into a non-dividing, quiescent state known as G0. Most cells in the body of adults are maintained in this G0 phase.

Cyclin dependent kinases (CDKs), along with their regulatory subunits, called cyclins, are the main engines that drive the cell cycle forward.

1.1.1 Cyclins and CDKs

The family of closely related cyclin proteins appear and disappear during the cell cycle in a strictly controlled, "cyclic" pattern. It was the discovery of cyclin (Evans *et al.*, 1983) that led to the model of an autonomous oscillator driving the cell cycle of early embryonic cells. Cyclins are accessory subunits that activate protein kinases known as "cyclin-dependent kinases" (CDKs). There are multiple cyclins and cyclin-dependent kinases, and they are involved in the cell cycle, transcription and differentiation (reviewed in (Murray, 2004)). Each cyclin associates with one or two CDKs, and most CDKs associate with one or two cyclins. However some, such as CDK1 in budding yeast, associate with as many as nine different cyclins. In the cell cycle there are cyclins associated with G1 (cyclin D), S phase (cyclins E and A), and mitosis (cyclins B and A). The cyclic appearance and disappearance of the cyclin proteins is mediated by

transcriptional activation of the cyclin genes, and ubiquitin-mediated degradation of the cyclin proteins, respectively.

CDKs are a family of serine-threonine protein kinases that are activated in a cell cycle stage-specific manner (reviewed in (Tessema *et al.*, 2004)). Association of CDKs with their regulatory subunit, the cyclin, is required for the kinase activity of the CDKs. Activities of the different CDKs are regulated both by availability of a particular cyclin, and also by binding of CDK-inhibitors (CKI), in addition to phosphorylation and dephosphorylation events, for example by CDK-activating kinase (CAK), or by CDK-associated protein phosphatase, respectively.

Approximately two thirds of the way through G1 the cell reaches the "restriction (R) point" (Pardee, 1989), when it assesses the environmental conditions (such as the presence of mitogens) and decides whether to continue through G1 and divide again, or to enter G0 and become quiescent. Activity of almost all CDKs are suppressed in G0 and early G1 by a combination of high CKI activity and low cyclin levels, and this absence of active CDK allows the retinoblastoma protein (pRB) to stay bound to the transcription factor E2F (see Figure 1.1). pRB inhibits E2F from activating transcription of genes important for DNA replication. D-type cyclins start to accumulate once the cell has received an extracellular signal that stimulates proliferation, and CDK4/6-Cyclin D becomes fully activated via phosphorylation by CAK. At the transition through R, CDK4/6-Cyclin D phosphorylates pRB (Bartek *et al.*, 1996; Weinberg, 1995), leading to the release of E2F transcription factors, and allowing transcription of genes that encode proteins required for entry into S phase. Active CDK2-Cyclin E and CDK4/6-Cyclin D together inactivate pRB completely, inducing more E2F-responsive genes required to drive cells through the G1/S transition and initiate DNA replication (see Figure 1.1).

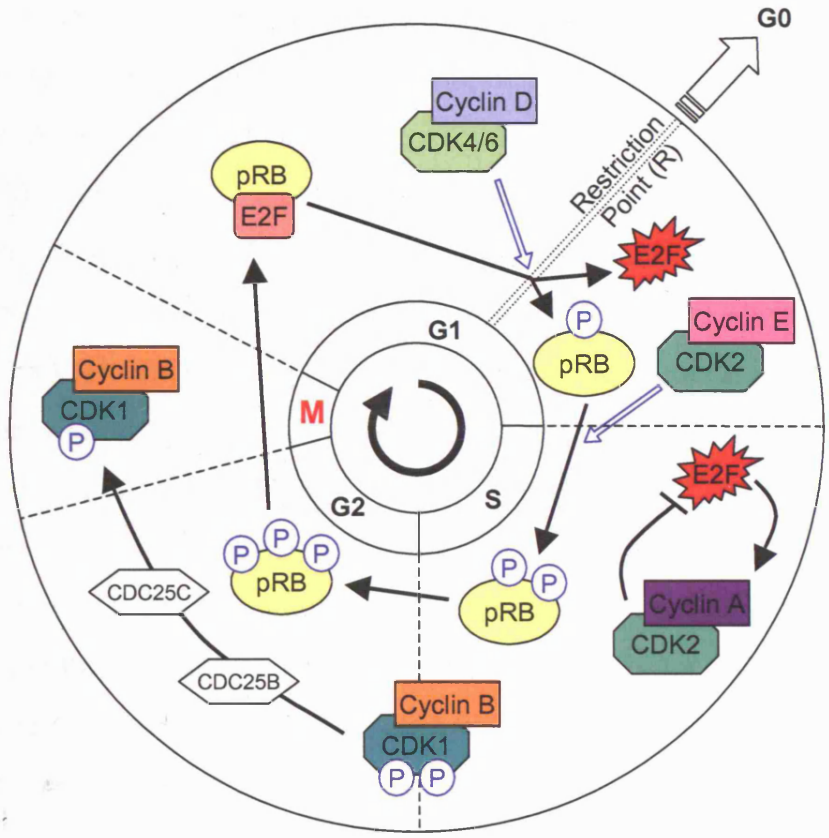

Figure 1.1: Cell cycle regulation.

A simplified summary of eukaryotic cell cycle regulation is shown with some of the major players represented. Progression through the cell cycle is regulated by sequential assembly and activation of cyclin-dependent kinase (CDK)-cyclin complexes.

Cyclin A starts to accumulate during S phase, and phosphorylation of components of the DNA replication machinery by CDK2-Cyclin A is important for initiation of DNA replication. E2F is responsible for activating the synthesis of Cyclin A, but E2F activity is also inhibited by CDK2-Cyclin A, forming a negative feedback loop (see Figure 1.1). Cyclin A is abruptly destroyed before metaphase (M phase) via ubiquitin-mediated proteolysis.

Cyclin A is also required for the G2/M transition. The entry into mitosis (G2/M transition) is triggered by CDK1-Cyclin B, also known as Maturation Promoting Factor (MPF). CDK1 (also known as cdc2) is kept in an inactive state during S and G2 phases by phosphorylation on two residues: Tyr15 and Thr14 (Hoffmann *et al.*, 1993). At the end of G2 MPF is activated via dephosphorylation by at least two phosphatases, CDC25B and CDC25C (Lee and Yang, 2001) (see Figure 1.1). Activated MPF is known to phosphorylate many substrates, including motor and microtubule-binding proteins important for chromosome condensation, nuclear envelope breakdown, spindle assembly and centrosome separation (Nigg, 2001).

Ultimately the degradation of Cyclin B is necessary to exit M phase and start a new cell cycle.

1.1.2 Mitosis

The cell cycle can be divided up into two phases: interphase (which contains G1, S and G2 phases), and mitotic phase (M phase). Mitosis has historically been separated into five phases: prophase, prometaphase, metaphase, anaphase and telophase, the definitions of which are based on morphology as seen via light microscopy. Mitotic phase consists of these five phases, also incorporating a process called cytokinesis (for a review, see (Sluder *et al.*, 2004)).

The start of mitosis is defined as prophase, which begins when condensing chromosomes are first clearly seen, and ends with breakdown of the nuclear envelope. As prophase progresses, the chromosomes become

progressively more condensed (Swedlow and Hirano, 2003), the nucleoli disappear, and the cytoplasmic microtubule array present at interphase becomes reorganised into two focal arrays, called asters, centred on the centrosomes. Centrosomes are the microtubule organising centres which will divide to organise the two poles of the mitotic spindle. The extent to which the asters are formed and separated by the time of nuclear envelope breakdown varies greatly from one cell to the next. In some cells the duplicated centrosomes show little evidence of astral microtubule assembly at the end of prophase, remaining close together. In others, by the end of prophase both asters may be well developed and have already separated to opposite sides of the nucleus (reviewed in (Rieder, 1990)).

Nuclear envelope breakdown signals the start of prometaphase, the stage when the mitotic spindle forms. During this phase, the cell establishes a bipolar spindle axis, the sister chromatids of each replicated chromosome become attached to opposing spindle poles (i.e. bioriented), and the chromosomes become aligned at or near to the spindle equator (Rieder, 1990).

The cell is considered to be in the metaphase stage of mitosis once all the chromosomes are bioriented and positioned near the spindle equator, i.e. once all chromosomes have aligned on the metaphase plate. During metaphase the spindle becomes progressively more compacted, resulting in a decrease in the distance between the spindle poles.

Anaphase begins when the sister chromatids of each replicated chromosome are separated to form two independent chromosomes, each of which moves towards its attached spindle pole. Anaphase ends when the poleward motion of the chromosomes is completed. Anaphase actually consists of two types of movement that act additively to increase the distance between the two separating groups of chromosomes: each chromosome moves to its respective pole (called Anaphase A), and the poles themselves move further apart (called Anaphase B). Anaphase A and B movements usually start simultaneously upon chromatid disjunction in vertebrates, but they can begin at different times in some organisms, suggesting that they can be

independently regulated (reviewed in (Mazia, 1961)). At some point in mid to late anaphase the process of cytokinesis (pinching the cytoplasm of the dividing cell in two between the separating sets of chromosomes) is initiated, although this is not always obvious (Oegema and Mitchison, 1997; Rappaport, 1969; Salmon, 1989; White and Borisy, 1983).

Telophase is the last stage of mitosis, consisting of events that complete cell division and allow the cell to exit mitosis. A nuclear envelope reforms around both masses of separated chromosomes. During telophase, the cell also continues the process of cytokinesis, cleaving between the separate nuclei. The cleavage apparatus (consisting of a circumferential band of actin and myosin) co-ordinately contracts and disassembles to prevent a mass of actomyosin from hindering the constricting furrow from completing cell division (Fishkind and Wang, 1993; Oegema and Mitchison, 1997). Before cleavage is complete, the two daughter cells remain attached via a midbody composed of tightly bundled microtubules embedded in a densely staining matrix material. Cleavage is completed when the midbody has been ruptured, thought to be caused by the daughter cells crawling apart.

1.1.3 Cell cycle checkpoints

Cell cycle checkpoints were first identified in yeast (Hartwell and Weinert, 1989) and are also present in mammalian cells. There are several checkpoints, each acting at a different stage of the cell cycle to ensure proper completion of cell cycle events. Some checkpoints act by blocking cell cycle progression until errors have been corrected (for example by requiring accurate DNA decatenation prior to mitotic entry (Deming *et al.*, 2001), or proper spindle formation and chromosome alignment prior to the initiation of anaphase (Bharadwaj and Yu, 2004)). Other checkpoints function to detect and correct errors that have occurred in previous steps (such as DNA damage checkpoints at G1 and G2 that prevent progression into S phase and mitosis, respectively (Mercer, 1998)). Many cell cycle checkpoints relate to DNA

metabolism, including DNA damage responses and the requirement for completion of DNA replication prior to mitotic entry (Sancar *et al.*, 2004). Other checkpoints monitor cytoskeletal function, including a pRB-dependent G1 checkpoint that monitors actin function (Reshetnikova *et al.*, 2000), a p53-dependent G1 checkpoint that monitors microtubule function (Andreassen *et al.*, 2001b), and the spindle assembly checkpoint which monitors microtubule polymerisation and ensures accurate segregation of sister chromatids at anaphase (Bharadwaj and Yu, 2004). Although the p53 tumour suppressor protein plays a role in both the G1/S phase and G2/M phase checkpoints in mammalian cells, no proteins homologous to p53 have been identified in yeast. However, several studies have suggested that certain aspects of p53 function may exist in yeast (Bischoff *et al.*, 1992; Koerte *et al.*, 1995; Nigro *et al.*, 1992).

1.2 THE SPINDLE CHECKPOINT

Every time a cell divides, it is crucial that each daughter cell receives one and only one copy of each chromosome. Failure to ensure the fidelity of sister chromatid segregation in each mitosis would result in aneuploidy (having a chromosome number that is not an exact multiple of the haploid number). Aneuploidy can lead to either cell death or the accumulation of cancer-causing mutations through gains or losses of DNA. The spindle checkpoint (also called "the spindle assembly checkpoint" and "the mitotic checkpoint") is a surveillance mechanism that blocks chromosome segregation until all sister chromatid pairs in the cell have successfully formed a bipolar attachment to spindle microtubules (for a recent review, see (Bharadwaj and Yu, 2004)). An interaction between the viral protein SV40 large T antigen (LT) and an important component of the spindle checkpoint pathway, Bub1, has recently been identified (Cotsiki *et al.*, 2004), suggesting that aneuploidy induced by SV40 LT may be caused by inhibition of the spindle checkpoint function of Bub1.

The sister chromatids of a dividing cell are held together by a protein bridge formed by a multiprotein complex called cohesin (reviewed in (Bharadwaj and Yu, 2004)). Proteolysis of the cohesin subunit Scc1 by a protease called separase triggers anaphase. However, separase is normally kept inactive by an associated inhibitor called securin, thus preventing progression to anaphase (see Figure 1.2). During prometaphase of mitosis, sister chromatids attach to microtubules emanating from opposite poles of the mitotic spindle via a specialised DNA-protein complex called the kinetochore, located at the centromere of each sister chromatid. If any kinetochores are unattached, or have not formed a bipolar attachment, an inhibitory signal generated by the spindle checkpoint blocks the transition to anaphase by inhibiting the activity of the anaphase promoting complex or "cyclosome" (APC/C), an E3 ubiquitin ligase.

Figure 1.2: Regulation of chromosome segregation by the spindle checkpoint.

A simplified diagram showing how the spindle checkpoint proteins function to regulate the metaphase-anaphase transition. For simplicity, spindle checkpoint proteins are represented by generic shapes (A more detailed description of the functions of the spindle checkpoint proteins in this pathway is shown in Figures 1.3 and 1.5).

When the spindle checkpoint is activated, separase is inhibited by securin from cleaving cohesin, and APC/C^{Cdc20} is prevented from lifting this inhibition by action of the spindle checkpoint (A).

Once all sister chromatids have formed a bipolar attachment with the mitotic spindle apparatus, the spindle checkpoint is deactivated and APC/C^{Cdc20} targets securin for proteolytic destruction, resulting in activation of separase which cleaves the cohesin subunit Scc1 (B), allowing onset of anaphase and chromosome segregation to occur (C).

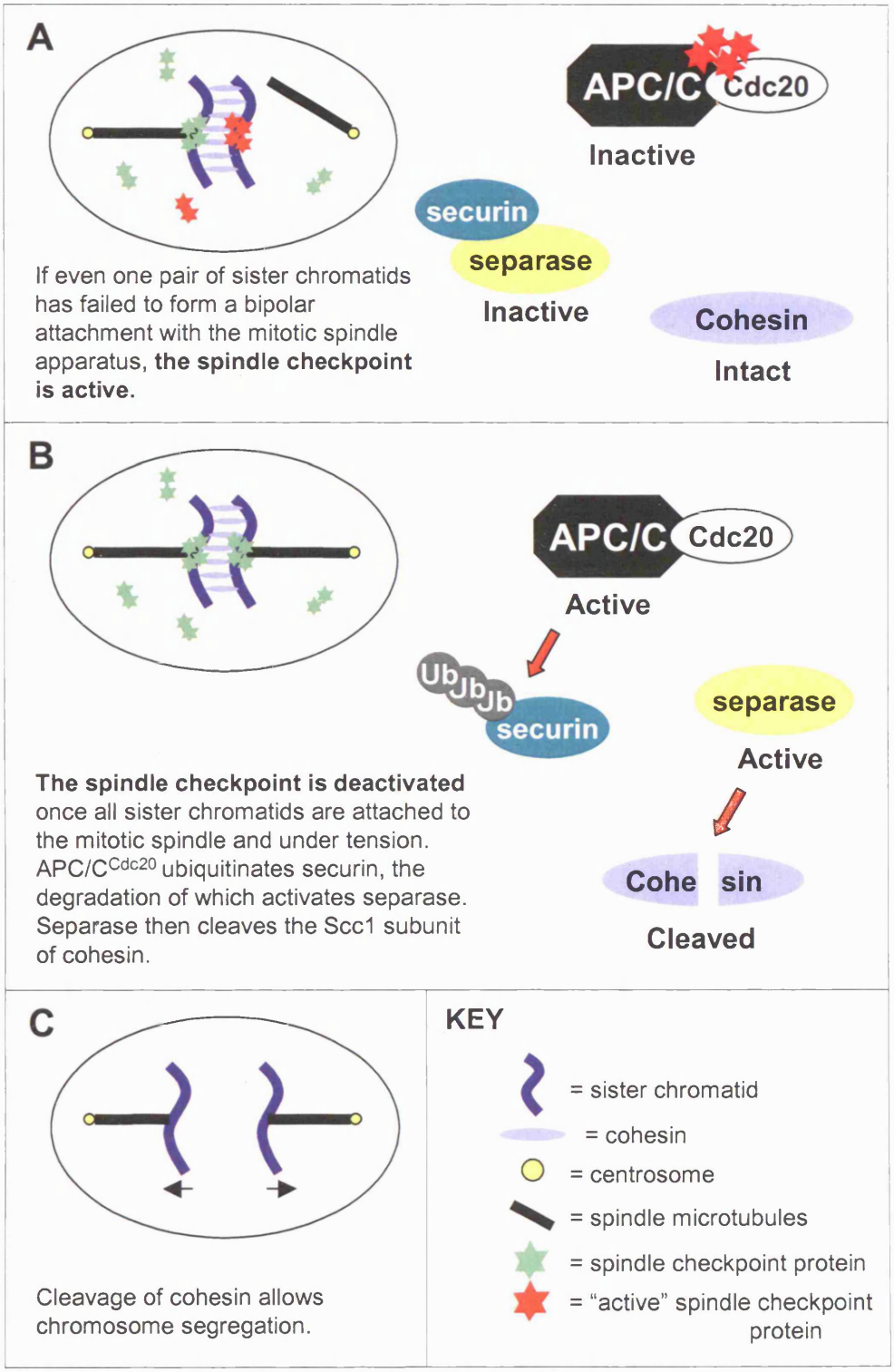

Figure 1.2: Regulation of chromosome segregation by the spindle checkpoint.

This prevents degradation of the securin proteins that are involved in chromatid cohesion, and thus causes mitotic arrest. However, once all sister chromatids in the cell have formed bipolar attachments with the mitotic spindle, the spindle checkpoint is satisfied, and APC/C is de-repressed. Securin is then ubiquitinated by APC/C, and destroyed by the proteasome. This leads to separase activation, Scc1 cleavage, loss of chromosome cohesion, and anaphase onset (see Figure 1.2). Later in anaphase and telophase, APC/C also targets Cyclin B for destruction, allowing mitotic exit to occur (Peters, 1999). It has also been shown that Cyclin B1-CDK1 is capable of blocking anaphase when present at high levels, indicating that both securin and Cyclin B1 must be degraded to allow separation of sister chromatids (Hagting *et al.*, 2002).

Binding of the substrate recognition factor Cdc20 to APC/C is required for the ubiquitination of securin, and it is the interaction of APC/C with Cdc20 that is modulated by the spindle checkpoint. A diffusible signal that inhibits the cytoplasmic pool of APC/C^{Cdc20} is generated by unattached kinetochores, preventing the separation of all (including already aligned) chromosomes (see Figure 1.2). Bub1 is thought to act as a scaffold for recruitment of other checkpoint proteins (Mad1, Mad2, Bub3 and CENP-E in *Xenopus*, and BubR1, CENP-F, CENP-E and Mad2 in mammalian cells) to unattached kinetochores (Chen, 2004; Johnson *et al.*, 2004; Sharp-Baker and Chen, 2001), and the activation of Bub1 kinase activity at unattached kinetochores correlates with generation of the spindle checkpoint signal that inhibits APC/C^{Cdc20} (Chen, 2004). Inhibition of Cdc20 (and thus of APC/C) is widely thought to be accomplished by the mitotic checkpoint complex (MCC, composed of Cdc20 and the spindle checkpoint proteins Mad2, BubR1 and Bub3), which is generated by unattached kinetochores and is conserved from yeast to humans (Fang, 2002; Fraschini *et al.*, 2001; Hardwick *et al.*, 2000; Millband and Hardwick, 2002; Sudakin *et al.*, 2001; Yu, 2002) (see Figure 1.3).

Figure 1.3: A simplified model for spindle checkpoint signalling

When the spindle checkpoint is activated (i.e. in the presence of one or more kinetochores which have not formed a bipolar attachment with the mitotic spindle), checkpoint proteins that act upstream in the spindle checkpoint pathway (e.g. the Bub1 and Mps1 kinases) may recruit and/or modify other spindle checkpoint proteins at the unattached kinetochore, resulting in production of the mitotic checkpoint complex (MCC), consisting of Mad2, BubR1, Bub3 and Cdc20 proteins. The MCC then inhibits APC/C, preventing destruction of securin, and resulting in a continued metaphase arrest, with no cleavage of cohesin.

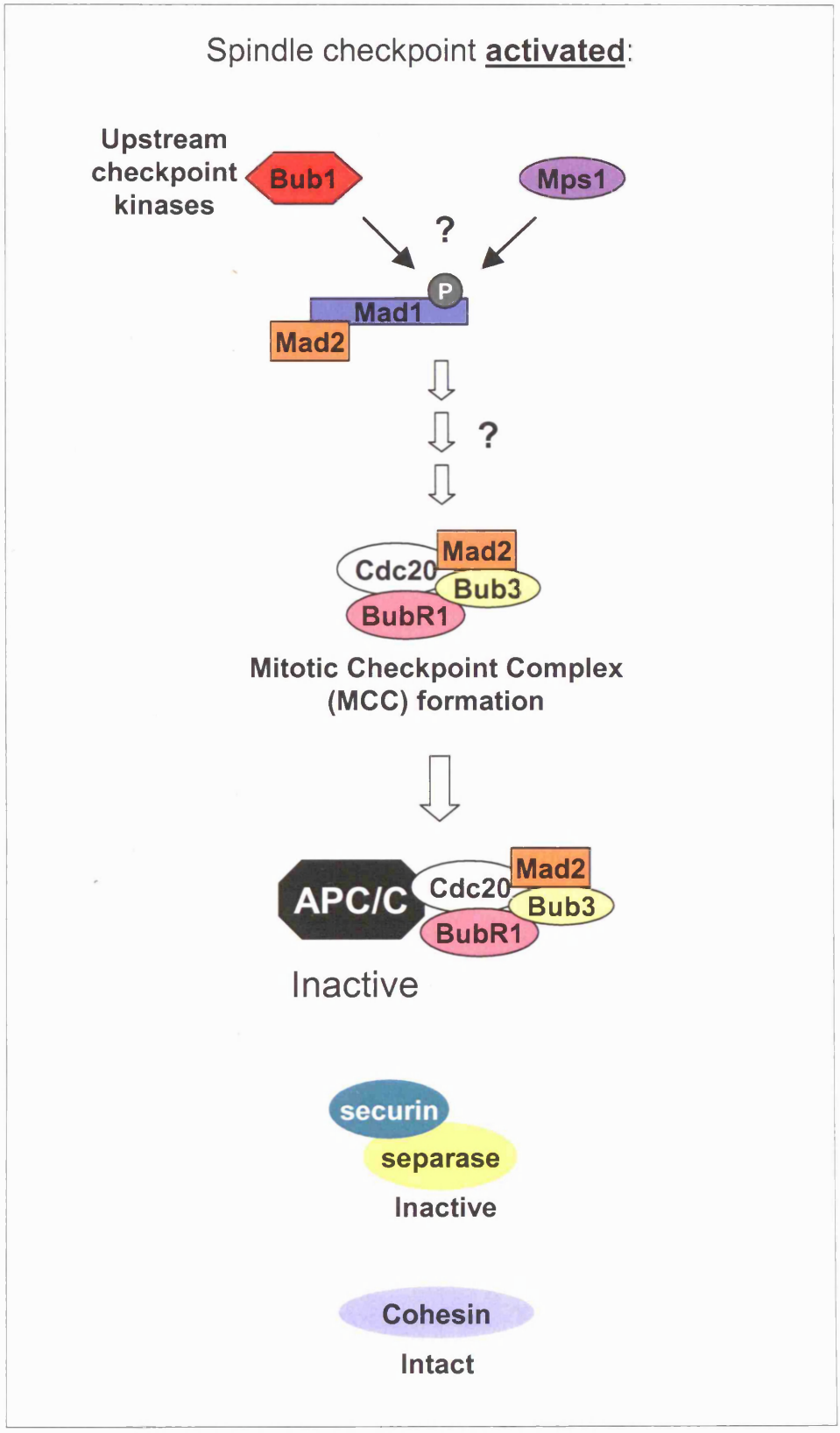

Figure 1.3: A simplified model for spindle checkpoint signalling

The MCC has been shown to have an APC/C-inhibitory activity that is 3000-fold greater than that of recombinant Mad2 in HeLa cells, also known to inhibit APC/C (Sudakin *et al.*, 2001). However, the precise details of the spindle checkpoint pathway remain to be determined, and there are many more components that play important roles in this pathway, as shall be discussed in more detail.

In addition to the spindle assembly checkpoint (SAC), a spindle orientation checkpoint (SOC) has been identified in fission yeast, activated in the absence of either an actomyosin division ring, or astral microtubules (Gachet *et al.*, 2001; Oliferenko and Balasubramanian, 2002). These two independent studies have shown that the SOC involves members of the SAC pathway, with both agreeing on the involvement of Bub1 in the two checkpoints. Mammalian cells also have a mechanism that monitors spindle orientation and positioning, and this is likely driven by interactions between astral microtubules, the motor protein dynein and the cell cortex (O'Connell and Wang, 2000). Perhaps this could represent a mitotic checkpoint mechanism equivalent to the SOC seen in fission yeast.

1.2.1 Discovery of the spindle checkpoint

Genetic studies in the budding yeast *Saccharomyces cerevisiae* initially identified six components of the spindle checkpoint - Bub1, Bub2, and Bub3 (Hoyt *et al.*, 1991) and Mad1, Mad2, and Mad3 (Li and Murray, 1991), each of which was essential for establishment or maintenance of the checkpoint. These genes are non-essential in yeast, but the *mad* (*m*itotic *a*rrest *d*efective) and *bub* (*b*udding *u*ninhibited by *b*enomyl) mutants ignore spindle abnormalities and attempt mitosis regardless. The *S. cerevisiae* Mps1 gene product, an essential protein kinase required for spindle pole body (SPB) duplication, is also required for spindle checkpoint function (Weiss and Winey, 1996).

Vertebrate homologues of several of these proteins are associated with the kinetochore, including Bub1 (Jablonski *et al.*, 1998; Taylor and McKeon, 1997), Bub3 (Taylor *et al.*, 1998), Mad1 (Chen *et al.*, 1998), Mad2 (Chen *et al.*, 1996; Li and Benezra, 1996), BubR1, a protein kinase with homology to both Bub1 and Mad3 (Cahill *et al.*, 1998; Chan *et al.*, 1999; Taylor *et al.*, 1998), and Mps1 (Stucke *et al.*, 2002).

Bub2 forms a separate branch of the spindle checkpoint that plays a role in the exit from mitosis (reviewed in (Gardner and Burke, 2000)).

1.2.2 Genetic instability and the spindle checkpoint

Genetic instability has been proposed to underlie neoplasia (Hartwell, 1992; Loeb, 1991), and can occur in two different forms. Microsatellite instability (MIN) is the result of defective mismatch repair and a consequentially increased mutation rate at the nucleotide level. Chromosomal instability (CIN) leads to an abnormal chromosome number, known as aneuploidy, and has been shown to be associated with loss of function of the spindle checkpoint protein Bub1 (Cahill *et al.*, 1998). In humans, aneuploidy is a hallmark of spontaneous abortions, birth defects and most cancers (Hassold and Hunt, 2001; Jallepalli and Lengauer, 2001; Thomas *et al.*, 2001). However, it has more recently been suggested that CIN cells do in fact undergo mitotic arrest in response to spindle damage, and that they possess a robust spindle checkpoint, although the checkpoint may nevertheless be compromised to some extent (Tighe *et al.*, 2001). While mutations in spindle checkpoint genes are rare in human tumours, the Adenomatous Polyposis Coli (APC) gene is frequently mutated in CIN cells, and Tighe *et al.* show that an APC mutant can compromise the spindle checkpoint response, perhaps contributing to CIN. The product of the APC gene, involved in familial colon cancer, has been shown to form a complex with the checkpoint proteins Bub1 and Bub3 during mitosis (Kaplan *et al.*, 2001). APC is a plus-end microtubule-binding protein that localises to kinetochores. Kaplan *et al.*

suggested that APC may be stabilising the microtubules and therefore aiding their attachment to the chromosomes. This appears to be supported by the recent finding that CIN tumour cells exhibit inefficient microtubule plus-end attachments during mitosis, and that this is correlated with the status of APC (Green and Kaplan, 2003). Despite the observed interaction between APC and the Bub proteins, APC has not been found to be necessary for the spindle checkpoint, although phosphorylation of APC by both Bub1 and BubR1 kinases may be involved in regulation of kinetochore-microtubule attachment (Kaplan *et al.*, 2001).

Deletion of one allele of Mad2, Bub3 or BubR1 in mice compromises the spindle checkpoint and results in higher rates of chromosome missegregation and tumour formation, suggesting a causal relationship between a weakened checkpoint and carcinogenesis arising from CIN (Babu *et al.*, 2003; Dai *et al.*, 2004; Michel *et al.*, 2001). Although initial weakening of the spindle checkpoint might enhance aspects of CIN-mediated tumourigenesis, further weakening or silencing of the spindle checkpoint pathway has been shown to rapidly lead to cell death, even in aggressive cancer cell lines (Kops *et al.*, 2004; Michel *et al.*, 2004). Kops *et al.* showed that depletion of BubR1 and Mad2 (or inhibition of BubR1 kinase activity) causes apoptotic cell death within six divisions in the cells, except when cytokinesis had been inhibited by addition of a microtubule poison (cytokinesis requires overlapping microtubules from the two spindle poles for recruitment of the component(s) necessary for cleavage, (Maddox and Oegema, 2003)). In the presence of microtubule poisons such as colcemid, nocodazole or taxol, reduced levels of BubR1 or Mad2 were shown to permit progression through the cell cycle without spindle checkpoint arrest, resulting in giant cells and nuclei as a consequence of continued cycling. Since the survival of CIN (and MIN) tumours depends on basal levels of spindle checkpoint signalling, Kops *et al.* suggest that drugs targeting essential spindle checkpoint functions such as BubR1 kinase activity could selectively kill these tumour cells.

1.2.3 The components of the spindle checkpoint pathway

The fine mechanistic details of the spindle checkpoint remain to be elucidated, but by dissecting the functions of the various members of the pathway a greater understanding of this complex process can be gained. This section gives a summary of some of the latest findings relating to the main players in the spindle checkpoint pathway.

1.2.3.1 Bub1

The human Bub1 (hBub1) is a protein of 1085 amino acids, with a predicted molecular weight of 122kDa (Ouyang *et al.*, 1998). hBub1 is localised to kinetochores during mitosis, and its expression is cell cycle regulated, peaking at G2/M phase (Taylor *et al.*, 2001). The amino-terminal region of hBub1 shows significant homology to yeast Mad3, and contains a nuclear targeting signal and also a domain homologous to the tail domain of murine kinesin-like protein (muKIF4, a microtubule-associated motor protein, (Sekine *et al.*, 1994)). hBub1 also has a GLEBS-like (GLE2p-Binding Sequence) motif at residues 249-264 that was shown to be sufficient for Bub3 binding (Wang *et al.*, 2001b). Wang *et al.* showed that the mRNA export factor Rae1 (also called GLE2) can also bind to this region of hBub1, and a separate study in mouse cells has suggested that Rae1 can cooperate with Bub3 in the spindle checkpoint pathway (Babu *et al.*, 2003). The carboxy-terminus of hBub1 contains a kinase domain and an ATP-binding site (see Figure 1.4).

The Bub1 protein is essential for spindle checkpoint function, acting as a scaffold for recruitment of other checkpoint proteins to unattached kinetochores. A recent study has shown that Bub1, Mps1 and CENP-E are dependent upon each other for their kinetochore localisation, and for the localisation of the other spindle checkpoint components (Vigneron *et al.*, 2004).

Mutations in the Bub1 gene have been shown to result in loss of spindle checkpoint function, and are related to the chromosome instability (CIN) phenotype in human neoplasias (Cahill *et al.*, 1998; Hempen *et al.*, 2003). hBub1 defects have also been observed in leukaemia and lymphoma cells (Ru *et al.*, 2002). Inhibition of Bub1 results in a CIN phenotype as well as induction of anchorage-independent growth in normal human fibroblasts, suggesting that failure of the spindle checkpoint and resulting aneuploidy could lead to transformation and tumourigenesis (Musio *et al.*, 2003).

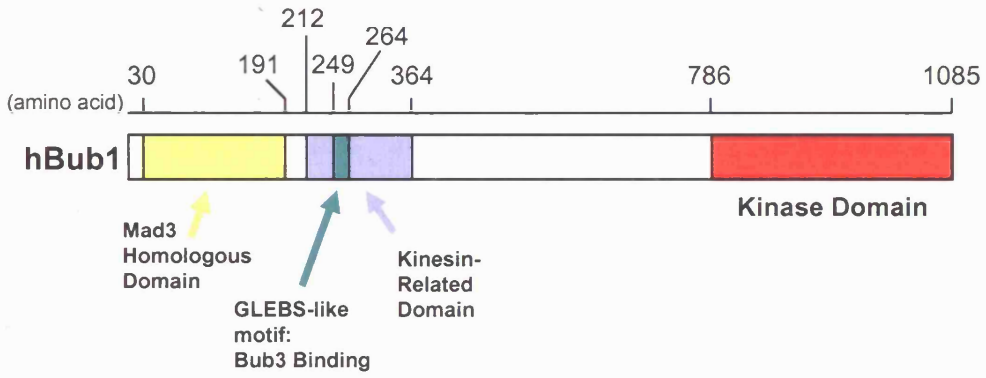

Figure 1.4: The Bub1 spindle checkpoint protein.

A representation of the domain structure of human Bub1 protein (hBub1). hBub1 is a protein of 1085 amino acids with a calculated molecular mass of 122kDa. It has a carboxy-terminal kinase domain, and the amino-terminal section (161 residues) shows a 26% amino acid identity to the Mad3 protein in budding yeast. Residues 249-264 are sufficient for binding to the spindle checkpoint protein Bub3. There also appears to be a domain (152 residues) that is homologous to the tail domain of murine kinesin-like protein, muKIF4. In addition, the kinase domain contains an ATP-binding site, and there is a putative nuclear localisation signal in the amino-terminal region of the protein (not shown).

The Bub1 protein is a serine/threonine kinase, and mutation of the carboxy-terminal kinase domain in budding yeast Bub1 results in a defective spindle checkpoint, suggesting that the kinase activity of Bub1 is critical for its function (Roberts *et al.*, 1994). Bub1 can phosphorylate itself as well as Bub3 (Roberts *et al.*, 1994) and Mad1 (Seeley *et al.*, 1999) *in vitro*. However, the kinase activity of fission yeast Bub1 is required but not sufficient for complete spindle checkpoint function (Yamaguchi *et al.*, 2003), and separate studies have shown that the protein kinase activity of Bub1 is not responsible for spindle checkpoint arrest induced by nocodazole, a microtubule-depolymerising agent (Sharp-Baker and Chen, 2001; Warren *et al.*, 2002). However, it has recently been suggested that the kinase activity of Bub1 modulates the strength of the checkpoint signal generated from each kinetochore (Chen, 2004). In experiments using *Xenopus* egg extracts, kinase-deficient Bub1 was found to be partially compromised in checkpoint function, with a reduced ability to recruit other checkpoint proteins to the kinetochore under conditions of low spindle damage (when only a few or even one kinetochore is unattached), whereas under optimal conditions for spindle checkpoint activation, kinase-deficient Bub1 is sufficient for full checkpoint function. It was therefore suggested that the kinase activity of Bub1 may become crucial in late prometaphase for efficient assembly of the complex that binds and inhibits Cdc20 at the few unattached kinetochores that remain.

Bub1 is associated with Bub3 throughout the cell cycle in budding yeast (Brady and Hardwick, 2000). Studies in human cells have shown that interaction with Bub3 is required for Bub1 to localise to kinetochores (Taylor *et al.*, 1998) and *Drosophila* Bub3 fails to localise to kinetochores when the Bub1 gene is deleted (Basu *et al.*, 1998), demonstrating a mutual dependency between Bub1 and Bub3 in kinetochore binding.

In budding yeast, there are two distinct forms of Bub1 during G1 phase of the cell cycle, and up to five forms during mitosis (Brady and Hardwick, 2000). Lambda protein phosphatase treatment revealed that these different forms of Bub1 are all due to phosphorylation. This modification of Bub1 was

not enhanced by spindle checkpoint activation. In contrast, the fission yeast Bub1 protein ("Bub1p") is directly phosphorylated by the cyclin-dependent kinase (CDK) Cdc2p in response to spindle damage in mitotic cells, and this phosphorylation is necessary for spindle checkpoint activation following spindle damage (Yamaguchi *et al.*, 2003). It has also been shown that human Bub1 is phosphorylated when the spindle is disrupted, but not during normal mitosis (Taylor *et al.*, 2001), and putative CDK sites are present in Bub1 from human, mouse, fly, budding yeast and *Xenopus laevis* (albeit without conservation of CDK site position). This suggests that CDK phosphorylation of Bub1 might play a role in the spindle checkpoint of eukaryotes generally. MAPK (mitogen-activated protein kinase) also contributes to hyperphosphorylation of *Xenopus* Bub1 on unattached kinetochores, resulting in activation of Bub1 kinase activity (Chen, 2004). Although Cdc2 is not involved in the phosphorylation of *Xenopus* Bub1, sequence alignment of the fission yeast and *Xenopus* Bub1 proteins indicates a homologous phosphorylation site for Cdc2 in fission yeast Bub1 and MAPK in *Xenopus* Bub1, suggesting that regulation of Bub1 by phosphorylation (albeit not necessarily by the same kinases) is evolutionarily conserved (Chen, 2004).

Bub1 is required for efficient kinetochore localisation of Mad1, Mad2, Bub3 and CENP-E in *Xenopus* (Chen, 2004; Sharp-Baker and Chen, 2001), and BubR1, CENP-F, CENP-E and Mad2 proteins in mammalian cells (Johnson *et al.*, 2004) (CENP-F is a kinetochore protein, CENP-E is a kinetochore-associated microtubule motor protein). In turn, the Aurora B protein (as described later) is required for kinetochore localisation of Bub1. BubR1 was not required for kinetochore localisation of Bub1, Mad2 or CENP-F in mammalian cells, in contrast to work carried out in *Xenopus* (Chen, 2002), suggesting that some transient kinetochore proteins may be recruited simultaneously in the *Xenopus* system. A recent study suggested that repression of Bub1 does not compromise spindle checkpoint function during either normal mitosis or in response to spindle damage (Johnson *et al.*, 2004), contradictory to previous observations in yeast, *Xenopus*, and HeLa cells

(Hoyt *et al.*, 1991; Roberts *et al.*, 1994; Sharp-Baker and Chen, 2001; Taylor and McKeon, 1997). However, the authors suggested that this observation could be caused by more than one pathway contributing to spindle damage-mediated arrest, with Bub1 or Aurora B only required for one pathway, or alternatively that inhibition of either Bub1 or Aurora B only partially inhibits the spindle checkpoint pathway.

Bub1 appears to have functions beyond its role in the spindle checkpoint pathway. Bub1 may be involved in regulating mitotic exit in response to incomplete DNA replication. This is suggested by the observation that Drosophila *dup* (double park) mutants, defective for initiation of DNA replication, arrest at the metaphase-anaphase transition, but *dup bub1* double mutants do not (Garner *et al.*, 2001). Bub1 is also thought to play a crucial role in meiosis, preventing loss of sister chromatid cohesion during the first meiotic division (meiosis I) of fission yeast (Bernard *et al.*, 2001). Bub1 is required for centromere localisation of Sgo1 (shugoshin) which is responsible for protection of Rec8, the Scc1 cohesin subunit counterpart in meiosis (Kitajima *et al.*, 2004). In addition, localisation of Sgo2, a paralogue of Sgo1 in fission yeast that is required for faithful mitotic chromosome segregation, was also shown to require Bub1.

1.2.3.2 Bub3

Bub3 is a small WD-repeat protein. The *S. cerevisiae* Bub3 consists of seven WD-repeat domains that fold together to form a β-propellor structure, devoted to protein-protein interactions, and perhaps acting as a stable platform to coordinate sequential and/or simultaneous interactions of several proteins (Fraschini *et al.*, 2001; Smith *et al.*, 1999). Bub3 function is required for both spindle checkpoint activation and for maintenance of a checkpoint arrest in *Xenopus* egg extracts (Campbell and Hardwick, 2003).

Bub3 is associated with Bub1 throughout the cell cycle in budding yeast (Brady and Hardwick, 2000). *Xenopus* Bub3 (XBub3) is found in complex with both XBub1 and XBubR1 kinases, although a complex of all

three proteins is not seen (Campbell and Hardwick, 2003). The authors observed that XBub3 has a diffuse nuclear localisation during interphase, and is recruited to kinetochores during early prophase, prior to the kinetochore localisation of XMad2 and XMad1. XBub3 staining of kinetochores is lost once all chromosomes have aligned at the metaphase plate. Bub3 protein has been localised to kinetochores in a number of species when the spindle checkpoint is active (Basu *et al.*, 1998; Martinez-Exposito *et al.*, 1999; Taylor *et al.*, 1998). Bub3 forms part of the mitotic checkpoint complex (MCC) that inhibits APC/C when the spindle checkpoint is activated.

While mice heterozygous for the mammalian Bub3 gene show no apparent abnormalities in development or fertility, Bub3 null mice fail to survive beyond day 6.5-7.5 postcoitus, with accumulation of mitotic errors early in development resulting in formation of micronuclei, chromatin bridges, lagging chromosomes and irregular nuclear morphology, similar to the defects seen in Mad2 null embryos (Dobles *et al.*, 2000; Kalitsis *et al.*, 2000).

1.2.3.3 Mad1

Budding yeast Mad1 is a 90kDa protein that becomes hyperphosphorylated during normal mitosis and when spindle assembly is disrupted (Hardwick and Murray, 1995). The upstream kinase for Mad1 is likely to be Mps1, the overexpression of which results in hyperphosphorylation of Mad1 and a mitotic arrest. However, phosphorylation of Mad1 also requires Mad2, Bub1 and Bub3 (Hardwick *et al.*, 1996; Weiss and Winey, 1996). Mad1 forms a complex with Mad2 and this interaction is essential for Mad1 phosphorylation in budding yeast (Chen *et al.*, 1999), and studies in *Xenopus* showed that Mad1 is required to recruit Mad2 to kinetochores (Chen *et al.*, 1996). In addition, human Mad1 binds to and is phosphorylated by Bub1 *in vitro* (Seeley *et al.*, 1999).

The human Mad1 protein was originally identified during a search for cellular targets of the Human T cell leukaemia virus type 1 (HTLV-1) oncoprotein Tax (Jin *et al.*, 1998), making it the first member of the spindle

checkpoint pathway to be found in complex with a viral oncoprotein. Unexpectedly, expression of human Mad1 is G1 rather than M phase specific, and intracellular levels of Mad1 correlate with the proliferative status of cells, both in primary and transformed cells (Iwanaga and Jeang, 2002). The same study found that human Mad1 promoter responds to mitogenic stimuli, but not to microtubule inhibitors. In addition, expression of human Mad1 was enhanced by a gain-of-function p53 mutant, suggesting that Mad1 could be a p53 downstream cellular factor that could link p53 to aneuploidy in human cells. This was in agreement with studies showing that human Mad1 mRNA is induced more than 10-fold by p53 (Polyak *et al.*, 1997), suggesting that p53 may have a true spindle checkpoint function, rather than simply serving to prevent cells from reinitiating DNA replication following errors in mitosis (Minn *et al.*, 1996).

1.2.3.4 Mad2

Human Mad2 is a 24kDa protein, and its expression is cell cycle regulated in human fibroblasts, peaking in mitosis (Hernando *et al.*, 2004). However, the budding yeast Mad2 protein remains at a constant level during the cell cycle (Chen *et al.*, 1999). Mad2 null yeast cells are viable but lose chromosomes at a higher rate than wild-type cells due to chromosome missegregation (Li and Murray, 1991). Mad2 null mice also missegregate their chromosomes, but they lose viability after day 6.5 postcoitus, highlighting the importance of chromosome stability for normal development (Dobles *et al.*, 2000). However, Mad2+/- mouse embryonic fibroblasts have enhanced chromosome instability without loss of viability, and consistent with this increased aneuploidy, Mad2+/- mice are tumour prone (Michel *et al.*, 2001). Partial reduction in Mad2 protein levels resulting in aneuploidy and tumourigenesis is consistent with the finding that several human tumour types have reduced levels of Mad2 protein expression (Li and Benezra, 1996; Wang *et al.*, 2002; Wang *et al.*, 2000). Mad2+/- cells cycle normally, form intact spindles and do not degrade Cyclin B prematurely. However, in response to

the microtubule poison nocodazole they degrade securin prematurely (but not Cyclin B) and exhibit premature sister chromatid separation with completely condensed chromosomes, suggesting that securin and Cyclin B degradation are uncoupled in the presence of one copy of Mad2 in these mammalian cells (Michel *et al.*, 2004; Michel *et al.*, 2001). This had not been shown in mammalian cells before, but uncoupling of Pds1 (securin) and clb2 (Cyclin B) destruction has been demonstrated in budding yeast, although the basis of this differential sensitivity of the two proteins to APC/C^{Cdc20} in yeast is unknown (Wasch and Cross, 2002; Yeong *et al.*, 2000).

Xenopus Mad2 is recruited to unattached kinetochores by Mad1 (Chen *et al.*, 1998). Mad2 is only a transient component of kinetochores, with a $t_{1/2}$ of 24-28 seconds (Howell *et al.*, 2000). Mad2 has been shown to bind phosphorylated but not unphosphorylated kinetochores, suggesting a link between attachment-sensitive kinetochore phosphorylation and the spindle checkpoint (Waters *et al.*, 1999) (see also Section 1.2.6).

Mad2 is a two-state protein that undergoes a dramatic conformational change in response to Mad1-binding, and adopts a very similar structure when bound to its molecular target, Cdc20 (Luo *et al.*, 2002). Luo *et al.* suggest a model in which Mad2 is recruited to unattached kinetochores via interaction with Mad1 when the checkpoint is activated. It is proposed that the Mad1-bound Mad2 protein is then transferred to Cdc20 to allow efficient formation of a Mad2-Cdc20-containing checkpoint complex, and that this could be facilitated by Mad2 transiently retaining its altered conformation. The empty preformed ligand binding site (induced by interaction with Mad1) would then also be recognised by Cdc20. Immunodepletion studies in *Xenopus* egg extracts have shown that Mad1-free Mad2 protein is required for establishment and maintenance of the spindle checkpoint response, but is unable to bind Cdc20, consistent with the model that Mad2-Cdc20 complex formation is facilitated by kinetochore localisation of Mad2 (Chung and Chen, 2002). Both Mad1-bound and Mad1-free Mad2 are required for spindle checkpoint function, and the ratio between Mad1 and Mad2 in the cell is

critical for maintaining a pool of Mad1-free Mad2. It was suggested that Mad2 may become activated and dissociated from Mad1 at kinetochores, and then replenished by the pool of Mad1-free Mad2. The human Mad2 protein is modified via phosphorylation on several serine residues in a cell cycle-dependent manner, and it is only unphosphorylated Mad2 that interacts with Mad1 or APC/C^{Cdc20} *in vivo* (Wassmann *et al.*, 2003). It was suggested that a phosphorylation-dephosphorylation cycle might be required to allow transfer of Mad2 from Mad1 to the APC/C^{Cdc20} complex. Mad2 is also a member of the MCC complex (along with Cdc20, BubR1 and Bub3) that inhibits APC/C.

It has recently been shown that Mad2 is a direct E2F target, and is as a consequence expressed aberrantly in cells with pRB (Retinoblastoma protein) pathway defects (Hernando *et al.*, 2004). The authors showed that Mad2 expression was increased, and was expressed at high levels throughout the cell cycle in cells with inactive pRB (due to expression of Adenovirus E1A, or knockdown of pRB levels via RNAi, as well as in carcinoma cell lines with inactive pRB). This can lead to aneuploidy, perhaps as the result of a hyperactive spindle checkpoint.

Mad2B, a novel human gene homologous to Mad2 has also been identified, and both genes are thought to be derived from a single ancestral Mad2 gene (Cahill *et al.*, 1999). Unlike Mad2, Mad2B does not interact with Mad1, and has been shown to inhibit APC/C^{Cdh1} *in vitro* and *in vivo* (Chen and Fang, 2001; Pfleger *et al.*, 2001b). (See Section 1.2.3.8 for more information about APC/C^{Cdh1}).

1.2.3.5 BubR1 (Mad3)

The budding yeast Mad3 gene encodes a 58kDa nuclear protein that is not essential for viability, but is an integral component of the spindle checkpoint (Hardwick *et al.*, 2000). Two regions of homology were identified between the budding yeast Mad3 and Bub1 proteins, and these regions are crucial for Mad3 interaction with Bub3, Mad2 and Cdc20 proteins (forming the MCC complex). The fission yeast Mad3 homolog is also nonessential

under normal growth conditions, but required for the spindle checkpoint response to microtubule-depolymerising agents (Millband and Hardwick, 2002). Like the budding yeast Mad3, fission yeast Mad3 forms a complex with Bub3, Mad2, and Slp1 (the fission yeast Cdc20 homolog). Genetic evidence also suggests that Mad3, along with Mad2 plays a crucial role in inhibition of APC/C, and showed that Mad3 is functioning either with or downstream of Mad2 to carry out this inhibition.

BubR1 is a mammalian Bub1 and Mad3 homolog. hBubR1 (human BubR1) is a 120kDa protein, identified by Cahill *et al.* (Cahill *et al.*, 1998), and is an essential component of the spindle checkpoint required for mitotic arrest in response to microtubule inhibitors (Chan *et al.*, 1999). Unlike the yeast Mad3 proteins, BubR1 is also necessary for normal mitotic progression as it prevents cells from prematurely entering anaphase.

Complete loss of BubR1 causes early embryonic lethality, but mice with low levels of BubR1 protein have been shown to develop progressive aneuploidy along with early onset of several aging-associated phenotypes including a severely shortened lifespan, and infertility (Baker *et al.*, 2004). The rate of tumours in mice with lowered BubR1 expression was very low despite substantial chromosome number instability, an unexpected finding because aneuploidy is a hallmark of most human cancers, and because BubR1 is also known to be mutated or expressed at low levels in a subset of colorectal carcinomas with CIN (Cahill *et al.*, 1998; Shichiri *et al.*, 2002). BubR1 expression was also shown to decline with age in several tissues of wild-type mice, indicating that BubR1 may be a key regulator of normal aging (Baker *et al.*, 2004). BubR1 haploinsufficiency in mouse embryonic fibroblasts has also been shown to result in a compromised spindle checkpoint, along with significantly reduced expression levels of securin and Cdc20 (Dai *et al.*, 2004).

Mammalian BubR1 has a C-terminal kinase domain, whereas Mad3 of both budding and fission yeast lack this domain (Millband and Hardwick, 2002). Human BubR1 (hBubR1) is cell cycle regulated, increasing

significantly in late S phase and G2 (Li *et al.*, 1999). Although hBubR1 is present throughout the cell cycle its kinase activity is detected only after cells have entered mitosis. The phosphorylation status of hBubR1 is also regulated during spindle disruption.

hBubR1 is associated with p55Cdc (the human homolog of Cdc20), and in response to spindle damage this interaction is enhanced and BubR1 phosphorylates p55Cdc (Wu *et al.*, 2000). BubR1 also associates with the kinetochore-associated kinesin motor protein CENP-E (Chan *et al.*, 1998), and spindle checkpoint activation or silencing was shown to be mediated through CENP-E-dependent activation or inactivation of the BubR1 kinase (Mao *et al.*, 2003). In addition, it has recently been shown that BubR1 (or Mad2) inactivation results in an accelerated mitosis, and that this regulation of mitotic timing is kinetochore-independent (Meraldi *et al.*, 2004a). It was proposed that BubR1 and Mad2 might be essential for restraining the onset of anaphase at a point early in mitosis when the kinetochores are still assembling. Finally, BubR1 mutation has recently been linked to the rare human disorder mosaic variegated aneuploidy, which has a high risk of malignancy (Hanks *et al.*, 2004). This supports the suggestion of a causal link between aneuploidy and cancer development.

1.2.3.6 Mps1

The founding member of the Mps1 kinase family in *Saccharomyces cerevisiae*, Mps1p, regulates many cell cycle-related processes, including the duplication of the spindle pole body (SPB) (Winey *et al.*, 1991), and the spindle checkpoint (Weiss and Winey, 1996). Spindle checkpoint activation in yeast leads to Mps1-dependent hyperphosphorylation of Mad1 and formation of a Mad1-Bub1-Bub3 complex, a crucial step in the spindle checkpoint mechanism (Brady and Hardwick, 2000; Hardwick *et al.*, 1996). Mps1 is highly homologous to a previously identified human gene TTK, now re-named hMps1 (Fisk and Winey, 2001; Mills *et al.*, 1992). However, while the human Mps1 kinase is required for the spindle checkpoint, it is not necessary

for centrosome duplication (Stucke *et al.*, 2002). The same study showed that hMps1 is a cell cycle regulated protein, with maximal protein levels and kinase activity occurring during mitosis. hMps1 is found in both the nucleus and cytoplasm of interphase cells, and localises to kinetochores during mitosis.

Mps1 is required for kinetochore recruitment and retention of active CENP-E protein in *Xenopus* egg extracts, which in turn is necessary for kinetochore association of the Mad1/Mad2 complex (Abrieu *et al.*, 2001). Hec1, a mammalian homolog of the budding yeast kinetochore-associated protein Ndc80p, is required for the kinetochore association of Mps1, and both Hec1 and Mps1 are necessary for recruitment of the Mad1/Mad2 complex (Martin-Lluesma *et al.*, 2002).

1.2.3.7 CENP-E

Centromere-associated protein-E (CENP-E) is a large (~300kDa) kinetochore-associated, kinesin-like microtubule motor protein that accumulates in G2 and is degraded in telophase (Brown *et al.*, 1994). CENP-E also binds to both spindle microtubules and to the kinetochore-associated checkpoint kinase BubR1 (Chan *et al.*, 1998; Putkey *et al.*, 2002; Yao *et al.*, 2000). Human CENP-E is detectable only in the cytoplasm of interphase cells (Yen *et al.*, 1992), whereas *Xenopus* CENP-E is a nuclear protein (Wood *et al.*, 1997). However, in both cases CENP-E is localised to kinetochores very early in mitosis.

CENP-E is required for the establishment and maintenance of the spindle checkpoint in *Xenopus* egg extracts (Abrieu *et al.*, 2000). Disruption of CENP-E function by immunodepletion results in failure to arrest in response to spindle damage, although the mitotic arrest is restored by addition of high levels of the Mad2 protein. This demonstrated that although CENP-E is necessary in *Xenopus* extracts for kinetochore-dependent signalling, it is not required for signal transduction further downstream in the checkpoint pathway. Paradoxically, inhibition of CENP-E function in mammalian

systems give results that contradict those seen in *Xenopus*, with suppression of CENP-E function resulting in a G2/M arrest due to a chronically activated spindle checkpoint (Chan *et al.*, 1999; Yao *et al.*, 2000). In the *Xenopus* system depletion of CENP-E prevents the association of Mad2 with kinetochores, and thus blocks the activation of Mad2 at kinetochores not yet attached to the mitotic spindle apparatus. Conversely, in human HeLa cells removal of CENP-E leaves active BubR1 and Mad2 in association with unattached kinetochores, perhaps offering an explanation for the discrepancy seen between the two model systems. However, a more recent study has demonstrated that CENP-E is essential for spindle checkpoint function in mammalian cells, with single unattached kinetochores depleted of CENP-E being unable to block entry into anaphase, resulting in aneuploidy (Weaver *et al.*, 2003). CENP-E enhanced the recruitment of BubR1 to each unattached kinetochore, and stimulated BubR1 kinase activity.

These discrepancies in CENP-E function are probably a reflection of species-specific distinctions between the spindle checkpoint of frogs and mammals or perhaps the difference between the meiotic state of egg extracts and the mitotic state of cultured cells. Although the spindle checkpoint pathway is itself widely conserved, its individual components are not and a prime example of this is the absence of a CENP-E-like protein in budding yeast. Also, the BubR1 protein with which CENP-E directly interacts is itself an apparent fusion of yeast Mad3 with the kinase domain of Bub1 (Taylor *et al.*, 1998). Nevertheless, CENP-E is a key vertebrate spindle checkpoint component that links checkpoint signalling to the binding of microtubules to sister chromatids.

1.2.3.8 APC/C

The anaphase promoting complex/cyclosome (APC/C) is a multi-subunit complex that acts as an E3 ubiquitin ligase, targeting proteins for destruction by the 26S proteasome. It functions at the metaphase to anaphase transition, as well as in late mitosis, G1 and in differentiated cells. APC/C

requires Cdc20 and Cdh1 proteins to recognise its substrates (reviewed in (Vodermaier, 2001)). APC/C^{Cdc20} and APC/C^{Cdh1} appear to have different substrate specificities (Visintin *et al.*, 1997). APC/C^{Cdc20} may target proteins such as securin whose destruction is required at the metaphase-anaphase transition, while APC/C^{Cdh1} may be targeting proteins such as Cyclin B whose degradation is important for mitotic exit. *In vitro*, APC/C^{Cdc20} recognises proteins that contain a destruction box (D-box), a loosely conserved motif with the consensus RxxLxxxxN, whereas APC/C^{Cdh1} is able to recognise proteins with either a D-box or a KEN box (a general targeting signal for APC/C^{Cdh1} composed of the amino acid sequence K-E-N) (Pfleger and Kirschner, 2000).

1.2.3.9 p55Cdc (Cdc20)

Cdc20 serves as a substrate receptor for APC/C, targeting securin for degradation by APC/C (Hilioti *et al.*, 2001; Pfleger *et al.*, 2001a). The level of Cdc20 is cell cycle regulated, rising in S phase, peaking in mitosis, and declining upon exit from mitosis in both yeast and mammalian cells (Kramer *et al.*, 2000; Prinz *et al.*, 1998; Shirayama *et al.*, 1998; Weinstein, 1997). The spindle checkpoint prevents activation of APC/C by Cdc20, thus blocking anaphase onset. Mad2 is an interacting protein for Cdc20 in both budding and fission yeast (the fission yeast Cdc20 homolog is called Slp1) (Hwang *et al.*, 1998; Kim *et al.*, 1998). Mutations in Slp1 or Cdc20 that disrupt their interaction with Mad2 result in a compromised spindle checkpoint. Cdc20 is also found in complex with Mad2, Bub3 and Mad3/BubR1 from various organisms, forming the mitotic checkpoint complex (MCC) that inhibits APC/C *in vitro* (Fang, 2002; Fraschini *et al.*, 2001; Hardwick *et al.*, 2000; Millband and Hardwick, 2002; Sudakin *et al.*, 2001; Yu, 2002).

In vitro CDK1-phosphorylated Cdc20 has been shown to interact with Mad2 rather than APC/C, suggesting that CDK activity is required to restrain

APC/C^{Cdc20} activation until completion of spindle assembly (D'Angiolella *et al.*, 2003).

p55Cdc is the mammalian homolog of Cdc20 (Weinstein *et al.*, 1994), but is also related to the Cdh1 protein (another substrate receptor for APC/C). The p55Cdc protein is degraded by APC/C^{Cdh1} during late mitosis, and recognition of p55Cdc by APC/C depends on the presence of a KEN box in the p55Cdc protein (Pfleger and Kirschner, 2000).

1.2.3.10 Securin

The budding yeast securin is called Pds1, and is an anaphase inhibitor that plays an essential role in both the spindle checkpoint and DNA damage pathways (Yamamoto *et al.*, 1996a; Yamamoto *et al.*, 1996b). In the DNA damage checkpoint, Pds1 is required for inhibition of cytokinesis and DNA replication as well as anaphase. In the spindle checkpoint pathway, Pds1 inhibits sister chromatid separation by binding and inhibiting the separase protein Esp1 (Ciosk *et al.*, 1998), a cysteine protease that causes cleavage of the cohesin Scc1 that binds sister chromatids together (Uhlmann *et al.*, 1999; Uhlmann *et al.*, 2000). In fission yeast, the securin protein is called Cut2, and the separase is called Cut1. The vertebrate separase is called separin. No sequence similarity has been found between Pds1 and Cut2, or between the yeast and vertebrate securin proteins, although the vertebrate securins share sequency similarity with each other (Zou *et al.*, 1999).

The human securin was identified via its association with the putative human separin, and is the product of the pituitary tumour transforming gene, PTTG-1 (also known as hPTTG) (Zou *et al.*, 1999). Human securin is regulated in a cell cycle-dependent manner, peaking in mitosis, and is phosphorylated by Cdc2 (also known as CDK1) during mitosis (Ramos-Morales *et al.*, 2000). Human securin, like Pds1 and Cut2, is required not only to inhibit the separase but also to generate the active form of the separase, and is essential for maintenance of euploidy (i.e. a chromosome number that is an

exact multiple of the haploid number for the species) (Jallepalli *et al.*, 2001). It has been shown that human securin can be ubiquitinated *in vitro* by both APC/C^{Cdc20} and APC/C^{Cdh1}, and that both a destruction box (D-box) and a KEN box within the securin protein have to be mutated to generate a non-degradable protein (Zur and Brandeis, 2001). Destruction of both securin and Cyclin B1 is initiated at the beginning of metaphase, well before sister chromatid separation, but degradation of a mutant form of securin lacking its D-box has been shown to occur later in mitosis, at anaphase (Hagting *et al.*, 2002). This destruction required a KEN box in the amino terminus of securin, perhaps indicating the time in mitosis when ubiquitination switches from APC/C^{Cdc20} to APC/C^{Cdh1}.

In budding yeast, mitotic arrest in response to DNA damage that occurs in metaphase is achieved by maintaining abundance of Pds1 (Sanchez *et al.*, 1999). It has been shown that Pds1 is phosphorylated by Chk1 (a conserved kinase that plays a critical role in the DNA checkpoint pathways) in response to DNA damage but not spindle disruption (Wang *et al.*, 2001a). This phosphorylation stabilises Pds1 without alteration of APC/C^{Cdc20} activity. The human securin protein (hPTTG) has also been implicated in DNA damage-response pathways by virtue of interaction with Ku, the regulatory subunit of the DNA-dependent protein kinase (DNA-PK), involved in repair of DNA double-strand breaks (DSBs) (Romero *et al.*, 2001). In addition, Zhou *et al.* have recently shown that human securin is a p53 target gene and may play a role in the p53-mediated DNA damage response pathway (Zhou *et al.*, 2003).

1.2.3.11 Aurora kinases

Aurora kinases have been shown to play critical roles in chromosome segregation and cell division, including roles in the spindle checkpoint (reviewed in (Meraldi *et al.*, 2004b)). This subfamily of serine-threonine kinases comprises three members in mammals, Aurora A, B and C, each with a different expression pattern, subcellular localisation and timing of activity.

All three Aurora kinases have been linked to cancer progression and are frequently altered in human tumours.

The Aurora A gene is commonly amplified in epithelial malignancies, and Aurora A overexpression, found in breast, colorectal and gastric cancers (up to 62% of breast cancers overexpress Aurora A), has been proposed to constitute an alternative mechanism for spindle checkpoint dysregulation during carcinogenesis (Anand *et al.*, 2003; Miyoshi *et al.*, 2001). Cells overexpressing Aurora A entered anaphase despite defective spindle formation and persistence of Mad2 at kinetochores indicating continued spindle checkpoint activation (Anand *et al.*, 2003). These abnormalities were suppressed by expression of a truncated (trans-dominant inhibitor) form of the Bub1 protein. This suggested that Aurora A overexpression is perturbing processes that are normally carried out or monitored by Bub1, resulting in instability of chromosome number during cell division. A separate study has shown that Aurora A overexpression is compromising the spindle checkpoint triggered by nocodazole by disrupting formation of the MCC (BubR1-Mad2-Bub3-Cdc20) complex, but that this is independent of Aurora A kinase activity (Jiang *et al.*, 2003). The results support a hypothesis in which Aurora A antagonises BubR1 function in spindle checkpoint regulation.

Aurora B is also proposed to regulate the spindle checkpoint, among other functions, and forms a tight complex with two proteins, INCENP (inner centromere protein) and survivin, although the precise role of this complex in spindle checkpoint signalling is unknown. Aurora B controls kinetochore localisation of both motors and checkpoint components, including dynein, CENP-E, BubR1 and Mad2 (Ditchfield *et al.*, 2003; Hauf *et al.*, 2003; Kallio *et al.*, 2002b; Lens *et al.*, 2003; Murata-Hori and Wang, 2002). Aurora B is also required for kinetochore localisation of Bub1, and it has been suggested that Aurora B increases the affinity of BubR1 and CENP-E for Bub1-positive kinetochores (Johnson *et al.*, 2004).

1.2.4 Spindle checkpoint function in a normal cell division

Many studies have provided evidence in favour of activation of the spindle checkpoint in each and every mitosis.

In budding yeast, Bub3, Bub1 and Mad1 form a complex upon checkpoint activation, but this complex is also found during a brief period of a normal cell cycle (unperturbed by microtubule poisons such as nocodazole) (Brady and Hardwick, 2000). It was suggested that this could be the period when the newly replicated centromeres have not yet formed stable kinetochore-microtubule interactions. The authors demonstrated that this complex formation was due to activation of the spindle checkpoint rather than cell cycle position by comparing levels of the complex in nocodazole-arrested cells with the level seen in *cdc26Δ* metaphase arrest. Cdc26 is a subunit of the anaphase promoting complex (APC/C) and *cdc26Δ* cells have inactive APC/C at their restrictive temperature, resulting in metaphase arrest. High levels of Mad1-Bub1-Bub3 were detected in the nocodazole-arrested cells, whereas very little was seen in the metaphase arrest in the *cdc26Δ* cells, in which the spindle microtubules would have been attached to kinetochores. It has been suggested that formation of a Bub3-Bub1-Mad1 complex causes the release of Mad2 from Mad1 (Brady and Hardwick, 2000; Sironi *et al.*, 2001). A similar Mad1-Bub1-Bub3 complex was also observed in *in vitro* experiments using recombinant mammalian proteins (Seeley *et al.*, 1999).

The spindle checkpoint protein hBubR1 has been shown to be essential during a normal mitosis, as it prevents cells from exiting mitosis prematurely (Chan *et al.*, 1999).

In addition, disruption of Bub1 or Mad2 function accelerates mitotic exit in human cells, suggesting that spindle checkpoint function may be required to complete normal somatic cell divisions (Gorbsky *et al.*, 1998; Michel *et al.*, 2001; Taylor and McKeon, 1997). Inactivation of the spindle checkpoint by targeting Mad2 with RNAi (RNA interference) has also been shown to result in a consistently shortened mitosis in mammalian cells,

providing direct evidence that the internal mitotic timing mechanism is much faster in cells that lack the spindle checkpoint and indicating a more general requirement for the spindle checkpoint, beyond its role in correcting errors in mitosis (Jones *et al.*, 2004).

However, a recent study has shown that while all known spindle checkpoint proteins are recruited to kinetochores during a normal mitosis in animal cells, in contrast, only Bub1 and Bub3 bind kinetochores in a normal cell cycle in budding yeast, with Mad1 and Mad2 only binding kinetochores in the presence of spindle damage or kinetochore lesions (Gillett *et al.*, 2004).

1.2.5 Activation of the checkpoint in response to spindle damage

The microtubule poisons taxol, nocodazole, and the colchicine relative colcemid all block normal chromosome segregation, activating the spindle checkpoint and causing cell cycle arrest in mitosis (reviewed in (Peterson and Mitchison, 2002)). Taxol stimulates microtubule polymerisation, while nocodazole and colcemid are microtubule-depolymerising agents. However, at low (nanomolar) concentrations, nocodazole has been shown to stabilise microtubules, causing spindle checkpoint activation by suppressing microtubule dynamic instability (the alternating periods of microtubule elongation and shortening), a process required for efficient mitotic spindle assembly (Vasquez *et al.*, 1997). Perhaps at low drug concentrations kinetochore-microtubule attachment remains largely unaffected, but the loss of microtubule dynamic instability results in lack of tension across the paired kinetochores, leading to spindle checkpoint activation (see also Section 1.2.6). Nocodazole is structurally related to benomyl, the microtubule-polymerisation inhibitor that was used in the initial genetic screens in *S. cerevisiae* that identified the Bub and Mad spindle checkpoint components (Hoyt *et al.*, 1991; Li and Murray, 1991), and is frequently used to study the spindle checkpoint pathway. In addition, nocodazole is used to conveniently synchronise cells because the arrest that it induces is reversible. Once cells have accumulated in

mitosis due to activation of the spindle checkpoint in response to nocodazole-induced microtubule-depolymerisation, they can be synchronously released by removing the compound from the media.

The spindle checkpoint can also be activated without directly affecting microtubule dynamics by use of the Eg5 kinesin inhibitor monastrol (Kapoor *et al.*, 2000). Instead of bipolar spindles, monastrol-treated cells produce monoastral spindles, resulting in syntelic (mono-oriented) kinetochore-microtubule attachments that lack tension (Mayer *et al.*, 1999), thus activating the spindle checkpoint, as will be discussed further in Section 1.2.6.

In addition, it has been shown that the spindle checkpoint can be activated in response to substantial DNA damage (Mikhailov *et al.*, 2002). The delay in mitosis observed is not due to the ATM-mediated DNA damage checkpoint pathway (reviewed in (Motoyama and Naka, 2004)), but is caused by defects in kinetochore attachment and function due to the presence of damaged DNA.

1.2.6 The spindle checkpoint signal: tension vs. attachment

The spindle checkpoint can detect a broad range of spindle defects, from the presence of a single unattached kinetochore, to the massive defects induced by microtubule-depolymerising drugs such as nocodazole. There are two models for generation of a "wait anaphase" signal by unattached kinetochores, leading to activation of the spindle checkpoint: the absence of tension at kinetochores vs. the simple presence of even a single unattached kinetochore. Alternatively, both attachment and tension could be monitored by the spindle checkpoint (Skoufias *et al.*, 2001).

The argument for tension being the signal was provided by studies using mantid spermatocytes (Li and Nicklas, 1995; Li and Nicklas, 1997). In these cells the presence of a single mono-oriented sister chromatid pair prevents progression into anaphase, due to arrest by the spindle checkpoint. However, cells were found to proceed into anaphase when tension was applied

to the unattached chromosome by use of a microneedle. A monoclonal antibody that recognised an unidentified phosphoepitope (3F3/2) was shown to bind to the unattached chromosome, but antibody binding was eliminated when tension was introduced via a microneedle, suggesting that it is the lack of physical tension that is translated into a chemical signal that leads to phosphorylation changes on kinetochore-associated proteins. The 3F3/2 phosphoepitope may be regulated by the mitogen-activated protein (MAP) kinase ERK (extracellular signal-regulated protein kinases 1 and 2: ERK1 and ERK2) at unattached kinetochores (Shapiro *et al.*, 1998). It was suggested that CENP-E could be the tension-sensitive 3F3/2 phosphoepitope at kinetochores, because MAP kinase can phosphorylate CENP-E *in vitro* at sites known to regulate its interactions with microtubules (Chen, 2004; Zecevic *et al.*, 1998). 3F3/2 has also been shown to bind directly to M-phase-specific phosphorylations on one or more components of the APC/C, suggesting that the checkpoint-sensitive staining of 3F3/2 at kinetochores could be due to kinetochore localisation of APC/C (Acquaviva *et al.*, 2004; Daum *et al.*, 2000).

Alternatively, in favour of the other model of checkpoint activation, loss of tension at kinetochores is not sufficient to localise the spindle checkpoint components Mad2 and Bub3 to kinetochores in vertebrate cells (Martinez-Exposito *et al.*, 1999; Waters *et al.*, 1998). Treatment of cells with the microtubule poison taxol leads to loss of tension at kinetochores but does not disturb kinetochore-microtubule attachment. In cells treated with taxol, 3F3/2 localises to all kinetochores, whereas Mad2 and Bub3 were only found to localise to kinetochores not yet attached to spindle microtubules. In addition, Skoufias *et al.* have shown that mammalian Bub1 and BubR1 respond to lack of tension, while Mad2 responds specifically to lack of microtubule attachment at kinetochores (Skoufias *et al.*, 2001).

However, a slightly different observation has been made in *Drosophila* cells, where Mad2 and Bub1 have been shown to monitor microtubule occupancy at the kinetochore, while BubR1 and Bub3 monitor tension across

attached kinetochores (Logarinho *et al.*, 2004). Mad2 has also been shown to be recruited to some kinetochores in which both sisters are attached to the same spindle pole, suggesting that the checkpoint is activated, possibly via a lack of tension, despite the presence of attached microtubules (Kapoor *et al.*, 2000). The authors therefore suggest that Mad2 may be sensing a subtler aspect of microtubule attachment such as the exact number of microtubules at the kinetochore or even the dynamic behaviour of kinetochores. It has also been proposed that binding of Mad2 is governed by tension-sensitive kinetochore phosphorylation (in addition to lack of microtubule attachment), whereas loss of Mad2 from kinetochores is largely governed by accumulation of kinetochore microtubules (Waters *et al.*, 1999).

Absence of tension is sufficient to activate the spindle checkpoint in budding yeast (Stern and Murray, 2001). However, a recent paper has shown that both tension-sensitive and attachment-sensitive spindle checkpoint pathways operate in budding yeast (Kitagawa *et al.*, 2003). It was shown that Bub1 associates with centromeric DNA via Skp1, a protein located within the core of the kinetochore, and while this interaction was required for mitotic delay in response to outer kinetochore or cohesion defects (lack of tension), it was not required for the response to spindle depolymerisation (lack of attachment). The authors therefore suggested that at least two different checkpoint signals are generated at the kinetochore of budding yeast, one for microtubule attachment (independent of Bub1-Skp1 interaction), and one for later events (dependent on Bub1-Skp1 interaction, assessing tension). Also, a recent study has shown that Mad1 and Mad2 are required for detection of bipolar orientation and/or tension at budding yeast kinetochores, whereas Mad3 is not (Lee and Spencer, 2004).

Finally, Aurora B kinase also appears to be involved in sensing both tension and attachment. Aurora B is thought to destabilise syntelic (mono-oriented) microtubule kinetochore interactions in a tension-sensitive manner, thereby favouring bipolar attachments (Buvelot *et al.*, 2003; Dewar *et al.*, 2004; Tanaka *et al.*, 2002). Aurora B is also required for checkpoint activation

in response to impaired microtubule attachment in metazoan cells, perhaps reflecting the role of Aurora B in kinetochore assembly (Meraldi *et al.*, 2004b).

1.2.7 Models for generation of the "wait anaphase", spindle checkpoint signal

Two models currently exist for how unattached kinetochores produce a diffusible signal in the cytoplasm that prevents activation of APC/C^{Cdc20}.

The "catalytic model" suggests that transient association of Cdc20 or its inhibitors with unattached kinetochores catalyses formation of the BubR1-Bub3-Mad2-Cdc20 (MCC) complex, resulting in inactivation of Cdc20 in the cytoplasm (Gorbsky *et al.*, 1998; Howell *et al.*, 2000; Kallio *et al.*, 1998; Kallio *et al.*, 2002a) (see Figure 1.5, Panel A).

Alternatively, the "APC/C sensitisation model" suggests that checkpoint-active kinetochores sensitise the APC/C to inhibition by cytoplasmic MCC, perhaps by phosphorylation (Sudakin *et al.*, 2001) (see Figure 1.6, Panel B). The MCC was shown to be present and active in interphase cells, indicating that it is not generated from kinetochores, but only APC/C from mitotic cells was sensitive to inhibition by MCC. This could occur via rapid exchange of APC/C with kinetochores, as there has been some evidence for APC/C kinetochore localisation in the literature (Acquaviva *et al.*, 2004; Huang and Raff, 2002; Jorgensen *et al.*, 1998; Topper *et al.*, 2002; Tugendreich *et al.*, 1995). Mps1 also binds APC/C (Liu *et al.*, 2003), and could therefore perhaps be the diffusible "wait anaphase" signal from an unattached kinetochore responsible for sensitising APC/C to inhibition by MCC.

A recent study has provided data with elements in support of both models for the spindle checkpoint pathway (Howell *et al.*, 2004). FRAP (fluorescence recovery after photobleaching) experiments in PtK_2 (Potoroo kidney epithelial) cells showed that Mad1 and Bub1 are relatively stable

components of the kinetochore, and unlikely to form part of the "wait anaphase" signal, whereas both BubR1 and Mad2 (Cdc20 inhibitors) cycle rapidly on and off unattached kinetochores but are depleted from kinetochores that have formed a bipolar attachment with the mitotic spindle apparatus. Cdc20 was also found to cycle rapidly through kinetochores, with 50% of the Cdc20 bound to unattached kinetochores also bound to Mad2.

Figure 1.5: Models for generation of the "wait anaphase" spindle checkpoint signal.

Two models exist for how unattached kinetochores produce a diffusible signal in the cytoplasm that prevents activation of APC/C^{Cdc20}. In Model A, the unattached kinetochore acts as a template to catalyse formation of the BubR1-Bub3-Mad2-Cdc20 complex (mitotic checkpoint complex, MCC), which then diffuses away from the kinetochore to inhibit APC/C. In Model B, APC/C is modified by the unattached kinetochore, promoting its association with MCC complex that is already present in the cytoplasm, leading to inhibition of APC/C. (Adapted from Bharadwaj and Yu, 2004).

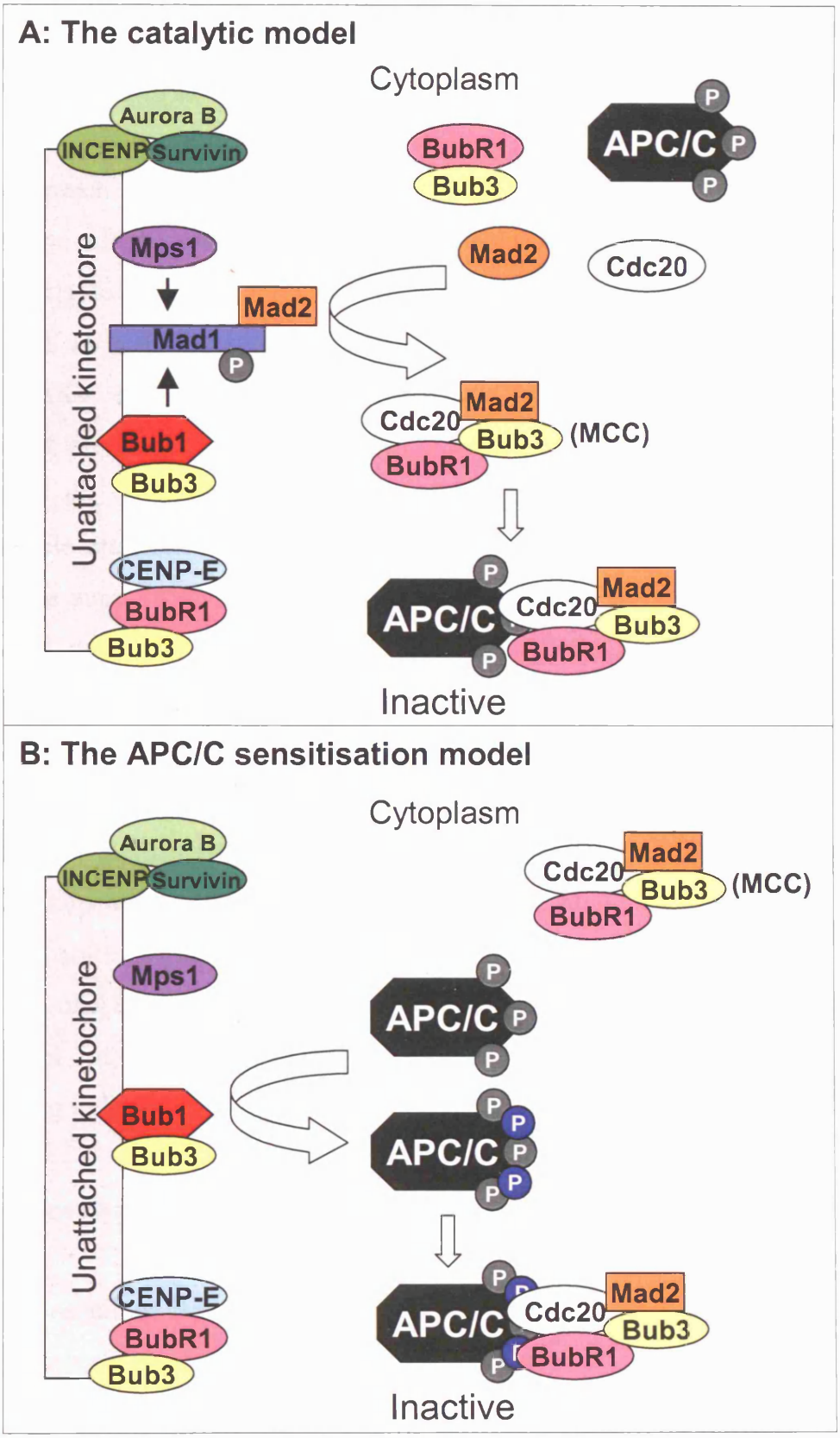

Figure 1.5: Models for generation of the "wait anaphase" spindle checkpoint signal.

This fraction of (Mad2-bound) Cdc20 dissociated from kinetochores with the same kinetics as the other MCC components, BubR1 and Bub3, in support of the catalytic model, in which Cdc20-Mad2 and MCC complexes are produced at the kinetochore, resulting in inhibition of APC/C^{Cdc20}. Howell *et al.* also reported much faster kinetics of Cdc20, BubR1 and Mps1, data that may support the APC/C sensitisation model, in which kinetochores modify these components to promote formation of Cdc20 inhibitory complexes in the cytoplasm. In a similar study, Shah *et al.* used the same technique (FRAP), also in PtK_2 cells, and showed that not only Mad1 and Bub1, but also a portion of the Mad2 in the cell is stably bound to unattached kinetochores (Shah *et al.*, 2004). While Mad1 and Mad2 were released following microtubule attachment of kinetochores, Bub1 remained kinetochore-bound. Their data supports the model in which an unattached kinetochore and its associated proteins acts as a catalytic platform for producing a Mad2-containing "wait anaphase" signal.

However, in disagreement with others (Sudakin *et al.*, 2001), Tang *et al.* have shown that Mad2 is not present in a mitotic checkpoint complex identified in HeLa cells, and that a BubR1-Bub3-Cdc20 complex inhibits APC/C independently of Mad2 (Tang *et al.*, 2001). Mad2 and BubR1 may be acting in parallel pathways and sequester different pools of Cdc20 to block the activation of APC/C, in agreement with the suggestion that Mad2 might sense attachment of microtubules to kinetochores, while BubR1 might be responding to lack of tension at kinetochores (Skoufias *et al.*, 2001).

1.2.8 Silencing the spindle checkpoint

Once all of the chromosomes in a cell are properly aligned on the metaphase plate the spindle checkpoint must be silenced to allow progression to anaphase. There are some clues to the mechanisms that lead to this spindle checkpoint silencing.

Dynein, a minus end-directed microtubule motor protein has been implicated in this process by studies in *Drosophila* neuroblasts and mammalian PtK_1 cells (Howell *et al.*, 2001; Wojcik *et al.*, 2001). It was suggested that dynein might function to switch off the checkpoint by transporting checkpoint proteins (including Mad2 and BubR1) from the kinetochores to the spindle poles, thus abolishing the wait anaphase signal.

However, the existing cytoplasmic APC/C inhibitory complexes such as MCC must also be dismantled for the spindle checkpoint to be silenced. A yeast two-hybrid screen has identified a novel human Mad2-binding protein called $p31^{comet}$ (formerly known as Cmt2, but now named $p31^{comet}$ for its comet tail-like cellular localisation pattern in mitosis) that may play a role in checkpoint silencing (Habu *et al.*, 2002). The association of $p31^{comet}$ with Mad2 coincides with the dissociation of the Mad2-Cdc20 interaction in HeLa cells. Also, depletion of $p31^{comet}$ by RNA interference (RNAi) results in cells escaping a spindle checkpoint-mediated arrest with significantly slower kinetics (Xia *et al.*, 2004). It was suggested that $p31^{comet}$ functions in spindle checkpoint silencing by counteracting the function of Mad2. Phosphorylation of Mad2 may also be involved in the mechanism of spindle checkpoint silencing. Mad2 phosphorylation increases as cells exit from a nocodazole-mediated mitotic arrest (Wassmann *et al.*, 2003). Since it is only the unphosphorylated Mad2 that can bind Mad1 or APC/C, it was suggested that phosphorylation of Mad2 inhibits its function and may be an important mechanism for checkpoint inactivation.

1.2.9 Adaptation of the spindle checkpoint: The G1 tetraploidy checkpoint

The spindle checkpoint (like the G2 checkpoint) is only maintained for a limited duration and following a period of time in arrest, cells can progress to the next stage of the cell cycle without the checkpoint being satisfied. This has been referred to as adaptation (reviewed in (Andreassen *et al.*, 2003)). Most mammalian cells undergo adaptation of the spindle checkpoint in the

presence of microtubule inhibitors. Adaptation with a half-time of 3 hours has been observed in mouse embryonic fibroblasts (Lanni and Jacks, 1998). The cells return to interphase in a tetraploid state, and thus exit from mitosis has occurred without satisfaction of the spindle checkpoint and the cells become micronucleated due to the failure of normal chromosome segregation (Andreassen *et al.*, 1996; Sablina *et al.*, 1998). This indicates that the cells have adapted to the checkpoint, and have not simply metabolised the microtubule poison or exported it from the cell. To counter this, mammalian cells have a G1 tetraploidy checkpoint that induces a stable G1 arrest of tetraploid cells that arise either following G2 or spindle checkpoint adaptation, or errors in mitosis (Andreassen *et al.*, 2001b; Borel *et al.*, 2002). It remains to be determined whether the G1 tetraploidy checkpoint would similarly arrest cells following aneuploidisation with gain or loss of only a small number of chromosomes (Margolis *et al.*, 2003).

Fibroblasts respond to spindle checkpoint adaptation and tetraploidisation by inducing G1 arrest in a p53-dependent manner, whereas lymphoblasts respond with a p53-dependent induction of apoptosis (Minn *et al.*, 1996). A recent study has suggested that propagation of cells arrested at the G1 tetraploidy checkpoint following spindle checkpoint adaptation is prevented by hBubR1-mediated apoptosis (Shin *et al.*, 2003).

Although experimental evidence has excluded a direct role for p53 in the spindle checkpoint, the response to long-term nocodazole-induced spindle damage in normal cells (triggering the tetraploidy checkpoint) has recently been shown to require an intact spindle checkpoint (Vogel *et al.*, 2004), suggesting a functional link between these two checkpoints. p53 is stabilised and activated during a damage-induced spindle checkpoint arrest, and this activation is due to the prolonged arrest rather than the nature of the damage. No accumulation of p53 is observed when the spindle checkpoint is activated during a normal mitosis. In addition, this spindle damage-induced activation of p53 is independent of ATM, ATR, Chk1 and Chk2 proteins, indicating that it does not require components of the DNA damage pathway. A p53-

dependent checkpoint mechanism that arrests cells in G2 upon prolonged spindle damage, preventing polyploid cells from re-entering mitosis, was also identified.

Interestingly, a recent study has demonstrated that triggering of the p53-dependent tetraploidy checkpoint involves Bub1-mediated phosphorylation of p53 at serine-37, suggesting that Bub1 could be the link between the spindle and tetraploidy checkpoints (Personal communication: Dr O. Gjoerup, Dana-Farber Cancer Institute, Boston, MA). It is therefore proposed that by interacting with Bub1, SV40 large T antigen (LT) is usurping a cellular mechanism normally active at the tetraploidy checkpoint, in order to stabilise p53. LT is thought to do this by acting as a scaffold to bring p53 into proximity with Bub1 (Cotsiki *et al.*, 2004), which phosphorylates p53 on serine-37. Bub1 is also shown to be required for LT binding to p300/CBP and the resulting acetylation of p53. LT could therefore induce p53 stabilisation in the absence of spindle damage by recruitment of Bub1 to phosphorylate p53 on serine-37, and also by inducing acetylation at lysines 373 and 382 of p53 via recruitment of p300/CBP. However, it is important to note that stabilisation of p53 by LT does not alter p53 activity, which is sequestered by LT (see Section 1.3.2.2).

1.3 SV40

Simian Virus 40 (SV40) is a member of the papovavirus family of DNA tumour viruses. It is a double stranded DNA virus of rhesus monkey origin, with a circular genome of 5243 base pairs (Tooze, 1981). SV40 was first isolated in the late 1950s as a contaminating virus from rhesus macaque monkey kidney cells that were being used to grow poliovirus for the early polio vaccine. It was later shown to be capable of inducing tumours in hamsters (reviewed in (Hilleman, 1998)).

The SV40 genome codes for seven gene products (see Figure 1.6).

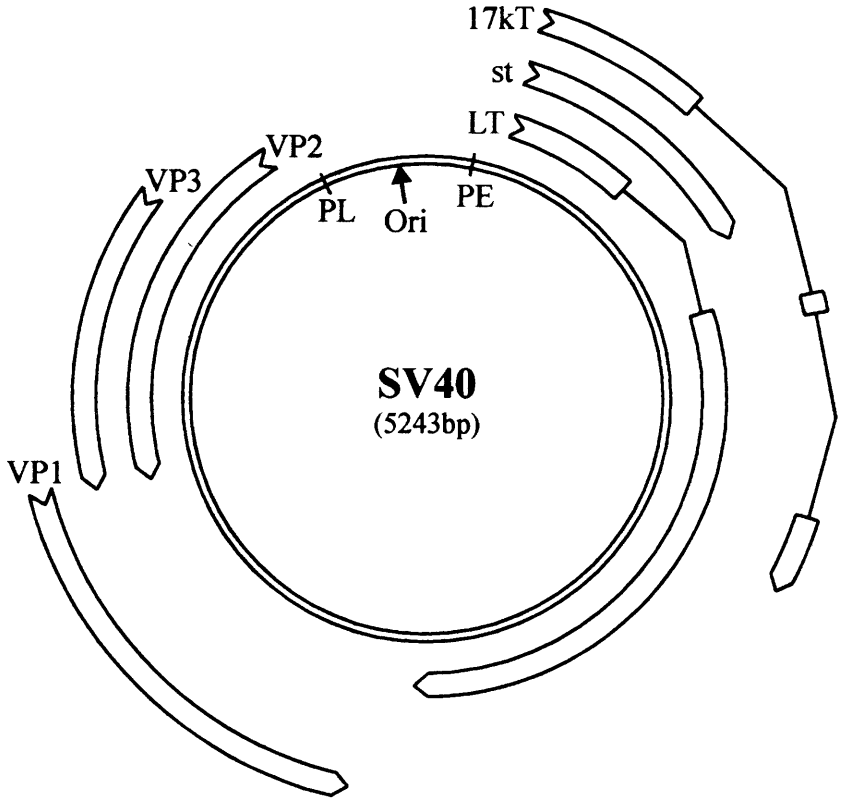

Figure 1.6: The genomic organisation of the SV40 virus.

SV40 virus has a circular double-stranded DNA genome, with promoters for early and late genes (PE and PL, respectively) located on either side of the origin of replication (Ori). The early genes encode the large T antigen (LT), small t antigen (st), and tiny t antigen (17kT) proteins, involved in regulation of early and late gene transcription, up-regulation of transcription in the host cell, replication of viral DNA and virion assembly, among other functions. The late genes encode VP1, VP2, and VP3, the structural proteins that form the viral capsid. The open reading frames that give rise to these proteins are indicated. (Adapted from Lock *et al.*, 2004).

The early genes are encoded by three alternatively spliced mRNAs that give rise to proteins that are identical for the amino-terminal 82 residues (referred to as "T/t common region"). These gene products are called large T antigen, small t antigen, and 17kT antigen (sometimes known as tiny t antigen). They are involved in many functions which include regulation of early and late gene transcription, up-regulation of transcription in the host cell, replication of viral DNA and virion assembly (reviewed in (Ali and DeCaprio, 2001; Conzen and Cole, 1995; Grand, 2001; Sullivan and Pipas, 2002)). These proteins were called T(umour) antigens because they were first identified when antisera from hamsters with SV40-induced tumours were used to search for antigens expressed in SV40 infected cells. SV40 also encodes the late gene products VP1, VP2 and VP3 which are generated from alternatively spliced mRNAs and alternative initiation codons, and which are the structural proteins that form the viral capsid (see Figure 1.6). SV40 also encodes the agno protein, a small highly basic polypeptide that is translated from the leader region of SV40 late mRNAs and may have a role in the assembly of the capsid and/or its release from the host cell (Cole, 1996; Jay *et al.*, 1981).

Replication of SV40 DNA begins when the virally encoded SV40 large T antigen binds to the SV40 origin, forming a double-hexameric structure (reviewed in (Simmons, 2000)). Three cellular proteins, DNA polymerase α/primase (pol/prim), followed by topoisomerase I (topo I) and replication protein A (RPA) then associate with SV40 large T antigen to form an initiation complex (Simmons *et al.*, 2004). Following initiation, the majority of DNA synthesis on both the leading and lagging strands occurs in response to additional cellular proteins such as polymerase δ, PCNA and RF-C, with approximately 11 cellular proteins needed to fully replicate the viral DNA. SV40 large T antigen has recently been shown to interact with Nbs1, the Nijmegen breakage syndrome (NBS) protein, involved in double-strand break repair (Wu *et al.*, 2004). Nbs1 plays a role in preventing DNA hyperreplication during the cell cycle, contributing to maintenance of genome stability, but LT targets Nbs1, thereby enhancing the yield of new SV40

genomes during viral DNA replication. This provides a further mechanism by which SV40 large T antigen is able to induce aneuploidy in its cellular host.

SV40 large T antigen (LT) is largely responsible for the functions of the virus that induce the host cell to produce the enzymes that are necessary for replication of the viral genome. Introduction of LT into primary rodent cells enables these cells to acquire an infinite proliferative potential (Jat and Sharp, 1989) but does not necessarily result in their transformation. Inactivation of LT in these immortal cells results in a rapid and irreversible loss of their proliferative potential in either G1 or G2 phases of the cell cycle, showing that LT is continuously required to maintain the proliferative state (Gonos *et al.*, 1996; Jat and Sharp, 1989). However, introduction of LT into immortalised cell lines can result in full transformation (reviewed in (Ali and DeCaprio, 2001)). The potency of LT for inducing both immortalisation and transformation of many cell types has led to its extensive use as a model system to study the critical steps for this process (recently reviewed in (Lock *et al.*, 2004)). These studies have provided a great insight into many cellular mechanisms, including the regulation of cell proliferation, senescence and apoptosis, in addition to the processes of immortalisation and tumourigenesis (see Section 1.3.1).

SV40 LT has been shown to rapidly disrupt mitotic checkpoints that help maintain genomic stability, suggesting mechanisms by which LT induces chromosome aberrations and promotes immortalisation and transformation of mammalian cells (Chang *et al.*, 1997). An interaction between SV40 LT and Ran, a small GTPase that regulates nucleocytoplasmic transport, cell cycle progression, and mitotic spindle organisation, has been demonstrated *in vitro* (De Luca *et al.*, 2003). This suggests that deregulation of the centrosome duplication cycle could be one mechanism by which SV40 LT causes genomic instability. In addition, elevated levels of Ran's exchange factor, RCC1, have been shown to abrogate the spindle checkpoint in *Xenopus* egg extracts, restoring APC/C activity and disrupting the kinetochore localisation of Mad2, CENP-E, Bub1 and Bub3 (Arnaoutov and Dasso, 2003). Similar effects were

seen when Ran's GTPase activating protein (RanGAP1) and its accessory factor (RanBP1) were depleted, suggesting that the spindle checkpoint is directly responsive to levels of Ran-GTP in the cell, and therefore leading to the possibility that SV40 LT interaction with Ran could be affecting the spindle checkpoint directly.

SV40 LT was recently shown to interact with the spindle checkpoint protein Bub1, leading to compromise of spindle checkpoint function (Cotsiki *et al.*, 2004), the subject of this project.

1.3.1 Immortalisation and Transformation

Immortalisation has been defined as the ability to produce cell lines that can be serially cultivated indefinitely without any overt signs of cessation of growth. It can be tested in a variety of cell types but the critical property the cells must possess is that they must only be able to undergo a finite number of divisions, because established cell lines have already undergone the changes necessary for immortalisation (i.e. are already genetically abnormal). Immortalisation is measured by the ability to obtain colonies upon transfection or infection of primary cultures and expansion of these colonies into cell lines that can be serially cultivated. The production of cell lines that can be serially cultivated is a critical component of this assay because it is possible to obtain an extension of life span without indefinite proliferation. The most common cell type used is embryonic fibroblasts, since they can be easily prepared and propagated *in vitro*.

In contrast, transformation has been defined as the process that gives rise to oncogenically transformed cells. The assays that are commonly used to measure transformation potential are production of dense foci, foci that overgrow a monolayer, growth in semi-solid medium i.e. anchorage-independent growth or growth in low serum concentrations or at high saturation densities. However, the ultimate test has to be whether tumours can be induced in either syngeneic or immunosuppressed animals. The closest correlate to tumours in experimental animals is anchorage-independent

growth. Transformation ability does not have to be measured in primary cells. It is usually carried out in established cell lines. In fact, if primary cells are to be used, then there may be a requirement for the presence of an active immortalising gene, because transforming genes such as activated *ras* induce premature senescence in the absence of an immortalising gene. Senescence is the process of cellular aging, with cessation of cell division.

Mouse embryo fibroblasts have the potential to undergo about 20 divisions before they cease dividing. However they will readily undergo spontaneous immortalisation, and thus great care needs to be taken when these cells are used for immortalisation assays. Rat embryo fibroblasts undergo slightly fewer divisions but immortalise spontaneously at a much lower frequency.

In marked contrast, human fibroblasts undergo many more divisions, approximately 50-70, defined as the Hayflick Limit (Hayflick, 1961) prior to undergoing senescence, and have never been demonstrated to undergo spontaneous immortalisation. The addition of an immortalising gene such as SV40 large T antigen into human cells does not cause immortalisation, but can extend the *in vitro* lifespan of the cells, adding an extra 20-30 population doublings for fibroblasts (reviewed in (Shay *et al.*, 1991)). At the end of the extended lifespan another proliferative decline known as "crisis" is observed. It has been proposed that senescence be defined as mortality stage I (M1), and that crisis be defined as mortality stage II (M2), to make a clear distinction between these two different states in the proliferative decline of human cells (Wright *et al.*, 1989). The inability of human cells to undergo spontaneous immortalisation has led to the proposal that human cells have acquired extra control mechanisms to prevent tumour formation i.e. a tumour suppressor mechanism. This most likely corresponds to the shortening of telomeres in human somatic cells (reviewed in (Sedivy, 1998)). In these cells the telomeres shorten each time the cells divide due to the end replication problem and the absence of functional telomerase activity in most human somatic cells. Telomerase activity can be reconstituted by ectopically expressing hTERT,

the catalytic subunit of telomerase (Bodnar *et al.*, 1998; Counter *et al.*, 1998; Vaziri and Benchimol, 1998). In fact, it has been proposed by some that reconstitution of telomerase activity is all that is required for immortalisation of human cells (Bodnar *et al.*, 1998; Ouellette *et al.*, 2000; Vaziri and Benchimol, 1998; Yang *et al.*, 1999). However, others have found that additional activities are required. These can be provided by Human papilloma virus 16/18 E7 protein or SV40 large T antigen (Hahn *et al.*, 1999; Kiyono *et al.*, 1998; O'Hare *et al.*, 2001). In contrast rodent cells have much longer telomeres and it is not possible to demonstrate telomere shortening upon serial passaging. Thus cellular senescence in rodent cells is not regulated by telomere dependent mechanisms (reviewed in (Itahana *et al.*, 2004)).

The loss of *in vitro* proliferative potential observed in rodent fibroblasts can be readily overcome by the action of any member of the family of immortalising genes, including SV40 large T antigen (reviewed in (Katakura *et al.*, 1998)). Furthermore, it has been shown that these cells only become dependent upon the immortalising gene to continue dividing when their endogenous life span has elapsed (Ikram *et al.*, 1994). If the immortalising gene is removed after this time, the resulting growth arrest becomes irreversible after about 72 hours, and can occur in both G1 and G2 phases (Gonos *et al.*, 1996; Jat and Sharp, 1989). The same result was obtained in other rodent cell types (myoblasts, neural cells) and human cells immortalised with a combination of hTERT and SV40 LT were similarly unable to maintain growth when LT was removed (O'Hare *et al.*, 2001). This property has led to large T antigen being one of the most frequently used agents for generating immortal cell lines.

1.3.2 SV40 large T antigen

SV40 large T antigen (LT) is a multifunctional phosphoprotein of 708 amino acids that localises mostly within the host nucleus via a nuclear localisation signal (NLS) in the N-terminal region of the protein (Kalderon *et al.*, 1984; Soule and Butel, 1979). However a very small fraction is bound to the plasma membrane (Santos and Butel, 1982). It has various biochemical activities (Fanning, 1992) including ATPase activity (Tjian and Robbins, 1979), and DNA and RNA helicase activity (Scheffner *et al.*, 1989) (see Figure 1.7). It can also bind to RNA covalently (Carroll *et al.*, 1988), as well as to DNA both specifically and non-specifically (Carroll *et al.*, 1974). While these activities are necessary for replication of the viral DNA, none of them are required for the immortalisation or transformation of rodent cells (Manos and Gluzman, 1984; Peden *et al.*, 1990; Stringer, 1982). LT can also activate and repress transcription from various viral and cellular promoters (Alwine *et al.*, 1977; Gilinger and Alwine, 1993; Gruda *et al.*, 1993; Hansen *et al.*, 1981; Mitchell *et al.*, 1987; Rice and Cole, 1993; Rushton *et al.*, 1997; Saffer *et al.*, 1990; Zhu *et al.*, 1991).

LT associates with a number of host cellular proteins, which include p53 (Lane and Crawford, 1979; Linzer and Levine, 1979), pRB (DeCaprio *et al.*, 1988), p107 (Dyson *et al.*, 1989; Ewen *et al.*, 1989), p130 (Hannon *et al.*, 1993), heat shock protein Hsc70 (Sawai and Butel, 1989), CREB-binding protein (CBP), p300 (Avantaggiati *et al.*, 1996; Eckner *et al.*, 1996), p400 (Lill *et al.*, 1997b), DNA polymerase α (Smale and Tjian, 1986), p185 (Kohrman and Imperiale, 1992), SUG1, a regulatory component of the proteasome (Grand *et al.*, 1999), TBP, the TATA-binding protein (Martin *et al.*, 1993), and the spindle checkpoint protein Bub1 (Cotsiki *et al.*, 2004) (see Figure 1.7). The abrogation of cellular pathways by SV40 large T antigen is summarised in Figure 1.8.

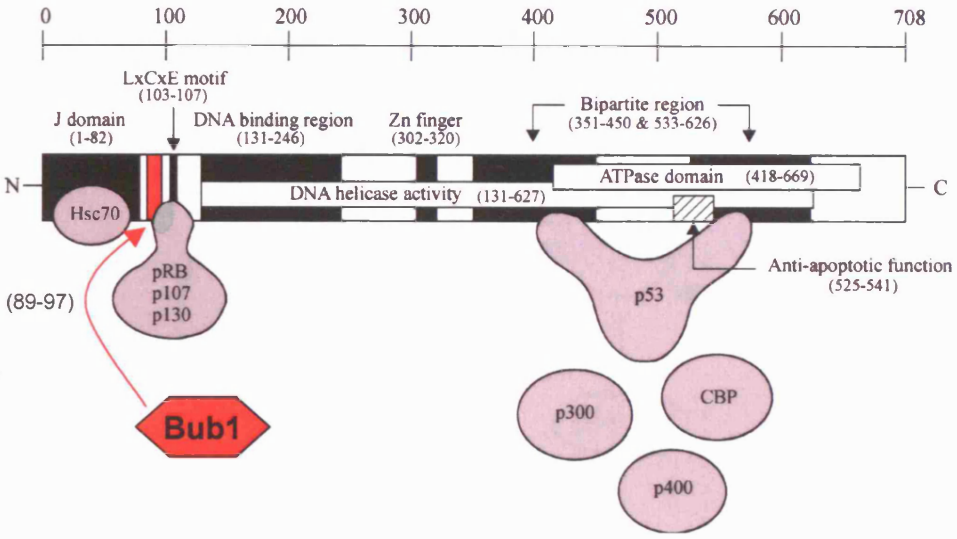

Figure 1.7: SV40 large T antigen.

The locations of the functional domains of SV40 large T antigen (LT) that are responsible for interaction with host proteins are indicated, along with the regions responsible for other activities of the protein. The interaction site of the spindle checkpoint protein Bub1 at amino acids 89-97 of LT is highlighted in red. (Adapted from Lock *et al.*, 2004).

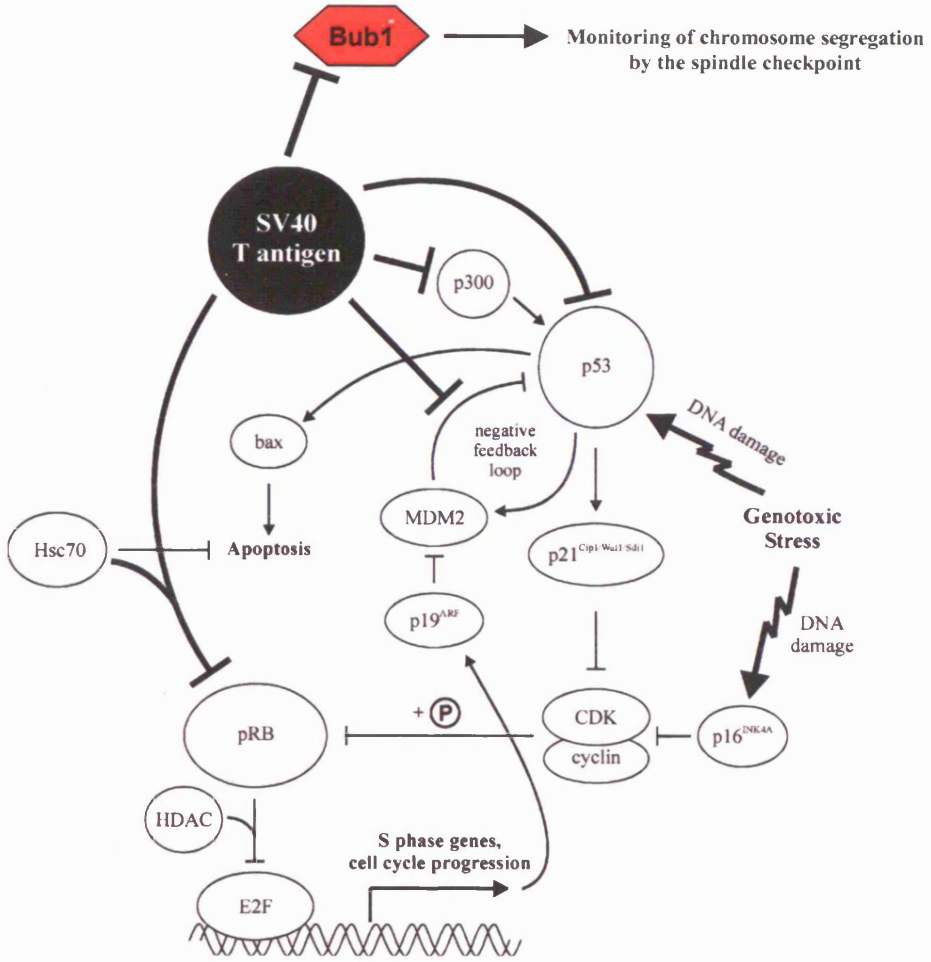

Figure 1.8: Cellular pathways affected by SV40 large T antigen.

This figure summarises some of the pathways that are involved in cell cycle progression, and shows the proteins that are affected by SV40 large T antigen (LT). Compromise of the spindle checkpoint by LT via interaction with the checkpoint kinase Bub1 is the focus of this project, and is highlighted in red. (Adapted from Lock *et al.*, 2004).

Mutational analyses of LT have indicated that three regions of the protein are critical for its immortalising activity (Conzen and Cole, 1995). These regions are the amino terminal 82 amino acids (the T/t common region), amino acids 102-114 and amino acids 350-560. It should be noted however that while all three regions are required for immortalisation, C3H10T1/2 cells (an established cell line) are still at least partially transformed by LT with mutations in the second or third regions, but mutations in the amino terminal 82 residues abrogate transformation of these cells. This illustrates the reduced requirement of LT functions for the transformation of established lines compared with immortalisation of primary cells. These regions of LT are all involved in interactions with host proteins, and these interactions and their possible functions will now be discussed in detail.

1.3.2.1 The Retinoblastoma family of proteins

The retinoblastoma protein (pRB) is the product of the retinoblastoma susceptibility gene, Rb1, which was the first tumour suppressor gene to be identified in humans. The RB gene as well as genes involved in the RB regulatory pathway are known to be mutated in a diverse range of human cancers (reviewed in (Malumbres and Barbacid, 2001)).

pRB is a ubiquitously expressed protein of 928 amino acids and contains at least three domains: an N-terminal domain, a central A/B (bipartite) pocket domain, and a C-terminal (C pocket) domain. There are two other pRB-family members, p107 and p130, and these proteins also possess the A/B pocket region, which is found to be the region with which most cellular and viral interacting proteins bind, and also the region in which most tumour-associated RB mutations occur (Classon and Dyson, 2001; Hu *et al.*, 1990; Huang *et al.*, 1990).

The pRB family of proteins functions to control proliferation, differentiation and apoptosis, by maintaining a tight control on cell cycle progression. pRB is phosphorylated and dephosphorylated during the cell cycle, and the site-specific phosphorylation of pRB appears to coincide with

the transition of the cell through R, the restriction point in G1 phase (Bartek *et al.*, 1996; Weinberg, 1995). pRB acts to prevent the cell-cycle transition from G1 to S phase partly via its interaction with E2F, a transcriptional activator for S phase-specific genes. It is only the active, underphosphorylated form of pRB that binds to E2F, thus inhibiting its transactivation activity. The interaction of pRB with E2F is regulated by phosphorylation of pRB by several cyclin-dependent kinases (CDKs), in a cell cycle-dependent manner (Adams, 2001) (see Figure 1.1).

SV40 large T antigen (LT) forms a stable complex with pRB, and this interaction is critical for immortalisation because mutants that are defective for binding pRB have a reduced immortalisation potential (DeCaprio *et al.*, 1988; Powell *et al.*, 1999). Some transformation defective mutants of LT are defective for binding to pRB, indicating the additional importance of this interaction for the transforming function of LT (reviewed in (Ali and DeCaprio, 2001)). All viral oncoproteins including SV40 LT and many cellular proteins that bind to pRB have in common the LxCxE motif, which is responsible for the interaction with the conserved pocket region of pRB (Lee *et al.*, 1998). The LxCxE motif of LT is located at residues 103-107, within the region of the protein that has homology to conserved region 2 (CR2) domain of adenovirus E1A and the human papilloma virus type 16 E7 protein (see Figure 1.7). The CR2 domain of each of these proteins is responsible for their interactions with the pRB family of proteins (DeCaprio *et al.*, 1988; Moran, 1988; Munger *et al.*, 1989). LT only binds to the underphosphorylated growth suppressing form of pRB that normally binds E2F, resulting in its sequestration (Ludlow *et al.*, 1989; Ludlow *et al.*, 1990). This has a similar effect to the phosphorylation-mediated inactivation of pRB. In the presence of LT, E2F is thus free to activate transcription, resulting in entry into S phase. LT also targets the other pRB family members, p107 and p130, similarly disrupting their interactions with E2F proteins, and additionally is able to perturb the phosphorylation state of p107 and p130 and stimulate p130 (but not p107) degradation (Stubdal *et al.*, 1996). It has been

suggested that p107 and p130 are the critical targets of LT for its immortalisation function, and that pRB may not be so important for this activity (Srinivasan *et al.*, 1997). The N-terminal "J domain" of large T antigen (residues 1-82) is also involved in the interaction with pRB family members, and it has been suggested that a functional J domain as well as the LxCxE motif are required for a productive interaction with pRB (Zalvide *et al.*, 1998).

1.3.2.2 p53

p53 was originally identified as a cellular protein that co-immunoprecipitated with SV40 LT using antisera from tumour-bearing animals (Lane and Crawford, 1979; Linzer and Levine, 1979). Interaction of LT with p53 leads to its stabilisation. Although it was originally believed that p53 was an oncogene, it was later found that wild-type p53 is a tumour suppressor, whereas mutant p53 is an immortalising gene. p53 has proven to be one of the most commonly mutated genes in human cancer (Hollstein *et al.*, 1994). It has sequence-specific DNA binding activity, and acts to increase the transcription of genes that cause growth arrest in G1 and G2, and to induce apoptosis in response to genotoxic stress. Its function as a tumour suppressor and "guardian of the genome" (Lane, 1992) has been attributed to its negative regulation of cell proliferation in the presence of DNA damage. p53 activity is also critical for maintenance of the senescent state, since microinjection of anti-p53 antibodies can induce DNA synthesis in senescent cells (Gire and Wynford-Thomas, 1998).

p53 is ubiquitously expressed in all cells, but is not stable due to its interaction with MDM2, a ubiquitin E3 ligase which targets it for degradation by the proteasome (Momand *et al.*, 2000). However, upon genotoxic stress such as irradiation, chemotoxin exposure, or unscheduled DNA synthesis induced by a virus, the normally short-lived p53 protein becomes stabilised, resulting in a corresponding increase in p53-mediated transcription (Kastan *et al.*, 1991; Kuerbitz *et al.*, 1992; Maltzman and Czyzyk, 1984).

Phosphorylation of p53 at theonine-18 or serine-20 in response to DNA damage causes p53 to dissociate from MDM2 resulting in its stabilisation (Kussie *et al.*, 1996). These modifications are also crucial for acetylation of C-terminal residues and these together result in the full p53-mediated response to genotoxic stress. Activation of p53 by ionising radiation requires the ATM protein, which mediates the direct phosphorylation of serine-15 and indirectly mediates the phosphorylation of serine-20 by controlling activation of chk2 (Turenne *et al.*, 2001). The ATM-Rad3-related protein ATR also regulates phosphorylation of serine-15 in response to UV DNA damage. Additional sites for DNA damage-induced phosphorylation at serine-33 and -37 may be regulated by ATR and other kinases (Tibbetts *et al.*, 1999). When the C-terminus of p53 is modified, the ability of this region to negatively regulate sequence-specific DNA binding is inhibited, resulting in activation of transcription of downstream targets in response to DNA damage (Appella and Anderson, 2001; Lill *et al.*, 1997a). This leads to a cascade of events that include the transcriptional activation of the CDK inhibitor $p21^{Cip1/Waf1/Sdi1}$, MDM2, as well as the apoptotic protein bax, cyclin G1 and several other factors. In addition, p53 can also repress the transcription of other genes including those encoding the anti-apoptotic protein bcl-2, pRB, the transcription factors c-*fos*, c-*jun*, and c-*myc* and the proliferating cell nuclear antigen (PCNA, a component of the DNA replication machinery that is required for both replication and repair of DNA) (Ginsberg *et al.*, 1991; Mercer *et al.*, 1991; Miyashita *et al.*, 1994; Moberg *et al.*, 1992; Shiio *et al.*, 1992).

If the DNA damage is too extensive to be repaired, p53 induces exit from the cell cycle and cell death via apoptosis. p53 can also halt DNA replication during S phase of the cell cycle if damage has occurred, again either promoting arrest until the DNA is repaired, or inducing apoptosis if the DNA is irreparable, indicating the pivotal role played by p53 as a signal integrator in the determination of cell fate. MDM2 acts to down-regulate p53, inducing its ubiquitin-mediated degradation and providing a negative

feedback loop mechanism that restores the normal functions of the cell once the genotoxic stress has diminished (Momand *et al.*, 2000).

It is not yet fully understood how the interaction of SV40 LT with p53 affects the functions of p53. However, it is generally accepted that LT inactivates p53 tumour suppressor function by directly binding to the region of p53 involved in specific DNA binding, preventing p53 from acting as a transcriptional activator of genes that induce cell cycle arrest in response to genotoxic stress. The failure of p53 to monitor the genome in SV40-immortalised cells is thought to be the reason behind the increased occurrence of mutations in these cells (Ray *et al.*, 1990; Stewart and Bacchetti, 1991; Woods *et al.*, 1994). Paradoxically, interaction of LT with p53 has also been shown to increase the half-life and steady-state levels of p53 (Deppert *et al.*, 1987; Oren *et al.*, 1981). The observation that MDM2 binds LT directly *in vitro* and co-precipitates in a complex with p53 *in vivo* has led to the suggestion that LT enhances the stability of p53 partly by entrapment of the p300/MDM2/p53 complex responsible for targeting its degradation (Brown *et al.*, 1993; Grossman *et al.*, 1998; Henning *et al.*, 1997).

The region of LT required for interaction with p53 is actually bipartite, consisting of amino acids 351-450 and 533-626 (see Figure 1.7). The C-terminal region of LT beyond amino acid 627 can be removed without loss of immortalisation, transformation or tumourigenic activity (Tevethia *et al.*, 1988). Interestingly, immortalisation of mouse cells is very much dependent upon the direct inactivation of p53 (Conzen and Cole, 1995), whereas rat cells can be immortalised by amino terminal fragments of large T antigen that cannot interact with p53 (Powell *et al.*, 1999; Sompayrac and Danna, 1991). However, it has been suggested that these mutants may be able to act downstream of p53 to inactivate the pathway, e.g. via pRB family binding (Michael-Michalovitz *et al.*, 1991; Quartin *et al.*, 1994; Rushton *et al.*, 1997). The sequestration of p53 by LT may also abrogate p53-mediated apoptosis (McCarthy *et al.*, 1994). In cell lines conditionally immortalised by a temperature-sensitive mutant of LT, its inactivation has in some studies

resulted in growth arrest without significant cell death (Jat and Sharp, 1989), while in others its inactivation resulted in cell death by apoptosis, perhaps caused by a sudden release of a large amount of stable p53 (Yanai and Obinata, 1994).

1.3.2.3 p300 and the CBP family of proteins

p300 was first identified as an adenovirus E1A interacting protein and has also been shown to bind to SV40 large T antigen (LT) (Avantaggiati *et al.*, 1996; Eckner *et al.*, 1996). p300 and the related proteins p400 and CBP (CREB-binding protein) are members of a family of transcriptional co-activators involved in coordinating the formation of specific transcription factor complexes (Struhl, 1998). They enhance the transcriptional activity of many proteins, including p53 and NFκB p65 subunit, either by directly interacting with transactivators, or by modulating the chromatin structure via recruitment of histone acetyltransferases (Goodman and Smolik, 2000; Hottiger and Nabel, 2000). p300/CBP acetyltransferases promote the acetylation of p53, thus activating p53-mediated transcription (Avantaggiati *et al.*, 1997). This activation of p53 by p300 is potentiated by ionising radiation.

In addition to their role in transcriptional regulation, these proteins may also be involved in cell cycle control and development. p300 and CBP may also have a tumour suppressor function, as mice with a null mutation in one allele of CBP are known to develop haematological malignancies (reviewed in (Janknecht, 2002)), and various human carcinomas have been linked to p300 mutations (Gayther *et al.*, 2000; Muraoka *et al.*, 1996). The binding site for p300 and CBP on LT has been mapped to both the N-terminal and the C-terminal domains of the protein (Eckner *et al.*, 1996; Lill *et al.*, 1997b). It is not clear if interaction of these proteins with LT is direct or via p53, but it has been shown that LT expression inactivates the transcriptional activation function of p300, and also changes the phosphorylation state of p300 (Avantaggiati *et al.*, 1996; Eckner *et al.*, 1996). This inactivation of p300 leads to the inhibition of p53 transcriptional activation activity, further helping

the virus to maintain an environment in which it can replicate in an uncontrolled manner.

1.4 AIM OF THE RESEARCH

The main aim of this project was to examine the function of SV40 large T antigen interaction with the checkpoint protein Bub1. The importance of this interaction was investigated in terms of the known functions of SV40 LT, and also as a model for mechanisms of the spindle checkpoint.

The first aim was to identify a LT mutant that is defective for Bub1 interaction. Such a mutant could then act as a tool for examining if interaction with Bub1 is critical for the cell cycle de-regulating functions of LT, such as the immortalising and transforming activities of the protein, in addition to its abilities to induce chromosomal instability.

The next aim was to examine the possibility that LT is inhibiting the spindle checkpoint function of Bub1, making use of a non-Bub1-binding mutant of LT as a negative control. The generation of good Bub1 monoclonal antibodies to aid in these experiments was also a priority.

If LT was shown to compromise spindle checkpoint function via interaction with Bub1, the final aim of the research was to investigate how this was achieved, perhaps also gaining insights into the spindle checkpoint function of Bub1 in the absence of LT.

2. Materials and methods

2.1 MAMMALIAN CELL CULTURE

2.1.1 Cell media

Tissue culture media and cell culture reagents were purchased from Invitrogen. All cell lines, except for hybridoma cells, were maintained in Dulbecco's modified Eagle medium (DMEM) (Invitrogen) supplemented with 2mM glutamine, 100 units/ml penicillin, 100 μg/ml streptomycin and 10% (v/v) heat inactivated foetal calf serum (FCS) for BOSC 23, U20S, Rat embryo fibroblast (REF) cell lines and other Rat cell lines, or 10% (v/v) heat inactivated donor calf serum (DCS) for NIH 3T3 cell lines. Hybridoma cells were maintained in RPMI 1640 Medium with GlutaMAX^{TM} I and 25mM HEPES (Invitrogen) supplemented with 2mM glutamine, 100 units/ml penicillin, 100ug/ml streptomycin, 10% (v/v) FCS and 1mM sodium pyruvate.

2.1.2 Cell culture conditions

All cell lines were maintained in a 5% CO_2 and 20% oxygen atmosphere at 37°C in medium supplemented with additives as above.

2.1.3 Primary cells

Rat embryo fibroblasts (REFs) were maintained in a 5% CO_2 and 20% oxygen atmosphere at 37°C in DMEM supplemented with 10% FCS, glutamine and antibiotics as above.

2.1.3.1 Preparation of REFs

REFs were prepared from 13-day-old Sprague-Dawley rat embryos. A 13-day-old day pregnant rat was sacrificed by cervical dislocation and the uterus was removed. The embryos were then isolated from the uterus under sterile conditions and immediately placed into Leibovitz's L-15 medium (Invitrogen). These first steps were carried out by the UCL Biological Services department. Heads and tails were then removed from the embryos and the remaining tissues were disaggregated by fine mincing followed by treatment with trypsin-EDTA (ethylenediaminetetraacetic acid) (Invitrogen) to produce a cell suspension. The cells were subsequently plated in 15 cm dishes (one dish was used for each embryo prepared). This was defined as passage 1 (P1). REFs were maintained in a 5% CO_2 and 20% oxygen atmosphere at 37°C in DMEM supplemented with 10% FCS, glutamine and antibiotics as above.

2.1.4 Sub-culturing of adherent cells

Cells were grown until a sub-confluent (80% confluence) state was reached. The media was then removed and the monolayer of cells was washed once with 1X trypsin-EDTA (0.25% v/v trypsin, 0.03% w/v EDTA). The monolayer was then detached using 1X trypsin-EDTA (1ml was used per 10 cm dish, for 5 min at 37°C) and the trypsin-EDTA was then inactivated by adding 10ml of complete media. The cells were then either plated at a defined ratio (e.g. 1 in 10 of the total cells were re-plated), or were counted using a haemocytometer and plated at the required density, and were then maintained at 37°C in a 5% CO_2 and 20% oxygen atmosphere.

2.1.5 Preservation of cells

Adherent cells from a sub-confluent (~80% confluence) dish were trypsinised, washed once in complete media and spun down at 1000rpm for

5min to remove any traces of trypsin, and resuspended in FCS (or DCS in the case of NIH 3T3 cell lines) with 10% DMSO (dimethyl sulphoxide) (BDH) (3ml for each 10cm dish of cells). 1ml aliquots were then transferred to cryotubes and frozen at -70°C wrapped in several layers of tissue for insulation. The tubes were transferred into liquid nitrogen after 24 hours.

Similarly, hybridoma cells were spun down at 1000rpm for 5min, resuspended in RPMI 1640 medium (Invitrogen) with 20% FCS and 10% DMSO, and frozen in aliquots as for other cell types.

2.1.6 Recovery of frozen cells

Cells were removed from liquid nitrogen storage and thawed rapidly at 37°C. The cells were added to 9ml of complete media in a 15ml falcon tube and then pelleted at 1000rpm for 5min to remove the DMSO-containing media. The pellet was then resuspended in 10ml of complete media and the cells split between two 10 cm dishes and incubated at 37°C in a 5% CO_2 and 20% oxygen atmosphere until sub-confluence was reached, at which point the cells were then sub-cultured.

2.1.7 DNA transfection of mammalian cells

Cells were transfected using FuGENE 6 Transfection reagent (ROCHE) according to manufacturer's instructions. The DNA:transfection reagent ratio was 1:2. Cells were plated at a density of 1 x 10^6 cells per 10cm plate the day prior to transfection. The following day the cells were ~50% confluent, and were transfected with 6μg of the vector DNA per plate. Where lysates were to be prepared from a transient transfection, media was changed the following day, and lysates prepared two days after the transfection.

2.1.8 Retroviral infection of rodent cells

2.1.8.1 Packaging the retroviral vectors

BOSC 23 cells (an ecotropic retroviral packaging cell line (Pear *et al.*, 1993)) were plated at 1.7 x 10^6 cells per 6cm plate the day prior to transfection. Cells were transfected the following day (at ~50% confluence) with 3μg of the retroviral vector DNA per plate using FuGENE 6 Transfection reagent (ROCHE) according to manufacturer's instructions. The DNA:transfection reagent ratio was 1:2. Media was changed the following day, adding only 3ml of media per plate rather than the usual 5ml, to concentrate the retroviral supernatant. Two days after the transfection, the retroviral supernatant was harvested, filtered through a 0.45μm filter, and quickly frozen in aliquots at -80°C.

2.1.8.2 Retroviral infection

Cells for retroviral infection were plated at 7 x 10^5 cells per 10cm plate for NIH 3T3 cells, or 1 x 10^6 cells per 10cm plate for REFs (2 days after preparation of the REFs, i.e. approximately passage 2). The following day at ~50% confluence), media was aspirated from the plates, and the cells were infected with retroviral supernatant (thawed on ice, volumes in the range of 0.1-0.5ml supernatant were used) mixed with 2ml of media per plate, and 8μg/ml polybrene, added dropwise of the surface of the plate. Cells were then incubated at 37°C for 2 hours, at which point the infection mixture was diluted out by adding a further 8ml of fresh medium per plate. Cells were maintained at 37°C, and 24-48 hours after infection, plates were split (1 in 10 and 1 in 50 to 10cm plates for NIH 3T3 cells, or 1 in 8 and 1 in 16 to 15cm plates for REFs). 48 hours following the infection, antibiotic selection was added (2μg/ml puromycin), and media (including antibiotic) was changed every 3-4 days.

2.1.8.3 Colony counting

Once cells transduced with the retrovirus had formed visible colonies (approximately 10 days for NIH 3T3 cells, and 15 days for REFs), media was removed from the plates and cells were stained with methylene blue (2% (w/v) methylene blue with 50% EtOH in ddH_20) at room temperature for 10-15 minutes. Plates were then gently rinsed with water, and cell colonies were counted to allow calculation of retroviral titre (from the NIH 3T3 colony counts), and efficiency of immortalisation of the retroviral constructs (from the REF colony counts, taking into account the retroviral titre calculated from the NIH 3T3 counts).

2.1.8.4 Isolation of clonal cell lines

After retroviral transduction and selection with 2μg/ml puromycin, single clones were expanded from the resulting colonies into cell lines. Single clones were picked using sterile cloning cylinders (Sigma). The growth medium was removed from each dish and a cloning cylinder (diameter 0.5 cm) was applied around each selected clone by pressing it lightly against the plate after the bottom edge of the cloning cylinder had been dipped into sterile silicone grease. Two drops of trypsin were then added and the cells incubated at 37°C for 5 min. The detached cells were then collected with a Pasteur pipette and the trypsin inactivated with complete medium. The cells were then plated into a 24 well plate and allowed to adhere and grow. When 80% confluence was reached (from a couple of days to a week, depending on the growth rate for each clone) the cells were transferred into 3 cm dishes. When 80% confluence was reached again the cells were transferred to 6 cm dishes and eventually to 10 cm dishes and subsequently passaged to new 10 cm plates after 1in 5 dilutions.

2.1.9 Focus formation assay

Cells were transduced with appropriate (equivalent) volumes of retroviral vectors as previously described, and 24 hours later cultures were split, but into medium with only 2% serum in the medium (rather than the usual 10%, to reduce the number of spontaneous foci), and with no antibiotic selection. Cells were maintained at 37°C with media changes every 3-4 days. 23 days post-transduction, all plates were washed twice with ice-cold 1X PBS (without $CaCl_2$ or $MgCl_2$), fixed with ice-cold methanol for 10min, and then stained at room temperature for 10min with 0.5% crystal violet (Sigma) solution (made in 25% methanol). Plates were then carefully rinsed in tap water, and allowed to dry at room temperature.

2.2 BACTERIAL MANIPULATIONS

2.2.1 Bacterial strains

The JS4 *Escherichia Coli* strain (kindly provided by J. Sedivy, Brown University) was used for plasmid manipulation and preparation. JS4 is a *rec*A1 derivative of MC1061, and has the following genotype: F$^-$*ara*D139, Δ(*ara*, *leu*)7697, Δ(*lac*)χ74, *gal*U, *gal*K, *hsd*R2 (rk$^-$ mk$^-$), *mcr*A, *mcr*BC, *rps*L (Strr) *thi*, *rec*A1.

E. coli strain BLR λDE3 pLysS (Novagen) was used for bacterial protein expression with the Novagen pET System. BLR λDE3 pLysS, is a *recA*- high-stringency derivative of *E. coli* strain BL21, and has the following genotype: F- *ompT* $hsdS_B$ (r_B^- m_B^-) *gal dcm* Δ(*srl-recA*)*306*::Tn*10* (DE3) pLysS. It is also resistant to chloramphenicol (34μg/ml).

2.2.2 Media and maintenance

E. coli cells were grown in Luria Broth, (LB medium, made up using 25 g/L Luria Broth Base, Invitrogen). 15g/L of Agar (Oxoid) was added when

plates were prepared. To make up the media all the components were dissolved in ddH_2O and autoclaved for 20 min at 37°C. When required, ampicillin (Sigma) was added to 100 μg/ml final concentration.

2.2.3 Preparation of competent bacteria

500ml of LB was inoculated with a single bacterial colony and incubated with shaking at 37°C overnight. 5ml of the overnight culture were then diluted into 500ml of LB and grown at 37°C with aeration for 2 to 2.5 hours until the OD_{600} reached 1.0-1.2 (mid-exponential phase). The bacteria were harvested by centrifugation at 2500rpm for 20 min, resuspended in 5ml ice cold 0.1M $CaCl_2$ and incubated on ice for 20 min. The bacteria were then centrifuged again and resuspended in 5ml of ice-cold 85:15 solution 0.1M $CaCl_2$ and glycerol. 50μl aliquots were frozen in pre-chilled 1.5ml tubes using liquid N_2, and then stored at -70°C.

2.2.4 Bacterial transformations

A single 50μl aliquot of frozen competent bacteria was thawed on ice. 950μl ice cold 0.1M $CaCl_2$ was added; 100μl of this mixture was then added to each DNA to be transformed. The DNA was incubated with the bacteria on ice for 30 min followed by heat shock at 42°C for 90 sec. The transformations were returned to ice for 2 min, after which 1ml of LB medium (without ampicillin) was added and the transformations incubated at 37°C with shaking for 30 min. The cells were then concentrated by centrifugation (2500rpm for 10 min) and resuspended in 100μl LB medium. The transformations were finally plated onto 10cm pre-warmed LB-agar plates containing 100μg/ml final concentration ampicillin and incubated overnight at 37°C.

2.3 DNA MANIPULATION

2.3.1 Polymerase Chain Reaction (PCR)

For PCR amplification of mBub1(1-561) and mBub1(562-1058), incorporating a 6x His-tag, and restriction sites (see Chapter 4, Figure 4.2 for primer sequences), 50µl PCR reactions were carried out (consisting of 1X Thermophil Buffer (New England Biolabs, contains 2mM $MgS0_4$), 200µM mixed dXTPs (nucleotides), 0.5µM mixed forward and reverse primers, 250ng of plasmid DNA (pcDNA3.1(+)-mBub1, "B3"), 0.5µl of Vent DNA polymerase (New England Biolabs), and ddH_20).

The following PCR program was used to amplify the mBub1(1-561) and mBub1(562-1058) DNA fragments, using a MJ Research Peltier Thermal Cycler: 94°C for 3min, then 5 cycles of denaturing at 94°C for 30sec, annealing at 51°C for 1min and extending at 72°C for 2min, followed by a further 25 cycles the same but with an annealing temperature of 64°C, and then finally a further extension at 72°C for 10min, followed by a 15°C hold. The two different annealing temperature were used to allow initial annealing of the vector sequence specific regions of the primers to the vector at a lower temperature, followed by more specific annealing at a higher temperature suitable for the entire length of the primers.

2.3.2 DNA sequencing

The following primers, in addition to the forward and reverse primers used for the initial PCR, were used to check the mBub1 DNA sequence in clones of the mBub1(1-561)-pET and mBub1(562-1058)-pET vectors:

Primer	Sequence (5'-3')	Designed from base no.
BUB1SEQ1 5'FW	ACTGGAATCCATTTGCCAGCTC	502
BUB1SEQ1 3'RV	ATGCAATTTCTTGTGAAGTTCA	960
BUB1SEQ2 5'FW	GAAATTGCATCAAGTGGTGGA	951
BUB1SEQ2 3'RV	GTCCATGATGAAACCTAATGC	1443
BUB1SEQ3 5'FW	GCATTAGGTTTCATCATGGAC	1423
BUB1SEQ3 3'RV	TCTTTATCTTCTGGAATCTGTACT	1895
BUB1SEQ4 5'FW	GATTCCAGAAGATAAAGAAAATGTGG	1878
BUB1SEQ4 3'RV	GGCTCCTTCTCCAAGAAGGTG	2373
BUB1SEQ5 5'FW	GCCTTTGCTCAAGTCTTTGAAG	2371
BUB1SEQ5 3'RV	GTTTCATATCTATACTCTGACCCAGGT	2842
BUB1SEQ6 5'FW	GATATGAAACTTTTCCCTAAAGGAAC	2833
BUB1SEQ6 3'RV	TCCATATTCATTTTATTTTCTTGAAC	3249

For each sequencing reaction, a mixture of 3.2pmol primer, 500ng plasmid DNA, 8µl ABI dRhodamine TRR Mix, made up to a final volume of 20µl with ddH_20, was submitted to 25 cycles of 95°C for 30sec, followed by 50°C for 30sec, and finally 60°C in a PCR machine (MJ Research Peltier Thermal Cycler). After the final cycle, sequencing reactions were cooled to 4°C, and cleaned using a DyeEx spin kit (QIAGEN), according to manufacturer's instructions. Samples were then vacuum dried, and run on a sequencing gel and analysed by the Ludwig Institute for Cancer Research DNA sequencing facility.

2.3.3 Plasmid DNA preparation

All the plasmid preparations (both small scale and large scale preparations) were carried out using QIAGEN kits, and following the manufacturer's instructions.

2.3.3.1 Small scale preparation

Bacterial stocks were kept at -70°C in LB containing 15% glycerol. Liquid cultures of bacteria picked from single colonies were grown in a bacterial shaker (vigorous shaking) overnight at 37°C in 5ml of LB medium with 100µg/ml ampicillin. 1.5ml of culture was then transferred to an eppendorf tube and microfuged at 13000rpm for 30sec. The pellet was

resuspended in 250µl of solution P1 (50mM Tris/HCl, pH 8.0, 10mM EDTA, 100 mg/ml RNAse A). Then 250µl of solution P2 (200mM NaOH, 1% sodium dodecyl sulphate (SDS)) was added and gently mixed by inverting the tube 4-6 times. To the same tube, 350µl of solution N3 (3.0M sodium acetate, pH 5.5) was added and immediately mixed by inverting the tubes 4-6 times. The mixture was then centrifuged in a microfuge for 10min at 13000rpm and the supernatant transferred to a QIAprep column. The column was then centrifuged for 30sec at 13000rpm and the flow-through discarded. The columns were first washed with 0.5ml of PB buffer (QIAprep Spin Miniprep kit, QIAGEN) and then 0.75ml of PE buffer (QIAprep Spin Miniprep kit, QIAGEN). The DNA was then eluted with 50µl of ddH_20. (All solutions used were from the QIAprep Spin Miniprep kit, QIAGEN)

2.3.3.2 Large scale preparation

200ml of LB containing 100µg/ml ampicillin was inoculated with an overnight culture of bacteria and grown overnight at 37°C with vigorous shaking. Bacteria were harvested at 7000rpm for 10min at 4°C and the pellet resuspended in 10ml of resuspension buffer P1 (50mM Tris-HCl pH 8.0, 10mM EDTA, 100 µg/ml RNAse A, stored at 4°C). 10ml of lysis buffer P2 (200mM NaOH, 1% SDS) were added. After 5min incubation at room temperature, 10ml of ice-cold neutralisation buffer P3 (3mM potassium acetate pH 5.5) were added and the mixture was further incubated on ice for 20min with occasional inversion. The cell debris was pelleted by centrifugation at 15000rpm in a Beckman JA-17 rotor for 30 min. The recovered supernatant was applied to a previously equilibrated QIAGEN-tip 500 column (equilibration buffer QBT: 750mM NaCl, 50mM MOPS [3 - (N-morpholino) propanesulphonic acid] pH 7.0, 15% Ethanol v/v, 0.15% Triton X-100) and allowed to enter the resin by gravity. The column was washed twice with 30ml of wash buffer QC (1M NaCl, 50mM MOPS pH 7.0, 15% Ethanol). The DNA was then eluted with 15ml of elution buffer QF (1.25M

NaCl, 50mM Tris-HCl pH 8.5, 15% Ethanol) and precipitated in 10.5ml of isopropanol at room temperature. Centrifugation was performed for 30 min at 15000rpm at 4°C in the same rotor previously used and the DNA pellet was then washed with 70% ethanol. The pellet was air dried for 5 min and resuspended in ddH_2O. The DNA obtained was then checked by appropriate restriction digests and run on an agarose gel. (All solutions used were from the QIAfilter Plasmid Maxi kit, QIAGEN)

2.3.3.3 DNA quantification

To determine DNA concentration, the optical density of the solution was measured at 260nm (OD_{260}) using a BioRad spectrophotometer (Bio-Rad Smart Spec™ 3000 Spectrophotometer). DNA concentration was calculated using the relationship:

1 OD unit at 260nm = 50μg/ml DNA.

The DNA was also checked by running 1μl on an agarose gel.

2.3.4 Restriction digests

Restriction digestions of DNA plasmids were performed using restriction enzymes from New England Biolabs and Boehringer Mannheim according to the specified conditions. The 10X buffer provided for each enzyme was diluted to 1X in the final reaction mixture. Bovine serum albumin (BSA, New England Bio Lab) was used at 1X dilution when required. Other conditions such as incubation time and temperature were performed according to the manufacturer's guidelines for the specific enzyme.

2.3.5 DNA agarose gel electrophoresis

DNA fragments were loaded with 1X DNA loading buffer (2.5% Ficoll, 0.04% (w/v) bromophenol blue and 0.04% Xylene) and fractionated by

electrophoresis on 1% (w/v) agarose (Invitrogen) gels, prepared in 1X TAE (40mM Tris-acetate and 2mM EDTA) with 1 μg/ml ethidium bromide (BDH). Electrophoresis in 1X TAE was carried out in electrophoresis tanks and DNA fragments were separated at a constant voltage of 80V for 1 or more hours. Samples were loaded alongside double stranded DNA molecular weight markers, 1kb-ladder (GibcoBRL). Ethidium bromide stained DNA fragments were then visualised on a UVP (Dual intensity ultraviolet trans-illuminator) and an image was produced and printed with a Sony video graphic printer.

2.3.6 Extraction of DNA from agarose gels

DNA restriction fragments separated on agarose gels were purified using the QIAquick Gel Extraction Kit (QIAGEN), according to the manufacturer's instructions. After agarose separation DNA was viewed with a long wavelength ultraviolet emission (UV) transilluminator and the desired band was cut out using a scalpel and transferred to an eppendorf tube. The gel slice was dissolved by adding 3 volumes (per weight of gel slice) of QG buffer (QIAquick spin kit, QIAGEN) and incubating at 50°C for 10 min. The sample was then transferred to a QIAquick spin column and centrifuged for 1 min after which the DNA in the column was washed with 0.75ml of PE buffer (QIAquick spin kit, QIAGEN). Traces of wash buffer were removed by centrifugation for 1min. Finally, the DNA was eluted by adding 30μl of ddH_20 and centrifugation for 1min at full speed in a microcentrifuge. The DNA was collected in a 1.5ml microfuge tube.

2.3.7 Ligation

All ligations performed during this project were cohesive-end ("sticky-end") ligations. Ligation reactions were performed using 1μl of T4-Ligase (New England Biolabs) in 1X ligation buffer (50mM Tris-HCl pH 7.5, 10mM $MgCl_2$, 10mM dithiothreitol, 1mM ATP, 25 μg/ml BSA). The amount of

DNA:vector to insert was dependent on the sizes of the two DNA fragments. The ligation mixture was incubated at 16°C overnight or at room temperature for at least 2 hours before transforming competent *E. coli* cells.

2.3.8 Plasmids used

pBabe-puro-L13V, D44N E90A, W91A, E92A, Q93A, W94A & W95A and dl89-97 (each containing mutated full-length SV40 LT cDNA), pBabe-puro-wild-type LT, pBabe-puro-(empty vector), pSUPERretro-Bub1 (Oligoengine vector allowing knockdown of Bub1 expression via RNAi interference (RNAi)), pSUPERretro(empty vector), pcDNA3.1(-)HA-mBub1 were kindly provided by Dr Ole Gjoerup of the Dana-Farber Cancer Institute, Boston, MA, USA.

mBub1 cDNA originally cloned into the NotI and SalI sites of the pcDNA3.1(+) (Invitrogen) expression vector by T. Puri, a final year undergraduate project student in the laboratory, was PCR amplified in two sections, incorporating restriction sites and a 6 x His-tag, and cloned into the pET-23a+ bacterial expression vector (Novagen) between the XbaI and BamHI sites.

2.4 PROTEIN ANALYSIS

2.4.1 Preparation of total protein extracts

Cells were either seeded (3 x 10^6 cells per 15cm plate for U20S, REF or NIH 3T3 cells, to give ~80% confluence on day of lysis), or were fed with fresh media the day prior to lysis. For the lysis, cells were washed twice with cold 1X PBS (Phosphate Buffered Saline (without $CaCl_2$ or $MgCl_2$)), and 1ml of 1X RIPA Lysis Buffer [150mM NaCl, 1% Triton-X-100, 0.5% sodium deoxycholate (NaDOC), 0.1% SDS and 50mM Tris pH 8.0] or 1X NP40 Lysis Buffer (150mM NaCl, 1% Nonidet P-40, 50mM Tris pH8.0, 5mM EDTA)

was added to each 15cm plate. 60µl of Protease Inhibitor Cocktail (Sigma P2714, 1 bottle dissolved in 10ml of ddH_20) was included per ml of lysis buffer. The cells were incubated for 30min on ice and then scraped and transferred to a 1.5ml microfuge tube. For the RIPA lysates only, the lysate was then passed three times through a 21 gauge needle to shear the DNA. The cell extracts were then centrifuged for 30min at 10000rpm at 4°C and the supernatant transferred to a fresh microfuge tube. The cell lysates were aliquoted and stored at -20°C.

2.4.2 Determination of protein concentration

Protein concentrations were determined using the Bio-Rad protein assay (Bio-Rad Laboratories), a protein assay based on the Bradford assay (Bradford, 1976). The dye reagent was diluted 1:5 in PBS. A BSA standard curve was established with protein dilutions ranging from 1 to 15µg/ml. 2µl of each sample were mixed with 1ml of freshly diluted dye and incubated at room temperature for 5 min. OD_{595} was measured (Bio-Rad Smart Spec™ 3000 Spectrophotometer) and plotted against protein concentration of standards. Regression coefficient was calculated and the unknown sample concentrations determined.

2.4.3 Sodium dodecyl sulphate-polyacrylamide gel electrophoresis (SDS-PAGE)

8% Sodium dodecyl sulphate-polyacrylamide gel electrophoresis (SDS-PAGE) gels were prepared from a 30% (w/v) acrylamide stock solution (containing a ratio of 29.2 acrylamide:0.8 NN'-methylenebisacrylamide; Genomic Solutions) in 375mM Tris-HCl pH 8.8 and 0.1% (w/v) SDS. Gels were polymerised by addition of ammonium persulphate (APS) (0.1% (w/v) final; Bio-Rad) and TEMED (N,N,N',N' tetraethylenemethyldiamine, 0.0006% (w/v) final; BDH Laboratory). For 12%

SDS-PAGE or 5-15% gradient SDS-PAGE gels, quantities of the polymerising agents were adjusted slightly.

For direct immunoblot 50μg of each cell lysate (unless otherwise stated) was heated at 90°C for 5min with 2X Laemmli sample buffer (1X final concentration, Sigma; 4% SDS, 20% glycerol, 10% 2-mercaptoethanol, 0.004% bromophenol blue and 0.125 M Tris-HCl, pH 6.8) and fractionated by SDS-PAGE on 8%, 12% or 5-15% gradient polyacrylamide gels, as more convenient. Electrophoresis was carried out at a constant voltage of 100-150V during the day (or 40V overnight) in running buffer (25mM Tris, 190mM Glycine, 0.1% (w/v) SDS). Proteins were stacked through 2cm of stacking gel (5% polyacrylamide, 125mM Tris-HCl pH 6.8 and 0.1% (w/v) SDS, polymerised by addition of APS and TEMED as before). Proteins were fractionated alongside broad-range prestained SDS-PAGE standards (Bio-Rad Laboratories).

2.4.4 Coomassie staining of SDS-PAGE

Following SDS-PAGE, for visualisation of total protein, the gel was incubated at room temperature for 4-5 hours in a stain containing 0.05% (v/v) Coomassie Blue, 10% (v/v) methanol and 10% (v/v) glacial acetic acid. The gel was then de-stained for several hours in the same solution but without the Coomassie Blue, and dried using a gel drier (Hoefer Scientific Instruments, San Francisco) attached to a vacuum pump.

2.4.5 Western blotting of SDS-PAGE

Following separation via SDS-PAGE, proteins were transferred to a nitrocellulose membrane Hybond-c extra (Amersham Life Science) by electrophoretic transfer in a wet tank blotting system (Bio-Rad Laboratories Trans-Blot cell). The transfer was carried out in transfer buffer (25mM Tris,

190mM glycine and 20% (v/v) methanol) for 4 hours at a constant voltage of 60V at 4°C or alternatively overnight at a constant voltage of 20V (4°C).

The nitrocellulose membrane was then blocked by incubation in 5% (w/v) skimmed milk powder (Marvel, Premier Brands) and 0.005% (v/v) Tween-20 (BDH Laboratory) in 0.5X PBS (PBS/Marvel) at room temperature for 1 hour (or overnight at 4°C). The filter was then incubated for 1 hour at room temperature, or overnight at 4°C with the primary antibody diluted in PBS/Marvel at the indicated dilutions (see Paragraph 2.4.8). The filter was then washed three times (15min each at room temperature) in 0.05% (v/v) Tween 20 and 0.5X PBS (PBS/Tween) prior to incubation with horseradish peroxidase (HRP) conjugated secondary antibody (Amersham Life Sciences ECL™ western blotting analysis system) diluted 1:2000 in PBS/Tween for 1 hour. Following three further washes (15min each at room temperature) in PBS/Tween, the filters were developed in HRP detection reagents for 90sec, according to manufacturer's instructions (ECL™, Amersham Pharmacia Biotech). The membrane was then wrapped with Saran-wrap and exposed to an auto-radiographic film for times varying from 10sec to 1hour (Fujifilm Super RX X-ray film). The films were developed with an AGFA X-ray film processor.

2.4.6 Immunoprecipitation

All immunoprecipitations (IPs) were carried out using pre-prepared NP40 lysates. 0.4-1mg of each lysate for IP was made up to a final volume of 500µl or 1ml, as appropriate, with NP40 lysis buffer in a 1.5ml eppendorf tube. Antibody for IP (50-100µl per IP for monoclonal antibody supernatants, or 2-5µl per IP for polyclonal antisera) was added, and lysates were mixed with the antibody on a wheel at 4°C for 1-2 hours. 50µl of 50% Protein A-sepharose beads in 1X PBS (Amersham Pharmacia Biotech) were added per IP, and the tubes were incubated at 4°C on the wheel for a further hour (Protein G-sepharose beads in 1X PBS (Amersham Pharmacia Biotech) were

used for IPs with IgG1 sub-class monoclonal antibodies). The beads were then pelleted at 6000rpm for 1min at 4°C, and washed three times with 800µl NP40 lysis buffer and further centrifugation. Following a final spin, the last remnants of the wash were removed, and 50µl of 2X Laemmli Sample buffer (Sigma) was added per tube. Each tube was then vortexed briefly, and heated at 90°C for 10-15min, after which the beads were pelleted at 6000rpm for 1min, and the supernatant was removed to a fresh eppendorf, ready for separation via SDS-PAGE, and western blotting.

2.4.7 Immunofluorescence

Cells were seeded at 3 x 10^3 cells per well onto glass coverslips in a 24-well plate. 3 days later cells were 50-70% confluent on the coverslips, and were fixed with ice-cold methanol for 10min at -20°C. All antibody incubations and washes were in "IF Buffer" (1X PBS with 1% BSA (bovine serum albumin) and 0.5% CHAPS (3-[(3-cholamidopropyl)dimethylamino]-1-propanesulphonate)), and were carried out at room temperature. Cells on each coverslip were blocked with 40µl 1:1 medium:IF Buffer for 10min, and washed 5 times (IF Buffer). Cells were then incubated with primary antibody for 30min, and washed 5 times. Finally, cells were incubated with secondary antibody for 30min (in the dark). Where used, propidium iodide (PI, 1:1000 dilution of 1mM stock) was included with the secondary antibody, to visualise the DNA. After 5 final washes, the coverslips were mounted on microscope slides using DAKO Fluorescent Mounting Medium, and images of the cells were obtained using a Zeiss LSM 510 confocal laser-scanning microscope (Welwyn Garden City, UK), using the accompanying LSM 510 software. Some of the immunofluorescence images presented in this thesis were captured from cells stained by Miss S. Klischies.

2.4.8 Antibodies used

Anti-Cyclin B1 mouse monoclonal (clone GNS-11), 1:1000 anti-Mad2 mouse monoclonal (clone 48), and 1:1000 anti-p55Cdc (clone 41) were from BD Pharmingen; anti-Mad2L1 mouse monoclonal (ab10691) was from Abcam; anti-hPTTG-1 rabbit polyclonal was from Zymed Laboratories Inc.; anti-actin mouse monoclonal (AC-40) was from Sigma.

Rabbit polyclonal antiserum raised against amino acids 1-303 of hBub1 fused in-frame to GST ("NT hBub1 serum Ab"), NT hBub1 affinity purified rabbit polyclonal, and rabbit polyclonal raised against amino acids 691-1085 of hBub1 fused in-frame to GST ("CT hBub1 serum Ab") were kindly provided by Dr Raimundo Freire (Hospital Universitario de Canarias, Tenerife, Spain). anti-Bub3 rabbit polyclonal "953", was a gift from Prof Peter Sorger (Massachusetts Institute of Technology, Cambridge, MA, USA). Anti-HA mouse monoclonal was kindly provided by Dr Claire Wells (LICR-UCL). Anti-SV40 LT mouse monoclonal antibodies PAb416, PAb419 and PAb423, and p53 mouse monoclonal antibody PAb421 (hybridoma supernatants) were harvested at LICR-UCL by Prof Parmjit Jat.

HRP (Horseradish peroxidase)-conjugated secondary antibody against whole mouse serum or against whole rabbit serum were from Amersham Pharmacia Biotech.

The antibodies used for western blots were diluted as follows: Cyclin B1 (GNS-11) 1:500; Mad2 (48) 1:1000; p55Cdc (41) 1:1000; Mad2L1 (ab10691) 1:1000 (used 2µl per 500µg lysate IP); hPTTG-1 1:125; actin (AC-40 1:10000; NT hBub1 serum Ab 1:2000; NT hBub1 Affinity Pure 1:2000 (used 3µl per 500µg lysate IP); CT hBub1 serum Ab 1:2000 (used 3µl per 500µg lysate IP); Bub3 (953) 1:2000 (used 3µl per 500µg lysate IP); HA 1:1000; PAb416 1:50; PAb419 1:50; PAb423 1:50; hybridoma tissue culture supernatants of anti-mBub1 mouse monoclonals generated during this project, 2B8, 13G9 and 17E9, were used at 1:25; HRP-conjugated secondary antibodies 1:2000.

For immunofluorescence, primary antibodies were diluted as follows: anti-mBub1 mouse monoclonals 2B8, 13G9, and 17E9 were used at 1:8; anti-β-Tubulin (Sigma) 1:100. FITC- and TRITC-conjugated secondary antibodies used for immunofluorescence were from Jackson Immunoresearch Laboratories Inc., and were used at 1:100.

2.5 GENERATION OF MONOCLONAL ANTIBODIES

2.5.1 Protein expression

2.5.1.1 IPTG induction of protein expression

500µl of an overnight culture of *E. coli* expression strain BLR λDE3 pLysS, transformed vector for expression of the protein of interest (mBub1(1-561)-pET or mBub1(562-1058)-pET) was inoculated in 5ml LB (with 100µg/ml ampicillin) and grown at 37°C with shaking until an OD_{600} spectrophotometer reading of 0.4-1 was reached. 1ml of the culture was saved as an "uninduced" sample, while a final concentration of 0.4mM IPTG (isopropyl-β-D-thiogalactopyranoside) was added to the remainder of the culture to induce protein expression. Protein expression was induced at 37°C for 2 hours.

To extract total protein from these induced samples, cells were harvested from both uninduced and induced samples by centrifugation at 10000rpm for 5min at 4°C. The pellets were washed with 1ml ice-cold PBS and resuspended in a 1:1 mix of PBS and 2X Laemmli Sample Buffer (Sigma), heated at 90°C for 5min, and run on an 8% SDS-PAGE gel. The gel was then Coomassie stained to check for induction of expression of the protein of interest.

2.5.1.2 Native protein mini-prep: protein solubility test

Protein expression was IPTG induced as described above, but following a 30°C induction for 3 hours (induces better than 37°C, but takes a

little longer), 2ml of the induced culture was pelleted at 10000rpm for 5min at 4°C, then air-dried on ice, and frozen at -20°C. The protein mini-prep under native conditions was carried out as suggested by QIAGEN (QIAexpressionist™ manual). The cell pellet was thawed on ice and resuspended in 100µl 1X Ni- Bind Buffer (50mM Tris-HCl pH 7.9, 300mM NaCl, 1mM imidazole), followed by incubation with 1mg/ml lysozyme for 30min on ice. Cells were then lysed by vortexing (avoiding frothing), spund down at 10000rpm for 10min (4°C) to remove cellular debris, and the supernatant was transferred to a fresh tube. 20µl of a 50% slurry of Ni-NTA His-Bind resin (QIAGEN) was added, and mixed on a wheel at 4°C for 30min. The resin was then pelleted at 6000rpm for 1min, and the resin was washed twice with 100µl of 1X Ni- Wash Buffer (50mM Tris-HCl pH7.9, 300mM NaCl, 10mM imidazole), with spinning at 6000rpm for 1min. The His-tag protein was then eluted three times with 20µl of 1X Ni- Elute Buffer (50mM Tris-HCl pH7.9, 300mM NaCl, 250mM imidazole), and half of each elution was mixed with 10µl 2X Laemmli Sample Buffer (Sigma) and separated on a 8% SDS-PAGE gel via Coomassie staining. Successful elution of the protein of interest indicated that the protein was expressed in a soluble form.

2.5.1.3 Bulk soluble protein purification

5ml of an overnight culture was used to inoculate each of 8 flasks of 500ml LB + antibiotics (50µg/ml ampicillin and 34µg/ml chloramphenicol) and grown at 37°C with shaking until an OD_{600} spectrophotometer reading of 0.4-1 was reached. Protein expression was IPTG induced (0.4mM IPTG) at 30°C for 4 hours, after which cells were harvested at 3000rpm for 20min and the cell pellets frozen on dry-ice/ethanol, and stored at -20°C overnight. Cell pellets were thawed on ice and resuspended in a total volume of 80ml Native Lysis Buffer (50mM NaH_2PO_4 pH 8.0, 300mM NaCl, 1mM imidazole), followed by incubation on ice for 30min with 1mg/ml lysozyme. The lysate was then sonicated on ice 6 times for 10sec, with 10sec breaks, followed by drawing the mixture 5 times through a 21-gauge needle. The lysate was then

cleared by centrifugation at 9000rpm for 20min at 4°C, and the supernatant was incubated with 1ml of a 50% slurry of Ni-NTA His-Bind resin (QIAGEN) for 60min on a wheel at 4°C. The supernatant/resin mix was then loaded onto a column (the flow-through was retained for a further preparation), and the resin was washed 5 times with 4ml Native Wash Buffer (50mM NaH_2PO_4 pH 8.0, 300mM NaCl, 10mM imidazole). His-tagged protein was then eluted 5 times with 0.5ml Native Elution Buffer (50mM NaH_2PO_4 pH 8.0, 300mM NaCl, 250mM imidazole), and stored at -20°C. The protein was later thawed on ice, dialysed into 1X PBS at 4°C, and concentrated 10-fold using Centricon-30 columns (No. 4208), ready for immunisation of mice.

2.5.1.4 Bulk insoluble protein purification

IPTG induction of protein expression and harvesting of cells was carried out as described for Bulk soluble protein purification (Section 2.5.1.3). Cell pellets were thawed on ice and resuspended in a total volume of 80ml of Denaturing Lysis Buffer (6M GuHCl (guanidine hydrochloride), 100mM NaH_2PO_4, 10mM Tris, adjusted to pH 8.0 using NaOH) and incubated on a wheel at room temperature for 30min, followed by vortexing until a clear, "translucent" solution was achieved. The lysate was then cleared by centrifugation at 9000rpm for 20min at room temperature, and the supernatant was incubated with 1ml of a 50% slurry of Ni-NTA His-Bind resin (QIAGEN) for 60min on a wheel at room temperature. The supernatant/resin mix was then spun down at 1000rpm for 1min (the supernatant was retained for a further preparation), and the resin was washed 2 times with 10ml of Denaturing Lysis Buffer for 30min on a wheel at room temperature, followed by 4 washes with 5ml of Denaturing Wash Buffer (6M GuHCl, 100mM NaH_2PO_4, 10mM Tris, adjusted to pH 6.0 using HCl) . His-tagged protein was then eluted 10 times with 1ml Denaturing Elution Buffer (6M GuHCl, 100mM NaH_2PO_4, 10mM Tris, adjusted to pH 3.0 using HCl) for 5min on a wheel at room temperature (for each elution, resin was spun down at 1000rpm for

1min, and supernatant (eluted protein) was removed and retained), and stored at -20°C. The protein was later thawed on ice, dialysed into 2M Urea at 4°C, and concentrated 10-fold using "Centriplus" Centricon YM-10 columns, ready for immunisation of mice.

2.5.2 Immunisations, generation of hybridomas, and ELISA screening

Immunisations of mice with the His-tag fusion proteins, generation of hybridomas via somatic cell fusions, single cell cloning, ELISA screening and isotyping of the resulting hybridomas was carried out by Dr T. Jowett (UCL monoclonal antibody facility).

2.5.3 Harvesting monoclonal antibody tissue culture supernatant

Hybridoma cells were cultured until large volumes (300-600ml) of media with dense cells was achieved. Dense cultures of cells were maintained at 37°C for 1-2 weeks, allowing the cells to die. Tissue culture supernatant was then harvested by centrifugation at 2000rpm for 15min at 4°C, followed by filtration using a 0.22μm Stericup™ filter (Millipore). Stocks of hybridoma tissue culture supernatant were stored at -20°C, supplemented with 0.1% NaN_3 (sodium azide).

2.5.4 Affinity purification of monoclonal antibodies

Affinity purification of monoclonal antibodies was carried out in collaboration with Dr G. Mallinson at the MRC Prion Unit, Institute of Neurology, UCL. Approximately 350ml of hybridoma tissue culture supernatant (without sodium azide) was concentrated down to approximately 40ml using an Amicon 8200 stirred cell with a Millipore Ultrafiltration membrane. The ÄKTA*prime* machine (automated liquid chromatography system from Amersham pharmacia biotech) was used to purify the

monoclonal antibodies, according to manufacturer's instructions. IgG proteins in the concentrated hybridoma tissue culture supernatant were bound to a 1ml HiTrap Protein G column (Amersham pharmacia biotech) with Buffer A1 (50mM sodium phosphate, pH 7.2), and the column was washed with the same buffer. Affinity purified IgG was eluted in Buffer B (100mM glycine-HCl, pH 2.5), and stored in aliquots at –80˚C with 0.1% NaN_3.

2.6 TIME LAPSE MICROSCOPY

Time lapse movies were created using Tempus software (Kinetic Imaging Ltd, Liverpool, UK) with images captured using a KPM1E/K-S10 CCD camera (Hitachi Denshi, Japan), in collaboration with Dr A. Entwistle (Ludwig Institute for Cancer Research Microscopy Facility, UCL branch, London).

2.7 KARYOTYPE ANALYSIS

2.7.1 Metaphase spreads

Cells were grown to 60-80% confluence, and 2 hours after feeding the cells with fresh medium, 0.1μg/ml colcemid (KaryoMAX colcemid solution Invitrogen) was added to the medium. Cells were incubated with colcemid for 4 hours at 37°C, after which time many "rounded" cells arrested in mitosis could be seen under the microscope. Cells were then trypsinised as usual, and pelleted at 700g for 5min. The pellet was then washed twice (700g for 5min) with 10ml 1X PBS, and carefully resuspended in 1ml of Hypotonic Solution (0.56% KCl) until a single cell suspension was obtained. A further 4ml of Hypotonic Solution was then added, and the cells were incubated in a 37°C waterbath for 5min. The cells were then pelleted at 300g for 5min, and the supernatant was removed, leaving 200-400μl behind, in which the pellet was resuspended. Cells were then fixed by very carefully adding ice-cold Fixative

(methanol:acetic acid, 3:1) dropwise for the first 7 drops (gently flicking the tube to mix it), and then gradually adding up to 5ml of the fixative, and leaving at room temperature for 5min. Cells were then spun down at 300g for 5min, the supernatant removed, and the fixing step repeated to a total of 2-3 times, after which cells were resuspended in 1-2ml of the fixative. 1-2 drops of cells were then dropped from a height of 30-50cm onto clean glass slides (the slides had been pre-soaked in 5% acetic acid in EtOH for a few hours and air dried). The slides were allowed to air dry overnight, after which they were stained with 5μM propidium iodide (PI) for 10min. The stain was blotted off with a tissue, and the slides were mounted under a coverslip with 5μM PI in glycerol and sealed with nail varnish.

2.7.2 Image capture of metaphase spreads

Images of metaphase spreads were captured using a Zeiss LSM 510 confocal laser-scanning microscope (Welwyn Garden City, UK).

2.8 FACS ANALYSIS

2.8.1 Fixing cells for FACS (fluorescence-activated cell sorting)

Cells plated at a density of 3 x 10^5 per 10cm plate were treated as required (e.g. drug treatment), and trypsinised as usual. Cells were then pelleted at 1000rpm for 5min, washed once with 1X PBS (1000rpm, 5min), and resuspended in a few remaining drops of 1X PBS. The cell suspension was then vortexed very gently while adding ice-cold 70% EtOH dropwise, up to a final volume of 4ml, transferred to a 5ml round-bottomed polypropylene tube (Falcon), and stored at 4°C for at least 30min, and until ready for FACS analysis.

2.8.2 Propidium Iodide (PI) staining of fixed cells for PI FACS (cell cycle) analysis

EtOH from the fixed cells was spun off at 2000rpm for 5min, and the cells were washed twice with 5ml 1X PBS (2000rpm, 5min), being careful to avoid cell loss when discarding the supernatant. To ensure that only DNA is stained, cells were next treated with 50µl of 100µg/ml RNase (Sigma) for 15min at room temperature. Cells were then incubated for a further 30min at room temperature with 200µl of 50µg/ml propidium iodide, at which point they were ready for analysis by flow cytometry.

2.8.3 PI FACS analysis

All FACS analysis was carried out by Dr Derek Davies (Cancer Research UK FACS laboratory), using a FACSCalibur machine (Becton Dickinson).

3. Mapping of the Bub1 interaction site on SV40 large T antigen

3.1 OBJECTIVES

The first objective of this study was to determine the exact residue(s) of SV40 large T antigen (LT) that are required for interaction with the spindle checkpoint protein Bub1. This was an important step for the project, as cells expressing a non-Bub1-binding mutant of LT would be an invaluable negative control in experiments examining the importance of the LT-Bub1 interaction for cell cycle control. In addition, it would also allow examination of whether Bub1 interaction is necessary for any of the well-characterised functions of LT, including its immortalisation and transformation functions. Part of the work presented in this chapter is already published (Cotsiki *et al.*, 2004).

3.2 EXPERIMENTAL STRATEGY

As previously described, the interaction of Bub1 with LT was first identified using the amino terminal 136 residues of LT as a bait in a yeast two-hybrid screen, and a HeLa cDNA library as prey. It was therefore already known that the binding site of Bub1 on LT was present within this region of the viral protein. For this reason, full length cDNAs of several previously characterised LT mutants within this region were transduced into primary Rat Embryo Fibroblasts (REFs), and the resulting cell lines generated were used to determine the Bub1-LT binding site via co-immunoprecipitation experiments. Primary REFs were used so that the immortalising efficiency could be determined concomitantly with the Bub1 binding efficiency of each of the LT mutants.

Initially, the LT mutations chosen for the mapping were the point mutants L13V and D44N, and the deletion mutant dl89-97. L13V and D44N

were chosen because they were previously known to affect various activities within the amino terminus of LT. dl89-97 was included because Professor Tom Roberts' laboratory had found that an unknown protein kinase binds to LT and this binding is disrupted in the dl89-97 mutant. It was hypothesised that this unknown kinase could be Bub1 and thus residues 89-97 would be the Bub1 interaction site on LT.

LT constructs containing single amino acid point mutations in conserved residues within the 89-97 region were also investigated for immortalisation efficiency and ability to interact with Bub1.

Finally, the ability of wild-type and dl89-97 LT to transform NIH 3T3 cells was investigated via focus formation assay, in both NIH 3T3(empty vector control), and NIH 3T3(Bub1 RNAi knockdown) cells.

3.3 RESULTS

3.3.1 Initial immortalisation efficiency and mapping experiments

3.3.1.1 All LT mutants tested were able to efficiently immortalise REFs

pBabe-puro- constructs for each of the LT mutants, wild-type LT or empty vector (see Figure 3.1, (Morgenstern and Land, 1990)) were packaged using the ecotropic retroviral packaging cell line BOSC 23 and used to transduce NIH 3T3 cells, to calculate the viral titre (NIH 3T3 is a line of Swiss mouse embryo fibroblasts that were immortalised spontaneously, and are highly contact inhibited). The viral titre is a measure of the total number of infected cells that grow into drug resistant colonies, and is calculated to allow normalisation between the different constructs. These constructs were kindly provided by Dr Ole Gjoerup of the Dana-Farber Cancer Institute, Boston, MA, USA. Retroviral transduction results in a greater efficiency of stable insertion of the gene of interest into the host cell genome, and each cell successfully transduced is likely to have a single copy of the gene inserted, rather than multiple copies as seen with DNA transfection.

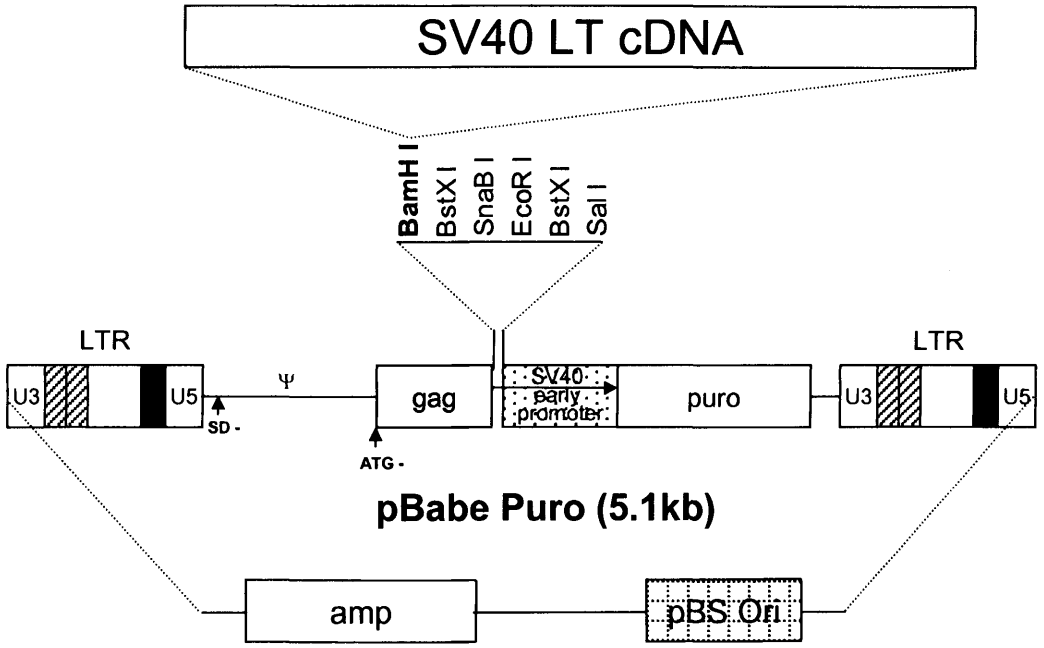

Figure 3.1: pBabe-puro vector used for transduction of SV40 LT cDNAs into rodent cells.

LT cDNAs with various mutations were cloned into the BamHI site in the pBabe-puro vector. The striped boxes represent 72bp enhancer repeats, and the blackened boxes the R (Repeat) region between the transcriptional start and the polyadenylation sites within the Mo MuLV LTRs (Moloney murine leukaemia virus Long Terminal Repeats). The Ψ-packaging site in the pBabe vectors is flanked by both an attenuated splice donor and ATG– *gag* sequences, to yield high viral titres. (Adapted from Morgenstern & Land, 1990)

Primary cells are also notorious for being difficult to transfect. For these reasons retroviral transduction was chosen to generate the cell lines needed to map the Bub1-LT interaction, and to determine immortalisation efficiencies for the LT mutants.

NIH 3T3 cells were seeded, and for each of the constructs, two plates were transduced with 100µl, and two plates with 500µl of the retroviral supernatant in the presence of 8µg/ml polybrene. This is a small, positively charged molecule that binds to cell surfaces and neutralises surface charge. This allows the viral glycoproteins to bind more efficiently to their receptors, because it reduces the repulsion between sialic acid-containing molecules. 24 hours post-transduction (to allow for expression of the resistance gene), the duplicate plates for each volume of retroviral supernatant were pooled and split 1 in 10 and 1 in 50 (in duplicate) into antibiotic selection media containing 2µg/ml puromycin, resulting in a total of 8 plates for each construct. The selective media was changed every 3-4 days, and 10 days post-transduction the NIH 3T3 cells had grown into colonies large enough to be stained with methylene blue and counted (see Table 3.1).

Colonies were counted on all plates for each construct, and the average counts from the 100µl retroviral supernatant, 1 in 10 split plates were used to calculate the viral titre using the following formula:

Formula 3.1:

Viral Titre (per ml of retroviral supernatant) = Average number colonies x 10 x 10 x 2

The x 10 factors in the equation account for the 1 in 10 split and the use of 100µl supernatant for the transduction, to give the number of colonies you would expect from 1ml of retroviral supernatant. The factor of 2 is included because the 100µl of retroviral supernatant was in fact divided equally between the two plates in the initial transduction step.

NIH 3T3:	Number of colonies									VIRAL	Volume (μl) retroviral
Retroviral vector	500μl retroviral supn., 1 in 50 split			100μl retroviral supn., 1 in 50 split			**100μl retroviral supn., 1 in 10 split**				supn equivalent to
pBabe-puro(ori-) -	Plate 1	Plate 2	Average	Plate 1	Plate 2	Average	Plate 1	Plate 2	Average	TITRE	500μl of 5.00E+03 titre virus:
empty vector	275	255	265	78	64	71	233	214	**224**	**4.48E+04**	**56**
wild-type LT	32	39	36	9	15	12	33	37	**35**	**7.00E+03**	**357**
L13V LT	36	41	39	7	8	8	28	29	**29**	**5.80E+03**	**431**
D44N LT	32	34	33	6	8	7	21	29	**25**	**5.00E+03**	**500**
dl89-97 LT	46	58	52	7	10	9	25	33	**29**	**5.80E+03**	**431**

Table 3.1: Retroviral transduction of NIH 3T3 cells with LT mutants to determine viral titres for initial mapping of Bub1-LT interaction.

All colony count data is shown, excluding counts from the 500μl retroviral supernatant, 1 in 10 split plates which had too many colonies to accurately count. The average counts from the 100μl retroviral supernatant, 1 in 10 split plates were used to calculate the viral titre because they had many colonies, while representing a large proportion of the original transduced population of cells. Volume of retroviral supernatant required for doses equivalent to 500μl of 5.00E+03 titre were calculated by dividing 5.00E+03 (titre wanted) by the viral titre and multiplying by 500(μl), for each construct.

The calculation was performed using the counts from these particular plates because they had enough colonies to ensure an accurate estimation of the transduction efficiency of the viral supernatants, but not too many to accurately count. The 500µl viral supernatant, 1 in 50 split plates also had a suitable number of colonies for the calculation, but it was thought that they would not give as accurate a result for the viral titre, as the sample is taken from a smaller proportion of the original population of cells, due to the 1 in 50 split.

The viral titres (calculated using Formula 3.1; see Table 3.1) were very similar in magnitude, except for the empty vector construct, which had a titre almost 10-fold higher than the other constructs. This is to be expected because the empty vector does not contain the LT cDNA, and is therefore much smaller, allowing more efficient packaging of the viral RNA.

The viral titres were then used to calculate the volume of retroviral supernatant that should be used for each construct to ensure an equal dose of viral particles when transducing REFs with the same retroviral supernatants (see Table 3.1). If all of the constructs were equally efficient at immortalising REFs, the use of equivalent doses of retroviral supernatant would result in all transduced REF plates having an equal number of colonies, making the colony counts more accurate for the immortalisation efficiency experiment. Primary REFs were seeded, and transduced in duplicate with an equivalent dose of retroviral supernatant for each of the constructs, and NIH 3T3 cells were also transduced with the same doses, to confirm the viral titres calculated previously. 48 hours later, the duplicate plates were pooled and split 1 in 10 and 1 in 50 in duplicate, into antibiotic selection (as before). The viral titres (per ml of retroviral supernatant) were calculated from the NIH 3T3 colony counts, 10 days post-transduction, this time using the following formula:

Formula 3.2:

$$\text{Viral Titre} = \text{Average number colonies} \times 50 \times 2 \times \frac{1000}{\text{Volume (µl) retroviral supernatant used to infect duplicate plates}}$$

All cells (NIH 3T3 and REF) were split 48 hours post-transduction on this occasion instead of 24 hours, in order to allow the REFs to recover prior to being split into antibiotic selection. This resulted in many more colonies than seen in the previous experiment, and so the 1 in 50 split NIH 3T3 plates were used to calculate the viral titre this time, accounting for the factor of 50 in the equation. Different volumes of retroviral supernatant were used for each construct, and each amount was divided between duplicate plates, accounting for the final factors in the equation.

When NIH 3T3 cells were transduced with the equivalent doses of the LT constructs, the viral titres were comparable to those seen previously, although 10 times higher (due to leaving the cells for 48 hours before splitting into selection, rather than 24 hours, thus allowing them to divide before being selected) See Table 3.2.

The REFs were split into selective media (with 2µg/ml puromycin) at the same time as the NIH 3T3 cells, but were split 1 in 8 and 1 in 16, and into 15cm plates rather than the 10cm plates used for NIH 3T3 cells. The REFs were plated at higher density than the NIH 3T3 cells because they were likely to result in fewer colonies due to some cells dying, others becoming senescent, and also because they generally grow slower than the NIH 3T3 cells. Selective media was changed every 3-4 days, and 17 days post-transduction the colonies on the REF plates were large enough to allow isolation via ring cloning, followed by staining and colony counting. 6 colonies were ring-cloned for each construct, and these were serially cultured for 5 passages to determine if they could be expanded into cell lines, and hence were truly immortal.

Table 3.2: Raw data for immortalisation efficiency of initial mapping constructs for Bub1-LT interaction site.

Duplicate experiments are shown (A & B). For each experiment the first table shows the viral titres re-calculated using NIH 3T3 colony counts from plates infected with the new, equivalent doses of retroviral supernatant (Formula 3.2). The second and third tables for each experiment show colony counts from the retroviral transduction of REFs, 1 in 8 and 1 in 16 (or 1 in 32) split plates, respectively. Immortalisation efficiencies relative to wild-type LT are calculated for each table (Formula 3.3), and number of colonies expanded are also shown. (Colonies were single cell cloned from a mixture of split plates for each construct, and so the number expanded shown in the second table for each experiment represents results from both split plates).

A: Immortalisation Efficiency Experiment 1

NIH 3T3: Retroviral vector pBabe-puro(ori-) -	Volume (μl) retroviral supn used to infect two plates of cells:	Number of colonies 1 in 50 split			VIRAL TITRE
		Plate 1	Plate 2	Average	
empty vector	56	270	281	276	4.93E+05
wild-type LT	357	203	254	229	6.41E+04
L13V LT	431	285	262	274	6.36E+04
D44N LT	500	295	247	271	5.42E+04
dl89-97 LT	431	346	314	330	7.66E+04

REF: Retroviral vector pBabe-puro(ori-) -	Volume (μl) retroviral supn used to infect two plates of cells:	VIRAL TITRE	Number of colonies 1 in 8 split			Immortalisation efficiency relative to wild-type LT (%)	Number colonies expanded
			Plate 1	Plate 2	Average		
empty vector	56	4.93E+05	2	0	1	1.22	(0/0)
wild-type LT	357	6.41E+04	68	67	68	100.00	6/6
L13V LT	431	6.36E+04	35	40	38	46.65	5/6
D44N LT	500	5.42E+04	34	55	45	55.88	5/5
dl89-97 LT	431	7.66E+04	134	151	143	145.76	6/6

REF: Retroviral vector pBabe-puro(ori-) -	Volume (μl) retroviral supn used to infect two plates of cells:	VIRAL TITRE	Number of colonies 1 in 16 split			Immortalisation efficiency relative to wild-type LT (%)	Number colonies expanded
			Plate 1	Plate 2	Average		
empty vector	56	4.93E+05	2	0	1	2.24	
wild-type LT	357	6.41E+04	32	41	37	100.00	(as
L13V LT	431	6.36E+04	16	24	20	45.13	above)
D44N LT	500	5.42E+04	19	20	20	45.64	
dl89-97 LT	431	7.66E+04	75	81	78	146.12	

B: Immortalisation Efficiency Experiment 2

NIH 3T3: Retroviral vector pBabe-puro(ori-) -	Volume (μl) retroviral supn used to infect two plates of cells:	Number of colonies 1 in 50 split			VIRAL TITRE
		Plate 1	Plate 2	Average	
empty vector	28	122	141	132	4.71E+05
wild-type LT	179	113	119	116	6.48E+04
L13V LT	216	117	124	121	5.60E+04
D44N LT	250	109	126	118	4.72E+04
dl89-97 LT	216	135	114	125	5.79E+04

REF: Retroviral vector pBabe-puro(ori-) -	Volume (μl) retroviral supn used to infect two plates of cells:	VIRAL TITRE	Number of colonies 1 in 8 split			Immortalisation efficiency relative to wild-type LT (%)	Number colonies expanded
			Plate 1	Plate 2	Average		
empty vector	168	4.71E+05	13	16	15	5.55	(0/0)
wild-type LT	1071	6.48E+04	211	262	237	100.00	6/6
L13V LT	1293	5.60E+04	162	143	153	61.88	5/6
D44N LT	1500	4.72E+04	153	(-)	153	63.28	5/5
dl89-97 LT	1293	5.79E+04	472	508	490	191.66	6/6

REF: Retroviral vector pBabe-puro(ori-) -	Volume (μl) retroviral supn used to infect two plates of cells:	VIRAL TITRE	Number of colonies 1 in 32 split			Immortalisation efficiency relative to wild-type LT (%)	Number colonies expanded
			Plate 1	Plate 2	Average		
empty vector	168	4.71E+05	10	7	9	8.87	
wild-type LT	1071	6.48E+04	92	85	89	100.00	(as
L13V LT	1293	5.60E+04	40	35	38	40.92	above)
D44N LT	1500	4.72E+04	63	66	65	71.59	
dl89-97 LT	1293	5.79E+04	165	182	174	181.24	

Table 3.2: Raw data for immortalisation efficiency of initial mapping constructs for Bub1-LT interaction site.

The average colony counts from both the 1 in 8 and the 1 in 16 split plates were used to determine the immortalisation efficiency of each construct, relative to wild-type LT, using the following formula:

Formula 3.3:

$$Im_A = 100 \times \frac{Av_A}{Av_{wt}\left(\frac{V_A T_A}{V_{wt} T_{wt}}\right)}$$

where:

Im_A = % Immortalisation efficiency of LT mutant A relative to wild-type LT.

Av_A = Average number colonies on LT mutant A (1 in 8 or 1 in 16 split) plates.

Av_{wt} = Average number colonies on wild-type LT (1 in 8 or 1 in 16 split) plates.

V_A = Volume (µl) of retroviral supernatant used for LT mutant A.

V_{wt} = Volume (µl) of retroviral supernatant used for wild-type LT.

T_A = Viral titre (per ml of retroviral supernatant) for LT mutant A

T_{wt} = Viral titre (per ml of retroviral supernatant) for wild-type LT.

This formula normalises the volume of retroviral supernatant used and the viral titre for each construct against these variables for the wild-type LT construct, allowing the REF colony counts (number of immortal cells) to be directly compared.

Colony count data collected from two independent immortalisation experiments in REFs (using the equivalent doses of the retroviral supernatants) revealed the relative immortalisation efficiencies of each of the LT mutants tested (Table 3.2).

These results are summarised in Figure 3.2. All LT constructs were able to efficiently immortalise REFs, and almost all colonies could be expanded into cell lines and cultured to passage 5.

A

REF:	Immortalisation Efficiency Relative to Wild-type LT (%)				
Retroviral vector pBabe-puro(ori-) -	Expt. 1 calculated using 1 in 8 split plates	Expt. 1 calculated using 1 in 16 split plates	Expt. 2 calculated using 1 in 8 split plates	Expt. 2 calculated using 1 in 32 split plates	Number colonies expanded
empty vector	1.22	2.24	5.55	8.87	(0/0)
wild-type LT	100	100	100	100	12/12
L13V LT	46.65	45.13	61.88	40.92	10/12
D44N LT	55.88	45.64	63.28	71.59	10/10
dl89-97 LT	145.76	146.12	191.66	181.24	12/12

B

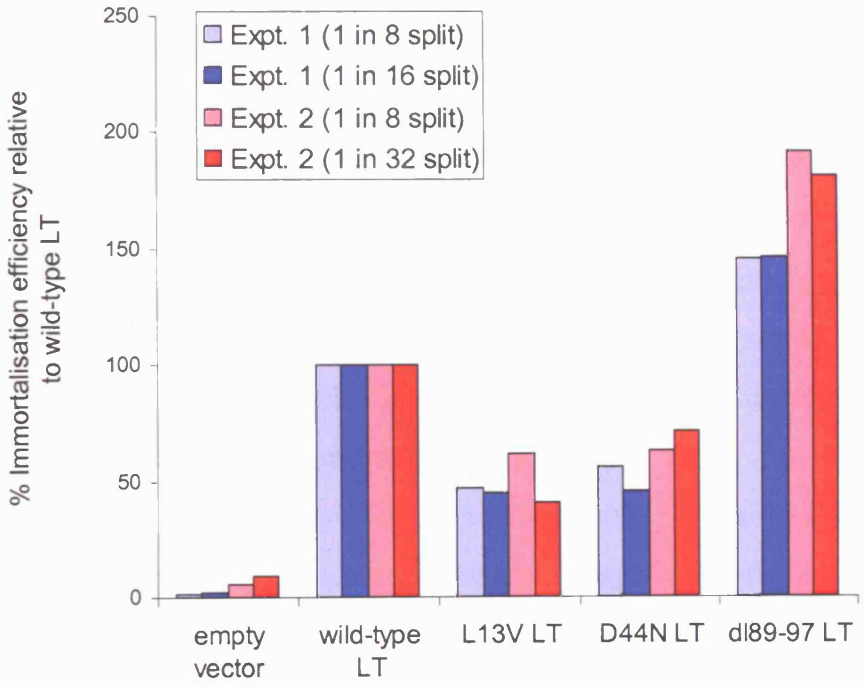

Figure 3.2: Immortalisation efficiency relative to wild-type LT of the initial Bub1-LT interaction site mapping constructs.

Summary of immortalisation efficiencies calculated from REF colony counts at two different plating densities, in two independent experiments, and the number of colonies that expanded (A). A graphical view of these results (B).

This was chosen as a measure of immortality because it has been observed in the laboratory that once cell lines have been cultured to passage 5 they are immortal and do not stop dividing thereafter. As expected, the empty vector construct was not able to efficiently immortalise REFs, and the small numbers of colonies seen on these plates were probably due to cells dividing a few times after infection (prior to senescence). The L13V and D44N LT mutants only immortalised approximately half as efficiently as the wild-type LT. The dl89-97 LT mutant seemed able to consistently immortalise REFs more efficiently than wild-type LT, an unexpected finding.

3.3.1.2 Bub1 interacts in the region of residues 89-97 of LT

Whole cell lysates were prepared from the immortalised REF lines, and compared in immunoprecipitation experiments. Lysates from one REF clone expressing either wild-type, L13V and D44N LT were compared with lysates from three REF clones expressing dl89-97 LT, and with lysate from a cell line called GSE-8, which is a REF line immortalised by a genetic suppressor element derived from p53 (Tarunina *et al.*, 2004) to act as a negative control. NIH 3T3 cells were not used to map the Bub1-LT interaction site due to difficulties with immunoprecipitating the mouse Bub1 protein using the antibodies available at this point in the project.

First of all, protein expression levels of Bub1, LT, Bub3 and p53 in the lysates were compared via western blotting. 30μg of the whole cell lysates were separated on SDS-PAGE and western blotted for Bub1 using a rabbit polyclonal antiserum raised against amino acids 1-303 of hBub1 fused in-frame to GST. This antiserum shows specificity to both the human and the rat Bub1 proteins when used for immunoblotting. See Figure 3.3A. A band of approximately 150kDa was observed in all lanes, at approximately the same intensity for each cell line expressing LT, demonstrating that the level of expression of Bub1 was not altered from wild-type by any of the mutations in LT.

Figure 3.3: The Bub1 interaction site on LT maps to residues 89-97.

REF cell lines, established by transduction with different mutants of LT, with wild-type LT, or with a p53-derived genetic suppressor element, were used to map the Bub1-LT interaction site. Co-immunoprecipitation of LT with Bub1 is observed for wild-type, L13V and D44N LT, but is not observed for dl89-97 LT in any of the 3 clonal REF cell lines tested. GSE-p53 cell line is included as a negative control, and the relative expression levels of Bub1, LT, Bub3 and p53 are shown for all cell lines (A). dl89-97 LT is further shown to be defective for Bub1 binding by immunoprecipitating with either affinity purified NT Bub1 antibody or a Bub3 antibody, and blotting for LT, using the same lysates as before (B).

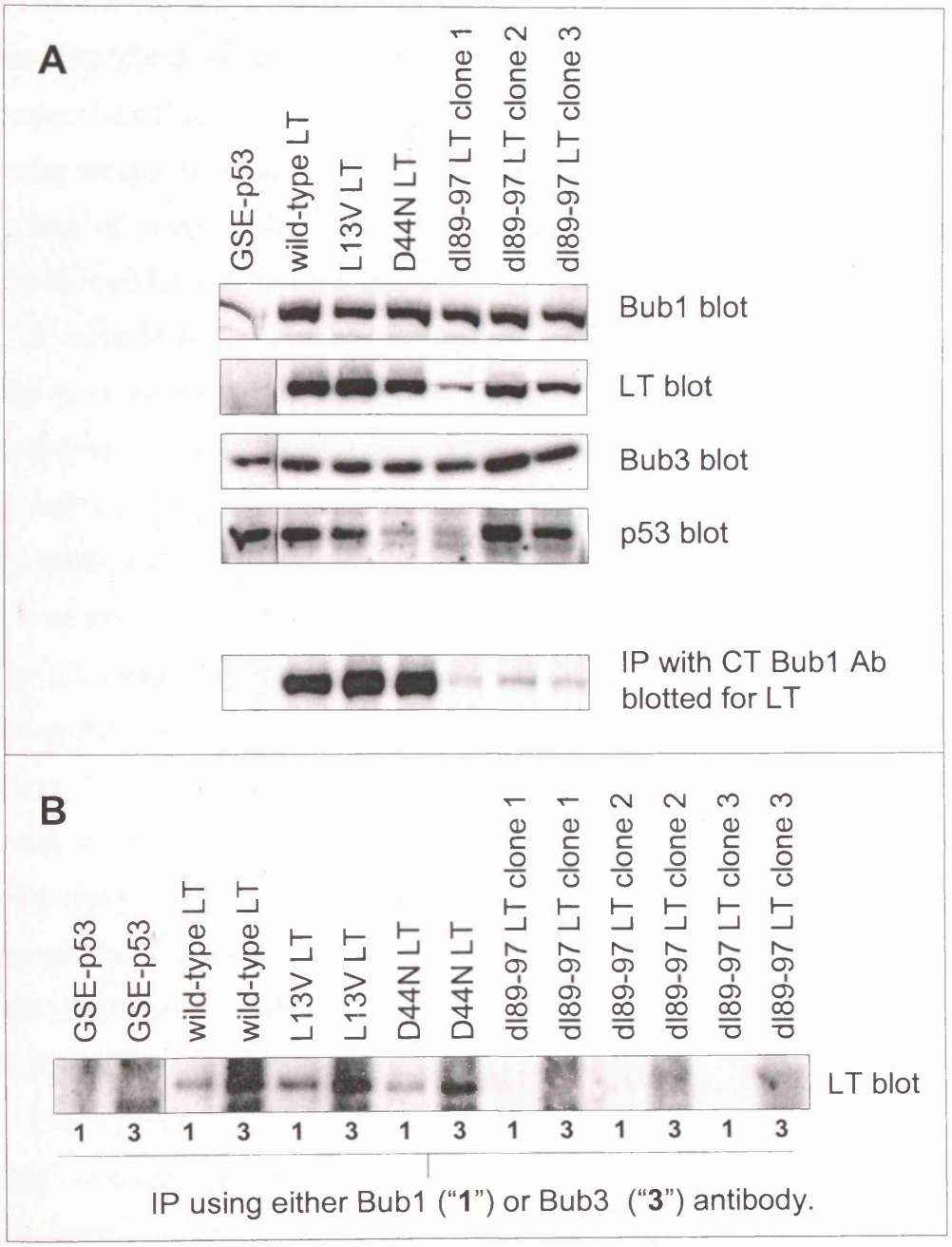

Figure 3.3: The Bub1 interaction site on LT maps to residues 89-97.

Bub1 has a predicted molecular weight of approximately 120kDa, but from examination of the specificity of the Bub1 monoclonal antibodies generated in this project (see Chapter 4), Bub1 appears to migrate to a higher than expected molecular weight of 150kDa.

5μg of each of the lysates were also separated on SDS-PAGE and western blotted for LT, Bub3 and p53.

A mixture of LT mouse monoclonal antibodies PAb416, PAb419 and PAb423 were used to show the relative levels of LT in the different cell lines. Approximately 100kDa bands were observed in all lanes for the cell lines expressing LT (wild-type or mutant). As expected, the GSE-p53 negative control lysate did not show evidence of LT expression. The intensity of the LT bands was very similar between the wild-type, L13V, D44N and clone 2 for dl89-97 LT lanes, but was not as intense for clones 1 and 3 of dl89-97 LT, indicating that these cell lines express LT at a lower level. Several clones of wild-type, L13V and D44N LT have been tested for level of LT expression (data not shown) and had consistently similar high levels of LT, whereas different clones of dl89-97 LT were observed to have different and always lower expression levels of LT than the other mutants. It was for this reason that three different clones of dl89-97 LT were used to determine the interaction of Bub1 with LT in Figure 3.3.

The western blot of the whole cell lysates using Bub3 rabbit polyclonal antibody resulted in 40kDa Bub3 bands in all lanes, and indicated approximately equal expression of the Bub3 protein in all of the cell lines tested. However, dl89-97 LT clone 2 demonstrated a slightly higher level of expression of Bub3 than the other cell lines. This appears to correlate with this clone also having the highest level of LT expression of all the dl89-97 cell lines, whereas Bub1 expression levels were the same for all LT lines.

The p53 mouse monoclonal antibody PAb421 was used to determine the relative expression level of p53 in each of the REF cell lines. LT is known to stabilise p53 protein (Lane and Crawford, 1979), and so the purpose of this blot was to determine if any of the mutations tested had an effect on the ability

of LT to carry out this function. Strong, approximately 50kDa bands were observed in all lanes except D44N LT and dl89-97 LT clone 1. There is a positive correlation between level of expression of p53 with that of LT in the dl89-97 LT lanes, presumably due to the p53-stabilising functions of LT previously described. This shows that the dl89-97 mutation does not affect the p53 stabilisation function of LT. However, there are two unexpected results in this blot. Cells expressing GSE-p53 display a high p53 expression level, with the p53 band being the same intensity as is seen for wild-type LT and L13V LT cells. This is seen in the absence of LT in the GSE-p53 cells, and in addition can not be a manifestation of the p53-derived genetic suppressor element used to immortalise these cells, as this was only a very small cDNA fragment of p53, much smaller than the 50kDa band seen here. This high level of p53 seen in the GSE-p53 line could be due to stabilisation resulting from interaction between the GSE polypeptide and the endogenous full length p53 protein, although this remains to be determined. The second unexpected observation from this blot is that only a very faint p53 band is seen in the D44N LT lane, despite the relatively high level of LT expression seen in these cells. This is a J domain mutant of LT, and it is not clear why a mutation at residue 44 of this region should prevent LT from stabilising the p53 protein, while a mutation at residue 13 of the J domain (L13V LT) does not.

To determine the ability of each LT mutant to interact with Bub1, an antibody raised against the carboxy terminal amino acids 691-1085 of hBub1 fused in-frame to GST was used to immunoprecipitate Bub1 from the REF lysates. It had been shown that an antibody raised against the amino terminal of human Bub1 (hBub1) was able to detect the rat Bub1, and so it was hoped that an antibody raised against the carboxy terminal of hBub1 would also recognise the rat protein, and perhaps immunoprecipitate the protein more efficiently than other antibodies tested. The carboxy terminal hBub1 antibody clearly detected rat Bub1 in co-immunoprecipitation experiments immunoblotted using the amino terminal hBub1 antibody, and was used to immunoprecipitate Bub1 from 1mg of whole cell lysate for each of the REF

cell lines. The resulting precipitates were then immunoblotted for LT using a mixture of LT mouse monoclonals PAb416 and PAb423 (see Figure 3.3A). As expected, no 100kDa LT band is co-immunoprecipitated with Bub1 in the GSE-p53 cell line, because this line does not express LT. A very strong approximately 100kDa LT band in the wild-type LT lane demonstrates the recently published interaction between LT and Bub1 (Cotsiki *et al.*, 2004). Equally strong 100kDa LT bands are seen to be brought down with Bub1 in REFs expressing L13V and D44N LT, indicating that these mutations do not compromise interaction of LT with Bub1. However, only extremely faint 100kDa LT bands could be seen in the dl89-97 LT lanes for the Bub1-LT co-immunoprecipitation experiment. When a comparison is made between the level of expression of Bub1 and LT in each cell line in Figure 3.3A, and the relative amounts of LT protein being co-immunoprecipitated with Bub1, it is clear that all three dl89-97 clones are deficient for Bub1 interaction. The faint bands seen in the dl89-97 LT co-immunoprecipitation lanes are likely to be due to LT being a relatively "sticky" protein, resulting in non-specific binding to Protein A-sepharose beads, as has been observed by others. Alternatively, it could be the case that these bands represent a low level of direct or indirect interaction between Bub1 and dl89-97 LT.

The same whole cell lysates were also used to immunoprecipitate either Bub1 (this time using an affinity purified rabbit polyclonal antibody raised against amino acids 1-303 of hBub1 fused in-frame to GST) or Bub3 (using a rabbit polyclonal antibody), and the resulting precipitates were immunoblotted for LT using mouse monoclonals PAb416 and PAb423 (see Figure 3.3B). The binding of Bub3 to Bub1 is thought to be critical for the kinetochore localisation of Bub1 (Taylor *et al.*, 1998) and it has been shown that LT, Bub1 and Bub3 are present in the same protein complex (Cotsiki *et al.*, 2004). When the Bub1 or Bub3 immunoprecipitates were western blotted for LT, 100kDa bands indicating co-immunoprecipitation were only observed in the wild-type, L13V and D44N LT lanes, where Bub1, Bub3 and LT are part of the same complex. As expected, no 100kDa LT bands are seen in the

immunoprecipitations from GSE-p53 in Figure 3.3B, because this cell line does not express LT. No 100kDa LT bands are observed in the dl89-97 lanes, indicating that neither Bub1 nor Bub3 were able to interact with dl89-97 LT in any of the three clones tested. Figure 3.3B therefore further demonstrates that LT mutant dl89-97 is defective for Bub1 interaction, and concomitantly for Bub3 interaction also.

3.3.2 Immortalisation efficiency and mapping experiments using single amino acid mutations to alanine in residues 89-97 of LT

A further examination of residues 89-97 of LT was undertaken, with the intention of mapping of the Bub1-LT interaction site in finer detail. Within the 89-97 region of LT a EWEXWW motif was found to be conserved between all large T antigens, with the exception of murine polyomavirus T antigen (see Figure 3.4, (Cotsiki *et al.*, 2004)). For this reason, the amino acids in this motif were mutated to alanine by Dr Ole Gjoerup using site-directed mutagenesis, and these mutated full length LT cDNAs were then cloned into the pBabe-puro vector as described previously (see Figure 3.1).

These retroviral constructs (pBabe-puro- E90A, W91A, E92A, Q93A, W94A & W95A) were packaged in BOSC 23 cells as before. The resulting retroviral supernatants were used to determine the immortalising efficiency and ability to interact with Bub1 for each of these single amino acid point mutations of LT, using the same methods as described for the initial immortalisation and mapping experiments in this chapter.

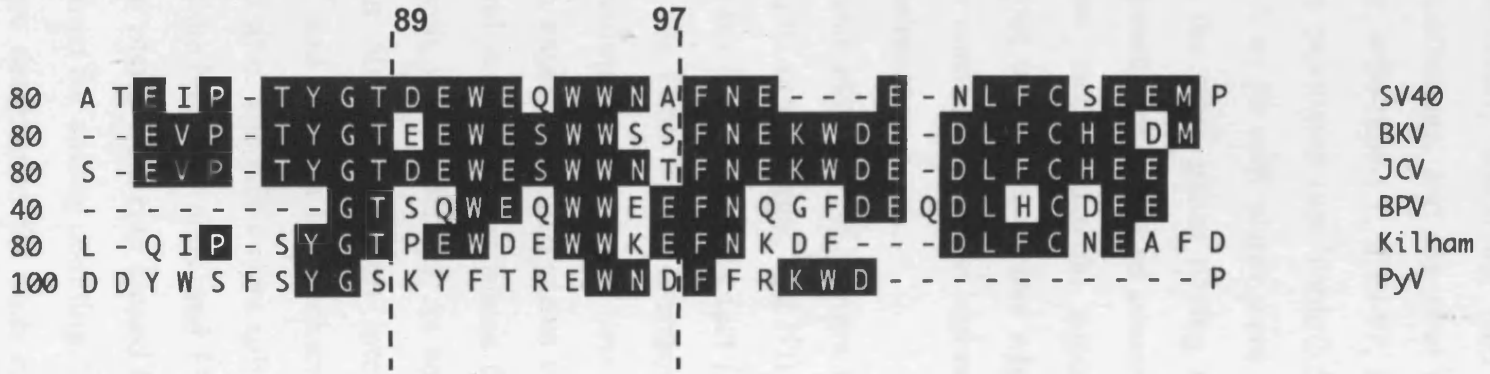

Figure 3.4: Conservation within the 89-97 amino acid region of SV40 LT, and other large T antigens.

Sequence alignment of the polyomavirus large T antigens: SV40, human BK polyomavirus (BKV), human JC polyomavirus (JCV), bovine polyomavirus (BPV), Kilham strain of polyomavirus (Kilham) and murine polyomavirus (PyV) were aligned using the DNASTAR program. The sequence (E/Q)W(E/D)XWW (amino acids 90-95 of SV40 LT) is conserved between SV40, BKV, JCV, BPV, and Kilham T antigens, but there is no obvious homologous sequence in the same region of PyV. (Adapted from Cotsiki *et al*, 2004)

3.3.2.1 Individual substitution mutations in the 89-97 region of LT were not able to disrupt the immortalising functions of LT.

As previously described, NIH 3T3 cells were transduced with the retroviral supernatants, and the viral titres for each construct (pBabe-puro-empty vector, wild-type LT, dl89-97, E90A, W91A, E92A, Q93A, W94A & W95A) were calculated (see Table 3.3). The colony counts from the 100μl supernatant, 1 in 50 split plates were used on this occasion to calculate the titre, due to the other plates having a very large number of colonies, and therefore a greater possibility of counting errors. The viral titres were used to calculate how much retroviral supernatant should be used to give an equivalent dose of each retrovirus when infecting the REFs. As before, the empty vector construct gave the highest viral titre, with comparable titres for the other constructs.

Duplicate plates of REFs were transduced with these equivalent doses of the retroviral supernatants, and NIH 3T3 cells were also transduced with half these doses (to counter the fact that they produce many more colonies than REFs). See Table 3.4. This retroviral transduction of REFs was in fact performed in duplicate, with the two experiments kept completely separate (i.e. for each experiment, two plates of REFs were initially transduced with each retroviral construct, and plates from each individual experiment were pooled and split, independently). As before, the NIH 3T3 cells were split 1 in 10 and 1 in 50 (in duplicate) into antibiotic selection 48 hours post-transduction, and 10 days later colonies were counted to determine a more accurate viral titre. The REFs were split 1 in 8 and 1 in 16 (in duplicate) at the same time as the NIH 3T3 cells, and 15 days post-transduction 3 to 5 colonies from the REF plates were ring cloned from each separate experiment, and the rest were stained for colony counting. Immortalisation efficiencies of each LT construct were determined for each experiment, using both the 1 in 8 split colony counts, and the 1 in 16 counts (See Table 3.4). The number of colonies that could be expanded to passage 5 are also shown for each separate experiment.

NIH 3T3:	Number of colonies									VIRAL	Volume (µl) retroviral
Retroviral vector	500µl retroviral supn., 1 in 50 split			100µl retroviral supn., 1 in 10 split			**100µl retroviral supn., 1 in 50 split**				supn equivalent to
pBabe-puro(ori-) -	Plate 1	Plate 2	Average	Plate 1	Plate 2	Average	Plate 1	Plate 2	Average	TITRE	500µl of 2.00E+04 titre virus:
empty vector	760	680	720	640	604	622	194	190	**192**	**1.92E+05**	**52**
wild-type LT	123	143	133	100	123	112	36	28	**32**	**3.20E+04**	**313**
dl89-97 LT	119	97	108	75	63	69	24	37	**31**	**3.10E+04**	**323**
E90A LT	56	54	55	57	55	56	20	18	**19**	**1.90E+04**	**526**
W91A LT	56	71	64	62	38	50	8	17	**13**	**1.30E+04**	**769**
E92A LT	77	113	95	64	58	61	17	23	**20**	**2.00E+04**	**500**
Q93A LT	138	124	131	115	99	107	27	37	**32**	**3.20E+04**	**313**
W94A LT	114	116	115	131	135	133	72	49	**61**	**6.10E+04**	**164**
W95A LT	120	147	134	135	150	143	28	20	**24**	**2.40E+04**	**417**

Table 3.3: Fine mapping of the Bub1-LT binding site: retroviral transduction of NIH 3T3 cells with LT substitution mutants to determine viral titres.

All colony count data is shown, excluding counts from the 500µl retroviral supernatant, 1 in 10 split plates which had too many colonies to accurately count. The average counts from the 100µl retroviral supernatant, 1 in 50 split plates were used to calculate the viral titres because the other plates had larger and possibly less reliable colony counts. Volume of retroviral supernatant required for doses equivalent to 500µl of 2.00E+04 titre were calculated by dividing 2.00E+04 (titre wanted) by the viral titre and multiplying by 500(µl) for each construct.

Table 3.4: Raw data for immortalisation efficiency of the LT substitution mutant constructs.

Duplicate experiments are shown (A & B). The first table in section A shows viral titres re-calculated using NIH 3T3 colony counts from plates infected with the new equivalent doses of retroviral supernatants (Formula 3.2). The tables of REF colony counts in A and B use these new titres to calculate the immortalisation efficiencies of the constructs relative to wild-type LT from the 1 in 8 and the 1 in 16 plates (Formula 3.3). The number of colonies that expanded for each construct are also shown for each experiment.

A: Alanine Linker Scan Immortalisation Efficiency Expt. 1:

NIH 3T3: Retroviral vector pBabe-puro(ori-) -	Volume (μl) retroviral supn used to infect two plates of cells:	Number of colonies 1 in 50 split			VIRAL TITRE
		Plate 1	Plate 2	Average	
empty vector	26	131	123	127	4.88E+05
wild-type LT	157	83	98	91	5.80E+04
dl89-97 LT	162	132	116	124	7.65E+04
E90A LT	263	12	42	27	1.03E+04
W91A LT	386	124	124	124	3.22E+04
E92A LT	250	37	63	50	2.00E+04
Q93A LT	157	80	48	64	4.08E+04
W94A LT	82	47	39	43	5.24E+04
W95A LT	209	89	97	93	4.45E+04

REF: Retroviral vector pBabe-puro(ori-) -	Volume (μl) retroviral supn used to infect two plates of cells:	VIRAL TITRE	Number of colonies 1 in 8 split			Immortalisation efficiency relative to wild-type LT (%)	Number colonies expanded
			Plate 1	Plate 2	Average		
empty vector	52	4.88E+05	(contam.)	(contam.)	-	-	(0/0)
wild-type LT	313	5.80E+04	34	35	35	100.00	1/3
dl89-97 LT	323	7.65E+04	71	57	64	134.34	2/3
E90A LT	526	1.03E+04	58	51	55	526.56	3/3
W91A LT	769	3.22E+04	136	142	139	291.16	5/5
E92A LT	500	2.00E+04	56	45	51	264.53	3/3
Q93A LT	313	4.08E+04	53	72	63	255.88	1/2
W94A LT	164	5.24E+04	41	60	51	307.82	4/5
W95A LT	417	4.45E+04	80	74	77	215.23	5/5

REF: Retroviral vector pBabe-puro(ori-) -	Volume (μl) retroviral supn used to infect two plates of cells:	VIRAL TITRE	Number of colonies 1 in 16 split			Immortalisation efficiency relative to wild-type LT (%)	Number colonies expanded
			Plate 1	Plate 2	Average		
empty vector	52	4.88E+05	(contam.)	(contam.)	-	-	
wild-type LT	313	5.80E+04	16	22	19	100.00	
dl89-97 LT	323	7.65E+04	23	34	29	112.14	
E90A LT	526	1.03E+04	29	(contam.)	29	511.44	(as
W91A LT	769	3.22E+04	98	(contam.)	98	378.15	above)
E92A LT	500	2.00E+04	27	29	28	267.53	
Q93A LT	313	4.08E+04	24	38	31	231.94	
W94A LT	164	5.24E+04	18	30	24	266.84	
W95A LT	417	4.45E+04	36	38	37	190.61	

B: Alanine Linker Scan Immortalisation Efficiency Expt. 2:

(Viral titres are identical for the two experiments, which were conducted simultaneously)

REF: Retroviral vector pBabe-puro(ori-) -	Volume (μl) retroviral supn used to infect two plates of cells:	VIRAL TITRE	Number of colonies 1 in 8 split			Immortalisation efficiency relative to wild-type LT (%)	Number colonies expanded
			Plate 1	Plate 2	Average		
empty vector	52	4.88E+05	0	1	1	2.98	(0/0)
wild-type LT	313	5.80E+04	30	18	24	100.00	1/3
dl89-97 LT	323	7.65E+04	69	62	66	202.04	3/3
E90A LT	526	1.03E+04	70	67	63	879.59	3/3
W91A LT	769	3.22E+04	120	145	133	406.28	5/5
E92A LT	500	2.00E+04	58	50	54	408.47	3/3
Q93A LT	313	4.08E+04	78	66	72	426.47	3/3
W94A LT	164	5.24E+04	31	32	32	281.67	5/5
W95A LT	417	4.45E+04	85	109	97	395.40	5/5

REF: Retroviral vector pBabe-puro(ori-) -	Volume (μl) retroviral supn used to infect two plates of cells:	VIRAL TITRE	Number of colonies 1 in 16 split			Immortalisation efficiency relative to wild-type LT (%)	Number colonies expanded
			Plate 1	Plate 2	Average		
empty vector	52	4.88E+05	2	0	1	4.77	
wild-type LT	313	5.80E+04	16	13	15	100.00	
dl89-97 LT	323	7.65E+04	31	24	28	137.14	
E90A LT	526	1.03E+04	33	37	35	781.85	(as
W91A LT	769	3.22E+04	78	66	72	351.91	above)
E92A LT	500	2.00E+04	31	24	28	338.87	
Q93A LT	313	4.08E+04	45	25	35	331.70	
W94A LT	164	5.24E+04	14	18	16	225.33	
W95A LT	417	4.45E+04	46	58	52	339.15	

Table 3.4: Raw data for immortalisation efficiency of the LT substitution mutant constructs.

The immortalising efficiencies of the constructs relative to wild-type LT are summarised and displayed in a graphical format in Figure 3.5. Within each separate experiment, and between the repeated experiments, the 1 in 8 and 1 in 16 split plate counts reveal consistent results for the immortalising efficiencies of the constructs tested. All LT constructs were able to efficiently immortalise REFs, and almost all clones tested could be expanded to passage 5, indicating that the cells really were immortal. Only 2 colonies out of 6 that were single cell cloned and passaged for the wild-type LT construct reached passage 5 on this occasion (See Figure 3.5A). This is in contrast to the results from the initial immortalisation efficiency tests (see Figure 3.2A) where all 12 wild-type LT-immortalised REF clones could be expanded, but should not be given too much importance because the clones that failed to grow did so at the first passage, most likely due to too few cells surviving the ring-cloning process.

As expected, empty vector is not able to immortalise REFs efficiently (See Figure 3.5B). Dl89-97 LT appears (as seen previously) to be a slightly better immortalising gene than wild-type LT. Surprisingly, each of the single amino acid mutations to alanine tested within the 89-97 region of LT cause LT to be an even more efficient immortaliser than the deletion mutant dl89-97.

3.3.2.2 Dl89-97 mutant of LT is the most defective for Bub1 binding.

Whole cell lysates were prepared from selected single cell clones of REFs expressing each of the LT substitution mutants, and wild-type LT and dl89-97 LT. Passage 2 (P2) REFs were lysed as a negative control, as these cells do not express LT, but are still proliferative as they have yet to senesce.

30μg of whole cell lysates were western blotted using a rabbit polyclonal antiserum raised against the amino terminal 303 residues of hBub1 (see Figure 3.6). A 150kDa Bub1 band was seen in all lanes, at approximately the same intensity for each lysate, indicating that the expression level of Bub1 protein was equivalent between the different cell lines.

A

REF:	Immortalisation Efficiency Relative to Wild-type LT (%)				
Retroviral vector pBabe-puro(ori-) -	Expt. 1 calculated using 1 in 8 split plates	Expt. 1 calculated using 1 in 16 split plates	Expt. 2 calculated using 1 in 8 split plates	Expt. 2 calculated using 1 in 16 split plates	Number colonies expanded
empty vector	-	-	2.98	4.77	(0/0)
wild-type LT	100	100	100	100	2/6
dl89-97 LT	134.34	112.14	202.04	137.14	5/6
E90A LT	526.56	511.44	879.59	781.85	6/6
W91A LT	291.16	378.44	406.28	351.91	10/10
E92A LT	264.53	267.53	408.47	338.87	6/6
Q93A LT	255.88	231.94	426.47	331.7	4/5
W94A LT	307.82	266.84	281.67	225.33	9/10
W95A LT	215.23	190.51	395.4	339.15	10/10

B

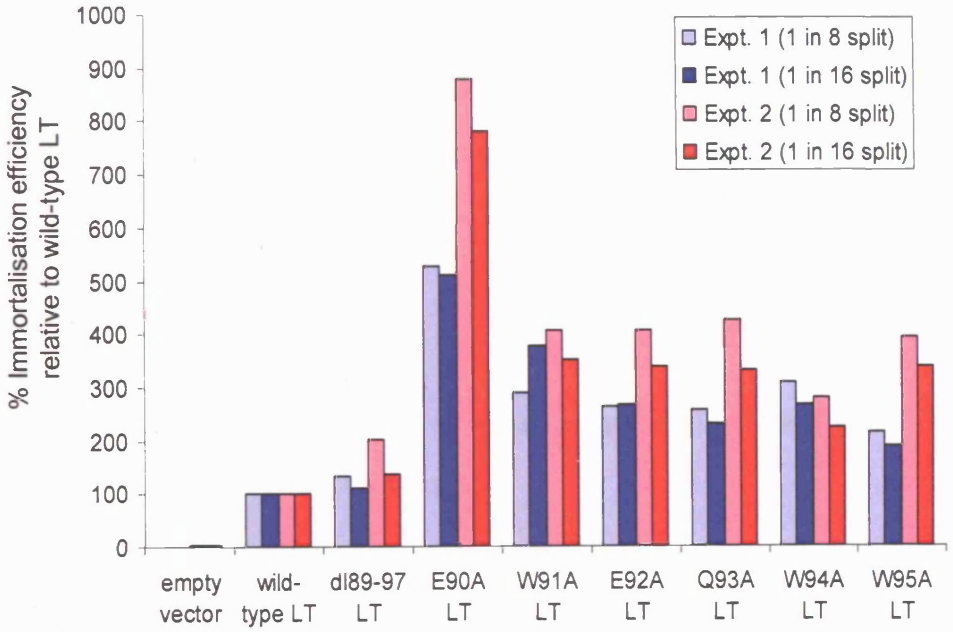

Figure 3.5: Immortalisation efficiency relative to wild-type of the LT substitution mutants.

Summary of immortalisation efficiencies calculated from REF colony counts at two different plating densities in two independent experiments, and the number of colonies that could be expanded (A). A graphical view of these results (B).

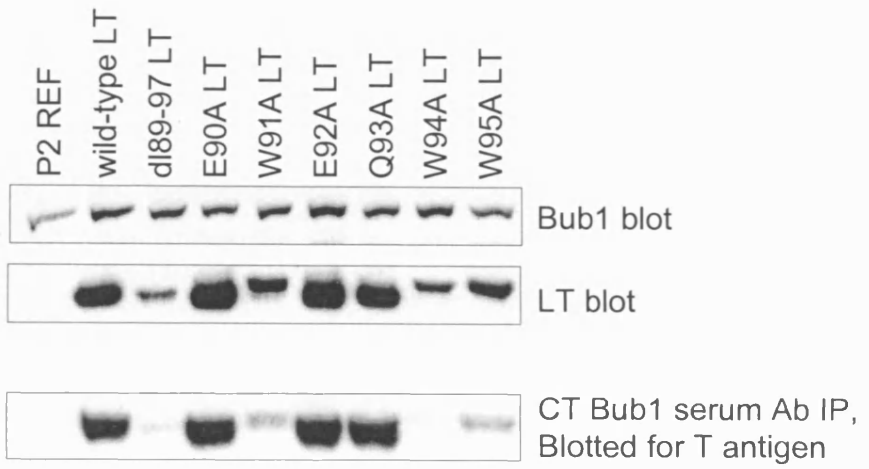

Figure 3.6: No single conserved residue in the 89-97 region of LT is necessary for Bub1 interaction.

REF cell lines, established by transduction with wild-type LT or with different substitution mutants of LT were used to fine map the Bub1-LT interaction site. In repeated co-immunoprecipitation experiments (one of which is shown here), the dl89-97 LT deletion mutant was very defective for Bub1 binding, and the tryptophan mutants W91A, W94A and W95A were also defective for Bub1 binding. E90A, E92A and Q93A LT mutants interact with Bub1 as strongly as wild-type LT. Passage 2 (P2) REF lysate is included as a negative control, and the relative expression levels of Bub1 and LT are shown.

Relative expression levels of the LT proteins in the different cell lines were demonstrated by western blotting 5μg of the whole cell lysates using a combination of LT mouse monoclonals PAb416, PAb419 & PAb423. 100kDa LT bands were observed for all cell lines except for the P2 REF negative control, as expected. However, it was noted that the dl89-97 and the tryptophan mutants, W91A, W94A and W95A of LT were expressed at a much lower level than wild-type LT, E90A, E92A or Q93A LTs. The dl89-97 LT clone shown in Figure 3.6 is "dl89-97 LT clone 2" as shown in Figure 3.3, where it appeared to have a similar level of expression to wild-type LT. However it is possible that the dl89-97 LT clone 2 lane shown in Figure 3.3 may have been overloaded (as suggested by the apparently higher expression level of Bub3 in the dl89-97 LT clone 2 lane of Figure 3.3, when compared to the other samples), resulting in an incorrect observation of equivalent LT expression level between wild-type LT and dl89-97 LT clone 2 in Figure 3.3. The LT mutants with lowered expression also demonstrated a slightly slower migration on SDS-PAGE, possibly due to a post-translational modification, and this was particularly noticeable for the tryptophan mutants (See Figure 3.6).

Bub1 was immunoprecipitated from 1mg of each of the whole cell lysates using a rabbit polyclonal antibody raised against the carboxy terminal amino acids 691-1085 of hBub1. The resulting precipitates were then immunoblotted for LT using a mixture of LT mouse monoclonals PAb416, PAb419 and PAb423, to determine which of the LT constructs was the most defective for interaction with Bub1 (Figure 3.6).

As expected, the P2 REF lane does not show Bub1-LT co-immunoprecipitation due to the absence of LT in these cells. LT is strongly co-immunoprecipitated with Bub1 in the wild-type LT, E90A, E92A and Q93A lysates, as can be seen by comparing the intensity of the 100kDa LT bands brought down via Bub1 with the level of LT expression seen in the whole cell lysates LT blot. In repeated experiments, the most defective for Bub1 binding was the original non-Bub1 binding mutant dl89-97 LT protein,

as virtually no LT band can be seen in the Bub1 immunoprecipitate for the cell line expressing this version of LT. The tryptophan mutants W91A, W94A and W95A appeared slightly defective for Bub1 binding, as the 100kDa LT bands seen in the Bub1 immunoprecipitations for cell lines expressing these LT proteins were of a lower intensity than would be expected given the amount of LT expressed in these cell lines. In the experiment shown in Figure 3.6 the tryptophan mutants appear to be just as defective for Bub1 binding as the dl89-97 deletion of LT. However when repeated they showed slightly more intense bands. Therefore, the co-immunoprecipitation data in Figure 3.6 should be treated qualitatively. One interpretation of the data could be that the LT mutants that co-immunoprecipitate decreased levels of Bub1 do so purely due to their lowered LT expression levels, and not because of a decreased ability of the LT to interact with Bub1. However the reduced interaction of dl89-97 LT (and to some extent W91A, W94A and W95A LT) with Bub1 has also been demonstrated very convincingly in experiments using the same LT mutants, but expressed in Rat-1 cells (Cotsiki *et al.*, 2004). The level of expression of LT in the Rat-1 cells was very similar between the wild-type and the mutant LT cell lines, due to prior screening of single cell clones for equivalent LT expression levels. Transient transfected cells or a pool of permanently transfected cells were not used because it was not possible to obtain pools of cells with equivalent LT expression between the cell lines. REFs expressing wild-type or mutant LT were also screened for single cell clones with high and equivalent expression levels of the LT protein, but unfortunately it was not possible to find clones of dl89-97, W91A, W94A or W95A LT expression any higher than that shown in Figure 3.6. Given more time a greater number of clones would have been screened for LT expression level to try to remedy this issue.

3.3.3 Transformation efficiency of wild-type LT versus dl89-97 LT

Bub1 mutations have been occasionally identified in certain types of human cancer characterised by chromosomal instability and aneuploidy, such as colorectal cancer (Cahill *et al.*, 1998; Ru *et al.*, 2002; Shichiri *et al.*, 2002), raising the possibility that interaction of Bub1 with LT might be contributing to its transforming activity. It has long been known that SV40 LT has the ability to transform, but that it is not a *bona fide* transforming gene such as *ras* or Polyoma middle T antigen. The Roberts laboratory have shown that when transfected with dl89-97 LT or one of the tryptophan substitution LT mutants, Rat-1 cells fail to form the dense foci indicative of transformation that are seen when the cells are transfected with wild-type LT or one of the other LT mutants (Cotsiki *et al.*, 2004).

These findings are reiterated by a similar focus assay, this time conducted in NIH 3T3 cells. NIH 3T3 cells stably transfected with either pSUPERretro (empty vector) or pSUPERretro-Bub1 (allowing knockdown of Bub1 expression via RNAi interference (RNAi); vectors kindly provided by Dr Ole Gjoerup, and described in more detail in Chapter 4) were transduced with retroviral supernatants containing packaged pBabe-puro(empty vector), pBabe-puro(wild-type LT) or pBabe-puro(dl89-97 LT), as described earlier in this chapter.

Viral titres calculated previously were used to determine the relative volume of each supernatant to use for equivalent infections. Untransfected NIH 3T3 cells were transduced with these volumes of supernatant, split 24 hours later (1 in 10 and 1 in 50, in duplicate) into puromycin selection, and stained with methylene blue 8 days later to count the number of colonies on each plate. Estimations for equivalent volumes of the retroviral supernatants were very accurate for pBabe-puro(wild-type LT) and pBabe-puro(dl89-97 LT), as can be seen by the average colony counts from the viral titre plates (see Figure 3.7A). The colony counts for these vectors were very similar, allowing focus assay plates using these volumes of retroviral supernatant for

the infection to be directly compared for the relative transformation potential of wild-type versus dl89-97 LT. The colony counts for the NIH 3T3 cells transduced with pBabe-puro(empty vector) were higher than those for the other vectors, but this was not so crucial as this vector was not expected to induce focus formation in the cells, and so using too much of this retrovirus would only highlight the relative inability of the empty vector to transform.

NIH 3T3(pSUPERretro-empty vector) and NIH 3T3(pSUPERretro-Bub1) cells were transduced (on duplicate plates) with four times the volume of pBabe-puro- retroviral supernatants used to confirm similar colony counts, as shown in Figure 3.7A. (four times the volume of supernatant was used compared to the viral titre infections, to account for the relatively low transformation efficiency of LT). 24 hours later, the duplicate plates were pooled, and split 1 in 8 to 4 plates, with only 2% serum (donor calf serum, DCS) in the medium. The reason for this reduction in serum concentration was to reduce the number of spontaneous foci that are seen when conducting this assay in NIH 3T3 cells. Puromycin selection was not used for the focus assay plates because the cells were already puromycin resistant, due to the pSUPERretro- vectors that they already carried.

Cells were maintained at 37°C with media changes every 3-4 days. 23 days post-transduction, all plates were stained with Crystal Violet, to visualise the transformed foci (see Figure 3.7B&C). The results of the transformation assay conducted by Dr Roberts laboratory in Rat-1 cells (Cotsiki *et al.*, 2004) is reiterated by this focus assay using NIH 3T3 cells, as seen in the representative plates shown in Figure 3.7B. pBabe-puro(empty vector)-transduced NIH 3T3(pSUPERretro-empty vector) cells do not show any dense foci, indicating that the low serum conditions have reduced spontaneous transformation of NIH 3T3 cells.

Figure 3.7: Transformation-competence of wild-type versus dl89-97 LT in NIH 3T3 cells with normal and lowered levels of Bub1 expression.

Table showing the relative proportions of retroviral supernatants used for each pBabe-puro construct (empty vector, wild-type LT or dl89-97 LT) for focus formation assays in NIH 3T3 cells, indicating that they result in approximately equal colony counts (and hence transduction efficiencies) for the LT constructs (A). Representative plates showing focus formation for each construct in NIH 3T3(pSUPERretro-empty vector) cells (B), and in NIH 3T3(pSUPERretro-Bub1) cells (C), which have reduced expression of the Bub1 protein.

Wild-type LT has the ability to induce foci (indicative of transformation) whereas dl89-97 (non-Bub1-binding) LT does not. The same result is seen in cells with both normal and reduced levels of Bub1 expression.

A

Retroviral vector:	Vol. (μl) retroviral supn. per infection	Colony counts: 1 in 10 split:		Average:	1 in 50 split:		Average:
pBabe-puro(empty vector)	30	1568	1504	**1536**	592	640	**616**
pBabe-puro(wild-type LT)	250	992	904	**948**	412	420	**416**
pBabe-puro(dl89-97 LT)	102	784	840	**812**	414	450	**432**

B

NIH 3T3(pSUPERretro):

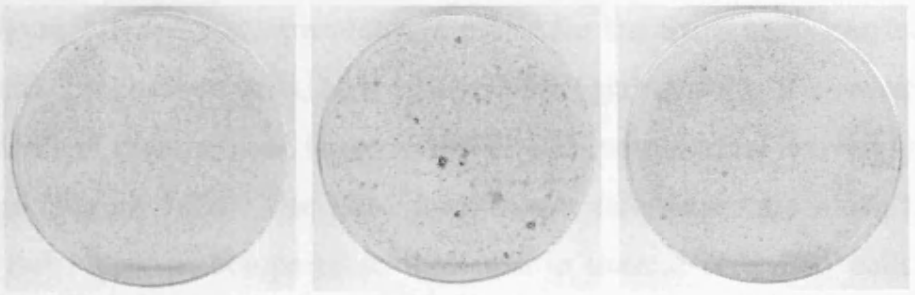

pBabe-puro-(empty vector)

pBabe-puro-(wild-type LT)

pBabe-puro-(dl89-97 LT)

C

NIH 3T3(pSUPERretro-Bub1):

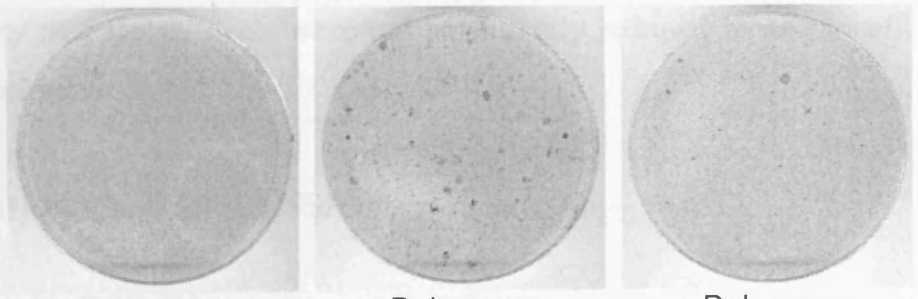

pBabe-puro-(empty vector)

pBabe-puro-(wild-type LT)

pBabe-puro-(dl89-97 LT)

Figure 3.7: Transformation-competence of wild-type versus dl89-97 LT in NIH 3T3 cells with normal and lowered levels of Bub1 expression.

The cells transduced with pBabe-puro(wild-type LT) show a moderate number of dense foci, indicating the transforming abilities of this protein. As seen in Rat-1 cells however, the dl89-97 LT-containing retrovirus induces a much lower number of dense foci than the wild-type LT, indicating that dl89-97 LT is transformation defective. The NIH 3T3 colony counts shown in Figure 3.7A are very similar between the wild-type and dl89-97 LT constructs, verifying that these focus assay plates can be directly compared.

Figure 3.7C shows representative plates for the focus assay carried out in the Bub1 knockdown cells, NIH 3T3(pSUPERretro-Bub1). The results are almost identical to those seen in the NIH 3T3 cells with normal levels of Bub1 expression (Figure 3.7B). The Bub1 knockdown cells express a much lower level of Bub1 protein compared to that seen in normal NIH 3T3 cells (see Chapter 4, Figure 4.15). It was proposed that if wild-type LT induces efficient transformation via sequestering Bub1, dl89-97 LT might be able to efficiently transform cells in which Bub1 levels have been reduced. However, this is not observed (compare Figure 3.7 sections B and C). This does not rule out the possibility that Bub1 levels were not sufficiently reduced to see an effect in this experiment.

3.4 SUMMARY & DISCUSSION

The results presented in this chapter demonstrate that residues 89-97 of the SV40 LT protein are necessary for interaction with the spindle checkpoint protein Bub1. Finer mapping of the interaction site indicated that residues 90, 92 and 93 of LT are not important, whereas the tryptophan residues (91, 94 and 95) are important for the interaction with Bub1. The binding of LT with Bub1 is not involved in the immortalisation functions of the LT protein, but LT-Bub1 interaction is necessary for the transformation functions of LT.

Although the results presented in this chapter highlight the importance of the tryptophan residues in the 89-97 region of LT for Bub1 binding, it remains to be seen if a particular set of these tryptophan residues delimit the

Bub1 binding site. The mapping experiments shown here have also been replicated in human U20S cells and in Rat-1 cells by members of Tom Roberts' laboratory at the Dana Farber Cancer Institute, Boston, MA (Cotsiki *et al.*, 2004), providing further validation for the results presented here. In Rat-1 cells the dl89-97 mutant and the tryptophan substitution mutants in this region showed a retarded mobility on SDS-PAGE and a lower level of expression than wild-type LT, reiterating the results seen in the REFs. The retarded mobility could be due to some form of post-translational modification of the LT protein caused by the mutations, or could merely be a consequence of the substitution or deletion mutations. Further experiments are required to find the cause of these mobility differences. The significance of the low expression level of the LT mutants defective for Bub1 binding is not clear, although it may be related to inability of the cells to survive high levels of expression of these particular LT mutants. It remains to be proven that the Bub1-LT interaction is direct. In the future, it would be interesting to try *in vitro* binding assays using recombinant Bub1 and LT proteins to try to answer this question.

Most importantly of all, the knowledge of the binding site of Bub1 on the LT protein opens up many avenues of research into the function of the interaction. The dl89-97 LT-expressing cell lines generated can now act as tools to study the effects that LT is having on the spindle checkpoint, as they provide a control for the difference between effects caused specifically by the Bub1-LT interaction, and effects caused by other functions of LT.

It has also been shown that an additional mutant of LT lacking residues 98-102 (dl98-102) fails to co-precipitate with Bub1, suggesting that residues 89-97 of LT may not represent the entire Bub1 interaction site (personal communication, Dr Ole Gjoerup). However the Bub1-LT interaction is sufficiently disrupted in cells expressing dl89-97 LT to prevent co-immunoprecipitation, and also to prevent the compromise of Bub1 spindle checkpoint functions seen in cells with wild-type LT (See Chapter 5). It would be interesting to investigate the immortalisation efficiency of the dl98-102 LT

mutant in the future, as well as to determine the checkpoint function of Bub1 in the context of this LT deletion mutant.

The Roberts laboratory has proposed that LT is acting as a scaffold to bring p53 into proximity with Bub1, causing p53 to be phosphorylated on serines 15 and 37 (Gjoerup *et al.*, submitted 2004: SV40 large T antigen reveals a functional connection between Bub1 and p53). They have demonstrated that this Bub1-mediated phosphorylation is essential for the stabilisation of p53 elicited by LT, and is also required for LT-induced acetylation of p53. In addition, it may also contribute to CBP/p300 binding by LT. It was also shown that the microtubule-depolymerising drug nocodazole induced phosphorylation of p53 on serines 15 and 37 in a Bub1-dependent manner. They suggest that LT is thus taking over a cellular signalling mechanism by recruiting Bub1 to phosphorylate p53 on serines 15 and 37 and inducing acetylation at lysines 373 and 382, leading to p53 stabilisation in the absence of spindle damage. In this way, LT is inactivating but at the same time stabilising one tumour suppressor, p53, in order to make a trap for a second tumour suppressor, p300. However, the data presented in Figure 3.3 of this chapter (showing the relative expression levels of p53 in REFs expressing different LT mutants) is contradictory to the findings of the Roberts laboratory. Two of the cell lines expressing dl89-97 LT displayed equally high levels of p53 as that seen in cells expressing wild-type LT, indicating that the protein is just as stable, even in the absence of Bub1 interaction. If these results were consistent with the Roberts laboratory, all dl89-97 clones would show low p53 expression, as seen in the p53 blot of dl89-97 LT clone 1. Further verification of these results would be needed to determine their significance, as currently no explanation can be given for these observations.

The inability of the dl89-97 LT to interact with Bub1 does not affect the ability of the protein to stably immortalise primary REFs. Furthermore, the results presented here suggest that inability to bind to Bub1 actually increases the immortalising efficiency of LT. The E90A LT mutant was the most efficient immortalising protein of all the mutants tested. However, this does

not appear to be directly related to Bub1 binding of LT because E90A was not defective for Bub1 binding. Perhaps the inability of dl89-97 LT to disturb the spindle checkpoint is in some way increasing the survival rate of its primary cell targets, possibly via protection from the problems associated with aneuploidy. Alternatively, this apparent gain of function could be due to an increase in proliferation (see Figure 5.2 for an indication of a faster growth rate of dl89-97 LT-expressing cells), or perhaps a decrease in apoptosis in the dl89-97 LT-expressing cells, resulting in observation of a higher than expected immortalisation efficiency. The LT mutants with single substitutions to alanine that were tested in the dl89-97 region appeared to be even more powerful immortalising proteins than dl89-97 or wild-type LT, although there is currently no obvious explanation for this. This result has been repeated and is therefore unlikely to be trivial, although further work is needed to determine the cause of the apparent increased immortalisation efficiency of LT mutated within residues 89-97. However this observation is very interesting and unexpected, and suggests that dl89-97 LT could in some way act as a more efficient immortalising agent than the wild-type LT protein.

Published data (Cotsiki *et al.*, 2004), along with data presented in this chapter demonstrate that dl89-97 LT is defective for transformation, while retaining the ability to immortalise primary cells. This demonstrates for the first time that the immortalisation functions of LT can be separated from the transformation functions of the protein. If the interaction with Bub1 turns out to be crucial for the ability of LT to induce aneuploidy, then this finding is given greater credence by the link between aneuploidy and tumourigenesis that has been suggested many times in the literature (Draviam *et al.*, 2004; Saraga *et al.*, 1997; Tutt *et al.*, 1999). It has also been shown that reduction of Bub1 levels in human fibroblasts results in a low frequency of aneuploid clones capable of anchorage-independent growth (another measure of transformation), providing more evidence in support of a role for Bub1 in LT-mediated oncogenic transformation (Musio *et al.*, 2003). Further work is necessary to demonstrate the link between LT, Bub1 and aneuploidy in

primary cells, especially in human cells, which are known to have a more stable genome. In fact, initial studies of the karyotype of human mammary fibroblasts and epithelial cells immortalised with hTERT and either wild-type or dl89-97 LT recently carried out in the laboratory indicate that while dl89-97-immortalised cells are near diploid, wild-type LT appears to induce an aneuploid phenotype.

Tom Roberts' colleagues have also shown that these Bub1-binding deficient LT mutants, along with D44N LT, are defective for replication of the SV40 viral DNA (personal communication). *In vivo* DNA replication assays were performed essentially using a previously described method (Gjorup *et al.*, 1994). Initiation of SV40 viral DNA replication requires formation of a complex at the SV40 origin, consisting of the virus-encoded LT protein, and three cellular proteins, replication protein A (RPA), DNA polymerase α/primase (pol/prim) and topoisomerase I (topo I) (reviewed in (Simmons, 2000)). Replication of SV40 DNA is initiated when LT binds to the SV40 origin and forms a double-hexameric structure. Pol/prim is the first cellular protein to interact with the origin-bound double-hexameric LT, followed by topo I and RPA (Simmons *et al.*, 2004). It has been shown that topo I binds LT at two sites, the first mapping to amino terminal residues 83-160 of LT, and the second mapping to carboxy terminal residues 602-708 (Roy *et al.*, 2003). The possibility therefore presents itself that the inability of dl89-97 LT to allow viral DNA replication could be due to deletion of residues crucial for the binding of topo I, although this remains to be determined. However, it could be the ability of LT to bind Bub1 that is critical for viral DNA replication and hence survival of the SV40 virus itself, and the inhibition of Bub1 function resulting in failure of accurate chromosome segregation could be secondary to this. The tryptophan residues in the 89-97 region of LT were the most critical for viral DNA replication (personal communication, Dr Ole Gjoerup), consistent with their importance for the transformation function of LT, and further suggesting a link between Bub1 and SV40 viral replication.

Future experiments that may aid in our understanding of the Bub1-LT interaction would include mutation of all 3 tryptophan residues in the 89-97 region of LT simultaneously, to determine if they constitute the core binding region of Bub1 on LT. Primary cells could also be transduced with the different LT mutants and their karyotype determined over successive passages, to further examine the possibility that LT is inducing aneuploidy via its interaction with the Bub1 spindle checkpoint protein. This seems a likely possibility, as temporary inhibition of Bub1 by RNAi and ribozyme-mediated methods in primary human fibroblasts has been shown to result in a statistically significant number of aneuploid cells (15%) (Musio *et al.*, 2003). Although most of these aneuploid cells underwent apoptosis, some were able to escape programmed cell death and gave rise, at low frequency, to anchorage independent clones. The aneuploidy phenotype persisted in culture, even though the inhibition of Bub1 was only temporary. It was noted however that these anchorage independent clones had not yet acquired a neoplastic phenotype, because they were unable to grow when injected subcutaneously in nude mice. This suggests that a second mutational event is required for the full transformation phenotype. It may therefore be interesting to inject nude mice with pools of clones expressing either wild-type LT, dl89-97 LT or the tryptophan point mutants of LT in this region to determine if the cells can induce tumours. Perhaps the inhibition by LT of p53, pRB and other host proteins could provide the primary event, and aneuploidy caused by LT inhibition of Bub1 could provide the secondary event required for effective neoplastic transformation. If the predictions made in this chapter are correct and dl89-97 LT-expressing cells have a stable chromosome content, these cells should not have the capacity to induce tumour formation in nude mice. Alternatively, the capacity of the LT mutants to induce tumours in mice could also be tested by generating transgenic mice expressing recombinant LT linked to the rat insulin promoter, as described in (Hanahan, 1985). Wild-type LT was shown to cause tumours exclusively in the beta-cells of the endocrine pancreas in these transgenic mice, and it would be interesting to determine if

the LT mutants deficient for Bub1 binding are capable of generating similar tumours.

A sequence alignment of the polyomavirus large T antigens demonstrated conservation within the 89-97 region of SV40 LT for several of these large T antigen proteins, in particular human BK polyomavirus, human JC polyomavirus, bovine polyomavirus, and Kilham strain of polyomavirus (see Figure 3.4). A prediction could therefore be made that each of these large T antigens is likely to interact with Bub1 in the same way as SV40 LT, due to the homology observed in these residues. However, this remains to be tested. Murine polyomavirus large T antigen did not show any obvious homology in this region of the protein, and so it would be interesting to determine if this protein is able to interact with Bub1. If all polyomavirus large T antigens are found to interact with Bub1, regardless of sequence homology to the 89-97 region of SV40 LT, perhaps the protein structure of these regions need to be studied rather than their sequence in order to further elucidate the features of the Bub1-LT interaction site. These kinds of studies may provide more information about the mechanism by which LT is inhibiting the function of the Bub1 checkpoint kinase.

4. Generation of monoclonal antibodies against Bub1

4.1 OBJECTIVES

High quality antibodies against the mammalian Bub1 protein were not readily available when this project was begun. There were no good commercial antibodies against this protein, and only very small quantities of Bub1 antibody were obtainable via request from other laboratories. Attempts to use the available Bub1 antibodies for immunoprecipitation and immunofluorescence studies of the Bub1-LT interaction in the mouse had not been very successful, and the antibodies tested did not appear to be particularly specific for Bub1 in either mouse, rat or human, recognising many bands on a western blot. For this reason it was decided to develop monoclonal antibodies against the mouse Bub1 protein to aid future studies of the Bub1-LT interaction in NIH 3T3 cells.

4.2 EXPERIMENTAL STRATEGY

The mouse Bub1 protein (mBub1) was cloned in two halves into the expression vector pET-23a(+), incorporating a histidine tag into the carboxy terminus of each protein sequence. The mBub1 protein is on the upper limit for expression of proteins in *E. coli* (1058 amino acids), and it was for this reason that it was decided to express it as two separate his-tag proteins, representing the amino-terminal (NT) and carboxy-terminal (CT) halves of the protein. A rabbit polyclonal antibody raised against the carboxy-terminal region of Bub1 immunoprecipitated Bub1 better than an antiserum raised against the amino-terminus of Bub1 (Personal communication, Dr Raimundo Freire). Conversely, Bub1 antibodies directed against the amino-terminus of Bub1 appeared to be particularly good for western blotting, while also being useful for immunoprecipitation. Also, the kinase domain of Bub1 is located in the carboxy-terminus of the protein, whereas the amino-terminus has other

activities. For these reasons, it was thought that raising antibodies against the Bub1 protein in two halves would increase the chances of obtaining reagents for future studies of the Bub1-LT interaction, and would possibly result in antibodies targeted against the different activities of the Bub1 checkpoint kinase.

His-tagged mBub1 proteins were expressed in the *E. coli* strain BLR λDE3 pLysS, and purified via affinity chromatography in sufficient quantities for immunisation. Several mice were immunised and boosted with either NT or CT mBub1 protein, and test bleeds were screened by western blotting. Splenocytes were prepared from the mice with the most promising test bleeds for the NT and CT mBub1 antibodies, and fused with a myeloma cell line to produce hybridomas. Pools of hybridoma cells then went through successive rounds of screening by ELISA, western blotting and immunoprecipitation, isotyping, and sub-cloning of the best pools until single cell clones secreting the best possible antibodies were obtained.

The specificities of the monoclonal antibodies generated were determined via several means, including western blotting of exogenously expressed HA-tagged Bub1 protein, western blotting of lysates with Bub1 levels knocked-down by RNAi, and immunolocalisation experiments. The monoclonal antibodies were also affinity purified using Protein G columns, and tested for their abilities to detect the Bub1-LT interaction.

4.3 RESULTS

4.3.1 Generation of mBub1 antigens

4.3.1.1 PCR and cloning strategy for generation of pET-23a(+)-mBub1-His-Tag expression vectors

The mBub1 cDNA (a gift from the McKeon laboratory that originally cloned it (Taylor and McKeon, 1997)) had previously been cloned into the pcDNA3.1(+) (Invitrogen) expression vector by Teena Puri, a final year

undergraduate project student in the laboratory, to allow ectopic expression of mBub1 in mammalian cells (see Appendix I for pcDNA3.1(+/-) vector map). This vector was used as a template for PCR amplification of the mBub1 cDNA in two sections, which were then cloned into the bacterial expression vector pET-23a(+) (Novagen). The cDNA sequence of mBub1 was divided into two sections of approximately equal size, representing codons 1-561 and 562-1058, and thus between them coding for the entire mBub1 protein. Residue 562 of mBub1 (a methionine residue) was chosen to begin the CT mBub1 protein sequence to prevent the need to add a start site to the sequence, possibly changing the structure of the protein.

The vector map for pET-23a(+) is shown in Figure 4.1. The pET system was developed for cloning and expression of recombinant proteins in *E. coli*. Plasmids are established in a non-expression host, and are later transformed into a host bearing the T7 RNA polymerase gene (λ DE3 lysogen) for expression of target proteins. Figure 4.2 shows the context in which the mBub1 PCR products were cloned into the pET-23a(+) vector, and the primer sequences used. The restriction sites of many of the favoured restriction enzymes present in the multiple cloning site of the pET-23a(+) vector were also found in the mBub1 cDNA sequence. For this reason, the restriction enzymes XbaI and BamHI were chosen for the cloning because the mBub1 cDNA sequence does not contain any restriction sites recognised by these enzymes (See Figure 4.2A). The XbaI site is upstream of the ribosome binding site in the pET-23a(+) vector, and for this reason it was necessary to include the ribosome binding site sequence in the forward primers for the PCR amplification of the two Bub1 proteins (See Figure 4.2B). The reverse primers were designed to incorporate a 6 residue histidine tag into the carboxy-terminus of the mBub1 proteins, and thus did not make use of the His-Tag sequence already incorporated into the pET-23a(+) expression vector.

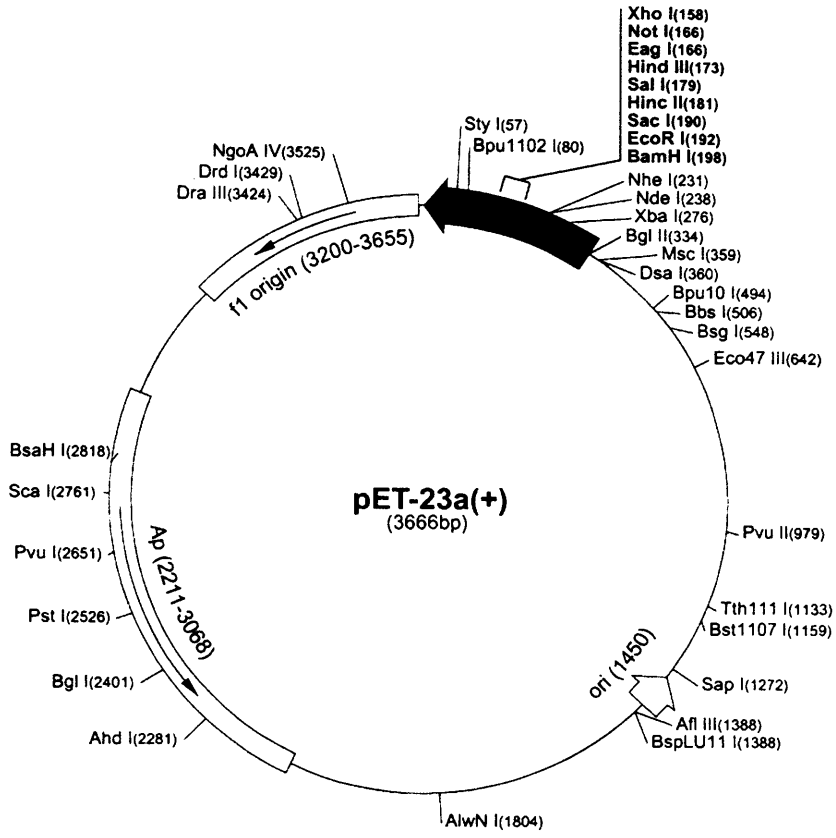

Figure 4.1: Vector map of expression vector pET-23a(+).

Vector designed by Novagen for expression of recombinant proteins in *E. coli* (plasmid map taken from novagen website, www.novagen.com). pET-23a(+) is an expression vector, and target genes are transcribed under control of the strong bacteriophage T7 promoter.

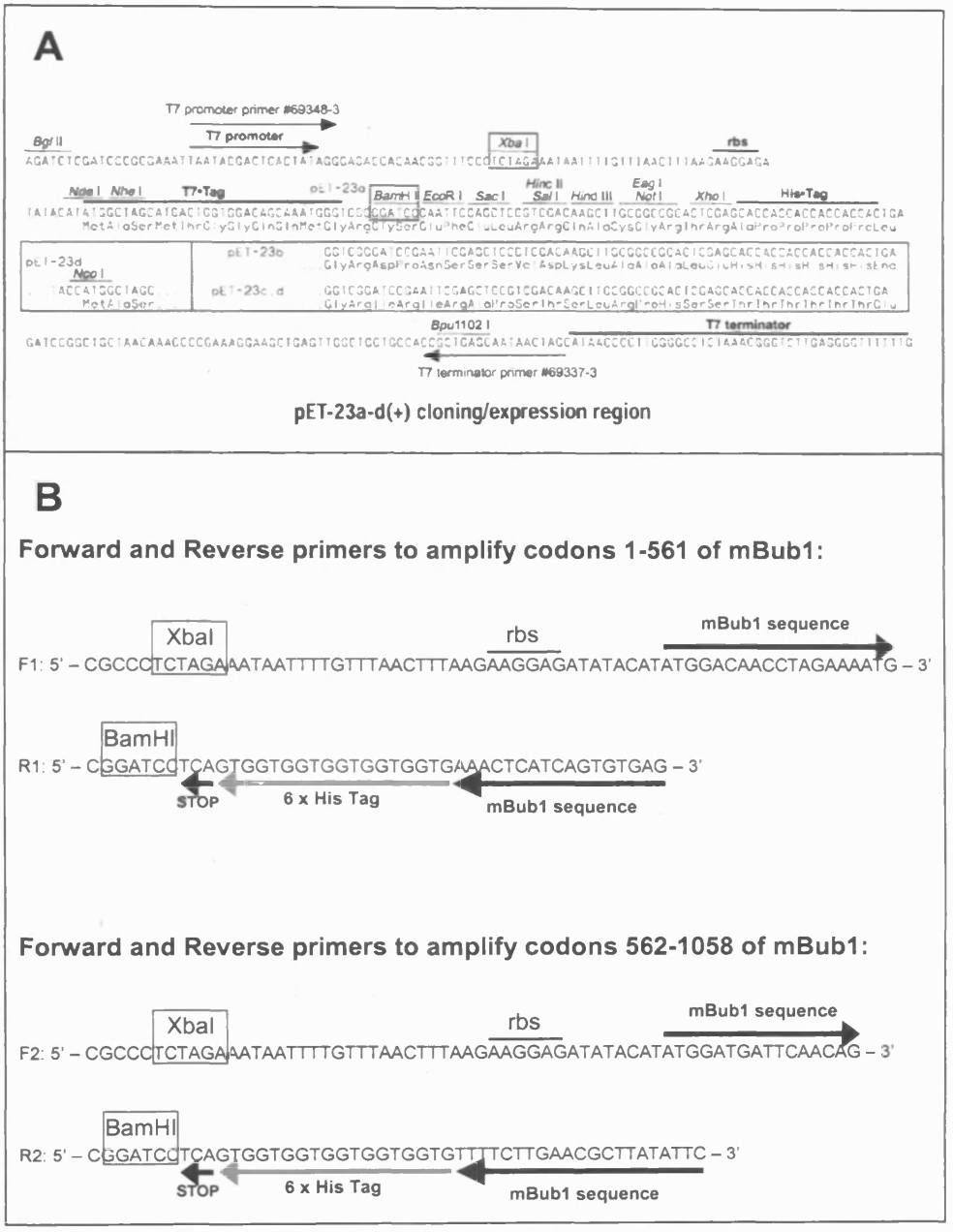

Figure 4.2: Cloning mBub1 into the pET-23a(+) expression vector.

Location of the XbaI and BamHI restriction sites in the pET-23a(+) vector used for cloning of mBub1 PCR products (A). Sequence of the forward (F) and reverse (R) primers used to PCR amplify mBub1 codons 1-561 and codons 562-1058 (B). A XbaI restriction site and the prokaryotic ribosomal binding site (rbs) are incorporated into each of the forward primers, and a BamHI restriction site, stop codon and 6 x Histidine Tag are incorporated into each of the reverse primers.

The NT- ("mBub1(1-561)") and CT- ("mBub1(562-1058)") halves of mBub1 were PCR amplified using each of the two sets of primers. The Vent (*Thermococcus litoralis*) polymerase was used because it has 3'-5' exonuclease function, resulting in a higher fidelity than that seen with other polymerases such as Taq. The resulting PCR products and the pET-23a(+) vector were then digested with XbaI and BamHI restriction enzymes (see Figure 4.3). Bands of 1746bp and 1554bp were expected for mBub1(1-561) and mBub1(562-1058) PCR products, respectively, when digested with XbaI and BamHI. The pET-23a(+) vector was expected to produce a band of 3588bp when digested with these enzymes. The digested DNAs showed bands of the expected sizes when separated on a 1% agarose gel containing Ethidium Bromide (See Figure 4.3). These digested DNAs were excised and gel purified using a Qiagen kit. Purified digested PCR products were then ligated to the cut pET-23a(+) vector using T4 DNA ligase, and transformed into $CaCl_2$-competent JS4 strain *E. coli* cells (Sedivy *et al.*, 1987). JS4 strain, a *rec*A1 derivative of MC1061 that does not contain the T7 RNA polymerase gene, was used for the cloning stage to eliminate plasmid instability caused by expression of proteins potentially toxic to the host cell. Colonies were grown overnight at 37°C on ampicillin selection agar plates, and these were PCR screened for positive transformants. The screen produced 6 mBub1(1-561)-pET-23a(+) and 4 mBub1(562-1058)-pET-23a(+) positives, all of which were then transformed into $CaCl_2$-competent cells of the protein expression *E. coli* strain BLR λDE3 pLysS. The DNA sequence of the mBub1 insert was checked for each resulting positive clone, concomitantly with testing protein expression, as described below.

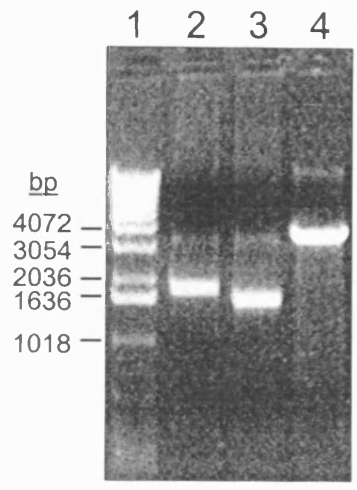

Lane:
1 – 1kb Ladder (GIBCO BRL)
2 – mBub1(1-561) PCR product, XbaI & BamHI restriction digest (expect 1746bp band)
3 – mBub1(562-1058) PCR product, XbaI & BamHI restriction digest (expect 1554bp band)
4 – pET-23a(+) vector, XbaI & BamHI restriction digest (expect 3588bp band)

Figure 4.3: Restriction digests of mBub1 PCR products and pET-23a(+)

PCR products encoding the amino- and carboxy-terminal halves of mBub1, along with the expression vector pET-23a(+) were digested with XbaI and BamHI restriction enzymes, yielding fragments of the expected sizes, ready for gel extraction and ligation.

4.3.1.2 Protein expression, solubility testing, and optimisation of protein purification

BLR λDE3 pLysS strain is a λDE3 lysogen derived from BL21 strain of *E. coli* and bears a copy of the T7 RNA polymerase gene under the control of the *lacUV5* promoter, which is inducible upon addition of isopropyl-β-D-thiogalactopyranoside (IPTG) to a growing culture (see Novagen website: www.novagen.com). T7 RNA polymerase transcribes the target DNA in the plasmid. Even in the absence of IPTG there is some residual expression of the T7 RNA polymerase from the *lacUV5* promoter, and therefore basal expression of the target protein. To minimise the effects of potential toxicity of the target protein to the host cells, this host strain is also pLysS. This means that it also contains a plasmid that provides a low level of T7 lysozyme, a natural inhibitor of T7 RNA polymerase. This plasmid also carries the chloramphenicol resistance gene. In addition, the BLR λDE3 pLysS strain is also recA-, allowing improved plasmid monomer yields, and stability of target genes containing repetitive sequences.

BLR λDE3 pLysS cells transformed with mBub1(1-561)-pET-23(a)+ and mBub1(562-1048)-pET-23(a)+ positive clones, were IPTG induced, and total protein was extracted from both "uninduced" and "induced" cultures. Samples were then run on 8% SDS-PAGE gels, and stained with Coomassie blue. All mBub1(1-561)-pET or mBub1(562-1058)-pET clones tested demonstrated expression of a 90kDa or a 70kDa protein, respectively, upon induction with IPTG (data not shown). It was therefore possible to check protein solubility and optimise purification conditions for the proteins, now that it was known that protein expression was being effectively induced by IPTG for both constructs.

Soluble proteins are fully folded in a (supposedly) native conformation, and often yield good monoclonal antibodies with relatively low injection doses. Monoclonal antibodies generated against a soluble protein are likely to be useful for immunoprecipitation, immunofluorescence, and other techniques where the target protein is in its native conformation (Carey Hanly *et al.*,

1995). Many proteins do not fold properly when expressed as recombinant proteins in bacteria, and form insoluble inclusion bodies in the cells. These insoluble proteins can be solubilised and if necessary refolded *in vitro*, although unfolded antigens are more immunogenic than antigens in their native form (Mayer, 2000), and often result in antibodies that are good at recognising the denatured form of the protein of interest, e.g. for use in western blotting.

To test the purification protocol for each of the mBub1 proteins, following IPTG-induction, the proteins were bound to nickel-nitrilotriacetic acid His-bind resin (Ni-NTA; Novagen) under native purification conditions, and tested for the ability to bind to and elute from the resin under these conditions. Ni-NTA resin has a very high affinity for proteins containing an affinity tag of six consecutive histidine residues - the 6xHis tag. Total protein extracts were prepared for "uninduced" and "induced" samples from two different clones of the mBub1(1-561)-pET construct (named 1-2-1 and 2-2-1), and for two different clones of the mBub1(562-1058)-pET construct (named 4-1-1 and 4-4-1). For each clone, 2ml of the induced culture that had not been subjected to total protein extraction was tested for solubility of the expressed protein, via protein mini-prep under native conditions. Cells were lysed and the His-tagged mBub1-derived protein was bound to Ni-NTA His-Bind resin, washed and eluted. The binding (and lysis) buffer contained a very low concentration (1mM) of imidazole, a small molecule which at high concentrations has a better affinity for the Ni-NTA resin than the His-tag proteins. This was included to reduce non-specific binding to the resin by proteins containing a few consecutive histidine residues. The wash buffer contained 10mM imidazole to wash away any proteins without a 6xHis-tag that had bound to the resin, and the elution buffer contained 250mM imidazole, to dissociate (elute) the protein of interest from the resin. Finally, samples were heated with Laemmli buffer, loaded on SDS-PAGE gels, and stained with Coomassie blue (See Figures 4.4 and 4.5).

Figure 4.4: Native mini-prep of mBub1(1-561)-His protein.

For each of two bacterial clones expressing (NT) mBub1(1-561)-His (clones 1-2-1 and 2-2-1), expression of a 90kDa protein (indicated by an arrow) is induced by IPTG (20μl (out of 100μl) of uniniduced (lanes 1 & 7) and IPTG-induced (lanes 2 & 8) total bacterial lysate are shown). This protein is successfully bound to Ni-NTA resin, as indicated by lack of this 90kDa protein in the "unbound protein" (20μl out of 100μl of the first resin wash) lanes (3 & 9). 20μl, successive elutions of the His-tag protein from each clone (lanes 4-6 & 10-12) demonstrate that this 90kDa protein can be purified in its soluble form.

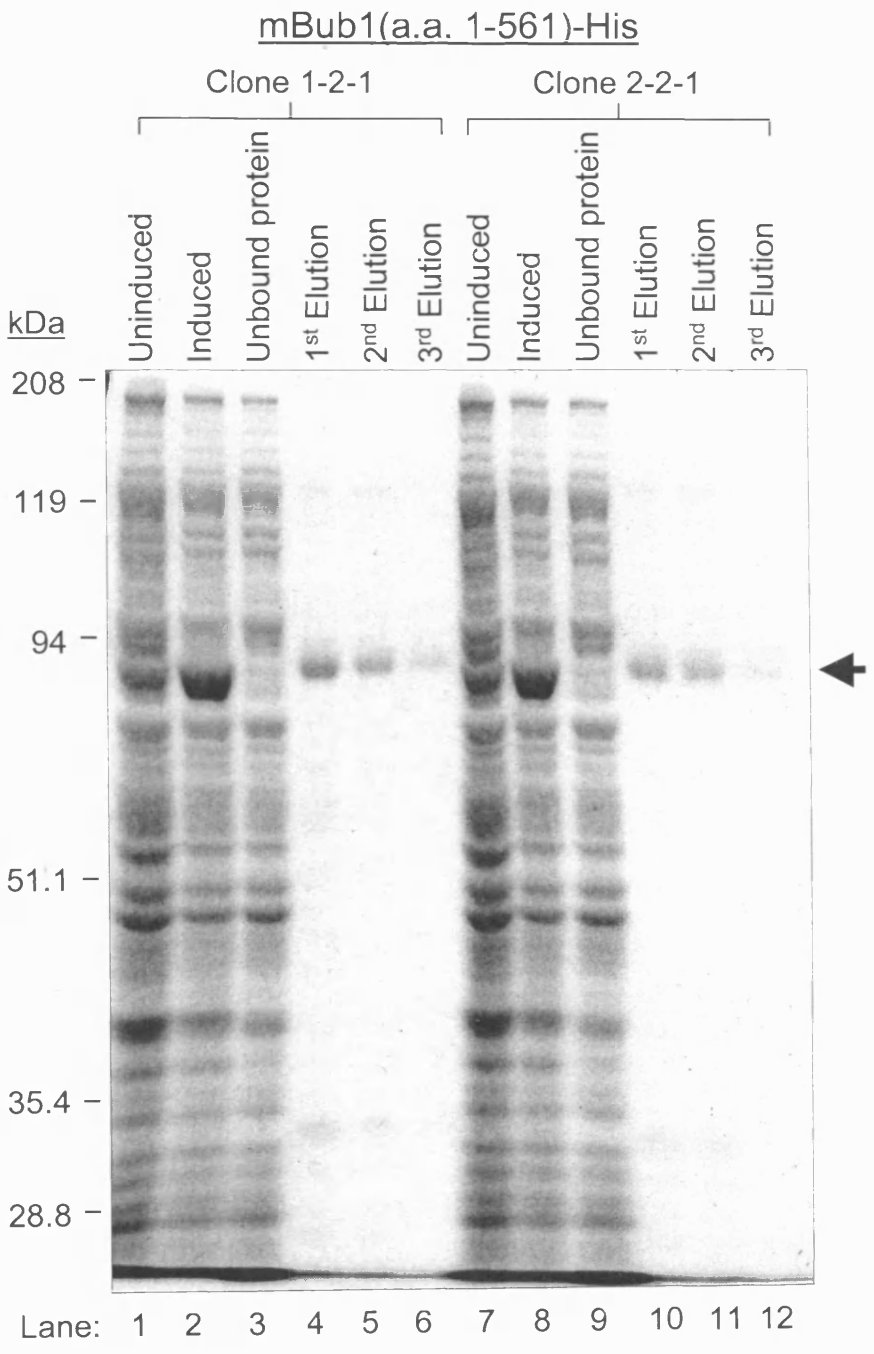

Figure 4.4: Native mini-prep of mBub1(1-561)-His protein.

Figure 4.5: Native mini-prep of mBub1(562-1058)-His protein.

For each of two bacterial clones expressing (CT) mBub1(562-1058)-His (clones 4-1-1 and 4-4-1), expression of a 70kDa protein (indicated by an arrow) is induced by IPTG (20μl (out of 100μl) of uniniduced (lanes 1 & 7) and IPTG-induced (lanes 2 & 8) total bacterial lysate are shown). This protein is successfully bound to Ni-NTA resin, as indicated by lack of this 70kDa protein in the "unbound protein" (20μl out of 100μl of the first resin wash) lanes (3 & 9). 20μl, successive elutions of the His-tag protein from each clone (lanes 4-6 & 10-12) demonstrate that this 70kDa protein could not be eluted from the affinity resin, and thus cannot be easily purified in its soluble form.

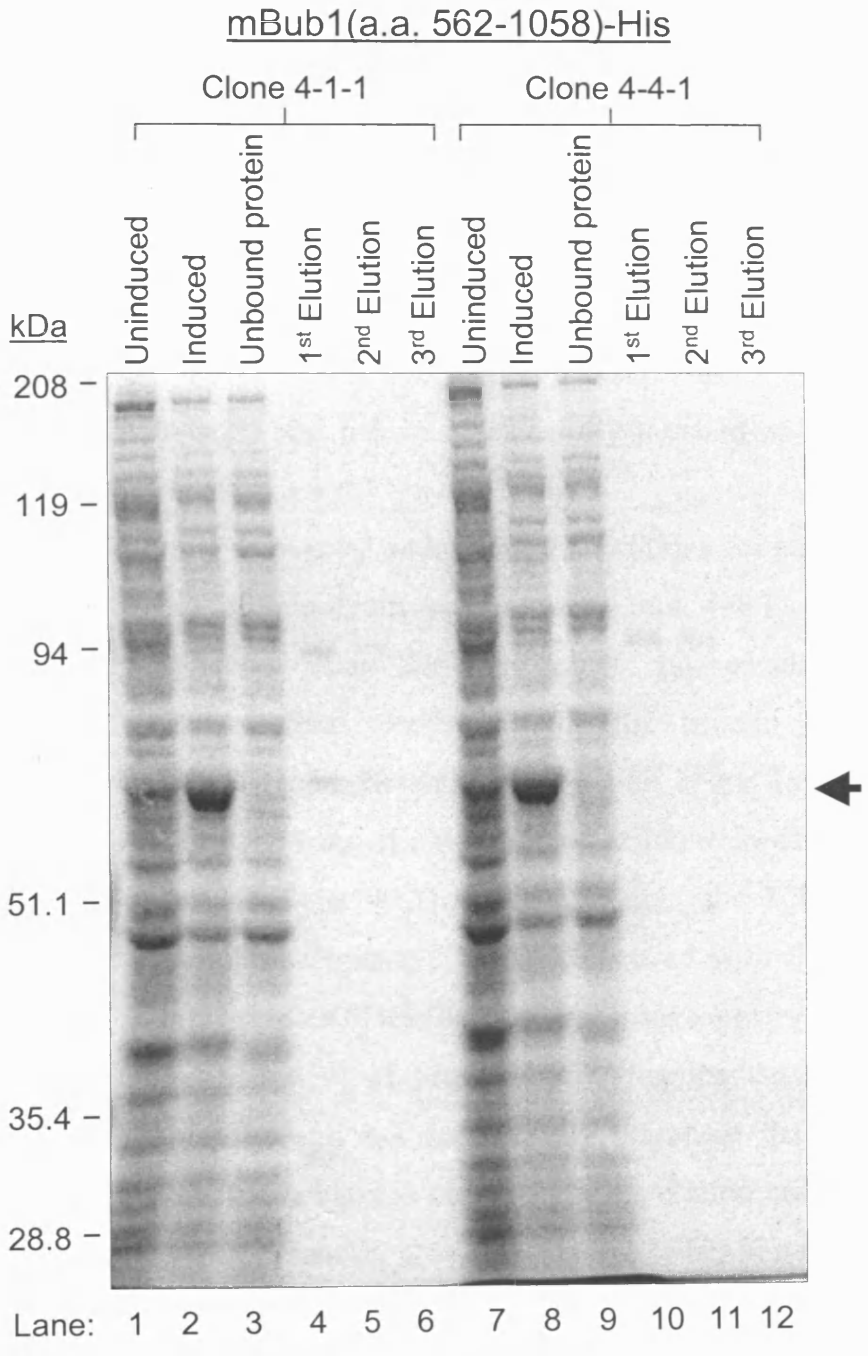

Figure 4.5: Native mini-prep of mBub1(562-1058)-His protein.

In Figure 4.4, it is clear that expression of a protein of approximately 90kDa is induced by addition of IPTG to the bacterial culture, in both mBub1(1-561)-pET clones 1-2-1 and 2-2-1, as a strong 90kDa band is seen in the "induced" lane that is not so strong in the "uninduced" lane for each clone (compare lane 1 with lane 2, and lane 7 with lane 8). This strong band is no longer detected in the "unbound protein" lane for each clone (lanes 3 and 9, representing the first wash of the protein-bound Ni-NTA resin), indicating that this protein is His-tagged, and has successfully bound to the His-bind resin. Finally, it is clear that the His-tagged NT mBub1 protein from both clones can be eluted very cleanly as a 90kDa band using native conditions for the mini-prep (see lanes 4-6 and 10-12). Therefore, mBub1(1-561) protein is approximately 90kDa in size, and can be successfully purified as a soluble protein.

Figure 4.5 shows the mini-prep under native conditions for purification of mBub1(562-1058)-His protein from clones 4-1-1 and 4-4-1. A strong 70kDa band in the "induced" lanes for each clone, not present in the "uninduced" lanes indicates that expression of this protein is being successfully induced by IPTG (compare lane 1 with lane 2, and lane 7 with lane 8). As would be expected from the number of residues in each of the mBub1(1-561) and mBub1(562-1058) His Tag proteins, the CT mBub1 protein has a lower molecular weight of 70kDa, compared with the 90kDa observed for the NT mBub1 protein. This 70kDa band is no longer seen in the "unbound protein" lanes (3 and 9) of Figure 4.5, indicating that it is the mBub1(562-1058)-His protein, and has successfully bound to the Ni-NTA resin. However, no strong 70kDa band is observed in the elution lanes of this figure (lanes 4-6 and 10-12) indicating that mBub1(562-1058)-His cannot be eluted and thus cannot be purified in its native form, and would need to be purified as insoluble protein. In fact, when attempting to purify this protein under native conditions, two faint bands were observed in the elution lanes when more sample was loaded, at 70kDa and also at 90kDa (data not shown).

Two clones of mBub1(1-561)-pET in BLR λDE3 pLysS cells, "1-2-1" and "2-2-1" were sequenced to confirm the fidelity of PCR, and that the correct sequence had been cloned. The DNA sequence of 1-2-1 contained a single base change, whereas the sequence of clone 2-2-1 was a perfect match to the sequence of mBub1 in the original pcDNA3.1-mBub1 plasmid. One clone of mBub1(562-1058)-pET, "4-1-1", was sequenced and perfectly matched the mBub1 sequence from the pcDNA3.1-mBub1 plasmid.

Therefore, clone 2-2-1 was chosen to express and purify (NT) mBub1(1-561)-His protein in bulk using a soluble protein purification method. Similarly, clone 4-1-1 was chosen to express and purify (CT) mBub1(562-1058)-His protein in bulk using an insoluble protein purification protocol.

Figure 4.6 shows samples from the native protein purification process for the NT mBub1 protein, mBub1(1-561)-His, run on an 8% SDS-PAGE gel and Coomassie stained. As expected, a strong approximately 90kDa protein is seen in the "induced" sample (lane 2), but not in the "uninduced" sample (lane 1). This protein is not seen in the "unbound protein" (lane 4) suggesting that it successfully bound to the Ni-NTA resin on the column. Only very faint 90kDa bands are seen in the "wash" (lanes 5 and 6) samples, indicating that very little was removed by the wash steps. The "cleared lysate" sample (lane 3) does not show a strong 90kDa band as would be expected. This may suggest that most of the 90kDa protein precipitated out and was lost to the pellet during the lysis. Nevertheless some of the protein of interest must have been present in the cleared lysate and then successfully bound to the Ni-NTA resin, because strong 90kDa protein bands can be seen clearly in the elution lanes (7-11 and 15-19). The 90kDa protein NT mBub1 protein appears to cleanly elute in elution fractions 2-5 (lanes 7-11) of the first prep, "Prep 1" (lanes 1-11). Prep 2 (lanes 12-19) represents "unbound protein" from Prep 1, loaded onto a fresh Ni-NTA resin column, and washed and eluted separately.

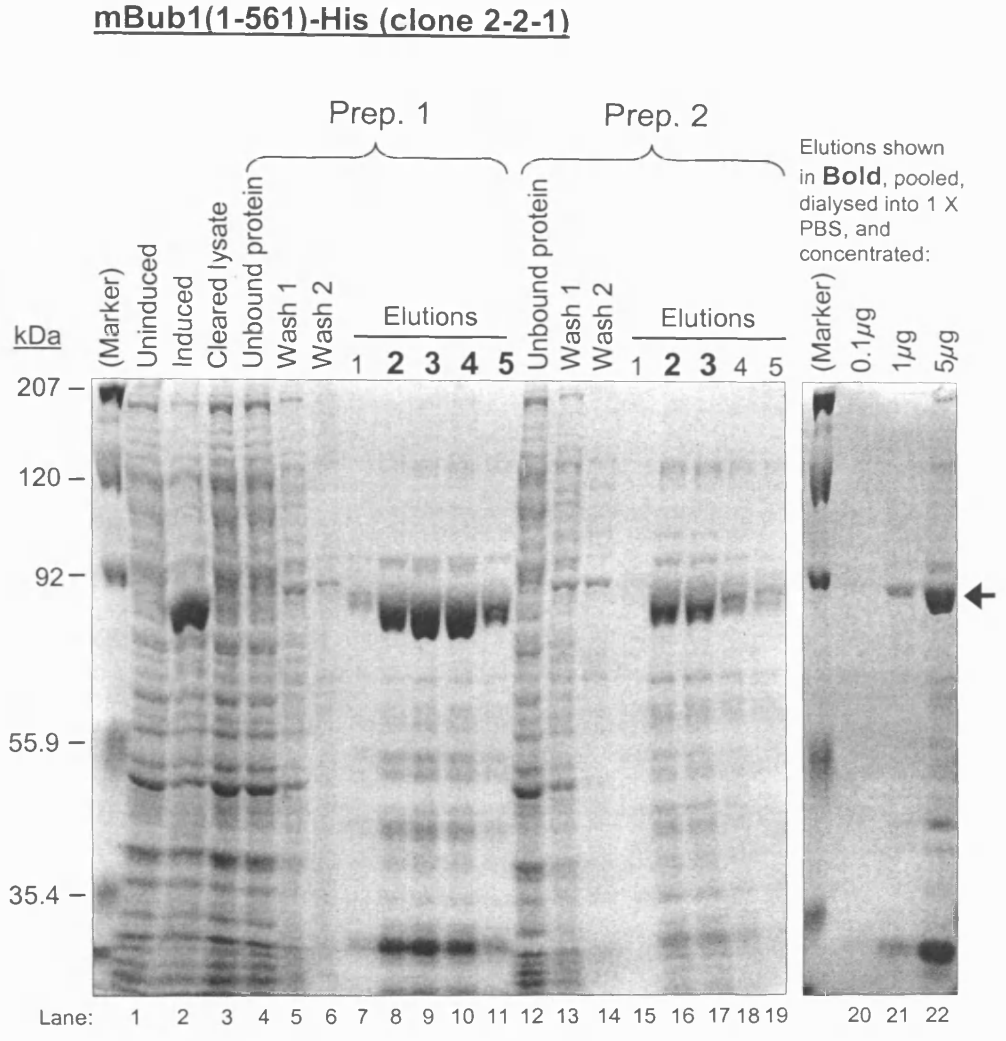

Figure 4.6: Bulk purification of soluble mBub1(1-561)-His protein.

Samples of all stages of the protein purification process are shown. The (arrowed) 90kDa (NT) mBub1(1-561)-His protein (expressed in clone 2-2-1) was eluted cleanly, and the strongest elution fractions were pooled and dialysed into 1 x PBS, ready for immunisation of mice for generation of monoclonal antibodies against NT mBub1.

(Equal volumes of the samples (5µl) were loaded in lanes 1-19).

The 90kDa protein is eluted cleanly in elution fractions 2 and 3 (lanes 16-17) of Prep 2, even though the unbound protein from Prep 1 (lane 4) did not appear to contain any of this protein. This indicates that not all NT mBub1 protein was binding to the Ni-NTA resin in the original prep. Elutions 2-5 of Prep 1 and elutions 2-3 of Prep 2 were pooled, dialysed into 1 x phosphate buffered saline (PBS), and concentrated (using 30 kDa NMWL (nominal molecular weight unit) columns from Millipore), ready for injection into mice. These elutions were chosen because they had the greatest quantity of the NT mBub1 90kDa protein (mBub1(1-561)-His). Figure 4.6 lanes 20-22 show 0.1μg, 1μg and 5μg samples of this pooled and concentrated protein, ready for immunisation of mice for monoclonal antibody production. The most abundant band was the Bub1 protein, and this was very clean in comparison to the crude "induced" sample (lane 2) from which it was purified.

Attempts to optimise the bulk denaturing purification of (CT) mBub1(562-1058)-His protein from clone 4-1-1 using urea-based buffers were unsuccessful. Buffers containing Guanidine-HCl were found to be much better for purification of the denatured 70kDa protein from 4-1-1. Figure 4.7 shows samples of total bacterial lysate from the uninduced and IPTG-induced 4-1-1 cells used for the purification (lanes 1 and 2, respectively), run on an 8% SDS-PAGE gel and Coomassie stained. As before, a strong ~70kDa protein is seen in the "induced" (lane 2) sample upon addition of IPTG, and this cannot be seen in the "uninduced" sample (lane 1). The 70kDa band was present in the cleared lysate lane as expected, but an equal amount was also seen in the "unbound protein" sample that didn't bind to the Ni-NTA resin (data not shown), indicating that not all of the available 70kDa HisTag protein successfully bound to the Ni-NTA resin. This was perhaps due to overloading the capacity of the resin. 10 elutions from the Ni-NTA resin were collected, and in addition the unbound protein sample was used as the starting material for a second prep, from which a further 10 elutions of the 70kDa CT mBub1 protein were collected.

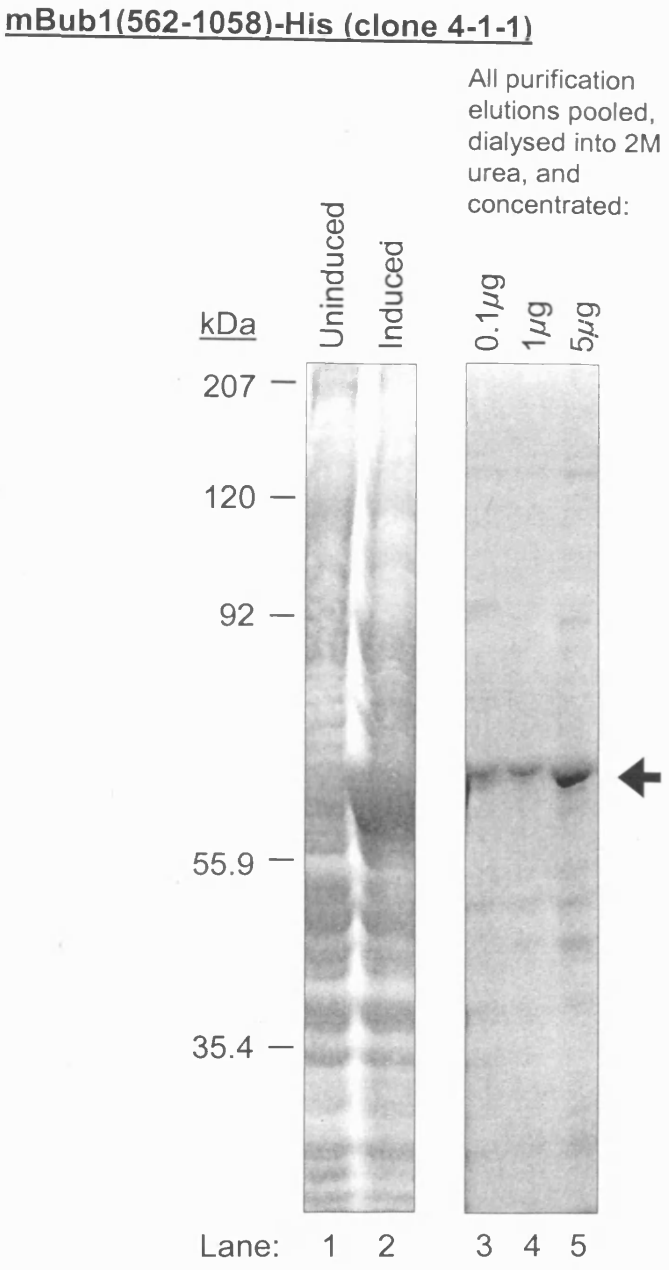

Figure 4.7: Bulk purification of insoluble mBub1(562-1058)-His protein.

Uninduced and IPTG-induced total bacterial lysate samples from clone 4-1-1 are shown (lanes 1-2). The 70kDa (CT) mBub1(562-1058)-His protein (arrowed) was eluted cleanly, and 20 separate elutions were pooled, dialysed into 2M urea and concentrated, ready for immunisation of mice for generation of monoclonal antibodies against CT mBub1.

These elution samples are not shown in Figure 4.7 because only a very small quantity of each was run on a SDS-PAGE gel and stained, so as to retain as much as possible for immunisation, and the bands seen were very faint. All 20 elutions (i.e. the elutions from both preps) were pooled, dialysed into 2M urea, and concentrated, ready for injection into mice. Figure 4.7 lanes 3-5 show 0.1μg, 1μg and 5μg samples of this purified mBub1(562-1058)-HisTag protein, and demonstrates that the 70kDa protein samples have very few impurities.

The bulk purifications detailed above resulted in sufficient protein for immunisation of mice for monoclonal antibody production and for antibody screening, for both NT and CT mBub1 proteins. The total yield was 200μl of (NT) mBub1(1-561)-HisTag (in 1 X PBS) at 2.1mg/ml, and 2ml of (CT) mBub1(562-1058)-HisTag (in 2M urea) at 2.2mg/ml.

4.3.2 Generation of hybridoma cell lines that secrete monoclonal antibodies specific to mBub1

4.3.2.1 Immunisation and test bleed validation

Immunisations of two mice for each purified mBub1 protein were carried out by Dr Terry Jowett at the UCL monoclonal antibody facility. Test bleeds were taken from the mice, and fusions were carried out for spleen cells derived from the most promising mouse for each of the mBub1 antigens.

Figure 4.8 shows western blot results using the test bleed samples from the immunised mice. NIH 3T3 whole cell lysate (lane 1), and uninduced and IPTG-induced whole bacterial lysates from antigen-expressing cells for both the NT (lanes 3 and 4) and CT (lanes 5 and 6) mBub1 were blotted with the test bleeds, and also with normal mouse serum (negative control), and rabbit polyclonal NT hBub1 antiserum (positive control).

Figure 4.8: Western blot analysis using test bleeds from mBub1-immunised mice.

Whole cell lysate from NIH 3T3 cells, and whole bacterial lysate from uninduced and induced bacteria expressing either NT mBub1 (mBub1(1-561)-His from clone 2-2-1) or CT mBub1 (mBub1(562-1058)-His from clone 4-1-1) were separated on SDS-PAGE and western blotted using either normal mouse serum (A), NT Bub1-immunised mouse 1 (B) or mouse 2 (C) test bleeds, CT Bub1-immunised mouse 1 (D) or mouse 2 (E) test bleeds, or rabbit polyclonal NT hBub1 antiserum (F). Specificities of the test bleed antisera for both endogenous mBub1 protein (predicted molecular weight 120kDa, as seen in the NIH 3T3 lane), and for the antigen expressed in bacteria (90kDa NT mBub1 protein, or 70kDa CT mBub1 protein) were used to select which mouse to recommend for hybridoma generation for each antigen.

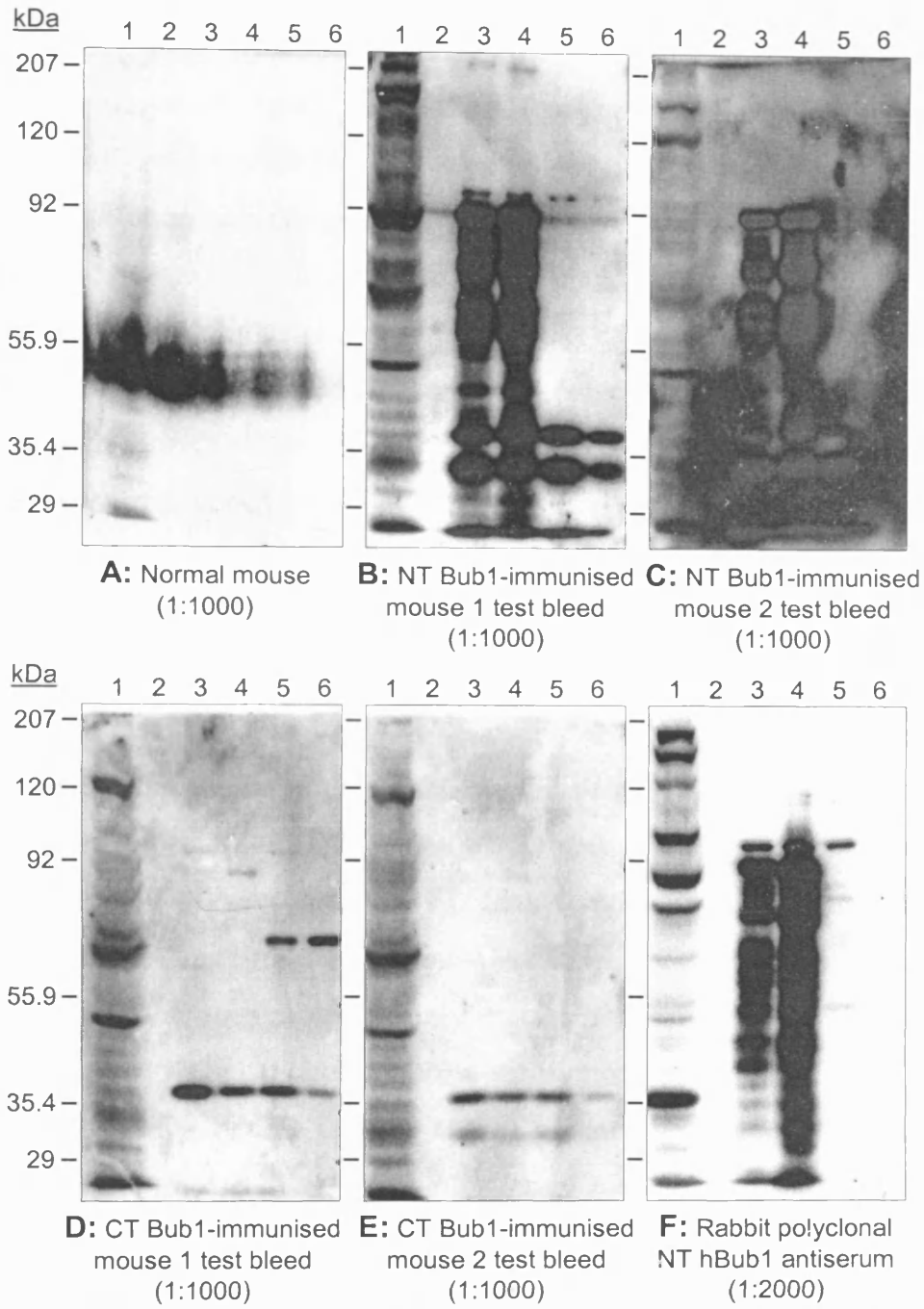

Lane:
1 = 50μg NIH 3T3 lysate
2 = (blank)
3 = NT Bub1 (clone 2-2-1) uninduced whole bacterial lysate, 20μl
4 = NT Bub1 (clone 2-2-1) IPTG-induced whole bacterial lysate, 20μl
5 = CT Bub1 (clone 4-1-1) uninduced whole bacterial lysate, 20μl
6 = CT Bub1 (clone 4-1-1) IPTG-induced whole bacterial lysate, 20μl

Figure 4.8: Western blot analysis using test bleeds from mBub1-immunised mice.

As expected, normal mouse serum (Figure 4.8A) did not show any strong bands of the expected size, i.e. ~120kDa is the predicted molecular weight of mBub1 in the whole cell lysate, while the NT mBub1 antigen is ~90kDa, and the CT mBub1 antigen ~70kDa. NT mBub1-immunised mouse 1 test bleed (Figure 4.8B) blotted several very strong bands at around 120kDa in the NIH 3T3 whole cell lysate lane (lane 1), and also showed strong recognition of the 90kDa antigen in both lanes 3 and 4. This is slightly surprising, as lane 3 is loaded with "uninduced" bacterial lysate from clone 2-2-1, and so would not contain as high a level of the NT mBub1 antigen as the "induced" sample in lane 4. Perhaps the pLysS plasmid in the BLR λDE3 pLysS cells does not reduce basal expression in the absence of IPTG as well as hoped, but it seems most likely that this result is simply indicative of the sensitivity of western blotting. NT mBub1-immunised mouse 2 test bleed (Figure 4.8C) showed fewer bands in lane 1 (NIH 3T3 lysate) than mouse 1, with very strong bands only at 120kDa (the predicted molecular weight of mBub1), and at ~150kDa. Similar to mouse 1, NT-mBub1-immunised mouse 2 showed very strong 90kDa bands in lanes 3 and particularly in lane 4, indicating recognition of the antigen. NT mBub1-immunised mouse 2 was chosen for monoclonal antibody production, due to its recognition of only two, rather than several very strong bands in lane 1. It was also chosen because it blotted equally strongly for the 120kDa and 150kDa bands, and the 120kDa band matched the predicted molecular weight for mBub1. Mouse 1 however blotted most strongly for a 150kDa and a 90kDa band in the NIH 3T3 lysate (lane 1), and so was not thought to be recognising the correct protein.

CT (carboxy-terminal) mBub1-immunised mouse 1 test bleed (Figure 4.8D) was specific to a 120kDa band in the NIH 3T3 lysate (lane 1), and was also able to recognise the 70kDa antigen in lanes 5 and 6 (although more strongly in lane 6, where the expression of the protein has actually been induced). CT mBub1-immunised mouse 2 test bleed (Figure 4.8E) was also specific to a 120kDa band in the NIH 3T3 lysate, but was not able to recognise the antigen in lanes 5 and 6, as no 70kDa band is seen in these

lanes. For this reason, CT mBub1-immunised mouse 1 was chosen for monoclonal antibody generation.

Figure 4.8F is a positive control, showing the same lysates blotted using rabbit polyclonal antiserum against the NT hBub1 (kindly provided by Dr Raimundo Freire). This demonstrates the relative non-specificity of this antibody, as many bands are strongly recognised in the NIH 3T3 lysate. It should also be noted that the 120kDa (predicted molecular weight of Bub1) band is not the strongest of these. Interestingly, the pattern of bands seen in lanes 3 and 4 of Figure 4.8F match the patterns seen in the equivalent lanes in panels B and C, providing further indication that these antibodies are recognising the same protein, and suggesting that the bands of molecular weight lower than 90kDa seen in these lanes are degradation products. Finally, the native, NT mBub1 protein resulted in a stronger immune response than that seen with the CT mBub1 protein. This is slightly unexpected, as it is usually the denatured, unfolded antigens that give the strongest immune response, as mentioned previously.

4.3.2.2 Fusion and initial screening

Spleen cells were isolated from NT mBub1-immunised mouse 2 and CT mBub1-immunised mouse 1, and were fused with myeloma cells to produce hybridomas by Dr Terry Jowett, using standard protocols. Initial screening of the hybridomas via ELISA (Enzyme-Linked ImmunoSorbent Assay), antibody isotyping and cloning and cultivation of hybridoma cells were also performed by Dr Jowett. The wells of the ELISA screen microtitre plates were coated with either the native NT mBub1 antigen, or the dialysed CT mBub1 antigen. Although unfolded proteins do not stick to ELISA plates, some of the CT mBub1 protein would have refolded in the dialysis buffer, and it was hoped that this would be sufficient to carry out the screen. It would of course have been better to use a soluble CT mBub1 protein for the ELISA, but this was not possible to purify. After blocking with BSA (Bovine Serum Albumin), hybridoma supernatants for each antibody were added to wells of

microtitre plates coated with the relevant antigen, and positives were detected by addition of HRP (Horseradish peroxidase)-conjugated secondary antibody against whole mouse serum, and an HRP-substrate. The use of anti-whole mouse serum:HRP secondary antibody (a standard protocol used by Dr Terry Jowett) resulted in detection of both IgM and IgG class antibodies by the ELISA screen.

Hybridoma supernatants that tested positive in these initial ELISA screens were tested via western blot and immunoprecipitation, and the positives from these screens were then single cell cloned, isotyped and re-screened by ELISA. It should be noted that the ELISA screen of the NT-mBub1 hybridoma supernatants produced many more positives than the ELISA screen of the CT-mBub1 hybridoma supernatants (40 versus 22, respectively), probably due to the dialysed (mostly unfolded) CT mBub1 antigen being used for the latter ELISA screen.

4.3.2.3 Screening via western blot and immunoprecipitation

Figure 4.9 shows the results of the western blot screen for 40 hybridoma supernatants from the NT mBub1 fusion, all of which gave positive results in the ELISA screen. Each supernatant was used at a dilution of 1:100 to western blot one lane of NIH 3T3 (expressing wild-type LT) whole cell lysate (50μg), and one lane of induced whole bacterial lysate from clone 2-2-1 (NT mBub1-expressing cells), transferred from an 8% SDS-PAGE gel. Autorads from each blot for the NT hybridoma supernatants are shown, along with blots for media only (negative control), and a rabbit polyclonal antiserum against NT hBub1 (positive control).

Figure 4.9: Initial western blot screen of the NT mBub1 hybridoma tissue culture supernatants.

NIH 3T3(wild-type LT) whole cell lysate and whole bacterial lysate expressing the NT mBub1 antigen were blotted with 1:100 dilution of each of 40 hybridoma supernatants from the NT mBub1 fusion that tested positive for antigen recognition in the ELISA screen. Strips blotted with supernatants giving the most positive results are enlarged. The 90kDa bacterial antigen is indicated by an arrow. The supernatants were single cell cloned, and new single cell clone names and the isotype of these clones are indicated. Negative (media only) and positive (rabbit polyclonal NT hBub1 antiserum) control strips are also shown.

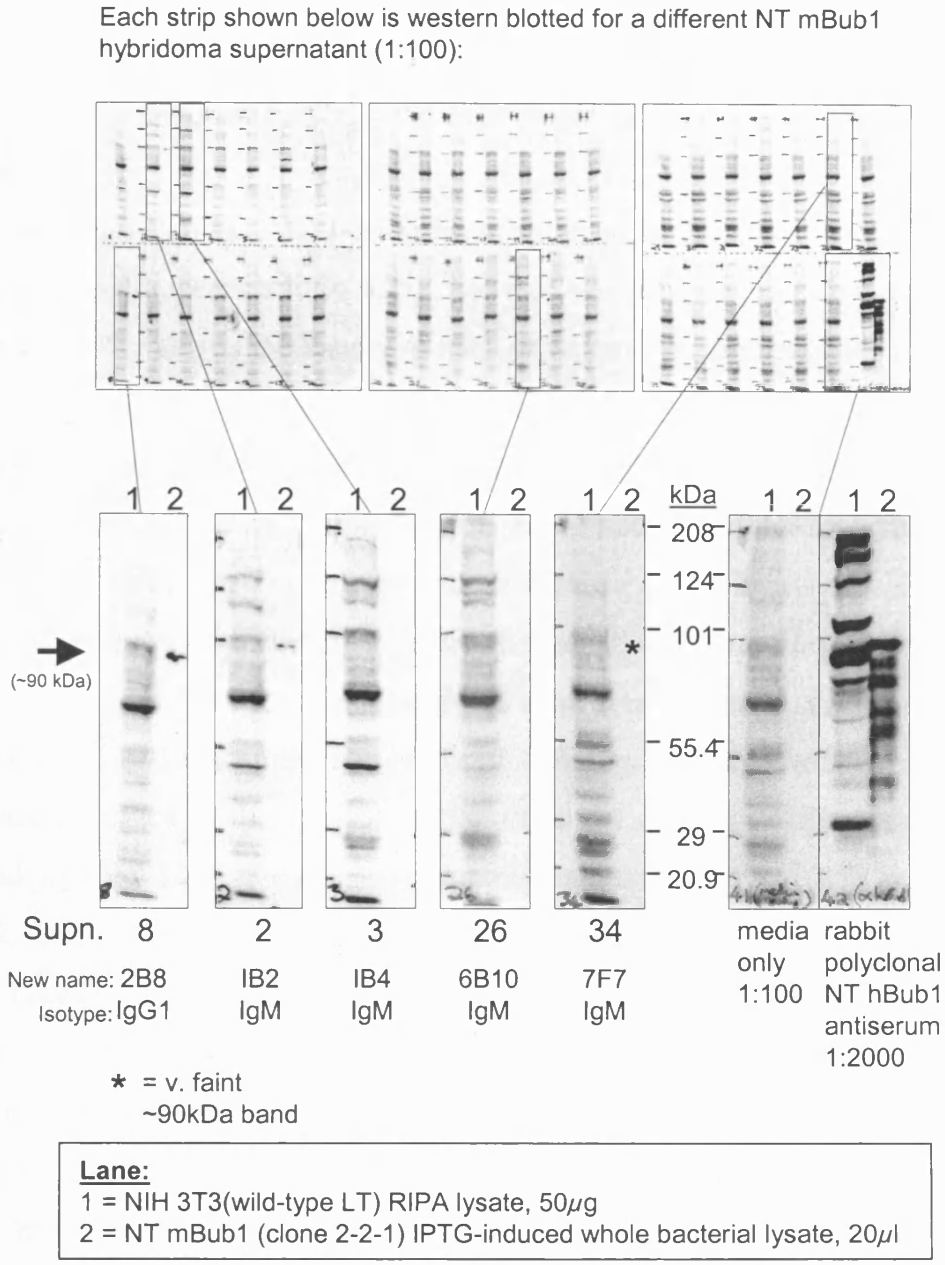

Figure 4.9: Initial western blot screen of the NT mBub1 hybridoma tissue culture supernatants.

The most interesting blots are enlarged in the bottom half of Figure 4.9, and these (no's 8, 2, 3, 26 & 34) were chosen for single cell cloning and for further analysis. NT Bub1 hybridoma supernatant no.'s 8 and 2 were chosen because they both strongly recognise the 90kDa NT mBub1 antigen in lane 2 (indicated by an arrow). (The 90kDa band in lane 2 of the supernatant 8 blot, although strong, appears a little fuzzy, but this was probably due to a running problem with the gel, as the band was seen on several exposures). Supernatant 2 also recognised a ~120kDa band (the predicted molecular weight for mBub1) in the NIH 3T3 lysate in lane 1, but a band of this size was not seen in lane 1 of the supernatant 8 blot. Supernatants 3 and 26 did not recognise the bacterial antigen in lane 2, but were chosen because strong bands of ~120kDa were seen in lane 1 for these supernatants. Supernatant 34 was chosen because an extremely faint 90kDa antigen band could be seen in lane 2, although this is not visible in the scanned image for this figure. As expected, no strong bands are observed in the 120kDa region of lane 1 and no 90kDa antigen is detected in lane 2 for the negative control, media only blot. The positive control strip, NT hBub1 rabbit polyclonal antiserum blot showed strong bands in the 120kDa region in lane 1, and a very strong 90kDa band (and other smaller bands representing either degradation products or prematurely terminated proteins) in lane 2. NT Bub1 hybridoma supernatants 8, 2, 3, 26 and 34 were single cell cloned and renamed (the new names for the single cell clones from these supernatants are shown in Figure 4.9). The single cell clones were also isotyped to determine their antibody sub-class, and they were all IgMs except for supernatant 8 (single cell clone name "2B8"), which was IgG1. The IgG (2B8) is likely to be a better antibody than the IgMs, as IgGs are produced by the stronger, secondary immune response, whereas IgMs are produced as the primary immune response and therefore may not be as specific as the IgG sub-class of antibodies. In hindsight, it would have been better to have used a mixture of anti-IgG antibodies (specific to the different mouse IgG sub-classes) conjugated to HRP to detect positives in the ELISA screen to prevent IgM antibodies from being selected for further validation,

allowing more time to be spent verifying the potentially more useful IgG candidate monoclonals.

All of the NT Bub1 hybridoma supernatants shown were also tested via immunoprecipitation, as shown in Figure 4.10. 50µl of each supernatant was used for immunoprecipitation from 500µg of NIH 3T3(wild-type LT) whole cell lysate. Media only and CT hBub1 rabbit polyclonal antibody (previously shown to immunoprecipitate well, but not western blot for Bub1, kindly provided by Dr Raimundo Freire) were used as negative and positive controls, respectively, for the immunoprecipitation. When blotted using the rabbit polyclonal antiserum against NT hBub1, the positive control (immunoprecipitation using polyclonal CT hBub1 antiserum) showed a very strong band in the 120kDa-200kDa region of the blot, in addition to several other very strong bands (data not shown, due to strong non-specific bands making scanning of a clear image difficult). The only other lane that showed a strong band in this region (co-migrating with the band in the positive control lane) was NT mBub1 hybridoma supernatant 8 (as previously mentioned, this was later single cell cloned and renamed 2B8, and was found to be IgG1 subclass). This was a very clear result and provided further evidence for the Bub1 specificity of this particular hybridoma supernatant, which when single cell cloned was identified as the only IgG from all those picked out from the western blotting screen in Figure 4.9, and the best monoclonal antibody generated against NT mBub1. It should also be noted that these immunoprecipitations were all carried out using Protein A-Sepharose beads. Protein A is a cell wall component of *Staphyloccocus aureus* that binds the Fc portion of IgGs from many species. However, 2B8 is IgG1, a sub-class that is not easily precipitated using Protein A (Protein G, a cell surface receptor from *Streptococcus* which is able to recognise both the Fc and Fab portions of a wide range of immunoglobulins, would have been better for immunoprecipitation experiments with this antibody, as it has a much greater affinity for IgG1).

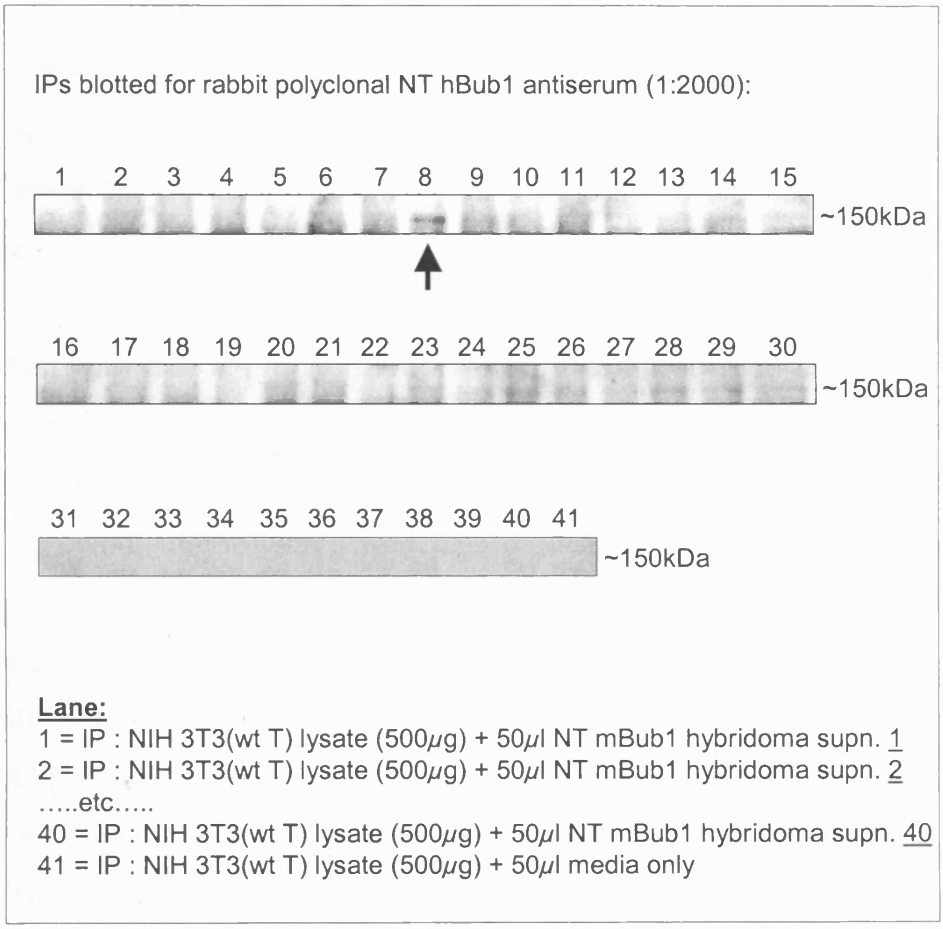

Figure 4.10: NT mBub1 hybridoma supernatant screening via immunoprecipitation.

50μl of each of the 40 NT mBub1 hybridoma tissue culture supernatants picked out from the ELISA screen was used to immunoprecipitate (IP) mBub1 from NIH 3T3(wild-type LT) whole cell lysate. IPs were then run on SDS-PAGE and western blotted using rabbit polyclonal NT hBub1 antiserum, to determine which if any supernatants were able to immunoprecipitate a band of approximately 120-200kDa (Bub1). The arrowed lane (NT mBub1 supernatant 8) was the only monoclonal to give a strong band in the region expected for Bub1. A negative control (media only, lane 41) is also shown.

This suggests that 2B8 must be a very effective antibody for immunoprecipitation, as Bub1 was effectively brought down even by the weak affinity this antibody has to Protein A. Immunoprecipitation experiments using antibody 2B8 and Protein G later in this chapter (see Figure 4.19), demonstrate that this antibody immunoprecipitates Bub1 extremely well.

Figure 4.11 shows the results of the western blot screen for 22 hybridoma supernatants from the CT mBub1 fusion, all of which gave positive results in the ELISA screen. Similar to the screen in Figure 4.9, each supernatant was used at a dilution of 1:100 to blot nitrocellulose strips, each with one lane of NIH 3T3(wild-type LT) whole cell lysate (50μg), and one lane of induced whole bacterial lysate from clone 4-1-1 (CT mBub1-expressing cells). Control strips were also blotted with media only (negative control), or a rabbit polyclonal antibody directed against NT hBub1 (positive/negative control).

Strips giving interesting results are enlarged at the bottom half of Figure 4.11. These hybridoma pools were all selected for single cell cloning (their new single cell clone names are shown) and the single cell clones were also isotyped. Supernatants 3, 12, 19 and 20 were chosen because they all strongly recognise the bacterially expressed 70kDa CT mBub1 antigen (indicated by an arrow in Figure 4.11) in lane 2. It is likely that the reason for these 70kDa bands being so strong (compare strength of 90kDa bands observed in Figure 4.9) is because the ELISA screen of these supernatants used insoluble protein. This would have been less efficient than a screen using soluble protein, and so the resulting positives must have had very strong affinities for the antigen. It should be noted that these hybridoma supernatants gave rise to single cell clones that were all IgG sub-class, whereas the other supernatants singled out for further analysis did not recognise the antigen in lane 2, and gave rise to IgM single cell clones.

Figure 4.11: Initial western blot screen of the CT mBub1 hybridoma tissue culture supernatants.

NIH 3T3(wild-type LT) whole cell lysate and whole bacterial lysate expressing the CT mBub1 antigen were blotted with 1:100 dilution of each of 22 hybridoma supernatants from the CT mBub1 fusion that tested positive for antigen recognition in the ELISA screen. Strips blotted with supernatants giving the most positive results are enlarged. The 70kDa bacterial antigen is indicated by an arrow. A 150kDa protein in the cell lysate that is recognised by many of the supernatants is indicated by an arrowhead. The supernatants were single cell cloned, and new single cell clone names and the isotype of these clones are indicated. Negative (media only) and positive (rabbit polyclonal NT hBub1 antiserum) control strips are also shown.

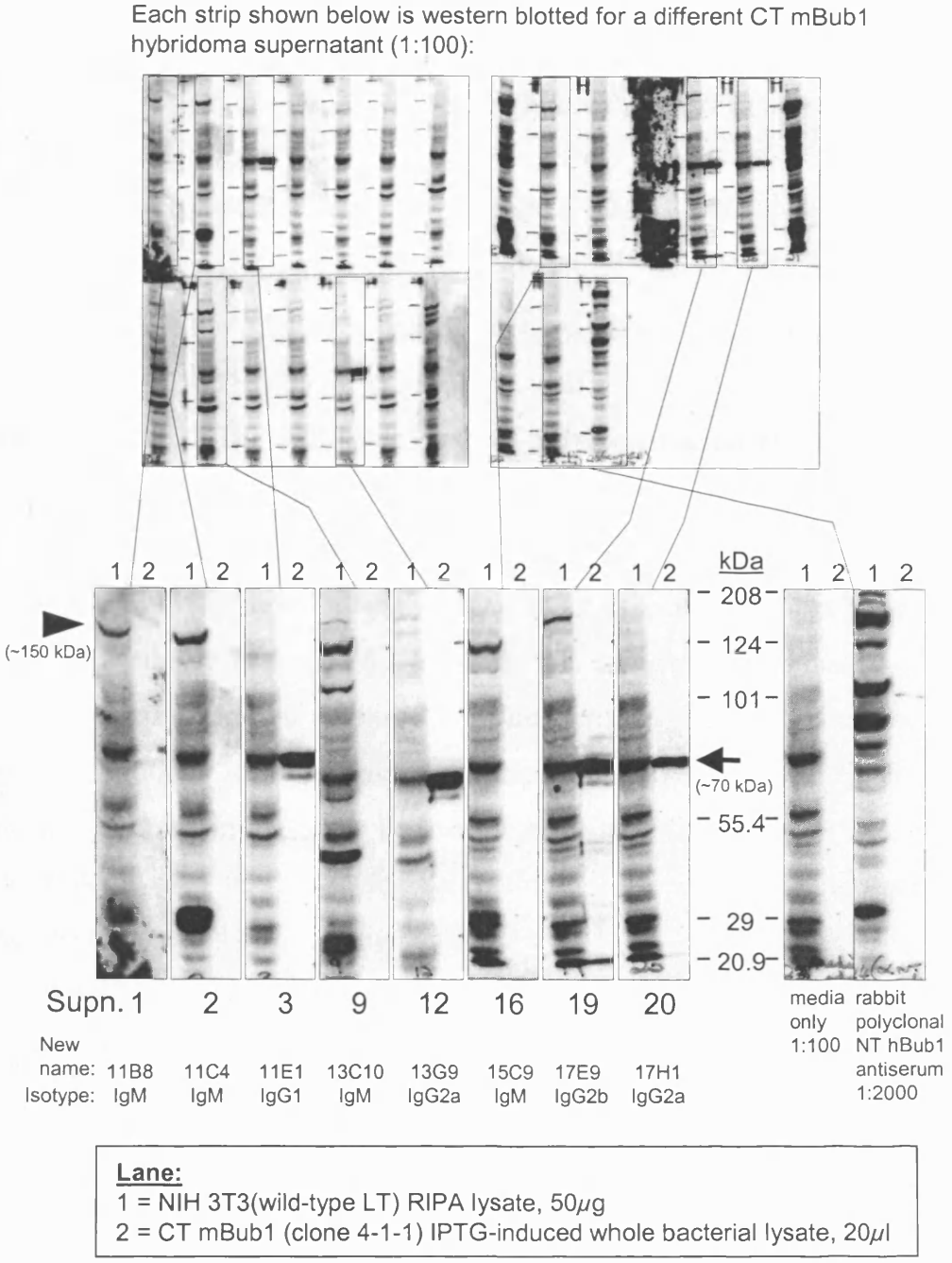

Figure 4.11: Initial western blot screen of the CT mBub1 hybridoma tissue culture supernatants.

Of the IgG sub-class hybridomas, 19 (and to some extent also hybridoma supernatant number 12) not only recognised the antigen in lane 2, but also recognised a band at around 150kDa (indicated in Figure 4.11 by an arrowhead). This band co-migrated with a very strong band seen in the positive control blot using the polyclonal NT hBub1 antiserum. Supernatants 1, 2, 9 and 16 were chosen because they all showed a strong band in the 120-150kDa region in the NIH 3T3 lysate, lane 1. As expected, media only did not show a strong 120-150kDa band in lane 1, and did not recognise the 70kDa antigen in lane 2. The NT hBub1 rabbit polyclonal antibody again (as in Figure 4.9) revealed a strong band at 120kDa (the predicted molecular weight of Bub1) and a particularly strong band at 150kDa, but did not recognise the 70kDa CT mBub1 antigen in lane 2. This is as expected, because the rabbit polyclonal antibody is prepared against the amino-terminus of human Bub1 protein that is not present in this CT mBub1 protein. The CT hBub1 rabbit polyclonal antibody (used for immunoprecipitation experiments in Chapter 3) could not be used in this case because it does not western blot. The weak 100kDa band seen in lane 2 for the rabbit polyclonal hBub1 antibody is presumed to be a non-specific interaction.

All 22 hybridoma supernatant pools for CT mBub1 were also screened by immunoprecipitating from 500μg of NIH 3T3(wild-type LT) whole cell lysate using 50μl of each supernatant, and western blotting using the rabbit polyclonal antiserum against NT hBub1 (see Figure 4.12). Media only (negative control) and rabbit polyclonal CT hBub1 antiserum (positive control) immunoprecipitations were also carried out. The CT hBub1 antiserum brought down a protein of ~150kDa that was recognised strongly by the NT hBub1 polyclonal antiserum, but as before this is not shown due to very strong non-specific bands making production of a clear scanned image very difficult. As for the immunoprecipitations shown in Figure 4.10, it was quite surprising that the immunoprecipitated band seen with these antibodies was 150kDa in size, because the predicted molecular weight for Bub1 is 120kDa.

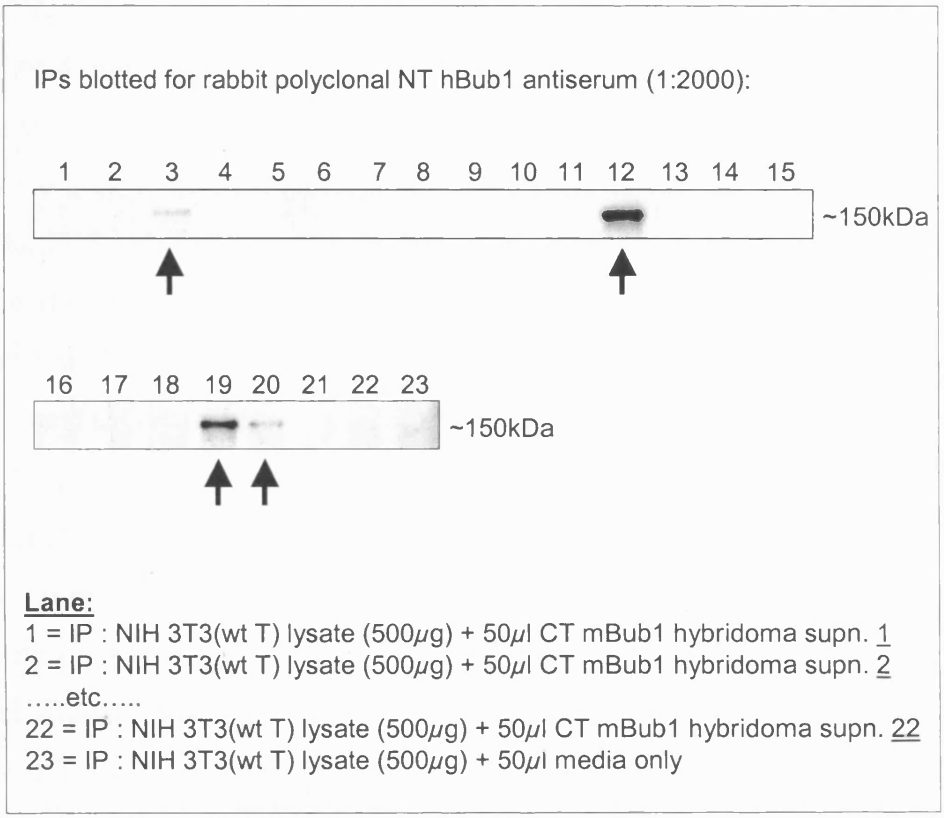

Figure 4.12: CT mBub1 hybridoma supernatant screening via immunoprecipitation.

50μl of each of the 22 CT mBub1 hybridoma tissue culture supernatants picked out from the ELISA screen was used to immunoprecipitate (IP) mBub1 from NIH 3T3(wild-type LT) whole cell lysate. IPs were then run on SDS-PAGE and western blotted using rabbit polyclonal NT hBub1 antiserum, to determine which if any supernatants were able to immunoprecipitate a band of approximately 120-200kDa (Bub1). The arrowed lanes (CT mBub1 supernatants 3, 12, 19 and 20) were the only monoclonals to give a strong band in the region expected for Bub1. A negative control (media only, lane 23) is also shown.

It is demonstrated that the 150kDa protein recognised by these antibodies is in fact Bub1 in section 4.3.3 below. Media only (lane 23) is not able to immunoprecipitate the 150kDa protein. Of the 22 hybridoma supernatants, only 3, 12, 19 and 20 are able to immunoprecipitate this 150kDa protein. The other hybridoma supernatants did not immunoprecipitate any proteins at all. It is interesting to note that these hybridomas were all chosen for single cell cloning from their western blotting abilities, and they represent all of the IgGs out of those shown in Figure 4.11. Also, 12 and 19 show very strong 150kDa bands in the immunoprecipitation experiment compared to the weak bands seen for 3 and 20. This was a further indication that 12 (IgG2a, single cell clone name "13G9") and 19 (IgG2b, single cell clone name "17E9") were the best of the CT mBub1 hybridoma supernatants chosen.

Single cell clones isolated from the hybridomas shown at the bottom of Figures 4.9 and 4.11 were further analysed and it was decided to concentrate on NT Bub1 hybridoma number 8 (IgG1 sub-class, which gave rise to three identical clones, 2B8/A4, 2B8/D2 and 2B8/H4, from now on known as "2B8"), CT Bub1 hybridoma number 12 (IgG2a, three identical clones, 13G9/A9, 13G9/B9 and 13G9/F11, from now on known as "13G9"), and CT Bub1 hybridoma number 19 (IgG2b, three identical clones, 17E9/E2, 17E9/E10 and 17E9/F3, from now on known as "17E9").

4.3.3 Confirmation that the antibodies truly detect Bub1, and species specificity tests

Having identified three potentially good monoclonal antibodies against mBub1, it was necessary to determine their specificity. The band detected by the mBub1 monoclonal antibodies via western blotting (150kDa) was not the expected molecular weight of Bub1 (120kDa). This 150kDa band had already been shown to co-migrate with a strong band recognised by a polyclonal NT hBub1 antiserum (see arrowhead, Figure 4.11), but further testing was required to determine if this band (rather than the 120kDa band also detected

by the polyclonal antibody) was actually Bub1. Species specificity of the antibodies was tested, followed by confirmation of the specificity of the antibodies to the Bub1 protein itself. Finally, immunolocalisation studies were carried out to investigate if the protein identified by these monoclonal antibodies localises as expected for Bub1, both spatially and temporally.

4.3.3.1 Species specificity

Although the monoclonal antibodies were developed to specifically recognise the mouse Bub1 protein, it was important to determine if they were also able to recognise the Bub1 protein of other species. Studies on the Bub1-LT interaction in the laboratory have focussed on rat and human cell lines in addition to experiments in mouse, and for this reason, western blotting of NIH 3T3 cells expressing wild-type LT (mouse), REFs expressing wild-type LT (rat) and U20S (human – no cells expressing LT were available for testing at this stage of the project) was used to examine the species specificities of the antibodies. As well as 50μg of each whole cell lysate, induced whole bacterial lysate of the relevant bacterial clone (2-2-1 for NT Bub1 monoclonal 2B8, and 4-1-1 for CT Bub1 monoclonals 13G9 and 17E9) were also blotted.

Figure 4.13 shows the results of these western blotting experiments using mBub1 monoclonals 2B8 (lanes 5-8), 13G9 (lanes 9-12) and 17E9 (lanes 13-16), and also using polyclonal antiserum against NT hBub1, for comparison (lanes 1-4). The polyclonal NT hBub1 antiserum (lane 1) and monoclonal 2B8 (lane 5) recognise the 90kDa NT mBub1 antigen band very strongly, and monoclonals 13G9 and 17E9 (lanes 9 and 13) recognise the 70kDa CT mBub1 antigen very strongly, as expected. The rabbit polyclonal hBub1 antibody detects a strong ~150kDa band (among others, including a faint 120kDa band) in the mouse, rat and human lysates (lanes 2-4). 2B8 is capable of recognising, albeit very weakly, a ~150kDa band in the mouse and human lysates (lanes 6 and 8, respectively), but not in the rat lysate (lane 7).

Figure 4.13: Species specificity of the Bub1 monoclonal antibodies.

Rabbit polyclonal NT hBub1 antiserum (1:2000) (lanes 1-4) or hybridoma tissue culture supernatants from each mBub1 monoclonal antibody (1:50) (lanes 5-16) were used to blot whole bacterial lysate expressing the antigen used for immunisation (20µl (of a 1 in 200 dilution) of a small scale induction was loaded), or 50µg of whole cell lysate from either mouse (NIH 3T3 (wild-type LT)), rat (REF (wild-type LT)) or human (U20S) cells. The rabbit polyclonal NT hBub1 antibody, and NT mBub1 monoclonal 2B8 recognise the 90kDa NT mBub1 antigen (indicated by an arrow, lanes 1 and 5), while CT mBub1 monoclonals 13G9 and 17E9 recognise the 70kDa CT mBub1 antigen (indicated by an arrow, lanes 9 and 13). A ~150kDa protein (indicated by an arrow) is detected in mouse, rat and human lysates by the rabbit polyclonal antibody (lanes 2-4), by monoclonal 2B8 (albeit very weakly in western blot) in mouse and human lysates (lanes 6 and 8), and by monoclonals 13G9 and 17E9 in mouse lysates only (lanes 10 and 14). Later experiments (see Figures 4.14 and 4.15) indicate that this ~150kDa band is Bub1.

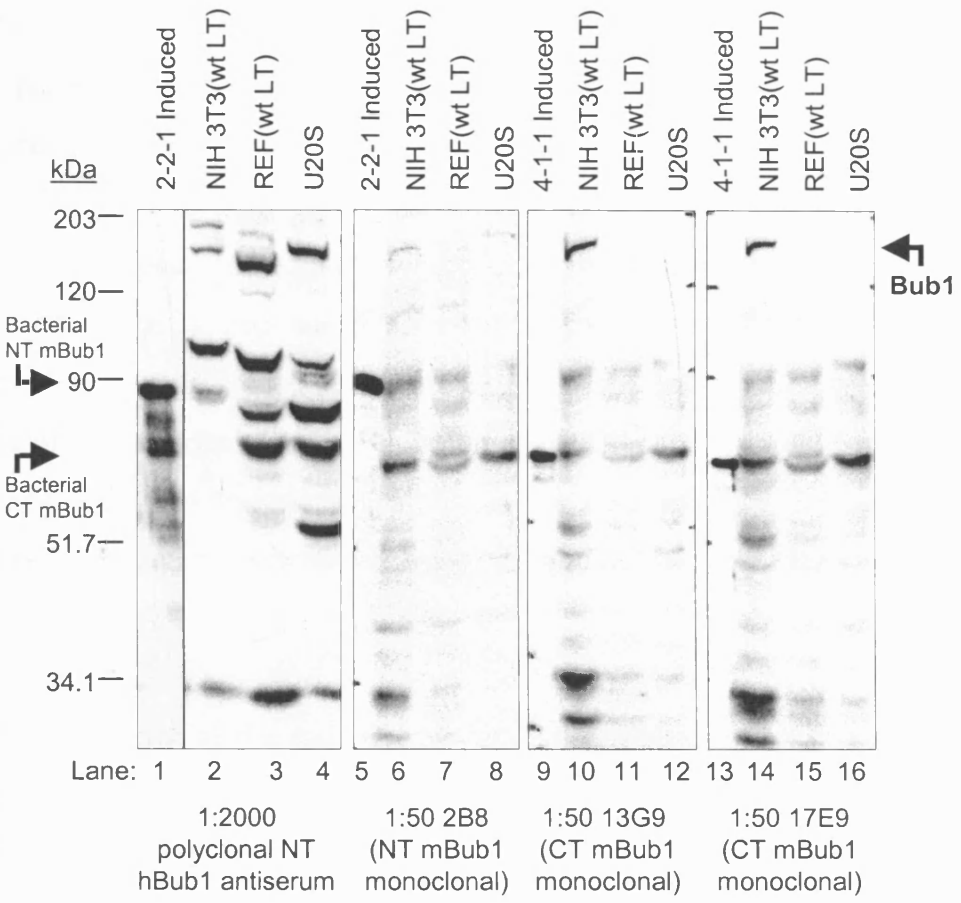

Figure 4.13: Species specificity of the Bub1 monoclonal antibodies.

Both 13G9 and 17E9 monoclonal antibodies are seen to detect a strong ~150kDa band in the mouse (NIH 3T3(wt LT)) lysate (lanes 10 and 14). However, neither antibody detects this protein in either the rat (lanes 11 and 15) or human (lanes 12 and 16) lysates. Therefore, 13G9 and 17E9 monoclonals are specific for the 150kDa mouse protein, but not for the rat or human proteins.

It is interesting to note that in the 2B8 blot, the human 150kDa band in lane 8 appears to migrate slightly slower than the mouse band in lane 6. The mouse, rat and human Bub1 proteins seen at ~150kDa in the polyclonal NT hBub1 antiserum blot (lanes 2-4) also appear to migrate at slightly different rates. The predicted molecular weights for the human and mouse Bub1 proteins are 122kDa and 119kDa, respectively, which could explain the differences in migration seen between them, but does not explain the observed mobility of these proteins at ~150kDa on SDS-PAGE. This could be due to post-translational modification(s), although the nature of this remains to be determined. Therefore it was important to prove the specificity of these antibodies to Bub1.

4.3.3.2 Specificity of the monoclonal antibodies to the Bub1 protein: HA-mBub1 and RNAi tests

Most important of all, it was necessary to determine the specificity of the monoclonal antibodies generated to the mBub1 protein itself. Several papers in the literature have suggested that antibodies raised against the Bub1 protein recognise a band of the correct predicted molecular weight for mammalian Bub1 of ~120kDa on SDS-PAGE (Grabsch *et al.*, 2004; Taylor *et al.*, 2001; Taylor and McKeon, 1997). The mBub1 monoclonal antibodies described in this chapter all appeared to be specific to a band that migrated to ~150kDa on SDS-PAGE, causing concern that the protein detected by these antibodies was not Bub1. However, in the papers mentioned above which describe Bub1 antibodies detecting a ~120kDa band in mammalian cell lysates, western blots are presented that appear to show that these antibodies

actually detect a slower migrating band of ~150kDa, as seen for the mBub1 monoclonal antibodies 2B8, 13G9 and 17E9. This suggested that the ~150kDa protein detected by the mBub1 monoclonal antibodies could be the Bub1 protein, even though it migrates much slower than the predicted molecular weight for mammalian Bub1 proteins of ~120kDa. Similarly, the Xenopus Bub1 homolog has a predicted molecular weight of 131 kDa, but antibodies raised against this protein have been shown to detect a protein migrating at 150kDa on SDS-PAGE (Sharp-Baker and Chen, 2001). When Bub1 immunoprecipitates prepared from mitotic extract were treated with lambda protein phosphatase, the apparent molecular mass of Bub1 was reduced to 140kDa, indicating that phosphorylation during mitosis was partly to blame for the slower migration of the Xenopus Bub1 protein.

To confirm the specificity of the mBub1 monoclonal antibodies, the finding that the monoclonals only detect the mouse protein was exploited. Experiments were undertaken to show that the protein that the antibodies detect co-migrates with a HA-tagged mouse Bub1 protein ectopically expressed in human cells ("HA" is influenza A virus haemagglutinin protein; it is a commonly used epitope tag). In addition, the ability of the mBub1 monoclonal antibodies to detect a reduction in Bub1 protein levels induced by RNAi (RNA interference) was also tested.

pcDNA3.1(-) vector (Invitrogen, see Appendix I for vector map) with HA-tagged, full length mouse Bub1 cDNA cloned into the BamHI site was kindly provided by Dr Ole Gjoerup. The species specificity tests detailed in section 4.3.3.1 had shown that only antibody 2B8 was able to detect human Bub1 protein, whereas all three monoclonals were able to detect the mouse Bub1. For this reason, the pcDNA3.1(-)HA-mBub1 vector was transfected into U20S (human) cells, to distinguish between endogenous Bub1 and the ectopically expressed HA-mBub1 protein.

Figure 4.14 shows the results of the HA-mBub1 specificity test for the mBub1 monoclonal antibodies.

Figure 4.14: Specificity of the mBub1 monoclonals to Bub1: HA-mBub1 experiment.

50μg of whole cell lysates from U20S (human) cells, U20S(empty vector), and U20S(HA-mBub1) (expressing HA-tagged mouse Bub1 protein) were western blotted using anti-HA antibody, to show expression of the tagged mBub1 protein (lanes 1-3). They were also blotted with hybridoma tissue culture supernatants for each of the mBub1 monoclonal antibodies, to demonstrate that they are specific to mBub1, and not some other protein of a similar molecular weight (~150kDa) (lanes 4-12). Finally, these lysates are blotted with rabbit polyclonal NT hBub1 antiserum (lanes 13-15), to demonstrate the strong specificity of the mBub1 monoclonals by comparison.

All three mBub1 monoclonal antibodies recognise the HA-mBub1 protein (indicated by an arrow).

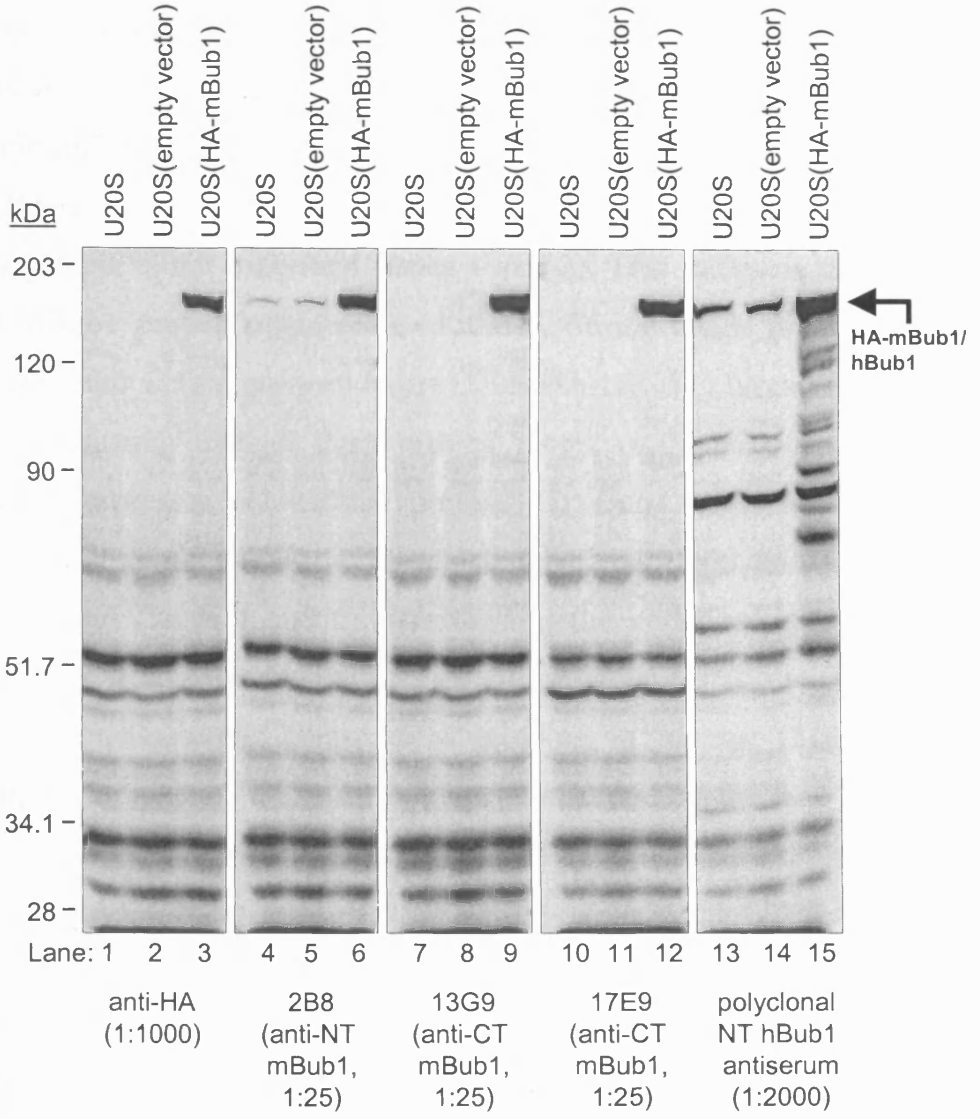

Figure 4.14: Specificity of the mBub1 monoclonals to Bub1: HA-mBub1 experiment.

50μg of whole cell lysates of either untransfected U20S cells, U20S transiently transfected with pcDNA3.1(-) (empty vector control), or U20S transiently transfected with the pcDNA3.1(-)HA-mBub1 vector were run on SDS-PAGE and western blotted using either anti-HA monoclonal antibody (positive control), each of the mBub1 monoclonal antibody tissue culture supernatants, or rabbit polyclonal antiserum against NT hBub1. In Figure 4.14, the anti-HA antibody detects a very strong ~150kDa protein in the U20S(HA-mBub1) lysate (lane 3), but not in the lysates where the HA-tagged mBub1 protein is not expressed (lanes 1 and 2). This indicates that the HA-tagged mBub1 protein migrates at ~150kDa. Strong bands migrating at the same molecular weight are seen in the U20S(HA-mBub1) lysates in lanes 6, 9 and 12, indicating that all three mBub1 monoclonal antibodies detect the ectopically expressed HA-mBub1 protein. NT Bub1 monoclonal 2B8 also detects, albeit more weakly, 150kDa bands in the U20S and U20S(empty vector) lysates (lanes 4 and 5), representing the endogenous human Bub1 protein. This is as expected because in the previous tests this antibody was able to detect mouse and human Bub1 proteins. In contrast 13G9 and 17E9 were unable to detect the human Bub1, as confirmed by the lack of bands in the 150kDa region of lanes 7-8 and 10-11 of Figure 4.14, indicating that these antibodies cannot detect endogenous hBub1 protein in the U20S lysates. The rabbit polyclonal NT hBub1 antibody (lanes 13-15) detected a 150kDa band in all three lysates, co-migrating with bands in lanes 3, 4-6, 9 and 12. This antibody was raised against the amino terminus of the human Bub1 protein, and so as expected detects both the endogenous human Bub1 (lanes 13 and 14), but more strongly detects the over-expressed HA-mBub1 protein, which is very abundant in the U20S(HA-mBub1) lysate (lane 15). It is also notable that there are also several bands at ~80 and 100kDa detected by this rabbit polyclonal antibody (possibly due to cross-reactivity of this antibody), not seen when blotting with any of the mBub1 monoclonal antibodies, or with the anti-HA monoclonal (see lanes 13 and 14), an indication that the new mBub1 monoclonal antibodies are cleaner reagents in comparison. The rabbit

polyclonal antibody also detects many extra bands of molecular weights ranging from ~70-150kDa in the U20S(HA-mBub1) lysate in lane 15, but these could perhaps be degradation products of the overexpressed HA-mBub1 protein, seen by this antibody due to its high efficiency of binding to the Bub1 protein (as well as to ~80 and 100kDa proteins, as seen in lanes 13 and 14). The strong bands of molecular weight below 60kDa in size seen in all five blots are most likely to be non-specific due to general stickiness of the primary or the secondary antibodies, as identical bands are seen in all blots.

This experiment confirms two important points. Firstly, it confirms that all three monoclonal antibodies tested are specific to the Bub1 protein, and not to some other protein of a similar molecular weight. Secondly, it also confirms that both the HA-tagged mBub1 protein, and in particular the endogenous hBub1 protein migrate at ~150kDa on SDS-PAGE, and not at the predicted molecular weight of ~120kDa. This is very clear in lanes 4-6 and 13-15 of Figure 4.14, where endogenous and ectopically expressed Bub1 are seen to co-migrate, even in the presence of the HA-tag (which is not surprising, as the HA-tag consists of only 9 amino acids (YPYDVPDYA)). Also, Figure 4.14 reiterates the species specificity results obtained in Figure 4.13.

The Bub1-specificity of the monoclonal antibodies was further verified via western blotting of lysates from cells where the expression level of Bub1 had been knocked down via RNA interference (RNAi). RNAi relies on the observation that double-stranded RNA (dsRNA) acts as a signal for gene-specific silencing of expression in many organisms, from the nematode worm, *C. elegans* to mammals (Sharp, 1999). pSUPERretro plasmid (see www.oligoengine.com, and Appendix II for vector map) with an oligo insert corresponding to a 19-nucleotide sequence within the mRNA of Bub1 (specific to both mouse and human Bub1) cloned into the HindIII and BglII sites was kindly provided by Dr Ole Gjoerup (this vector is called "pSUPERretro-Bub1"). The transcript of this recombinant vector is designed so that it will fold back on itself to form a 19-base pair stem-loop structure. This transcript is then cleaved in the cell to produce a functional short

interfering RNA (siRNA), which can mediate strong and specific suppression of gene expression (Brummelkamp *et al.*, 2002). The pSUPERretro-Bub1 vector, and an empty vector control (pSUPERretro) were packaged into retroviruses using the ecotropic packaging line BOSC 23, and the retroviral supernatant harvested was used to infect NIH 3T3 cells in the presence of polybrene. Stable transductants were selected for by culturing in media with 2μg/ml puromycin, and several colonies were isolated and expanded into cell lines. Whole cell lysates were then harvested from these clones, and tested for Bub1 knockdown via western blotting using the three mBub1 monoclonal antibodies, and the rabbit polyclonal NT hBub1 antiserum, to demonstrate that the protein recognised by these antibodies is being silenced by RNAi.

Figure 4.15 shows the results of these western blots. Each blot has 4 lanes, loaded as follows: lane 1 contains NIH 3T3 lysate, lane 2 contains lysate from a clone of NIH 3T3(empty pSUPERretro vector), lane 3 contains lysate from a clone of NIH 3T3(pSUPERretro-Bub1), and lane 4 contains lysate from an independent clone of NIH 3T3(pSUPERretro-Bub1). 60μg of whole cell lysate were loaded for the 13G9 and 17E9 blots, whereas 100μg were loaded for the 2B8 strip, and 30μg for the rabbit polyclonal Bub1 antiserum strip. Different quantities were loaded to account for the different antibody affinities observed when blotting with each antibody, to allow a clear result for each. For all three mBub1 monoclonal antibodies (blots A-C), blotting of these lysates detected strong ~150kDa bands in lanes 1 and 2 in the absence of Bub1 RNAi, but weaker 150kDa bands in lanes 3 and 4 where the Bub1 RNAi transcript is being expressed, and is thus resulting in knockdown of Bub1 protein levels. These results are reiterated by the rabbit polyclonal NT Bub1 antiserum positive control (blot D). Actin levels are also shown to indicate protein loading levels for each blot. This experiment provides further evidence of the specificity of the mBub1 monoclonal antibodies for the Bub1 protein, and again confirms that the Bub1 protein migrates at the higher than expected molecular weight of 150kDa on SDS-PAGE.

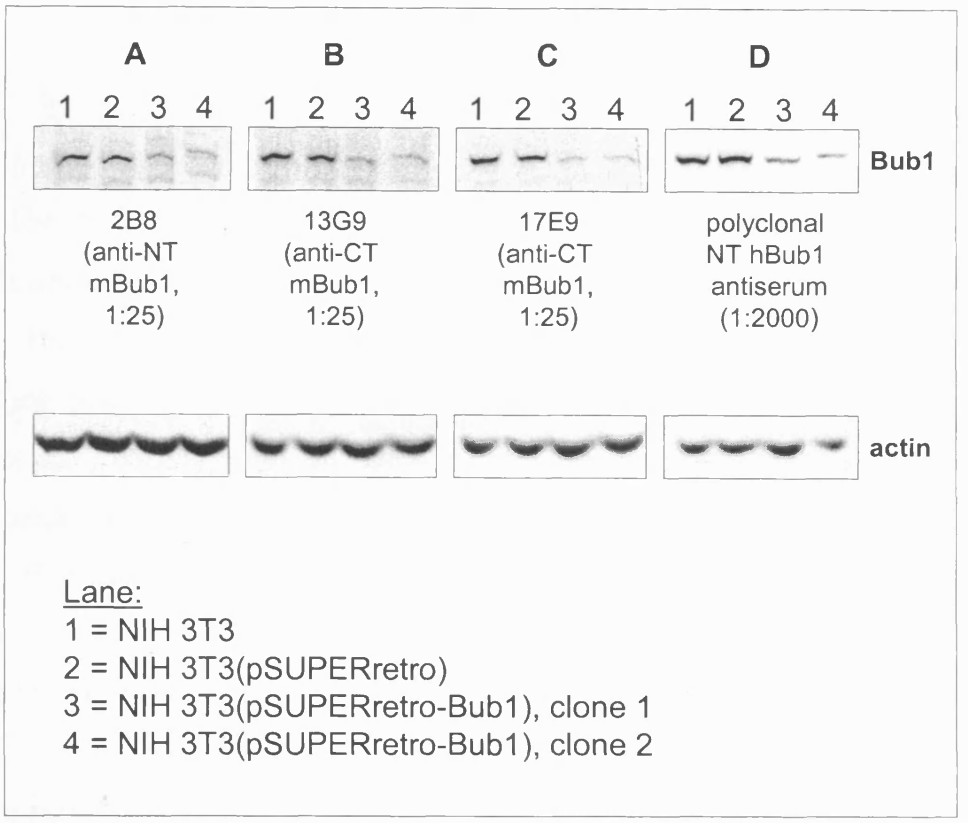

Figure 4.15: Specificity of the mBub1 monoclonals to Bub1: RNAi experiment.

Whole cell lysate from untransfected NIH 3T3 and NIH 3T3 transfected with empty vector control (lanes 1 and 2) show a strong ~150kDa Bub1 band, whereas NIH 3T3 in which Bub1 has been knocked down via RNAi (lanes 3 and 4) show a weak ~150kDa Bub1 band, when blotted using the mBub1 monoclonal antibodies (blots A-C) or with rabbit polyclonal NT hBub1 antiserum (blot D). This shows that these antibodies are specific for the mBub1 protein (migrating at ~150kDa), and not some other protein of similar molecular weight. Actin re-blots of each strip are shown below, indicating protein loading levels.

N.B. 100μg of each lysate was loaded for blot A, 60μg of each lysate for blots B and C, and 30μg of each lysate for blot D, to account for different affinities of the antibodies.

These tests led to the conclusion that monoclonal antibodies against the mouse Bub1 protein had been successfully generated.

4.3.3.3 Immunolocalisation of Bub1 as seen with the mBub1 monoclonal antibodies

The three mBub1 monoclonal antibodies were then used to determine the localisation of the Bub1 protein. There were several reasons for doing this. Firstly, Bub1 antibodies available prior to generation of the monoclonal antibodies described here detected non-specific proteins in addition to Bub1 via western blotting, and so were not suitable for localisation studies. Nevertheless attempts had been made to use these polyclonal antibodies for immunofluorescence in the laboratory, but there had been no success. It was therefore important to determine if the new Bub1 monoclonals were useful for this technique. Secondly, a further test of the specificity of the antibodies was possible by double staining cells with the Bub1 monoclonals, which was possible because they are fortunately all different IgG sub-classes. Finally, the antibodies were used to determine the subcellular localisation of Bub1 throughout the different stages of the cell cycle in cells expressing LT, something that had not been shown before.

Figure 4.16A shows a field of several cells as seen via confocal microscopy, all of which are in interphase except for one cell (indicated by the arrow) which has entered early prophase. Asynchronous NIH 3T3 cells expressing LT ("SE" cells) were grown on glass coverslips and fixed with ice-cold methanol. NT mBub1 monoclonal 2B8 (IgG1) was used to determine Bub1 localisation in Figure 4.16A (Bub1 shown in green), and was visualised using a FITC (Fluorescein)-conjugated secondary antibody. Propidium Iodide (PI) was added to the secondary antibody to stain the DNA in the cells, shown in red. It has previously been shown that Bub1 localises to the kinetochore during mitosis in normal mammalian cells (Taylor and McKeon, 1997).

Figure 4.16: Immunofluorescence in LT-expressing cells using the mBub1 monoclonal antibodies: detection of Bub1, and co-localisation of epitopes.

(A): Staining of NIH 3T3(wild-type LT) cells ("SE") with PI (for DNA localisation) and NT mBub1 monoclonal 2B8. The arrowed cell has entered mitosis (prophase) and shows punctate spots of Bub1, a protein that is known to be localised to the kinetochores at this stage of the cell cycle in normal cells. (B): Double staining using pairs of mBub1 monoclonal antibodies in prometaphase cells, to demonstrate co-localisation of epitopes. The upper panels show double staining of NT mBub1 monoclonal 2B8 and CT mBub1 monoclonal 13G9, the lower panels show co-localisation of the two CT mBub1 monoclonals (13G9 and 17E9). (Scale bars represent 10μm).

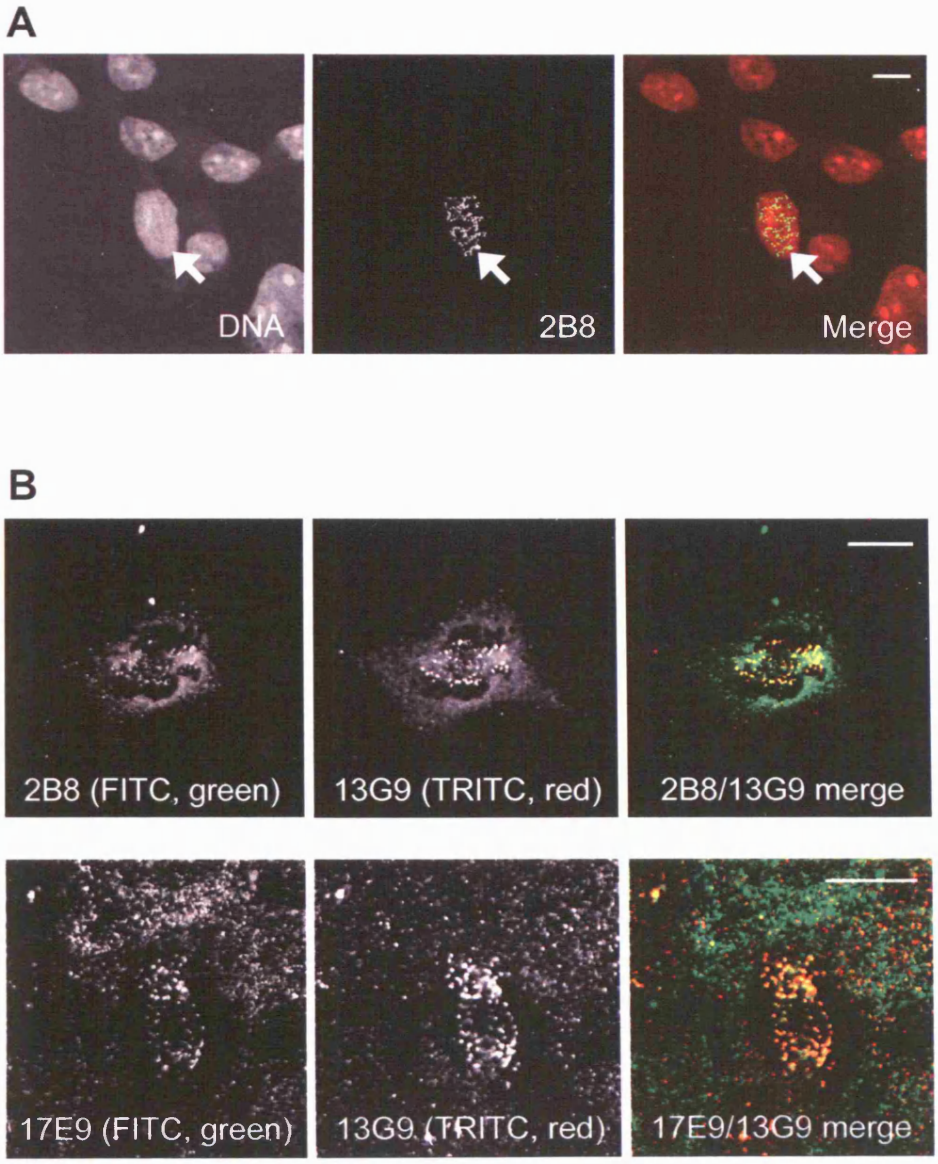

Figure 4.16: Immunofluorescence in LT-expressing cells using the mBub1 monoclonal antibodies: detection of Bub1, and co-localisation of epitopes.

Kinetochores are present on each replicated chromosome, and can be described as two macromolecular protein complexes located on opposite sides of the primary constriction, at the centromeres (Rieder and Salmon, 1998). Some kinetochore proteins, including Mad2 and Bub1 are only found transiently at the kinetochore, during mitosis (Chen *et al.*, 1996; Taylor and McKeon, 1997). The arrowed cell in Figure 4.16A is representative of a small proportion of mitotic cells in the population, and the green dots seen in the nucleus of this cell are visualised using the Bub1 monoclonal 2B8, possibly suggesting labelling of the kinetochore via Bub1. This cell is in early prophase of mitosis, because the DNA is not very noticeably condensed as seen by the red PI staining of the cells. The interphase cells in the field do not show the punctate Bub1 staining because Bub1 is not localised to a well defined structure such as the kinetochore at this stage in the cell cycle, and also because Bub1 levels are low in interphase due to its expression being cell cycle regulated, peaking at G2/M phase (Davenport *et al.*, 1999). This demonstrates that the Bub1 monoclonal antibody 2B8 recognises a protein via immunofluorescence that appears to have the same spatial and temporal localisation proposed for Bub1, a further validation of the specificity of this antibody. However it remains to be demonstrated that the punctate dots recognised by the Bub1 monoclonal antibodies in mitotic cells are actually located at the kinetochore. Figure 4.16A also perhaps suggests that the localisation of Bub1 described in the literature is unaffected by the presence of LT in these NIH 3T3 cells.

The three monoclonal antibodies raised against mBub1 were also used in pairs for immunofluorescence, to demonstrate co-localisation of the proteins recognised by the antibodies, and hence specificity. The upper three panels of Figure 4.16B show a prometaphase SE cell stained with 2B8 (NT mBub1 monoclonal, visualised with FITC-conjugated secondary antibody) and 13G9 (CT mBub1 monoclonal, visualised with TRITC (tetramethylrhodamine isothiocyanate)-conjugated secondary antibody). Preparation of these double-stained immunofluorescence slides was carried

out by Sabine Klischies, a short term student in the laboratory. The yellow dots in the merged image of the upper panels in Figure 4.16B show co-localisation of the proteins identified by 2B8 and 13G9, indicating that they identify the same protein. 2B8 and 13G9 were raised against different recombinant proteins (NT and CT mBub1, respectively), making this co-localisation an even better indication of the specificity of the antibodies to mBub1. Similarly, the lower three panels of Figure 4.16B show a prometaphase SE cell, but this time stained with 17E9 (CT mBub1) and 13G9 (CT mBub1), and again yellow dots indicate co-localisation of the epitopes for these two antibodies. Therefore, co-localisation of protein detected by all three mBub1 monoclonal antibodies further verifies their specificity to the same protein, Bub1.

Although punctate dots had been observed when staining mitotic SE cells with the mBub1 monoclonals, it had not been determined whether they localised to the kinetochores, as would be expected if Bub1 was behaving in the same way in LT-expressing cells as it does in cells with no LT. Unfortunately however, it was not possible during the course of the project to obtain good CREST serum, (an anti-centromere antibody highly specific for CREST syndrome (Calcinosis cutis, Raynaud's phenomenon, Esophageal dysmotility, Sclerodactyly and Telangiectasias)), to enable verification of kinetochore localisation of Bub1 in LT-expressing cells using the mBub1 monoclonal antibodies. Time permitting, it would have been appropriate to have tried to verify this using antibodies raised against alternative centromere proteins such as CENP-A. However, an observation made when capturing immunofluorescence images of SE (NIH 3T3/LT) prometaphase cells stained with the mBub1 monoclonal antibodies suggested that the punctate dots seen in these cells could be localised specifically at the kinetochores of the sister chromatids: the chromosomes of several of the prometaphase cells were forming a ring-like structure, with the punctate, Bub1 dots located in the centre of the ring (see Figure 4.17).

Figure 4.17: Immunolocalisation of Bub1 at the centre of prometaphase chromosome rosettes was observed using the mBub1 monoclonal antibodies.

(A): During prometaphase of the cell cycle, mammalian chromosomes form a rosette structure, with their centromeres (and associated kinetochore proteins) oriented towards the middle of the ring (adapted from Nagele *et al.*, 1995). (B): Staining of two prometaphase NIH 3T3(wild-type LT) "SE" cells for DNA (using PI) and Bub1 (using NT mBub1 monoclonal 2B8) shows that the Bub1 antibody recognises a protein that is localised to the centre of a chromosome rosette, at the same apparent location as the kinetochores in this structure. (Scale bars represent 5μm).

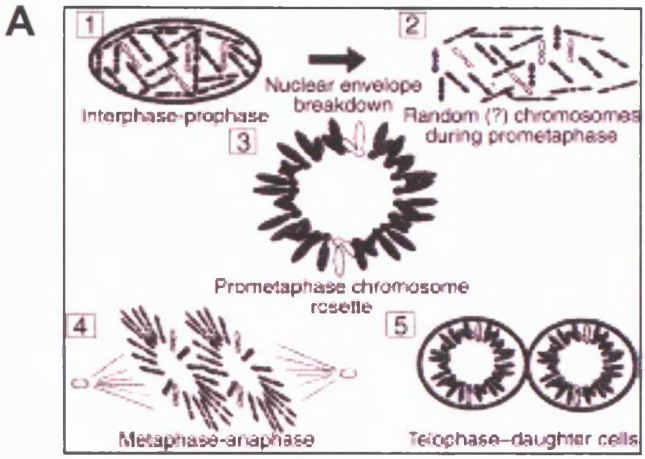

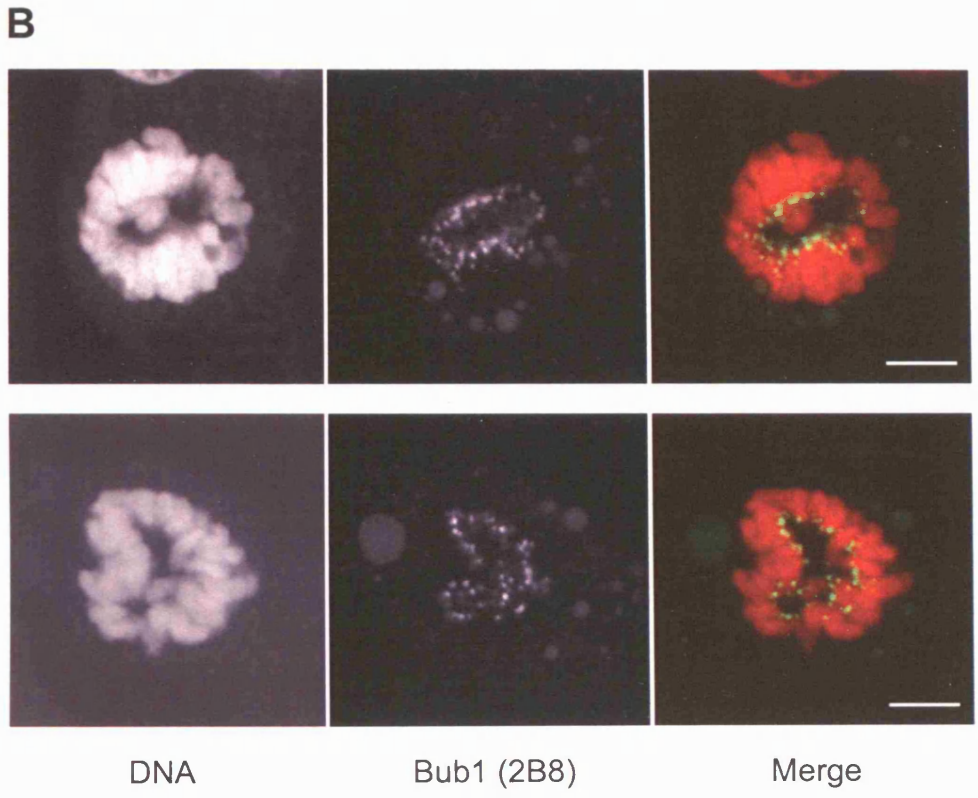

Figure 4.17: Immunolocalisation of Bub1 at the centre of prometaphase chromosome rosettes was observed using the mBub1 monoclonal antibodies.

During a short period in prometaphase all mammalian chromosomes are aggregated into a single, wheel-shaped ring known as a chromosome rosette, with most chromosomes oriented with their arms projecting outward, and their centromeres (and therefore also their kinetochores) in a ring in the centre, (Nagele *et al.*, 1995) as shown in Figure 4.17A. Figure 4.17B shows two different prometaphase SE cells observed to be forming chromosome rosettes, stained for mBub1 monoclonal antibody 2B8 (shown in green), and with their DNA also stained using PI (shown in red). It is clear that the punctate green dots seen with the mBub1 monoclonal in these LT-expressing cells are forming a ring in the centre of the chromosome rosettes, as would be expected if they were co-localised with the kinetochore. Furthermore, murine Bub1 has previously been noted to localise at the kinetochores in the centre of a prometaphase chromosome rosette (Taylor and McKeon, 1997). However, it should be noted that although this observation does not provide absolute proof of kinetochore localisation of Bub1 in these cells, it does suggest that the localisation of Bub1 in LT-expressing cells, as seen by the mBub1 monoclonals, is very similar to that observed by others in cells with no LT.

Finally, an examination of the localisation of Bub1 in LT-expressing cells (SE) through the different phases of mitosis was undertaken in collaboration with S. Klischies. Figure 4.18 shows images of one cell in each stage of mitosis, stained for DNA (red, PI), Tubulin (green), or Bub1 (blue, CT mBub1 monoclonal 13G9), with merged, colour images on the right-hand side. Many examples of each mitotic stage were observed, but only one representative cell is shown for each stage, for clarity.

The subcellular localisation of mBub1 in LT-expressing cells shown in Figure 4.18 suggests that LT is not altering Bub1 localisation from that observed in normal cells (Taylor and McKeon, 1997). The stage of mitosis for each cell in Figure 4.18 was determined by observation of both the DNA staining, the degree of chromosome condensation, and also by observation of the tubulin staining, looking for spindle pole duplication and positioning within the cell.

Figure 4.18: Subcellular localisation of mBub1 during mitosis does not appear to be affected by the presence of LT.

Asynchronous NIH 3T3(wild-type LT) "SE" cells were fixed and stained for DNA (shown in red), tubulin (shown in green) and Bub1 (using CT mBub1 monoclonal 13G9, shown in blue). Representative cells for the different stages of mitosis are shown, and indicate that Bub1 localisation through these stages does not differ in cells expressing LT from the pattern previously described in the literature for normal cells. Bub1 is seen in punctate spots (presumably at the kinetochores of condensed chromosomes) from prophase until prometaphase, but once all chromosomes have formed a bipolar attachment to the mitotic spindle at the metaphase plate, the spindle checkpoint is inactivated, Bub1 dissociates from kinetochores, and cells undergo anaphase. (Scale bars represent 10μm).

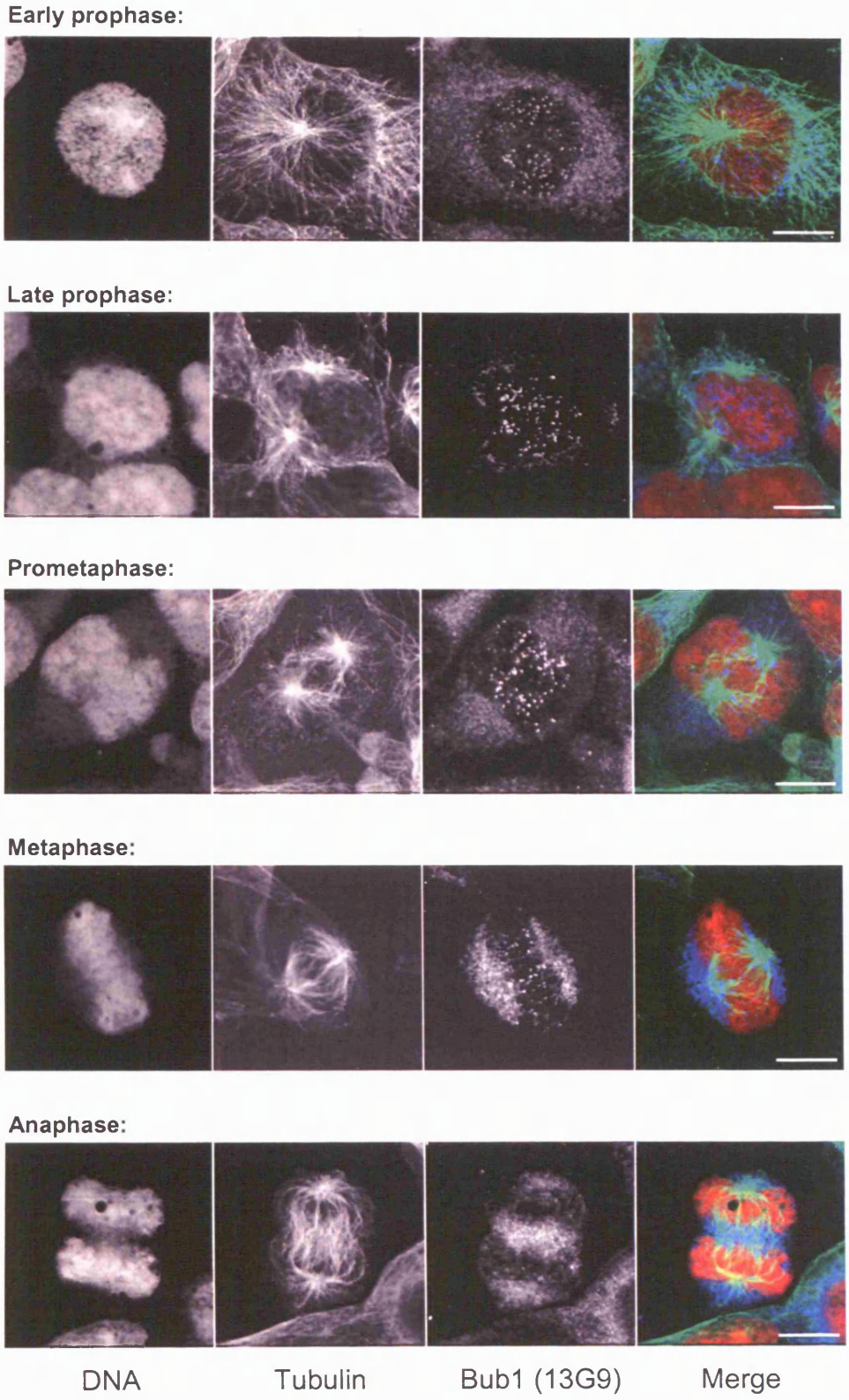

Figure 4.18: Subcellular localisation of mBub1 during mitosis does not appear to be not affected by the presence of LT.

The Bub1 staining first appears as punctate spots (presumably at the kinetochores, although again this has not been confirmed) when the DNA begins to condense, in early prophase. By late prophase, and prometaphase, the punctate spots of Bub1 are very clearly seen. In the cell labelled as metaphase there is still some punctate Bub1 staining, but this may be indicative of not all chromosomes actually being properly aligned at the metaphase plate with a bipolar attachment, rather than mislocalisation of Bub1, which is expected to have dispersed from the kinetochores by this stage. At anaphase the punctate Bub1 spots have disappeared, as is also seen in normal cells with no LT (Taylor and McKeon, 1997). In addition to the punctate spots of Bub1 localised in the same region as the DNA in these cells, the Bub1 images in Figure 4.18 also appear to show dispersed staining in the regions of the cell not occupied by the DNA. It has not been determined if this is also Bub1 protein or if it is simply due to some non-specificity of either the mBub1 monoclonal antibodies or the secondary antibodies used for immunofluorescence. It should be noted that double staining for LT and Bub1 localisation was also carried out in SE cells (data not shown), but no obvious co-localisation was observed. Dispersed nuclear staining was observed for LT throughout the cell cycle, with no punctate dots seen that might indicate any possible localisation with Bub1. This does not rule out the possibility that Bub1 and LT may co-localise in small quantities at some stage during the cell cycle, not necessarily during mitosis.

4.3.4 Affinity purification of mBub1 monoclonal antibodies

The mBub1 monoclonal antibodies that were generated had previously been tested using hybridoma tissue culture supernatants. Although good results were obtained for the specificity and utility of the antibodies, it was thought that the sensitivity of the antibodies could be improved by affinity purification.

Protein A, Protein G and Protein L are three bacterial proteins whose antibody-binding properties have been well characterised. These proteins have been purified from recombinant producers and used routinely for affinity purification of antibodies from a variety of species. Proteins A, G and L bind to antibodies at sites other than the antigen-binding domain, and for this reason are useful for the purification of general immunoglobulin from a crude sample. It was decided to use Protein G immobilised to a solid support in columns to affinity purify general IgG from the hybridoma tissue culture supernatants, for two reasons. Firstly, it was not seen as necessary to use the antigen itself rather than Protein A or G (or any of the other commonly used IgG-binding proteins) for the purification from these supernatants, because they contained monoclonal antibodies with a proven "clean" and high specificity for mBub1. Monoclonal antibodies by definition have a single specificity due to them being derived from a single hybridoma clone. In contrast, a polyclonal antibody would contain only a very small proportion of IgG specific to the antigen of interest. Secondly, as described previously, Protein G is able to bind a greater range of mouse IgG sub-classes than Protein A, and in particular has a much greater affinity for IgG1, the sub-class of monoclonal 2B8. Protein G was therefore suitable for affinity purification of all three sub-classes of monoclonal antibody.

All steps of the antibody purification process were carried out at the MRC Prion Unit in the Institute of Neurology, UCL, under the supervision of Dr Gary Mallinson.

Each antibody supernatant was concentrated by ultrafiltration, and bound to a Protein G column, washed, and eluted, using the ÄKTA*prime* machine, an automated liquid chromatography system from Amersham Biosciences. The elution fractions containing the most protein (typically fractions 2-4, as determined from the UV reading recorded during the purification process, data not shown) were pooled, and 0.1% NaN_3 was added to inhibit bacterial growth.

The following yields of affinity purified antibody were obtained from 350ml of initial hybridoma tissue culture supernatant: 3.6ml of NT mBub1 monoclonal 2B8 at 0.8mg/ml, 1ml of CT mBub1 monoclonal 13G9 at 2.22mg/ml, and 2ml of CT mBub1 monoclonal 17E9 at 1mg/ml. Storage of the antibodies at these relatively high protein concentrations has the advantage that it tends to stabilise the native structure of the immunoglobulin molecule.

NIH 3T3 (mouse) and U20S (human) whole cell lysates were western blotted using the concentrated, affinity purified mBub1 monoclonals, and it was found that these reagents can be used at a dilution of 1:250, i.e. 10-fold greater than the 1:25 dilution necessary when using tissue culture supernatant (data not shown). The affinity purified antibodies showed the same species specificities seen previously (2B8 detects both mBub1 and hBub1, whereas 13G9 and 17E9 only detect the mBub1 protein). The non-specific bands seen when western blotting with hybridoma tissue culture supernatant previously (see Figures 4.13 and 4.14) were not greatly reduced in intensity upon affinity purification of the antibodies, although it was hoped that the affinity purification would at least have removed the majority of unwanted immunoglobulin proteins present in the BSA and other tissue culture medium components in the hybridoma supernatant, leaving almost exclusively the mouse IgG proteins specific to mBub1.

4.3.5 Validation of utility of mBub1 monoclonals for Bub1-LT interaction studies

The focus of this project is the interaction between Bub1 and LT, and therefore it was very important to determine the ability of the newly generated monoclonal antibodies against Bub1 to detect the Bub1-LT interaction via co-immunoprecipitation.

Figure 4.19 shows the results of immunoprecipitation experiments carried out using both mouse (NIH 3T3) and human (U20S) whole cell lysates, either untransfected, or expressing wild-type LT or dl89-97 (non-

Bub1-binding) LT. 500μg of whole cell lysate was immunoprecipitated with either no antibody at all, with 3μl of either 2B8, 13G9 or 17E9 affinity purified mBub1 monoclonal antibody (the concentrated affinity pure antibodies), with 3μl of rabbit polyclonal CT hBub1 antiserum (as previously described), or with 30μl of PAb423, a monoclonal antibody (tissue culture supernatant) directed against the carboxy-terminal region of LT. The immunoprecipitates were then run on 8% SDS-PAGE and western blotted for Bub1 (using polyclonal NT hBub1 serum), followed by re-blotting for LT (using PAb423). These immunoprecipitations were all carried out using Protein A-sepharose beads, except for the immunoprecipitations using antibody 2B8, for which Protein G-sepharose beads were used.

In NIH 3T3 (mouse) cells, Bub1 was immunoprecipitated equally well from all three cell lines (with or without wild-type LT or dl89-97 LT) with each of the mBub1 monoclonals, 2B8, 13G9 and 17E9, all of which brought down strong 150kDa Bub1 bands, as seen by blotting with the rabbit polyclonal antiserum against NT hBub1 (See Bub1 blot of lanes 4-12 in Figure 4.19). The CT hBub1 rabbit polyclonal antiserum also immunoprecipitated a strong 150kDa band in each NIH 3T3 cell line, as seen in the NT hBub1 antiserum blot of lanes 13-15, but these bands appeared a little "smeary", probably due to the fact that each of these antibodies recognise non-specific bands quite strongly, a problem not seen with the new, clean Bub1 monoclonals. No 150kDa Bub1 bands are seen in the control lanes where NIH 3T3 lysates were immunoprecipitated without antibody (Bub1 blot of lanes 1-3), as is to be expected. Also, no 150kDa Bub1 band was observed when the lysates were immunoprecipitated for LT with PAb423 (Bub1 blot of lanes 16-18), whereas a band would be expected in the lane containing NIH 3T3 (wild-type LT) (Bub1 blot of lane 17), the LT that is able to interact with Bub1, as shown previously.

Figure 4.19: Co-immunoprecipitation of LT with Bub1 using the affinity purified mBub1 monoclonal antibodies.

Whole cell lysates from NIH 3T3 (mouse) or U20S (human) cells, either untransfected, or expressing wild-type (wt) LT or dl89-97 LT were immunoprecipitated using either no antibody (negative control), affinity purified mBub1 monoclonal antibody (2B8, 13G9 or 17E9), rabbit polyclonal CT hBub1 antiserum (positive control), or PAb423 (anti-LT monoclonal), and blotted for Bub1 (using NT hBub1 polyclonal antiserum) or LT (using PAb423). CT mBub1 monoclonal 2B8 is able to co-immunoprecipitate LT from NIH 3T3 cells expressing wild-type LT.

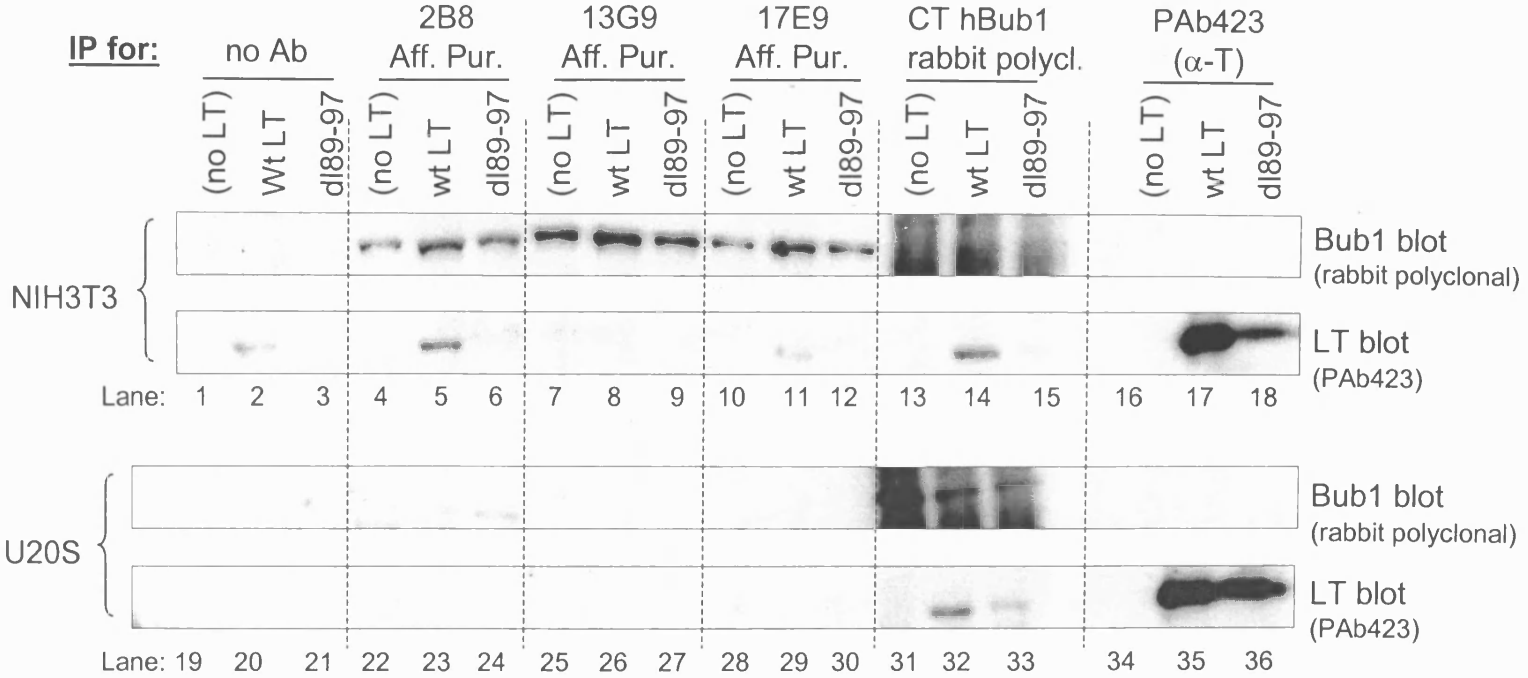

Figure 4.19: Co-immunoprecipitation of LT with Bub1 using the affinity purified mBub1 monoclonal antibodies.

This has been a continuing problem during the course of this project, because even with many attempts at optimising conditions, it has not been possible to demonstrate the LT-Bub1 interaction by co-immunoprecipitating Bub1 with LT (although it is readily observed when lysates are immunoprecipitated for Bub1 and blotted for LT, as shown in Chapter 3). Perhaps this observation is due to only a very small proportion of the LT in the cells interacting with Bub1, resulting in the majority of the immunoprecipitated LT protein not bringing Bub1 with it. The difficulty in detecting this small quantity of Bub1 could be exacerbated by the relative insensitivity of the Bub1 antibody in comparison to the LT antibody for western blotting. Conversely, even if only a small quantity of immunoprecipitated Bub1 is bringing down LT with it, the strong specificity of the LT antibody PAb423 allows its detection. However, PAb423 has been shown to be capable of co-immunoprecipitating Bub1 by previous members of the laboratory (Cotsiki *et al.*, 2004), although the reasons for the current difficulties remain elusive. Perhaps the exact cell lines used in the present study are in some way different to those used previously, but this would need further investigation. Given more time it would have been interesting to see if expression of an epitope-tagged LT protein and immunopreciptation using an antibody specific to the epitope tag would have allowed visualisation of the LT-Bub1 interaction via co-immunoprecipitation.

When the Bub1 immunoprecipitations in NIH 3T3 cells were re-blotted for LT (using monoclonal antibody PAb423), a strong 100kDa LT band was seen to co-immunoprecipitate with Bub1 in the wild-type LT-containing cells only when immunoprecipitating with either Bub1 monoclonal 2B8 (see Figure 4.19, LT blot of lane 5), or with the rabbit polyclonal antiserum against CT hBub1 (LT blot of lane 14). As expected, no 100kDa LT bands were precipitated by any of the Bub1 antibodies from the NIH 3T3 lysate that did not contain LT, or from the NIH 3T3(dl89-97 LT) lysate where the Bub1 interaction site on LT is deleted. A weak 100kDa LT band is co-immunoprecipitated by the Bub1 monoclonal 17E9 from the NIH 3T3(wild-type LT) lysate (LT blot, lane 11), but this does not indicate a strong co-

immunoprecipitation of LT with Bub1 by this antibody, as a 100kDa band of equal strength can be seen in the equivalent lane for the co-immunoprecipitation using no antibody, (LT blot, lane 2, probably seen due to the observation noted in the laboratory that LT expressed in mouse cells appears to stick to Protein A-sepharose beads). However, this does not offer an explanation for why no 100kDa band is seen at all in the NIH 3T3(wild-type LT) lysate immunoprecipitated using antibody 13G9 (LT blot, lane 8). Perhaps the epitope on Bub1 recognised by 13G9 is important for this observation. As expected, in the LT blot, no LT is seen to be immunoprecipitated by LT antibody PAb423 from NIH 3T3 cells that express no LT in the first place. The LT immunoprecipitation, blotted for LT shows a very strong 100kDa wild-type LT band (lane 17), and a less strong 100kDa dl89-97 LT band (lane 18), indicating the relative expression levels of these proteins.

The same collection of immunoprecipitation experiments was conducted using whole cell lysates from untransfected U20S cells, or U20S cells expressing wild-type LT or dl89-97 LT, as shown in the bottom half of Figure 4.19 (lanes 19-36). As seen in the NIH 3T3 cells, the CT hBub1 rabbit polyclonal antiserum was able to immunoprecipitate strong 150kDa Bub1 bands in all three U20S cell lines, as seen in the NT hBub1 polyclonal antiserum blot (Bub1 blot of lanes 31-33). The only other antibody able to immunoprecipitate the 150kDa human Bub1 protein was NT mBub1 monoclonal 2B8, as seen by the faint 150kDa bands in each lane for that antibody (Bub1 blot, lanes 22-24). As expected, no Bub1 bands were seen when immunoprecipitations were carried out in the absence of antibody (lanes 19-21). 13G9 and 17E9 immunoprecipitations blotted for Bub1 (lanes 25-30) do not show any 150kDa bands either, indicating that these CT mBub1 monoclonal antibodies are not able to immunoprecipitate the human Bub1 protein. As observed in the NIH 3T3 co-immunoprecipitation using LT monoclonal antibody PAb423, no Bub1 could be seen to co-immunoprecipitate with LT from the U20S lysates (Bub1 blot, lanes 34-36).

When these U20S immunoprecipitations were re-blotted for LT using PAb423, the only Bub1 antibody seen to be capable of co-immunoprecipitating LT from human cells was the rabbit polyclonal antiserum raised against CT hBub1, as indicated by a strong 100kDa LT band in the U20S(wild-type LT) lane (LT blot, lane 32). This antibody also appears to reveal a weak interaction between the dl89-97 LT and Bub1 in U20S cells (weak 150kDa band in LT blot, lane 33), although this may be due to an indirect interaction, as suggested in Chapter 3. This explanation is further validated by the LT immunoprecipitation in the U20S cell lines using PAb423, blotted using the same antibody (LT blot, lanes 35 and 36), which indicated that the level of LT expression was approximately equal in the U20S(wild-type LT) and the U20S(dl89-97) LT cells.

4.4 SUMMARY & DISCUSSION

In conclusion, three good monoclonal antibodies, 2B8, 13G9 and 17E9, have been generated against the mouse Bub1 protein. 2B8 is an IgG1 sub-class monoclonal and is specific to the amino-terminus of mBub1, 13G9 and 17E9 are independent monoclonals specific to the carboxy-terminal region of mBub1, and are IgG2a and IgG2b sub-class, respectively. The specificity of all three antibodies for the Bub1 protein itself has been verified by use of several techniques, including ectopic expression of HA-tagged mBub1 protein, and RNAi. The CT-specific mBub1 monoclonals are specific to the mouse Bub1 protein, which they recognise strongly and very specifically in western blots, whereas the NT-specific mBub1 monoclonal detects both the mouse and human Bub1 proteins, but does not western blot so strongly. All three monoclonals immunoprecipitate Bub1 well from mouse whole cell lysate, but only 2B8 can effectively co-immunoprecipitate LT. 2B8 is also able to immunoprecipitate Bub1 from human lysate (albeit very weakly), but unfortunately the Bub1-LT complex cannot be demonstrated in U20S(wild-type LT) cells using this antibody. Although it was more difficult to purify

sufficient native Bub1 protein for monoclonal antibody production in comparison to the large quantities of denatured protein that were more easily purified, the results achieved here suggest that it was worth the effort, as it was the native antigen (mBub1(1-561)) that produced the most effective monoclonal for immunoprecipitation studies, a technique used frequently in this project for investigation of the LT-Bub1 interaction. In the future it would be interesting to see if the reciprocal co-immunoprecipitation, using PAb423 to bring down Bub1 would work if one of the new mBub1 monoclonal antibodies was used for the blotting, rather than the rabbit polyclonal antiserum against NT hBub1 used in Figure 4.19. This has been tried before without success, but perhaps the immunoprecipitation conditions could be further optimised.

Problems were initially encountered in deciding where on an SDS-PAGE gel the Bub1 protein actually migrates, as the predicted molecular weight of 120kDa for Bub1 was much lower than that observed during the screening of the Bub1 monoclonals. Also, it had been suggested in the literature that Bub1 migrates at 120kDa on SDS-PAGE. Subsequent experiments verified that Bub1 actually migrates at around the 150kDa region, and it is thought that this could be due to some as yet unidentified post-translational modification. A good example of proteins that migrate on SDS-PAGE much slower than their molecular weight prediction would suggest, is the adenovirus E1A proteins. The primary translation products of the 12S and 13S mRNAs synthesised from the E1A region have apparent molecular weights of 42 and 45 kDa, respectively, when run on SDS-PAGE, significantly different from their predicted molecular weights (26 and 32 kDa). It was suggested that these aberrant migrations are probably due to the unusually high content of proline and acidic residues in these proteins, but in addition, approximately 60 polypeptide species of the 12S and 13S products have been resolved via high-resolution two-dimension gels, induced by differential phosphorylation of serine residues (Richter *et al.*, 1988). Had this information been known at the beginning of the project, the decision on which

of the NT mBub1-immunised mice to choose for hybridoma generation would have been different, perhaps resulting in even better NT mBub1 monoclonal antibodies than 2B8. Nevertheless, the information obtained during the course of these experiments suggested that the 150kDa band seen in western blotting experiments really is Bub1, making future studies of Bub1 and the LT-Bub1 interaction much easier.

All three monoclonal antibodies against mBub1 were also shown to be very useful for immunofluorescence studies in mouse cells, and were used to demonstrate Bub1 localisation in cells expressing LT, throughout the cell cycle. The immunolocalisation studies in SE cells using the mBub1 monoclonal antibodies suggest that the subcellular localisation of Bub1 is not disrupted by the presence of LT at any point during the cell cycle. However, parallel immunolocalisation studies in cells with no LT, or in cells expressing dl89-97 LT would be necessary to establish for certain that the subcellular localisation of Bub1 is not affected by LT interaction. In addition, it would be very interesting to determine if localisation of Bub1 in LT-expressing cells deviates from wild-type behaviour in any way in cells treated with the microtubule-depolymerising drug nocodazole.

Although the purpose of generating monoclonal antibodies against mouse Bub1 was for use in subsequent experiments to study the effect of the LT-Bub1 interaction on the spindle checkpoint, later on in the project it became clear that the most meaningful information about this mechanism was going to come from studies in human cells, and not from mouse cells. It seems that the spindle checkpoint is more robust in human cells than mouse cells, as seen in experiments conducted in this laboratory. NT mBub1 monoclonal 2B8 was shown to be capable of detecting by western blot and immunoprecipitating the human Bub1 protein, but unfortunately was not capable of co-immunoprecipitating LT. However Dr Raimundo Freire (Hospital Universitario de Canarias, Tenerife, Spain) had kindly provided sufficient CT hBub1 rabbit polyclonal antiserum to enable studies of the Bub1-LT interaction in human cells to go ahead.

The monoclonal antibodies generated against mouse Bub1 will nevertheless provide a very useful tool for future studies of the localisation of Bub1 in mouse cells expressing LT or dl89-97 LT, under the influence of the microtubule-depolymerising drug nocodazole, for example. Dr Ole Gjoerup at the Dana Farber Cancer Institute in Boston, MA, USA is particularly interested in the kinase functions of Bub1, and has also been testing these newly generated mBub1 monoclonal antibodies. He reports that all three are able to immunoprecipitate the Bub1 kinase in an active form, providing a further future use for these antibodies.

In summary, several highly specific monoclonal antibodies with multiple uses have been generated against the mouse Bub1 protein, providing cleaner reagents for future studies centred on this spindle checkpoint protein. In addition, monoclonal antibodies against the human Bub1 protein have now been generated in the laboratory using information learnt from this study, to complement the reagents currently available for this project.

5. Effects of SV40 LT-Bub1 interaction on cell cycle regulation

5.1 OBJECTIVES

The work described in the previous chapters provided the cell lines and reagents necessary to study the function of the LT-Bub1 interaction. The aim of the experiments detailed in this chapter was to use these tools to examine the possibility that LT is able to inhibit spindle checkpoint function by virtue of its interaction with the checkpoint kinase Bub1. Attempts were made to elucidate the mechanism by which LT could be carrying out this function. In addition, a karyotyping study was performed to determine if it would be possible to detect aneuploidy caused specifically by this interaction. Finally, the effect of LT-Bub1 interaction on the G1/S (p53-dependent) tetraploidy checkpoint was examined, to determine if this post-mitotic checkpoint is abrogated by both wild-type and non-Bub1-binding LT, and to look at the potential down-stream effects on genomic stability.

5.2 EXPERIMENTAL STRATEGY

Initial attempts to determine the ability of NIH 3T3 (mouse) and U20S (human) cell lines either untransfected, or expressing wild-type LT or non-Bub1-binding, dl89-97 LT to arrest at the spindle checkpoint in response to treatment with the microtubule-depolymerising drug nocodazole involved synchronisation of the cells prior to nocodazole treatment. Cells were synchronised either using the mitotic shake-off technique (M phase block), or using L-Mimosine (S phase arrest). The response of each cell line to drug treatment was monitored via fluorescence-activated cell sorting (FACS), or via western blotting. However, spindle checkpoint compromise was best

demonstrated by treating asynchronous cultures with nocodazole, and this method was used for all subsequent experiments.

The soluble and insoluble fractions of protein lysates from cells treated with nocodazole were compared via western blot to determine if observed differences in protein levels were due to changes in subcellular localisation of the proteins of interest. Also, the effect on securin levels of varying lengths of nocodazole treatment was examined to establish whether different growth or checkpoint adaptation rates were the cause of the differences seen between cell lines, rather than a direct effect on the spindle checkpoint by LT via Bub1.

Having demonstrated differences in spindle checkpoint activation via western blot for cells expressing wild-type LT, in comparison to cells expressing either dl89-97 LT or no LT at all, the same conditions and nocodazole treatments were used to begin to examine the mechanism via co-immunoprecipitation experiments.

Time lapse microscopy was used to investigate the effect of nocodazole on REFs expressing either wild-type LT or dl89-97 LT.

A preliminary investigation of the effect of wild-type LT on genomic stability was carried out by investigating the karyotype of tumourigenic versus non-tumourigenic wild-type LT-expressing cell lines.

To investigate the ability of wild-type LT versus dl89-97 LT to override the p53-dependent G1/S tetraploidy checkpoint, NIH 3T3 cells expressing either of these LT proteins, or untransfected cells were treated with the drug dihydrocytochalasin B (DCB) that prevents the growth of actin filaments, thereby inhibiting cytokinesis and triggering the tetraploidy checkpoint. The chromosome content of the cells was monitored via FACS at 24 hours following release from the drug, and also at 48-hour and 5-day release points.

5.3 RESULTS

5.3.1 LT inhibits spindle checkpoint function via interaction with Bub1

The ultimate aim of this project was to determine whether the interaction of SV40 LT antigen with Bub1 functionally affects the spindle checkpoint.

5.3.1.1 Examination of spindle checkpoint function using FACS and western blot analysis, with synchronised cells

Spindle checkpoint function experiments were first carried out in untransfected NIH 3T3 cells and NIH 3T3 cells expressing wild-type LT or dl89-97 LT, with the aim of identifying conditions under which a checkpoint defect can be demonstrated. It was then intended that the mBub1 monoclonal antibodies generated (see Chapter 4) would be used in immunoprecipitation experiments to investigate spindle checkpoint function in these cell lines.

In initial experiments, NIH 3T3 cells (untransfected or expressing wild-type LT or dl89-97 LT) were treated with different doses of the microtubule-depolymerising drug, nocodazole (De Brabander *et al.*, 1976). Nocodazole prevents microtubule polymerisation and hence formation of the mitotic spindle, resulting in activation of the spindle assembly checkpoint and cell cycle arrest in mitosis. The ability of this drug to block normal chromosome segregation in a reversible manner has led to its widespread use for cell cycle synchronisation of cultured cells, and for studies of mitosis and the spindle checkpoint (reviewed in (Peterson and Mitchison, 2002)). Asynchronous cultures of each of the NIH 3T3 cell lines were seeded and cultured at 37°C for 12 hours, at which point they were treated with nocodazole doses ranging from 10-100ng/ml (encompassing the range of nocodazole doses commonly used for spindle checkpoint activation in the literature), for 12 hours. Cells were then fixed for PI (Propidium iodide) FACS (fluorescence-activated cell sorting) analysis to determine the proportion of cells in different phases of the

cell cycle in each cell line. PI FACS analysis is a form of flow cytometry, the measurement (meter) of certain physical and chemical characteristics of single cells (cyto) as they flow in suspension one by one past a series of detectors. Cells are first stained with Propidium iodide (PI), a DNA intercalating fluorescent dye that excites at 495nm. PI does not penetrate the cell membrane, and thus requires cells to be fixed or permeabilised prior to staining. PI interacalates RNA as well as DNA, and so to ensure that the fluorescent signal observed is purely from the DNA, ribonuclease (RNase) was included in the staining procedure to degrade the RNA. As the PI-stained cells flow through the FACS machine, each cell scatters some light and the labelled cells generate fluorescent signals from the dye. These two parameters (light scatter and fluorescent signal) are gauged by photodetectors to generate a histogram indicating the relative DNA contents of the cell population, and hence the proportion of cells in G1 (2N DNA content), S and G2/M (4N DNA content) phase of the cell cycle, as well as any polyploid (>4N DNA content) cells. Control samples of the NIH 3T3 cell lines with no drug treatment were also examined by PI FACS at two time points corresponding to the addition of nocodazole to the other samples, and the point at which the drug-treated samples were fixed.

Cell cycle analysis was carried out at the FACS laboratory at Cancer Research UK (Lincoln's Inn Fields, London), in collaboration with Dr Derek Davies, using the BD FACSCalibur^{TM} system. Samples were PI stained, followed by analysis of 20,000 events (cells) via FACS. It was postulated that if interaction of LT with Bub1 compromises spindle checkpoint function, a lower proportion of cells would arrest in M phase at the checkpoint in response to spindle damage in the NIH 3T3(wild-type LT) cell line compared to untransfected NIH 3T3 or NIH 3T3(dl89-97 LT) cells. Several nocodazole concentrations were tested because it was not known how sensitive to level of spindle damage this experiment would be, and previous experiments had suggested a link to low levels of spindle damage and checkpoint leakiness. In repeated experiments, it did not seem possible to find a significant difference

in the proportions of 4N (G2/M phase) cells between the cell lines, and this was the same for all drug concentrations tested, although there was a hint that slightly fewer NIH 3T3(wild-type LT) cells were being arrested at the spindle checkpoint by nocodazole than NIH 3T3(dl89-97 LT) or untransfected cells (data not shown).

It is possible that the difficulties in detecting differences between the responses to nocodazole were partly due to starting with asynchronous cultures, with slightly different proportions of cells for each cell line already in G2/M phase when the drug was added. These cells would contribute to the G2/M peak in the FACS histograms, and thus their initial variability would make any subtle differences between the cells lines due to spindle checkpoint defects difficult to detect. For this reason, it was decided to try synchronising the NIH 3T3 cells so that virtually no cells were in G2/M phase of the cell cycle prior to carrying out the nocodazole treatment and subsequent FACS analysis.

It was noted during the initial experiments with nocodazole and FACS that the M phase arrest seen with 30ng/ml of the drug and higher was extremely efficient, with around 90% of the cell population arresting with 4N DNA content. For this reason, the NIH 3T3 cell lines were treated with 50ng/ml nocodazole for 12 hours, at which point arrested cells were isolated via mitotic shake-off, and re-plated. Samples of these cells were fixed at regular time points up to 24 hours and analysed by PI FACS to determine the release time required for the cells to enter S phase, but without passing through to the next round of mitosis. Unfortunately, no time point could be found at which all three cell lines had reached the correct phase of the cell cycle, due to the cell lines each having different growth rates. To try to combat this problem, attempts were made to pulse label S phase cells with bromodeoxyuridine (BrdU) following an 11 hour release from mitotic shake-off (the point at which many cells in each cell line were in S phase, although not in equal proportions), and then to specifically examine the cell cycle profiles of these BrdU-labelled cells following treatment with nocodazole.

BrdU is an analogue of thymidine and is taken up into the DNA of cycling cells. This is then detected by unwinding the DNA (using acid, alkali or enzyme) and then using an antibody against BrdU. In this way, G1, S and G2/M cells can be separated. This method still failed to reveal any significant results, as the cells quickly appear to become asynchronous again following mitotic shake-off and release (data not shown).

It has been suggested that human cells might be more easily synchronised than NIH 3T3 (mouse cells), and so attempts to demonstrate spindle checkpoint defect in LT-expressing mouse cells was abandoned in favour of U20S cell lines, generated and kindly provided by our collaborators in Tom Roberts' laboratory (Dana Farber Cancer Institute, Boston, MA, USA). At their suggestion, attempts were made to synchronise U20S cells, and U20S cells expressing wild-type LT or dl89-97 LT, with L-Mimosine (β-*N*-[3-hydroxy-4-pyridone]-α-amino-propionic acid), a naturally-occurring rare amino acid derivative isolated from *Mimosa* and *Leucaena* plants. This drug is an inhibitor of DNA replication in mammalian cells, arresting cells (reversibly) in S phase, at a point after DNA synthesis has begun (Hughes and Cook, 1996). Because the arrest caused by mimosine is at S phase, a point in the cell cycle only separated by a relatively short time from M phase (the phase at which nocodazole arrests), it was thought that problems caused by different growth rates of the cell lines could be reduced by making use of mimosine followed by a short release. U20S cell lines (untransfected, or expressing wild-type LT or dl89-97 LT) were treated with 200μM mimosine for 18 hours to arrest growth, followed by washes in medium to remove the drug, and a 6 hour release in fresh medium to allow the cells to progress further into S phase. At this point, cells were treated for 12 hours with nocodazole at concentrations between 0 and 100ng/ml, and the cells were then fixed for PI FACS analysis. Samples of cells taken immediately after mimosine treatment, and immediately before nocodazole treatment were also fixed for cell cycle analysis. The FACS results (data not shown) did not show a strong synchronisation of the U20S cells, as a small proportion of cells

appeared to remain at G2/M phase. The 6 hour release from mimosine did appear to send many cells into late S phase, as hoped, although once treated with nocodazole no significant difference between the cell lines could be seen for the proportion of cells arrested at the spindle checkpoint in M phase.

Since FACS analysis did not provide a convincing demonstration of a spindle checkpoint defect caused by LT, subsequent experiments used western blotting of lysates from cells treated with nocodazole, to examine any differences in levels of proteins that indicate spindle checkpoint arrest, e.g. securin and Cyclin B. These proteins are destroyed once the spindle checkpoint has been satisfied, immediately prior to anaphase, and so an accumulation of these proteins in response to nocodazole treatment is indicative of spindle checkpoint arrest occurring in the treated cells.

The first attempt at using western blotting for securin and Cyclin B to demonstrate a spindle checkpoint defect in nocodazole-treated cells was carried out in the U20S cell lines, with mimosine synchronisation. As for the FACS analysis experiments, untransfected U20S cells, and U20S cells expressing wild-type LT or dl89-97 LT were treated with 200μM mimosine for 18 hours, followed by a 6 hour release in fresh medium. Cells were then treated with different doses of nocodazole ranging from 0-100ng/ml. Following 12 hours of nocodazole treatment, plates were lysed with RIPA buffer and 10μg samples of each were loaded on a 12% SDS-PAGE gel and blotted for securin (using a rabbit polyclonal antibody against human PTTG-1 (PTTG-1 (Pituitary Tumour-Transforming Gene 1) is the vertebrate homolog of securin (Zou *et al.*, 1999)), Cyclin B (Cyclin B1 is the major mitotic cyclin), and actin (for loading levels). This experiment was carried out twice, but neither experiment gave a very convincing result for a spindle checkpoint defect in wild-type LT-containing cells, although a very slightly lower level of securin was seen in these cells compared with cells with no LT, or dl89-97 LT (data not shown). It was presumed that difficulties in seeing a difference in securin and Cyclin B levels between the cell lines in this experiment could be due to either ineffective mimosine synchronisation, some cells failing to

continue cycling following mimosine treatment, or perhaps due to different growth rates of the cell lines.

At this point members of Tom Roberts' group had demonstrated that LT does in fact cause a spindle checkpoint defect via interaction with Bub1, by determining the mitotic index of nocodazole treated cells (Cotsiki *et al.*, 2004). They also showed that bypass of the spindle checkpoint by LT is accompanied by increased endoreduplication (accumulation of cells with a DNA content greater than 4N) in the presence of nocodazole, as is to be expected if the LT-Bub1 interaction is causing a spindle checkpoint defect (Taylor and McKeon, 1997). These findings only served to reinforce the importance of finding reproducible conditions under which securin (and Cyclin B) levels were significantly lower in response to nocodazole treatment in U20S(wild-type LT) cells than in untransfected U20S or U20S(dl89-97 LT) cells, so that these conditions could then be used to examine the biochemical mechanism by which LT inhibits the spindle checkpoint.

One final attempt was made at using synchronised cells to examine the effect of nocodazole treatment on levels of securin and Cyclin B in U20S cells (untransfected, or expressing wild-type LT or dl89-97 LT). Although FACS analysis using mitotic shake-off synchronised lysates had not given a strong indication of a spindle checkpoint defect caused by LT in the NIH 3T3 cell lines, it was thought that the synchronisation itself had been very effective. For this reason, three attempts at using western blotting to demonstrate protein level differences (securin and Cyclin B) between the U20S cell lines in response to nocodazole treatment were made, one of which is shown in Figure 5.1. U20S cell lines were treated with 100ng/ml nocodazole overnight (for 15 hours), and the rounded cells (arrested in mitosis) were shaken-off, harvested and re-plated on several plates per cell line at 1.75 x 10^5 per 10cm plate. This low plating density was used to ensure that cells could not reach confluency or near-confluency during the course of the experiment, which would cause cell cycle arrest in G0 due to contact inhibition.

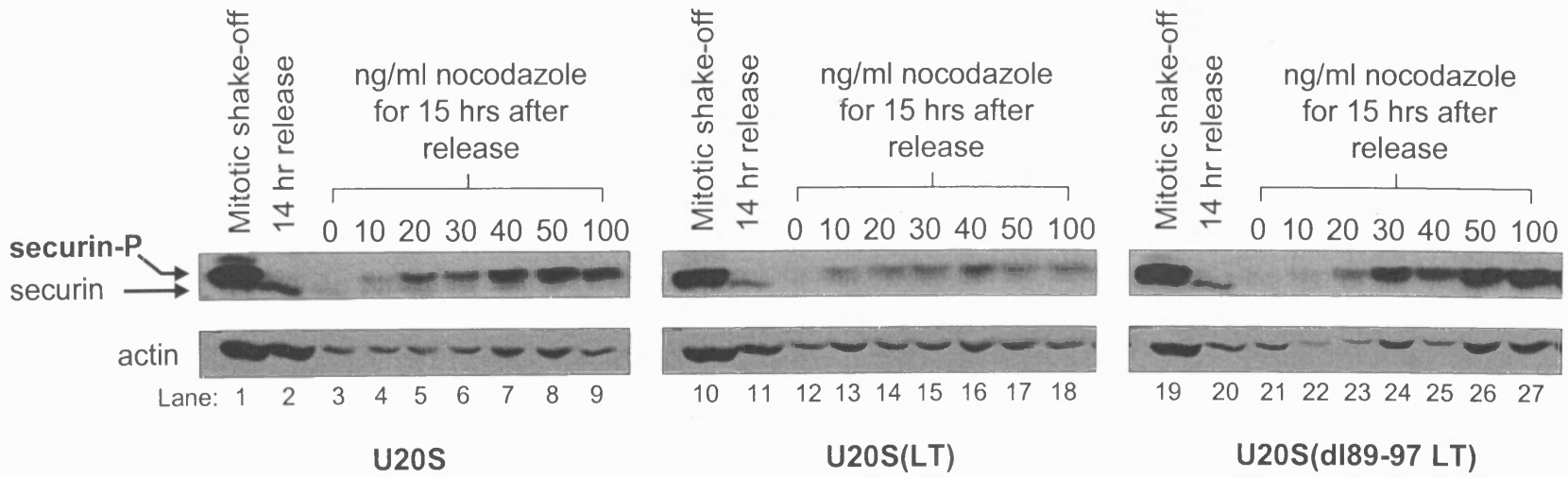

Figure 5.1: Nocodazole treatment of synchronised cells reveals a spindle checkpoint defect of wild-type LT-expressing cells.

U20S cells (lanes 1-9), U20S expressing wild-type LT (lanes 10-18) or U20S expressing non-Bub1-binding, dl89-97 LT (lanes 19-27) were treated with nocodazole overnight, and mitotic cells were then collected by shake-off (lanes 1, 10 and 19). These cells were re-plated, and released in fresh medium for 14 hours (lanes 2, 11 and 20), at which point they were treated with nocodazole at doses ranging from 0 to 100ng/ml, to activate the spindle checkpoint. Following 15 hours of drug treatment, lysates were prepared from all plates. Half of the total lysate samples were run on 12% SDS-PAGE and western blotted for securin and actin. "securin-P" indicates the slower migrating form of securin, phosphorylated by Cdc2 (also known as Cdk1) during mitosis.

These re-plated cells were then allowed to progress through the cell cycle, i.e. they were "released" from mitotic arrest, for 14 hours, at which point individual plates were treated with nocodazole doses ranging from 0-100ng/ml, for 15 hours at 37°C. The experiment shown in Figure 5.1 uses these conditions, which were optimised through several previous similar experiments using different release times and nocodazole treatment times. The 14 hour release was necessary to allow a large enough proportion of the relatively slow growing untransfected U20S cells to recover from the shake-off, without allowing the fast growing U20S(dl89-97 LT) cells to proceed as far as mitosis. Cells were treated for 15 hours with nocodazole, again to allow sufficient time for accumulation of spindle checkpoint-arrested untransfected U20S cells, for comparison with the relatively fast growing U20S(dl89-97 LT) cells (see Figure 5.2 later for a comparison of growth rates of the U20S cell lines, and further explanation of the problems encountered in trying to synchronise for spindle checkpoint experiments). Following nocodazole treatment, all plates were lysed with equal volumes of RIPA buffer, and equal volumes (50µl, i.e. half of the total lysed protein for each sample) were loaded on 12% SDS-PAGE, western blotted for securin levels, and re-blotted for actin levels (see Figure 5.1). Equivalent quantities of whole cell lysate were also loaded for cells collected at the time of mitotic shake-off (Figure 5.1, lanes 1, 10 and 19), and for cells collected immediately after the 14 hour release from shake-off, prior to nocodazole addition (lanes 2, 11 and 20). The actin levels shown in Figure 5.1 are not entirely even because the nature of the experiment generated too little lysate to allow accurate protein concentration determination via the Bradford Assay. However, equal volumes of lysate were loaded, relying on the fact that all plates were seeded at the same cell density for the experiment, and comparison of the loading levels is sufficient to allow confident conclusions to be drawn from the results.

The mitotic shake-off samples for U20S, U20S(wild-type LT) and U20S(dl89-97 LT) (lanes 1, 10 and 19, respectively) show very strong ~28kDa securin bands, indicating that these cells are arrested at the spindle

checkpoint, at which point securin has not been degraded. Human securin (also known as hPTTG or hPTTG-1) has been shown to begin to accumulate at the onset of S phase, and peak at G2-M phases, in parallel with Cyclin B1 (Zou *et al.*, 1999). After a 14 hour release from mitotic shake-off, all three cell lines (lanes 2, 11 and 20) show much reduced securin levels, with slightly faster migrating ~28kDa securin bands (compare strong, slower migrating securin band in lane 1 with weaker and faster migrating securin band in lane 2, and similarly compare lane 10 with 11, and 19 with 20). The reduced securin levels in lanes 2, 11 and 20 are expected because securin is degraded by anaphase promoting complex-mediated proteolysis at the metaphase-anaphase transition, i.e. during the 14 hour release. The difference in migration seen is due to phosphorylation. The mitotic kinase Cdc2 (also known as CDK1, and $p34^{cdc2}$, see (Doree and Hunt, 2002) for a review) phoshorylates securin at Serine-165 in mitosis (Ramos-Morales *et al.*, 2000), resulting in the highly phosphorylated, slower migrating form seen in lanes 1, 10 and 19. The low level of faster migrating (unphosphorylated) securin seen in lanes 2, 11 and 20 of Figure 5.1 is probably representative of a low level of expression of securin in G1 and S phases of the cell cycle.

Cells lysed after 15 hours of no drug treatment (following the 14 hour release from mitotic shake-off) show very low, almost undetectable levels of securin (see lanes 3, 12 and 21 of Figure 5.1), an indication that these cells are not in mitosis. However, 15 hour treatments with increasing doses of nocodazole resulted in increasing levels of the slower migrating, phosphorylated form of securin in both the U20S (lanes 4-9) and U20S(dl89-97 LT) cell lines (lanes 22-27). This demonstrated that nocodazole was arresting the cells at the spindle checkpoint in these cells, resulting in high levels of the phosphorylated securin being maintained. It also showed that the spindle checkpoint is robust in both normal U20S cells, and also in U20S cells expressing dl89-97 (non-Bub1-binding) LT. The apparent accumulation of securin seen with increasing nocodazole dosage in these cell lines is thought to be due to higher nocodazole doses causing more severe spindle damage and

resulting in a greater proportion of the population of cells arresting at the spindle checkpoint. Low (nanomolar) concentrations of nocodazole (N.B. 10ng/ml nocodazole is equivalent to 33nM) have been shown to stabilise rather than de-polymerise microtubules, causing spindle checkpoint activation by suppression of microtubule dynamic instability (the alternating periods of microtubule elongation and shortening (Vasquez *et al.*, 1997). Perhaps this suppression of dynamic instability at low nocodazole doses does not result in as frequent or rapid generation of unattached kinetochores as the spindle depolymerisation that results from higher nocodazole doses. This could lead to fewer cells in the population arresting at the checkpoint, resulting in detection of a lower level of phosphorylated securin in the cell lysates (e.g. compare lane 4 with lane 5, and lane 22 with lane 23).

Interestingly, this "accumulation" of phosphorylated securin seen in the lysates with increasing nocodazole was not detected in U20S cells expressing wild-type LT (Figure 5.1, lanes 13-18). Instead, these cells show a low level of phosphorylated securin when treated with 10ng/ml nocodazole (lane 13), (comparable with the securin levels seen in the equivalent lanes for the other cell lines (lanes 4 and 22)), but the securin levels in the cell population do not accumulate further with higher doses of nocodazole (lanes 14-18), remaining at the same approximate level as in lane 13, even with 100ng/ml nocodazole treatment (lane 18). It should be noted that the securin that is seen in U20S(wild-type LT) lanes 13-18, although not accumulating with nocodazole, is nevertheless phosphorylated, and is at a higher level than that seen in lane 12 (cells not treated with nocodazole), indicating that some cells are arrested at mitosis, albeit far fewer than seen in the equivalent lanes for the other cell lines. However, many U20S(wild-type LT) cells must be escaping spindle checkpoint arrest prematurely, or not arresting at all in response to spindle damage, as seen by lack of securin accumulation in response to increasing nocodazole. In contrast, the U20S cells expressing LT with the Bub1 binding site deleted (dl89-97, lanes 19-27) appeared to have a spindle checkpoint response that was just as robust as that seen in the absence of LT (lanes 1-9),

demonstrating that interaction of LT with Bub1 is crucial for the ability of LT to disrupt spindle checkpoint function.

This experiment clearly demonstrates that cells expressing wild-type LT are not able to effectively arrest at the spindle checkpoint in response to spindle damage, and that interaction of LT with Bub1 is crucial for this checkpoint inhibition.

5.3.1.2 Inhibition of spindle checkpoint function by LT is most clearly demonstrated using asynchronous cell cultures

Many of the problems encountered in demonstrating a spindle checkpoint defect in the U20S cells were thought to be the result of different growth rates of the cell lines, which also made the synchronisations very difficult. The growth rates of the U20S lines were examined, as shown in Figure 5.2. U20S, U20S(wild-type LT) and two independent clones of U20S(dl89-97 LT) cells ("#2", and "#4", the clone used in Figure 5.1 and all remaining figures in this chapter) were seeded to several 10cm plates at 3 x 10^5 cells per plate. At approximately 24 hour intervals over the next 4 days, two plates for each cell line were independently trypsinised and the cells were counted using a haemocytometer. Counts from all 4 corner squares of the haemocytometer were recorded for each plate, resulting in 8 counts for each cell line, at each time point (See Appendix III for raw data and normalised values for these counts).

Figure 5.2 shows the relative growth rates of the four cell lines, calculated as normalised (average) cell count values plotted against time (see also Appendix III). The growth curves in this graph show that U20S and U20S(wild-type LT) grow at very similar rates, while the two clonal U20S cell lines expressing dl89-97 LT both grow at a noticeably faster rate. However, several independent clones of each cell line would need to be tested to confirm with confidence that cells expressing this LT mutant always proliferate faster than cells expressing wild-type LT or untransfected control cells.

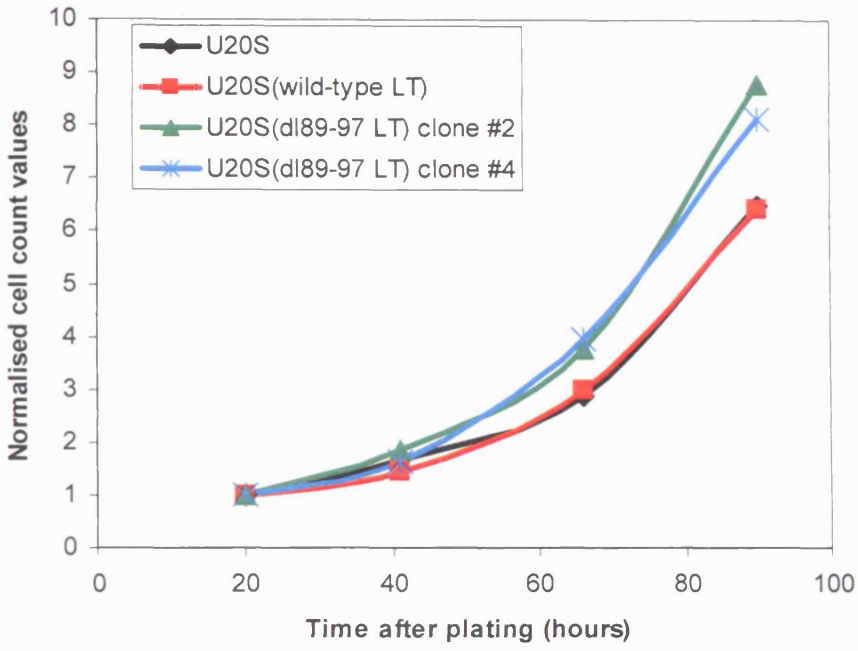

Figure 5.2: Relative growth rates of control U20S cells and U20S cell lines expressing wild-type LT or dl89-97 LT.

Untransfected U20S control cells, U20S(wild-type LT), or U20S(dl89-97 LT) cells (two independent lines expressing this mutant) were seeded, and the number of cells were counted for two plates from each line at regular intervals over 4 days. Cell counts were averaged for each line and normalised to allow comparison of growth rates over time for the lines. These values are plotted against time after plating for each cell line.

An observation made while collecting mitotic shake-off cells from the different cell lines for the experiment shown in Figure 5.1 provided a further indication of the spindle checkpoint defect in U20S(wild-type LT) cells. Far fewer rounded up cells could be collected from the U20S(wild-type LT) line than from the U20S or U20S(dl89-97 LT) cell lines. This was seen even when the flasks treated with nocodazole for mitotic shake-off had been seeded at the same density, and could not be a consequence of the different growth rates shown in Figure 5.2 because the U20S and U20S(wild-type LT) cell lines have very similar growth rates. This indicated that fewer U20S(wild-type LT) cells were arresting in response to nocodazole. It also showed that the cells that did arrest (and were re-plated following mitotic shake-off) still had the potential to override the spindle checkpoint, due to the observation of reduced securin accumulation in these re-plated U20S(wild-type LT) cells upon subsequent nocodazole treatment (see Figure 5.1 lanes 13-18) in comparison to the other cell lines (Figure 5.1 lanes 4-9 (U20S) and 22-27 (U20S(dl89-97 LT)).

The observation of a lower yield of mitotic shake-off cells from the U20S(wild-type LT) line suggested that perhaps synchronisation of the cell lines would not be necessary to demonstrate a spindle checkpoint defect in response to nocodazole.

U20S, U20S(wild-type LT) and U20S(dl89-97 LT) cells were seeded on several 10cm plates at 1 x 10^6 cells per plate, and 24 hours later when the plates were 40-60% confluent, they were treated with doses of nocodazole ranging from 0 to 400ng/ml. Cells were lysed in RIPA buffer following 15 hours of nocodazole treatment, protein concentrations were estimated via the Bradford Assay, and 10μg samples were run on 12% SDS-PAGE, and western blotted for securin, followed by re-blotting for Cyclin B, Mad2, and actin. It was necessary to load this relatively small quantity of protein (10μg) for each sample to allow a clear comparison of securin levels (See Figure 5.3).

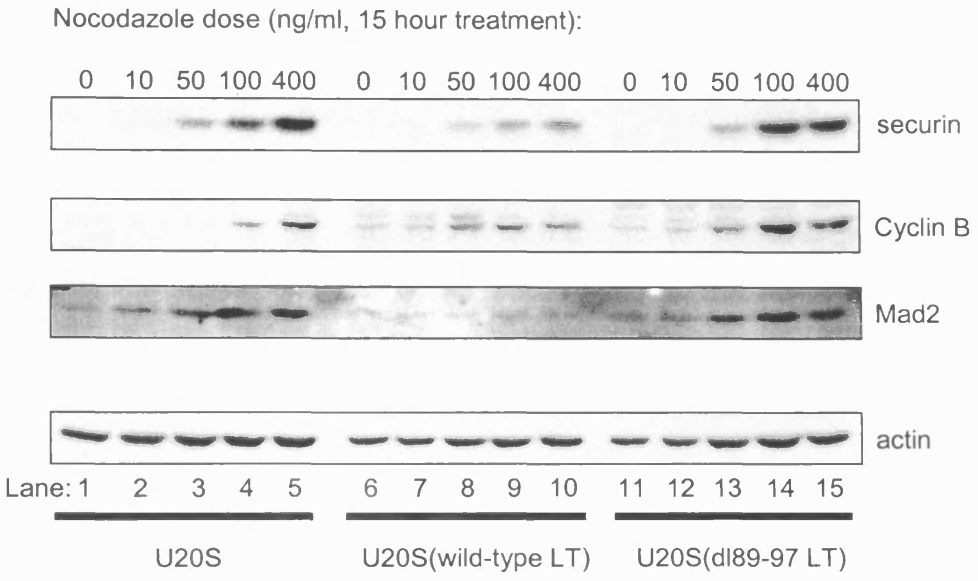

Figure 5.3: SV40 large T antigen compromises spindle checkpoint function via interaction with Bub1.

Asynchronous cultures of U20S (lanes 1-5), U20S(wild-type LT) (lanes 6-10) and U20S(dl89-97 LT) (lanes 11-15) cells were lysed following a 15 hour treatment with doses of nocodazole ranging from 0-400ng/ml. 10μg samples were loaded on 12% SDS-PAGE and western blotted for securin, Cyclin B, Mad2 and actin levels. Relative protein levels indicated that untransfected cells and cells expressing non-Bub1-binding (dl89-97) LT were arresting at the spindle checkpoint in response to nocodazole, but that far fewer wild-type LT-expressing cells were arresting, resulting in lowered securin, cyclin B and Mad2 levels in the lysates from this cell line. Therefore interaction of LT with Bub1 is crucial for the ability of LT to compromise spindle checkpoint function.

When treated with 0 or 10ng/ml nocodazole for 15 hours, no securin is detected in any of the cell lines (see Figure 5.3, securin blot of lanes 1-2, 6-7 and 11-12). This indicates that in the asynchronous cultures 10ng/ml nocodazole did not cause enough spindle damage to induce cells to arrest at the spindle checkpoint in significant numbers to allow detection of securin, a protein whose expression peaks at G2/M. The weak, unphosphorylated form of securin observed in Figure 5.1 is not detected in the securin blot of Figure 5.3, perhaps a further indication of its low abundance. However when treated with nocodazole doses of 50, 100 and 400ng/ml, the 28kDa securin protein can be detected in all three cell lines, but at different levels (see lanes 3-5, 8-10 and 13-15). U20S and U20S(dl89-97 LT) cell lines both show progressively more securin protein (presumably the phosphorylated form) with increased nocodazole dose, ranging from a relatively weak ~28kDa band at 50ng/ml nocodazole treatment (lanes 3 and 13) to a very strong band when treated with 400ng/ml of the drug (lanes 5 and 15). This accumulation of securin with nocodazole dose appears very similar between these two cell lines, with the exception that a greater proportion of the cells expressing dl89-97 LT appear to respond to 100ng/ml of nocodazole by arresting with high levels of securin than that seen in the U20S cells (compare lane 14 with lane 4). However, the cells expressing the wild-type LT (see lanes 8-10) do not appear to respond to spindle damage induced by nocodazole as well as the U20S or U20S(dl89-97 LT) cell lines, with only a moderate amount of the 28kDa securin protein being detected in the lysates from the U20S(wild-type LT) cells, even when treated with the highest drug dose, 400ng/ml (compare lanes 8-10 (wild-type LT) with lanes 3-5 (no LT) and 13-15 (dl89-97 LT)). Strong, ~50kDa actin bands of approximately equal intensity can be seen in all lanes (actin blot, lanes 1-15), demonstrating that all lanes were loaded equally, and that the differences seen in securin levels are real.

Cyclin B levels show a similar trend to that seen for securin levels in the nocodazole-treated U20S cell lines (see Cyclin B blot, Figure 5.3). The level of ~62kDa Cyclin B1 protein is seen to increase with increased doses of

nocodazole in the U20S and U20S(dl89-97 LT) cells (lanes 1-5 and 11-15, respectively), but not to the same extent in the U20S(wild-type LT) cells, staying at a relatively low level at the higher drug doses (lanes 8-10).

Cells expressing SV40 large T antigen have long been known to have elevated protein levels and/or associated activities of Cyclin B in comparison to untransfected cells (and also Cyclin A, Cdc25C and $p34^{cdc2}$) (Chang *et al.*, 1997; Chang and Schlegel, 1996; Kaufmann *et al.*, 1995). This explains why asynchronous U20S(wild-type LT) (lane 6) and U20S(dl89-97 LT) (lane 11) cells have a higher level of Cyclin B than the untransfected U20S cells (lane 1), and also explains why Cyclin B accumulates to a higher level in response to nocodazole in U20S(dl89-97 LT) cells in comparison to U20S cells (compare lanes 11-15 with lanes 1-5, respectively). It also emphasises the difference in Cyclin B accumulation between cells expressing the Bub1-binding (wild-type) and non-Bub1-binding (dl89-97) LT proteins: Cyclin B levels are almost identical in the 0-50ng/ml drug treatment lanes for these cell lines (compare lanes 6-8 with 11-13), but at 100 and 400ng/ml nocodazole doses the level of Cyclin B in the U20S(wild-type LT) cells did not increase further (62kDa bands in lanes 8-10 are approximately equal intensity), whereas the amount of Cyclin B protein in the U20S(dl89-97 LT) lysates increases greatly in the 100 (and 400) ng/ml nocodazole treatments compared to that seen at 50ng/ml (see lanes 13-15). A slower migrating band is also observed in the Cyclin B blot, possibly a phosphorylated (or otherwise modified) form of this protein. Interestingly, this is most clearly seen in the U20S(wild-type LT) cells treated with 50ng/ml nocodazole (lane 8).

The membranes were also re-blotted for Mad2. Mad2 forms a ternary complex with Cdc20 and Cdc27, a component of the anaphase-promoting complex/cyclosome (APC/C), to inhibit APC/C^{Cdc20}-dependent ubiquitylation and degradation, thereby causing a cell cycle arrest in metaphase (Fang *et al.*, 1998; Kallio *et al.*, 1998; Li and Benezra, 1996; Li *et al.*, 1997; Wassmann and Benezra, 1998). Mad2 is therefore an essential spindle checkpoint component because it acts as a negative regulator of the mitotic APC/C,

preventing progression to anaphase in the presence of even a single unattached kinetochore.

Mad2 levels in the nocodazole-treated U20S cell lines shown in Figure 5.3 are consistent with the securin levels seen in these cell lines (c.f. securin and Mad2 blots, lanes 1-15). In the U20S and U20S(dl89-97 LT) lysates, the intensity of the 24kDa Mad2 bands appear to increase with dose of nocodazole (see lanes 1-5 and 11-15, respectively). However in the U20S(wild-type LT) cells (lanes 6-10), Mad2 levels do not appear to respond to nocodazole treatment in the same way, only increasing a moderate amount with increased nocodazole.

Although the budding yeast Mad2 protein remains at a constant level during the cell cycle (Chen *et al.*, 1999), a recent study has shown that Mad2 is cell cycle regulated in human fibroblasts (IMR90 cells), peaking at G2/M phase (Hernando *et al.*, 2004). This offers a simple explanation for the Mad2 protein levels observed in Figure 5.3: as for securin and Cyclin B, lack of Mad2 accumulation with increased nocodazole in the U20S(wild-type LT) cells (lanes 6-10) indicates a spindle checkpoint defect in these cells, with cells failing to arrest in mitosis (the point at which Mad2 levels peak) in response to spindle damage.

It has been previously shown that some cancer cells displaying chromosome instability (CIN) also have reduced steady-state levels of Mad2, and an associated loss of spindle checkpoint control (Li and Benezra, 1996; Wang *et al.*, 2002; Wang *et al.*, 2000). However from the Mad2 blot in Figure 5.3 (and subsequent experiments) wild-type LT-expressing cells do not appear to have reduced steady-state levels of Mad2 (compare lanes 1, 6 and 11, and also see Mad2 blot in Figure 5.6).

50μg of the same lysates shown in Figure 5.3 were also run on a 8% SDS-PAGE gel and western blotted for other spindle checkpoint-related proteins, and for LT (see Figure 5.4).

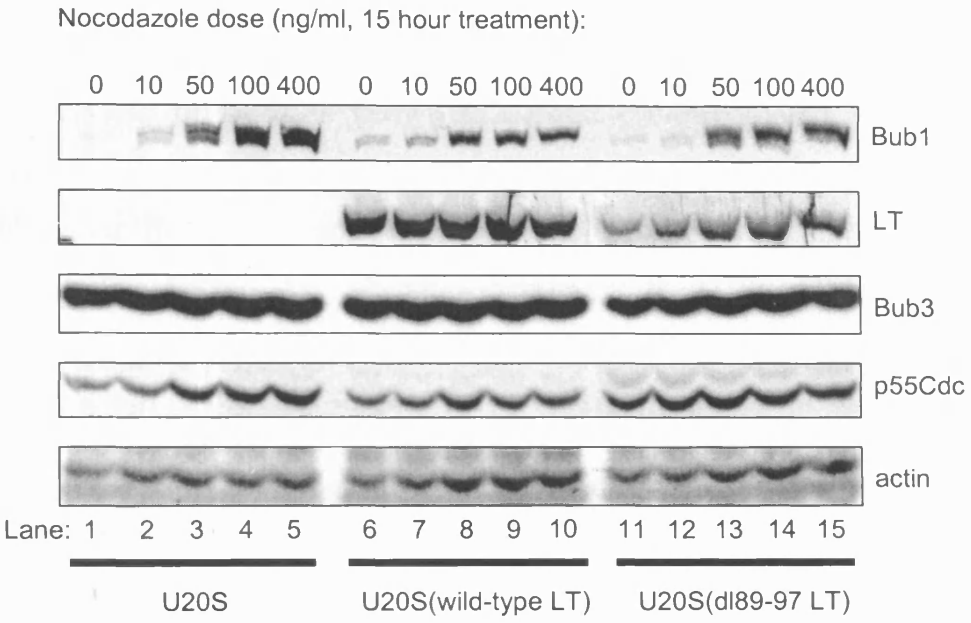

Figure 5.4: Relative expression levels of proteins involved in the spindle checkpoint, under conditions of checkpoint activation.

Lysates are the same as shown in Figure 5.3. 50μg samples were loaded on 8% SDS-PAGE and western blotted for Bub1, LT, Bub3, p55Cdc/hCdc20 and actin levels. Bub1 protein levels, observed as multiple bands, increase with increasing nocodazole treatment in all three cell lines, but to a lesser extent in U20S(wild-type LT) cells. Bub3 levels remain constant, and LT and p55Cdc levels do not appear to accumulate with nocodazole treatment in either the U20S(wild-type LT) or the U20S(dl89-97 LT) cells. However, p55Cdc does accumulate with nocodazole in untransfected U20S cells, as would be predicted by its cell cycle-regulated expression.

Lysates were blotted for Bub1 (using NT hBub1 polyclonal antiserum), and re-blotted for LT (using anti-LT monoclonal PAb423), Bub3, p55Cdc (also known as hCdc20, p55Cdc is the human homolog of Cdc20), and actin. Attempts were also made to blot these lysates for BubR1 and Mad1 levels, but unfortunately no good antibodies that detected the human homologs of these proteins could be obtained during the course of the project.

Expression of Bub1 is known to be cell cycle-regulated, peaking at G2/M phase (Davenport *et al.*, 1999; Taylor *et al.*, 2001), and thus the accumulation of Bub1 with increasing nocodazole observed for all cell lines in Figure 5.4 is as expected. Asynchronous cultures of the U20S cell lines (Bub1 blot, lanes 1, 6 and 11) show a faint ~150kDa band, but upon treatment with nocodazole, more cells accumulate in M phase, resulting in detection of stronger ~150kDa Bub1 bands (lanes 2-5, 7-10 and 14-15). The Bub1 blots in Figure 5.4 appear to show multiple forms with slightly different migrations, rather than single bands. This is true for all lanes, whether arrested in M phase by nocodazole or not, and is probably due to phosphorylation of the Bub1 protein. However, some studies of Bub1 phosphorylation have stated that Bub1 is not significantly phosphorylated during a normal mitosis, and is only hyperphosphorylated (by MAP kinase, (MAPK)) in response to unattached kinetochores (Chen, 2004; Taylor *et al.*, 2001). This would not explain the apparent Bub1 "doublets" seen with 0 or 10ng/ml nocodazole treatment (lanes 1-2, 6-7 and 11-12), but 2-Dimensional SDS-PAGE would be needed in order to determine exactly how many Bub1 bands are present. The intensity of the Bub1 bands in lanes 8-10 (U20S(wild-type LT)) appears slightly lower than that seen in lanes 3-5 (untransfected U20S), suggesting as in Figure 5.3 that more of the nocodazole-treated U20S(wild-type LT) cells in the population have escaped spindle checkpoint arrest (and therefore have reduced Bub1 expression). However, this spindle checkpoint defect is much more clearly demonstrated by the lack of accumulation of securin and Cyclin B in U20S(wild-type LT) cells in Figure 5.3.

The LT blot in Figure 5.4 shows that expression of wild-type LT (lanes 6-10) and dl89-97 LT (lanes 11-15) is not affected by stage of the cell cycle, as seen by the effect of nocodazole on the cells. The level of dl89-97 LT appears to rise slightly with increasing nocodazole, but this is not significant due to a slight rise in actin (loading) levels in these lanes (11-15). As observed previously, wild-type LT (a very strong ~100kDa band is seen in lanes 6-10) appears to be expressed at a higher level than dl89-97 LT (strong ~100kDa band seen in lanes 11-15), and as expected no 100kDa LT band is observed in the untransfected U20S lysates (lanes 1-5).

Bub3 protein levels do not appear to be affected by the presence of either wild-type or dl89-97 LT, or by treatment with nocodazole (see Bub3 blot, Figure 5.4 lanes 1-15, a very strong 37kDa Bub3 band is observed in each lane). This is in agreement with previous findings that Bub3 levels are constant throughout the cell cycle in budding yeast (Brady and Hardwick, 2000; Fraschini *et al.*, 2001), and also in human cells (Martinez-Exposito *et al.*, 1999).

p55Cdc (the human homolog of Cdc20 (Weinstein *et al.*, 1994)) mediates association of Mad2 to the APC/C and is required for the metaphase-anaphase transition (Kallio *et al.*, 1998). The level of p55Cdc protein fluctuates during the cell cycle. Synthesis is initiated at G1/S, with protein levels peaking in M phase, and the protein is abruptly degraded at the M/G1 transition (Fraschini *et al.*, 2001; Weinstein, 1997). Degradation of p55Cdc is blocked by proteasome inhibitors, suggesting that it is targeted by ubiquitin-mediated proteolysis. As expected, in Figure 5.4 p55Cdc appears to accumulate upon nocodazole treatment in the untransfected U20S cells (compare the strong ~55kDa p55Cdc bands in lanes 3-5 with the weaker bands in lanes 1-2). This p55Cdc accumulation with nocodazole treatment is clearly observed by comparing the p55Cdc and actin blots in Figure 5.4 lanes 1-5. In agreement with previous observations for this experiment, when comparing the p55Cdc and the actin blots for U20S(wild-type LT) cells (Figure 5.4, lanes 6-10), no p55Cdc accumulation in response to nocodazole is

observed, with the p55Cdc bands remaining at a relatively weak level that is unaffected by increasing the nocodazole dose. This is as would be expected if the wild-type LT-expressing cells are overriding nocodazole-induced spindle checkpoint arrest. Interestingly, the U20S(dl89-97 LT) cells do not show an accumulation of p55Cdc protein upon nocodazole treatement (see Figure 5.4 lanes 11-15, compare p55Cdc and actin blots), as might be expected from the securin and Cyclin B accumulation seen in these lysates in Figure 5.3. Instead, strong p55Cdc bands are seen in lanes 11-15, and the protein levels do not appear to be affected by the nocodazole treatment.

5.3.1.3 Compartmentalisation of spindle checkpoint proteins is not affected by LT

The next task was to confirm that the differences seen in securin and Mad2 levels between the U20S(wild-type LT) and U20S or U20S(dl89-97 LT) cells in response to nocodazole treatment in Figure 5.3 were due to a spindle checkpoint defect in the wild-type LT-expressing cells, rather than being caused by the method of detecting the protein levels present. It was possible that the lower levels of securin, Mad2 (and perhaps Bub1, see Figure 5.4) were due to a change in subcellular localisation of these proteins in the U20S(wild-type LT) cells, making them difficult to extract. The lysates shown in Figures 5.3 and 5.4 were prepared using RIPA buffer, saving only the soluble fraction (supernatant) of the lysis. RIPA buffer contains the non-ionic detergent Triton X-100, capable of solubilising membrane proteins, as well as the ionic detergents sodium dodecyl sulphate (SDS) and sodium deoxycholic acid (NaDOC). The RIPA-soluble (supernatant) fraction of the lysis contains predominantly soluble, cytosolic proteins as well as some proteins from membranous organelles that are also solubilised by the lysis buffer. The RIPA-insoluble (pellet) fraction, that was discarded when making the lysates in Figures 5.3 (and 5.4), would be composed primarily of intermediate filaments, remnant nuclei and their associated polypeptides, and also chromatin (Napolitano *et al.*, 1987).

U20S, U20S(wild-type LT) and U20S(dl89-97 LT) cells were seeded on several 10cm plates at 1.2 x 10^6 cells per plate, and 24 hours after plating were treated for 15 hours with either 0, 50 or 100ng/ml nocodazole. Cells were then lysed with 200µl of RIPA buffer, and both the soluble (supernatant) and insoluble (pellet, resuspended in 100µl 2x Laemmli Sample buffer and heated at 90°C for 10 minutes) were retained. Protein concentrations of the soluble samples were estimated by the Bradford Assay, and 50µg soluble samples were mixed with 2x Laemmli sample buffer, heated at 90°C for 10 minutes, and loaded on a 5-15% SDS-PAGE gradient gel, and western blotted. 30µl of each insoluble sample was also loaded on the same gel (it was not possible to estimate protein concentrations for the pellet samples solubilised in Laemmli buffer using the Bradford Assay) for comparison.

Figure 5.5 shows these samples western blotted for Bub1, and re-blotted for securin, Mad2, LT and actin. As observed previously in Figures 5.3 and 5.4, Bub1 levels appear to increase with nocodazole treatment (arrest in G2/M) in the soluble fractions, but this increase is less prominent in the U20S(wild-type LT) cells (compare strength of 150kDa Bub1 bands in lanes 4-6 with the lanes 1-3 and 7-9). Securin and Mad2 levels in the soluble samples behave similarly, as previously described, with less protein accumulation in the U20S(wild-type LT) cells. Both the unphosphorylated securin and the slower migrating phosphorylated form of securin are visible in all three cell lines (~28kDa securin bands, Figure 5.5 lanes 1-9), due to better resolution of proteins in this gradient gel. As before, LT levels in lanes 4-9 are not affected by nocodazole treatment, and actin levels in the soluble fractions are very even (lanes 1-9), indicating equal protein loading.

Actin levels in the insoluble fractions of the lysates (Figure 5.5 lanes 10-18) appear to increase with nocodazole treatment. This is unlikely to be a consequence of the drug treatment however, because the actin levels in these lanes correlate with the relative protein concentrations of the equivalent soluble fractions of the lysates (as calculated using the Bradford Assay, data not shown).

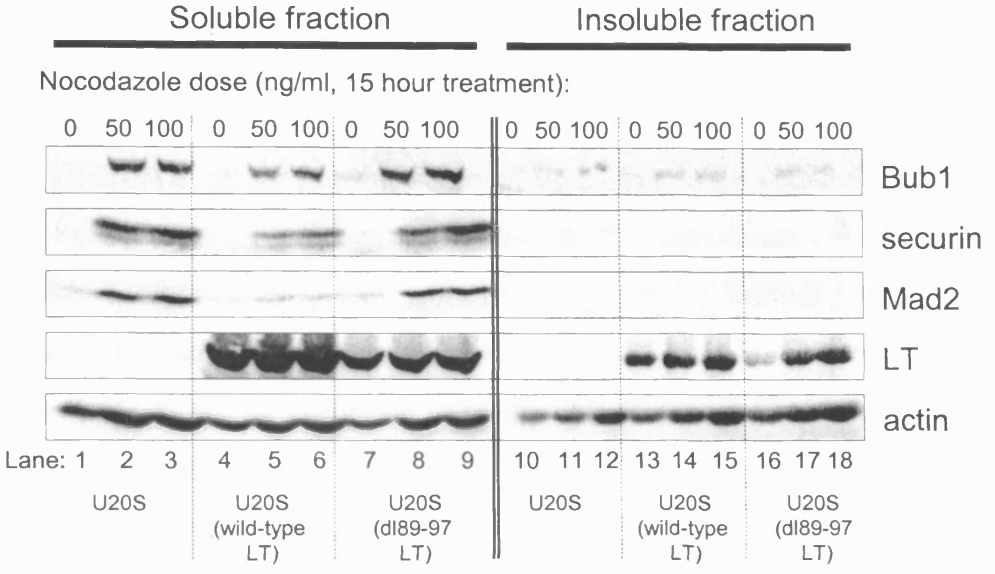

Figure 5.5: Observation of a reduced response to nocodazole in wild-type LT-expressing cells is not caused by difficulties in extracting total protein from different cell lines.

Comparison of protein levels in the RIPA-soluble (supernatant, lanes 1-9) and RIPA-insoluble (pellet, lanes 10-18) fractions of RIPA lysates from nocodazole-treated U20S, U20S(wild-type LT) and U20S(dl89-97 LT) cells. The lower Bub1, securin and Mad2 protein levels in nocodazole treated U20S(wild-type LT) are not due to a change of subcellular localisation of these proteins in the cells, because the difference cannot be accounted for by examining the insoluble fraction as well as the soluble.

It was not possible to estimate protein concentration from the pellet fractions solubilised in Laemmli buffer, and it was for this reason that equal volumes were loaded for these samples. However, qualitative interpretation of the results is not affected by the slightly uneven loading. A fairly significant proportion of the LT protein in both the U20S(wild-type LT) (lanes 13-15) and the U20S(dl89-97 LT) cells (lanes 16-18) appears to be found in the insoluble fraction of the lysis, probably bound to the chromatin, although the relative proportions present in the soluble versus insoluble fractions does not appear to be affected by nocodazole treatment (compare lanes 4-9 with lanes 13-18; however the relatively low amount of dl89-97 LT in lane 16 may need further investigation). A very small amount of the total Bub1 in each lysis appears to have been localised in the insoluble fraction (see faint 150kDa Bub1 bands in lanes 11-12, 14-15 and 17-18), but the relative strengths of these bands does not give any indication of a change of subcellular localisation of the Bub1 protein caused by expression of wild-type LT, because all bands are of similar relative intensities in lanes 10-18 as those seen in lanes 1-9. Finally, no securin or Mad2 is detected in any of the insoluble fraction lanes, in any of the cell lines, under any of the conditions tested (see lanes 10-18). This indicates that the lower levels of securin observed in lanes 4-6 compared to lanes 1-3 or 7-9 are due to compromise of the spindle checkpoint, and not simply an artefact of change of subcellular distribution of these proteins in the wild-type LT-expressing cells. Similarly, this also confirms that the low expression of Mad2 observed in asynchronous culture (lanes 1, 4 and 7), compared to the higher levels seen in nocodazole-arrested cells (lanes 2-3 and 8-9) is due to cell cycle regulated expression of Mad2 in these cells, with Mad2 expression peaking at G2/M phase.

Therefore, this experiment further confirms that wild-type LT (but not dl89-97, non-Bub1-binding LT) is able to compromise the spindle assembly checkpoint.

5.3.1.4 The spindle checkpoint itself, rather than rate of adaptation to the checkpoint is affected by LT

The spindle checkpoint is known to have only a limited capacity to maintain cell cycle arrest in response to spindle damage, resulting in eventual "adaptation" and progression to the next phase of the cell cycle in a tetraploid state, without correction of errors and satisfaction of the checkpoint (reviewed in (Andreassen *et al.*, 2003)). It is possible that the spindle checkpoint defect of the U20S(wild-type LT) cells could be that they are adapting to the checkpoint at a much faster rate than normal, rather than a failure of the error sensing and signal transduction mechanisms of the checkpoint itself.

To test this hypothesis, asynchronous U20S, U20S(wild-type LT) and U20S(dl89-97 LT) cells were treated with 0, 50 or 200ng/ml nocodazole for 2, 4, 6, 8, 10, 12 or 15 hours. All samples were lysed with RIPA buffer, and 20μg samples were run on 5-15% SDS-PAGE and western blotted for securin and actin. No accumulation of securin in response to nocodazole was observed in any of the cell lines until the 15 hour treatment time point, at which point results similar to those seen in Figure 5.3 were observed (data not shown). This indicated that the U20S(wild-type LT) cells were not simply adapting to the spindle checkpoint faster, because if they were, securin bands should have been observed earlier than the 15 hour time point to indicate a transient spindle checkpoint arrest. Instead, it appears that the U20S(wild-type LT) cells never achieve a spindle checkpoint arrest in response to nocodazole that can be detected as an increase in securin protein levels in the cell population.

Longer time points of nocodazole treatment were not tested, because prolonged exposures to the drug of 15 hours or more were expected to lead to adaptation in all the cell lines (Taylor and McKeon, 1997), and hence would not be informative because it would not be possible to differentiate between low securin levels induced by override of the spindle checkpoint, or by entry into the next cell cycle (via adaptation). As will be discussed later, LT-expressing cells are defective for the p53-dependent tetraploidy checkpoint at

G1 that would otherwise permanently block propagation of tetraploid cells that have adapted to the spindle checkpoint.

5.3.1.5 Preliminary experiments to search for a mechanism by which LT is inhibiting spindle checkpoint function: examination of protein complexes via co-immunoprecipitation

Having identified conditions under which it could be demonstrated that LT was inhibiting spindle checkpoint function, it was then possible to begin to examine the protein complexes present in the U20S cell lines under these conditions.

Asynchronous U20S, U20S(wild-type LT) and U20S(dl89-97 LT) cells were plated at a relatively low density (to prevent cell cycle arrest due to contact inhibition), and as before (see Figure 5.3), 24 hours after plating, the cells were treated for 15 hours with nocodazole doses ranging from 0-100ng/ml. Cells were then lysed using NP40 lysis buffer, which contains the non-ionic detergent Nonidet P40 which is less stringent than the RIPA buffer used in previous experiments. From previous experience, the LT-Bub1 interaction can not be detected under the stringent conditions of RIPA lysis, but can be seen when cells are lysed with NP40 lysis buffer. Therefore to maintain intact LT-Bub1 complexes (and any other complexes) in the cells, NP40 lysis buffer was used.

Figure 5.6 panel A shows 50μg of each sample run on a 5-15% SDS-PAGE (gradient gel), and western blotted to demonstrate relative protein levels of securin, Mad2, Bub1, LT, Bub3 and actin in these lysates. The protein levels seen in Figure 5.6 panel A re-iterate those seen for the same treatments of these cell lines previously. Securin levels accumulate in the cell population with increased dose of nocodazole in the untransfected U20S (Figure 5.6A, lanes 1-5) and U20S(dl89-97 LT) (lanes 11-15) cells, but not as much in the U20S(wild-type LT) cells (lanes 6-10), again indicating disruption of the spindle checkpoint by LT-Bub1 interaction.

Figure 5.6: Co-immunoprecipitation experiments conducted to begin to dissect the mechanism by which LT is compromising spindle checkpoint function.

U20S, U20S(wild-type LT) and U20S(dl89-97 LT) cells were treated for 15 hours with 0-100ng/ml nocodazole, and lysed using NP40 lysis buffer. (A): 50μg samples were analysed for securin, Mad2, Bub1, LT, Bub3 and actin levels via western blotting. (B): 500μg samples were immunoprecipitated using Bub1 antibody, and western blotted for Bub1 and LT levels. (C): 500μg samples were immunoprecipitated using Mad2 antibody, and western blotted to look for co-immunoprecipitating Bub1 and LT proteins.

By looking at protein complexes present in the different cell lines under conditions where the checkpoint is functional or abrogated, the aim was to gain some insight into the mechanism by which LT might be affecting the spindle checkpoint via interaction with Bub1.

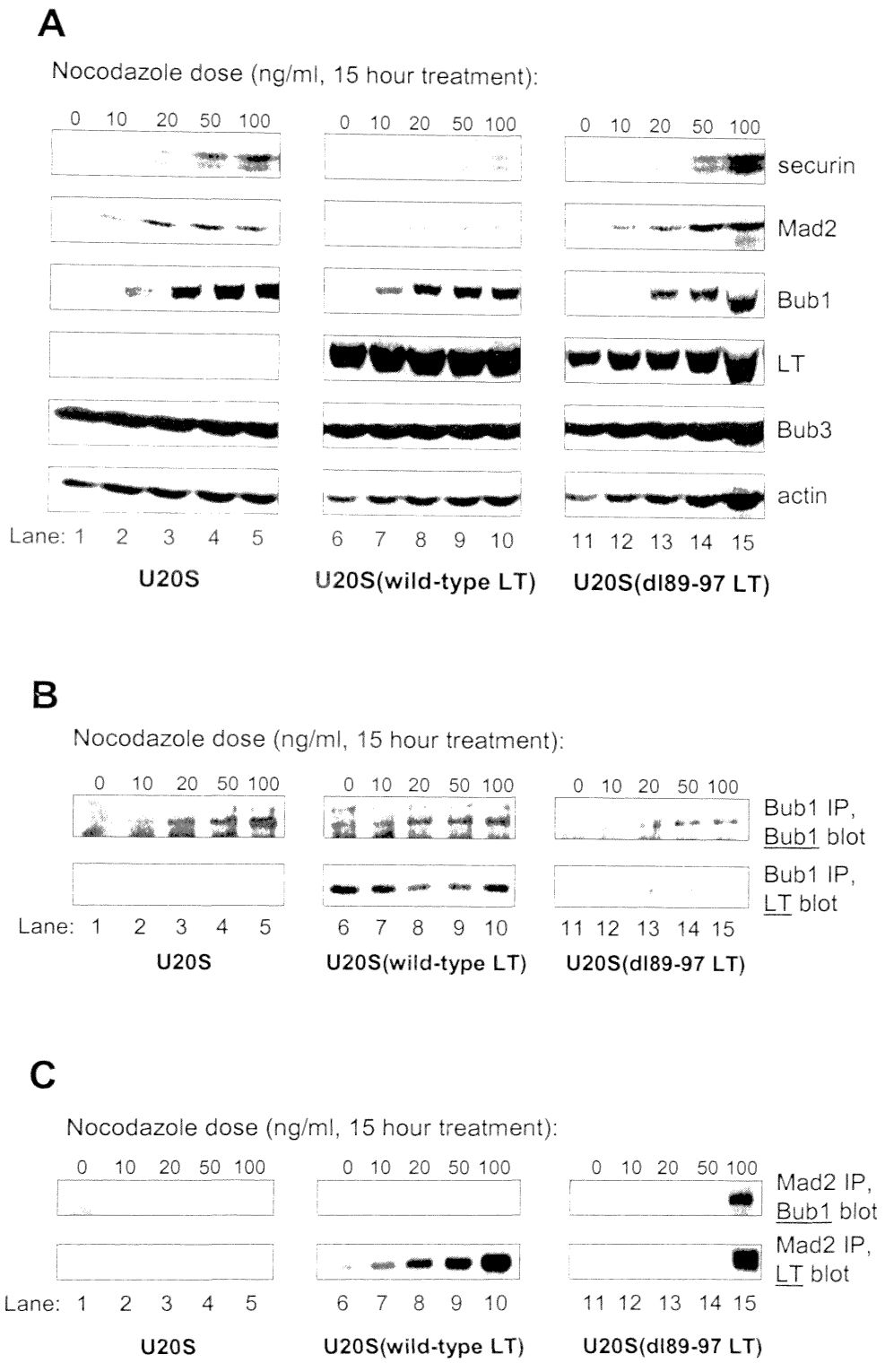

Figure 5.6: Co-immunoprecipitation experiments conducted to begin to dissect the mechanism by which LT is compromising spindle checkpoint function.

The securin doublets are seen in Figure 5.6 panel A, and as before it is presumed that the lower band represents the unphosphorylated form of securin, and the upper, stronger band represents the phosphorylated form of securin seen in mitosis. Both bands in the securin doublet seen in U20S(dl89-97 LT) cells treated with 100ng/ml nocodazole (lane 15) appear to be equally strong, but the equivalent lane of U20S cells (lane 5) shows the upper securin band to be stronger, as would be expected in mitosis. This abberantly strong lower securin band in lane 15 could be caused by slight overloading of this lane (see actin blot, lane 15), perhaps resulting in saturation in the securin blot of this lane. The actin blot of Figure 5.6 panel A shows that the protein loading was very even, but perhaps with slight underloading of lane 11 and overloading of lane 15. This allowed direct comparison of the protein levels in this figure, which are consistent with previous experiments using RIPA lysates. Mad2 levels accumulate with nocodazole in the lysates in lanes 1-5 (untransfected) and 11-15 (dl89-97 LT), but do not accumulate to the same extent in lanes 6-10 (wild-type LT). Bub1 levels accumulate when cells arrest in M phase in response to nocodazole-induced spindle damage in all three cell lines, but perhaps slightly less in wild-type LT-expressing cells (lanes 6-10). LT expression is not affected by nocodazole in either the U20S(wild-type LT) (lanes 6-10) or the U20S(dl89-97 LT) cells (lanes 11-15). Bub3 levels are not affected by spindle damage in any of the cell lines (40kDa bands of equal intensity are seen in lanes 1-15).

Figure 5.6 panel B shows Bub1 immunoprecipitations of the lysates from panel A, western blotted for Bub1 (control) and for LT. Bub1 was immunoprecipitated using CT hBub1 polyclonal antiserum and Protein A-Sepharose beads. The immunoprecipitates were loaded on a 5-15% SDS-PAGE gradient gel, and western blotted for Bub1 (using NT hBub1 polyclonal antiserum), and LT (using anti-LT monoclonal PAb423). As expected, an accumulation of Bub1 with increased nocodazole is observed in the Bub1 blot of the Bub1 immunoprecipitations in all three cell lines (Figure 5.6B, lanes 1-15). The Bub1 bands seen in Figure 5.6 panel B are not very clear, and in

particular look fainter than expected in lanes 11-15, the U20S(dl89-97 LT) cell line. The high number of non-specific bands also recognised by the NT hBub1 polyclonal antiserum used to blot the immunoprecipitations was the cause of this problem. Unfortunately at this stage in the project there were no other antibodies available that were good for western blotting human Bub1.

The LT blot in Figure 5.6 panel B showed approximately equal levels of LT co-immunoprecipitating with Bub1 in the U20S(wild-type LT) line, regardless of the extent of spindle damage (100kDa LT bands are of approximately equal intensity in Figure 5.6B lanes 6-10). It is not clear why the amount of LT being co-immunoprecipitated with Bub1 does not correlate with the levels of Bub1 being immunoprecipitated in the cells, but perhaps this is an indication that only a small proportion of the LT in the cell interacts with Bub1. Only very faint 100kDa LT bands are observed to co-immunoprecipitate with Bub1 in the U20S(dl89-97 LT) lanes (Figure 5.6B, lanes 11-15). These co-precipitating bands may be caused by an indirect interaction of this LT mutant with Bub1 via p53 (personal communication, Dr Ole Gjoerup), rather than the interaction of LT residues 89-97 with Bub1 observed in lanes 6-10 in the wild-type LT-expressing cell line.

Figure 5.6 panel C shows Mad2 immunoprecipitations of the lysates from panel A, western blotted for Bub1 and LT. The method used for the immunoprecipitations was the same as that used for panel B, except that anti-Mad2L1 (an alternative name for human Mad2) monoclonal antibody was used to immunoprecipitate the Mad2 protein from the lysates, and Protein G- rather than Protein A-Sepharose beads were used for the immunoprecipitation (because the Mad2 antibody was IgG1 sub-class, and therefore would not have high affinity for Protein A, as discussed in Chapter 4). As before, the immunoprecipitates were run on a 5-15% SDS-PAGE gradient gel, and western blotted with antibodies against Bub1 (using NT hBub1 polyclonal antiserum) and LT (using anti-LT monoclonal PAb423).

It has previously been shown that Mad2 does not associate with Bub1 in mammalian cells, even in the presence of nocodazole-induced spindle

damage (Skoufias *et al.*, 2001), and so the Mad2-Bub1 co-immunoprecipitation results shown in Figure 5.6 panel C were quite unexpected and novel. No co-immunoprecipitation of Bub1 with Mad2 is observed in any of the control (untransfected) U20S lysates, as would be expected from previous observations by others (Figure 5.6C, lanes 1-5, N.B. a non-specific smear was observed in the Bub1 blot of lane 1, but no clear 150kDa Bub1 band was seen). Similarly, no Mad2-Bub1 association is suggested in the U20S(wild-type LT) lysates treated with 0-50ng/ml nocodazole (see Figure 5.6C, Bub1 blot, lanes 6-9). However, when 100ng/ml nocodazole treatment was used, a very faint 150kDa Bub1 band appeared to be co-immunoprecipitating with Mad2, (lane 10, unfortunately it was difficult to demonstrate this clearly in the scan of the autorad shown in Figure 5.6C). The U20S(dl98-97 LT) cells treated with 100ng/ml nocodazole showed a strong 150kDa Bub1 band co-immunoprecipitating with Mad2 (Figure 5.6C lane 15, Bub1 blot), but no Bub1 was found to be associated with Mad2 when U20S(dl89-97 LT) cells were treated with lower doses of the drug (lanes 11-14).

The Mad2 immunoprecipitations were also blotted for LT, to look for association of these proteins in the three cell lines under conditions of increasing levels of spindle damage (see LT blot, Figure 5.6 panel C). As expected, no LT is detected in the untransfected U20S cells (lanes 1-5, no 100kDa LT bands are detected). However, when Mad2 is immunoprecipitated from the U20S(wild-type LT) lysates, LT appears to co-immunoprecipitate, as seen by the strong 100kDa LT bands in lanes 6-10. In addition, the amount of LT co-immunoprecipitating with Mad2 appears to increase with nocodazole dose (see lanes 6-10). Interaction of the spindle checkpoint protein Mad2 with SV40 LT has not been shown before, and was an unexpected and novel finding. The association of these proteins also appears to be greatly enhanced by spindle damage in the U20S(wild-type LT) cells, because the quantity of LT that is co-immunoprecipitated with Mad2 increases with nocodazole dose, even though the Mad2 levels remain relatively constant when these cells are

treated with nocodazole (see Mad2 blot in Figure 5.6 panel A, lanes 6-10). This relatively constant level of Mad2 in the U20S(wild-type LT) cells treated with increasing nocodazole doses should result in immunoprecipitation of an equal quantity of Mad2 protein in each of lanes 6-10 of Figure 5.6 panel C. Therefore, the accumulation of Mad2-associated wild-type LT seen in this figure seems most likely related to the level of spindle damage in the cells. In contrast, no such accumulation of Bub1-associated LT was observed in response to spindle damage, as shown by the 100kDa wild-type LT bands of equal intensity in lanes 6-10 of Figure 5.6 panel B. Mad2 also appears to associate with dl89-97 LT (see Figure 5.6C, LT blot, lanes 11-15), but only at high levels of spindle damage, (see lane 15). Very faint 100kDa dl89-97 LT bands are seen to co-immunoprecipitate with Mad2 at nocodazole concentrations from 0-50ng/ml (lanes 11-14), but these bands are much fainter than the intense band seen in lane 15.

These co-immunoprecipitation experiments revealed some very unexpected results, especially the Mad2 association with Bub1 and LT in the U20S(wild-type LT) and U20S(dl89-97 LT) cells. Attempts were made to verify that the Mad2L1 antibody was specifically immunoprecipitating the Mad2 protein, but this was very difficult to prove. A Mad2 western blot of the Mad2 immunoprecipitations was not informative, because the 24kDa Mad2 protein migrates at the same molecular weight as the IgG light chain (data not shown). The only other antibody available to us that could verify specificity of the Mad2L1 antibody was the p55Cdc antibody used earlier in this chapter. Mad2 is known to associate with Cdc20 (the human homolog of Cdc20 is p55Cdc) (Fang *et al.*, 1998; Sudakin *et al.*, 2001; Wassmann and Benezra, 1998), and therefore it was thought that detection of co-immunoprecipitation of p55Cdc with Mad2 would provide further evidence in support of the efficiency of the Mad2 immunoprecipitations for bringing down the real Mad2 protein. However, western blotting of the Mad2 immunoprecipitation for p55Cdc levels also failed to provide informative results, because the 55kDa protein co-migrates with IgG heavy chain and was not easily distinguishable

on the autorad (data not shown). However, the Mad2L1 antibody was able to detect the 24kDa Mad2 protein clearly in a western blot, demonstrating the same relative Mad2 levels in the different cell lines in response to nocodazole as seen in Figure 5.3 (data not shown), suggesting that the co-immunoprecipitation results seen in Figure 5.6 panel C are real.

Further investigation of the results seen in Figure 5.6 would be necessary to draw any firm conclusions about what is happening in the different cell lines. The co-immunoprecipitation shown in lane 15 of Figure 5.6 panel C has been repeated and yielded identical results, but unfortunately when more lysate was made for all samples and the experiments in Figure 5.6 were repeated in full, the interesting results could not be reproduced. However the results shown in Figure 5.6 were very convincing, and given more time it would be nice to investigate them further to determine for certain if they can be reproduced.

If the results are reproducible, the experiments shown in Figure 5.6 reveal three important and novel findings: Mad2 interaction with Bub1 (only in LT-expressing cells, and only with high spindle damage), interaction of Mad2 with wild-type LT (increasing with increased spindle damage), and interaction of Mad2 with dl89-97 LT (only in the presence of high spindle damage).

5.3.1.6 Time lapse microscopy of REFs reveals that LT-Bub1 interaction affects the cellular response to spindle damage

The importance of LT-Bub1 interaction for the spindle checkpoint defect observed in cells expressing wild-type LT was also examined via time lapse microscopy, in collaboration with Dr Alan Entwistle (LICR-UCL Light Microscopy Facility). REF(wild-type LT) or REF(dl89-97 LT) cells, as described in Chapter 3, were treated with several different concentrations of nocodazole and their real time response to each concentration was monitored overnight via time lapse microscopy. At nocodazole concentrations greater than 15ng/ml no difference was observed between the behaviour of the wild-

type and dl98-97 LT-expressing cells, with both cell lines responding by arresting in mitosis, observed as rounded up cells. At nocodazole concentrations lower than 15ng/ml, the drug did not appear to elicit a noticeable increase in numbers of mitotic, rounded cells (mitotic index) in either cell line (data not shown).

However, when the cell lines were treated with 15ng/ml nocodazole, differences were observed in the behaviour of the wild-type versus the dl89-97 (non-Bub1-binding) LT-expressing cells. Nocodazole was added at a final concentration of 15ng/ml to one flask of each cell type. After incubation at 37°C for 30 minutes they were then placed on an inverted time lapse microscope, and a phase-contrast image of one field was captured for each flask every two minutes, using a cooled CCD camera. A total of 450 images were collected from each cell line. These images have been collated into movies, which can be viewed from the supplemental CD attached to this thesis. Selected images from the movies are also displayed in Figure 5.7 (REF(wild-type LT)) and Figure 5.8 (REF(dl89-97 LT)).

Figure 5.7 shows the response of REF(wild-type LT) cells to treatment with 15ng/ml nocodazole. Several of the cells in the field of view have been induced to arrest in mitosis, as seen by the bright, rounded up cells that begin to accumulate in the population after ~3 hours of nocodazole treatment. Three different cells that have rounded up are indicated by arrowheads (distinguished by different colours, blue, green and red), to aid in the observation of behaviour of the cells in response to the drug. Each indicated cell is seen to round up at a slightly different time during the 15 hours shown, but each is seen to periodically change shape from a perfectly rounded structure to form elongated, dumb bell-like structures. The cell indicated by the blue arrowhead stretches into the dumb bell shape, and then following 5 hours of arrest (a normal mitosis is completed in less than an hour in vertebrate cells, (Rieder *et al.*, 1994)) appears to adapt to the spindle checkpoint by re-adhering to the flask without going through cytokinesis, presumably now in a tetraploid state.

Figure 5.7: Time lapse analysis of REF(wild-type LT) cells in response to 15ng/ml nocodazole.

450 phase-contrast images (one every 2 minutes), a selection of which are shown here, were captured to create a time lapse movie of REF(wild-type LT) cells treated with 15ng/ml nocodazole (see Supplemental CD). Three cells (indicated by arrowheads) demonstrate the general response to the drug. Arrested cells form dumb bell-like shapes in an apparent attempt to segregate their chromosomes, even in the presence of a nocodazole-induced arrest. (Scale bar represents 100μm).

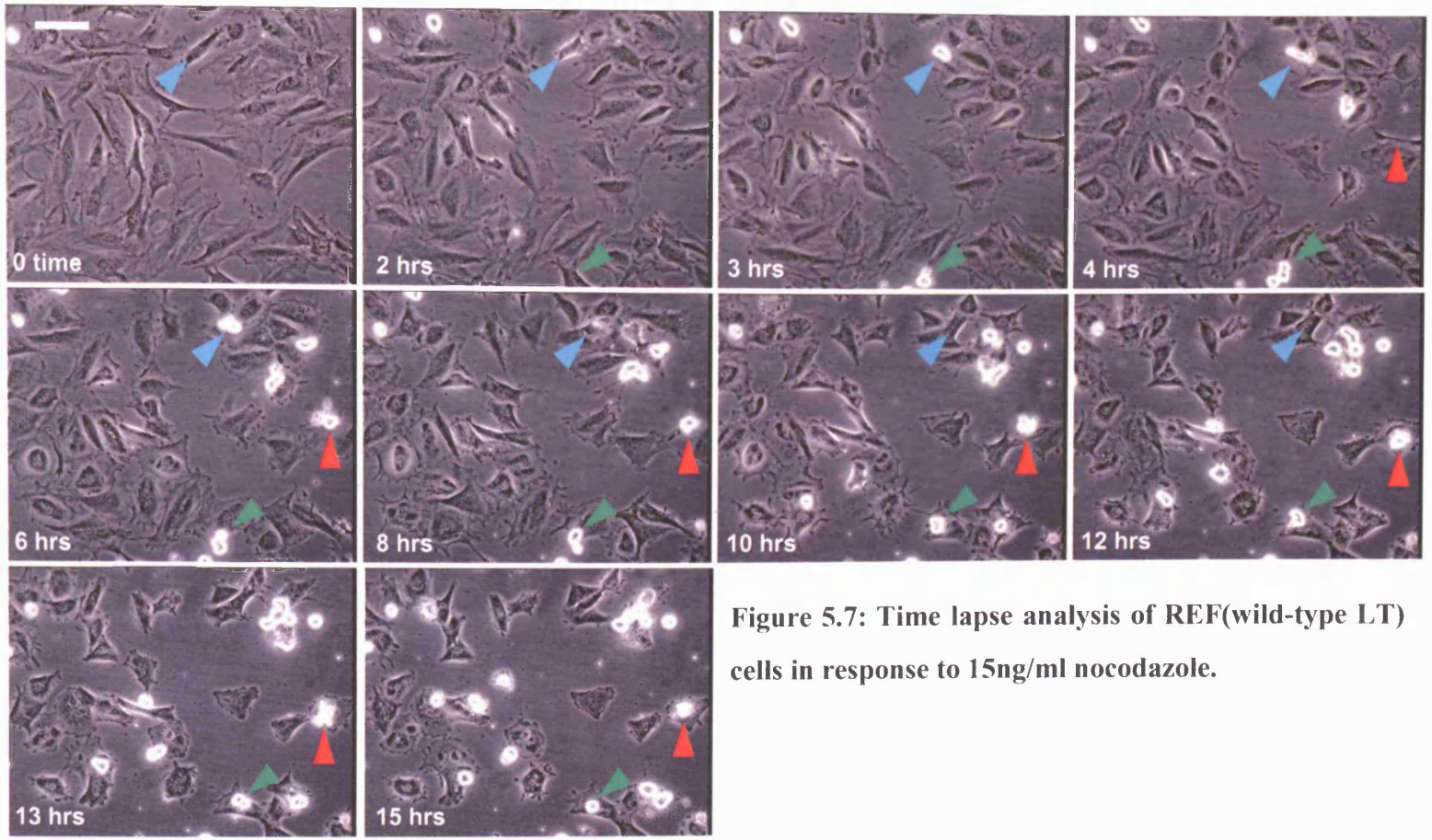

Figure 5.7: Time lapse analysis of REF(wild-type LT) cells in response to 15ng/ml nocodazole.

Figure 5.8: Time lapse analysis of REF(dl89-97 LT) cells in response to 15ng/ml nocodazole.

450 phase-contrast images (one every 2 minutes), a selection of which are shown here, were captured to create a time lapse movie of REF(dl89-97 LT) cells treated with 15ng/ml nocodazole (see Supplemental CD). Three cells (indicated by arrowheads) demonstrate the general response to the drug. Arrested cells remain in a stable, rounded conformation, indicative of a stable, nocodazole-induced spindle checkpoint arrest. (Scale bar represents 100μm)

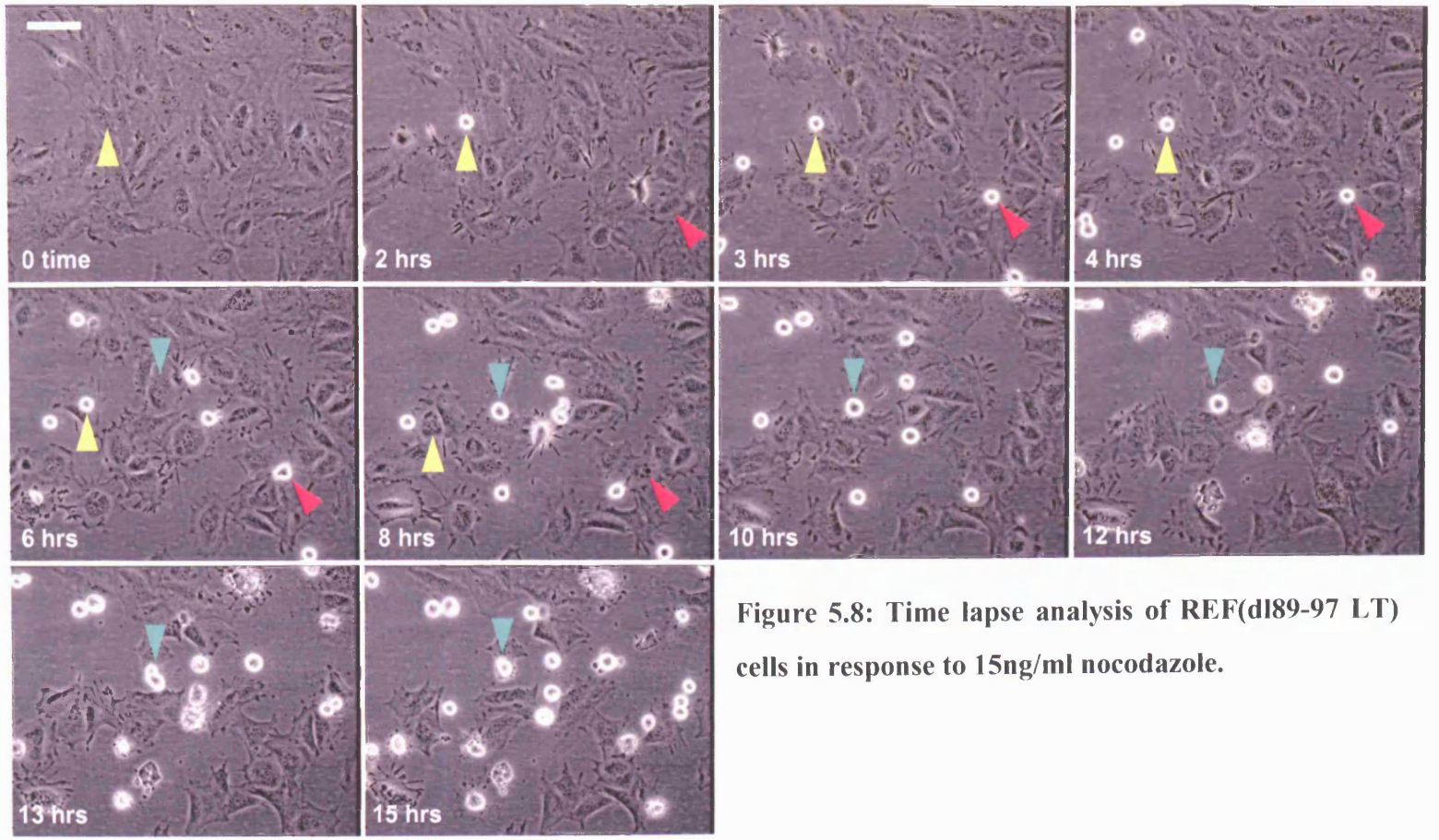

Figure 5.8: Time lapse analysis of REF(dl89-97 LT) cells in response to 15ng/ml nocodazole.

The other two indicated cells appear to stretch back and forth, but during the time of the movie do not adapt to the spindle checkpoint (i.e. are not seen to re-adhere to the flask). The overall view of the movie for the REF(wild-type LT) cells treated with 15ng/ml nocodazole is of cells rounding up, stretching back and forth in an apparent attempt to segregate the chromosomes, but then adapting to the spindle checkpoint, and re-adhering to the flask without undergoing cytokinesis.

In contrast, the REF(dl89-97 LT) cells in Figure 5.8 appear to behave differently in response to the same dose of nocodazole (15ng/ml). As for the wild-type LT-expressing cells in Figure 5.7, the rounded-up dl89-97 LT-expressing cells arrested at the spindle checkpoint begin to accumulate in the population after ~3 hours of nocodazole treatment. Three representative rounded-up cells are indicated by different coloured arrowheads (yellow, pink and turquoise). The cell indicated by the yellow arrowhead remains in a perfectly rounded shape for 8 hours, at which point it appears to adapt to the spindle checkpoint, and re-adheres to the flask without undergoing cytokinesis. The cell indicated by the pink arrowhead behaves in a similar manner. The turquoise arrowhead points to a cell that arrests much later during the time lapse analysis (after ~8 hours of nocodazole treatment), but again remains in a very rounded shape, arresting at the spindle checkpoint for at least 7 hours. In contrast to the wild-type LT-expressing cells shown in Figure 5.7, the dl89-97 LT-expressing cells in Figure 5.8 do not appear to attempt to segregate their DNA at all, remaining in a perfectly rounded, arrested state, and not contorting into dumb bell-like shapes.

These time lapse experiments suggest that cells expressing wild-type LT make an attempt at segregating their chromosomes even in the presence of a nocodazole-induced spindle checkpoint arrest. This observation appeared to be dependent on interaction of LT with the checkpoint protein Bub1.

5.3.2 *Karyotype analysis of tumourigenic and non-tumourigenic LT-expressing cells*

A potential end result of a disturbance in spindle checkpoint activation caused by LT could be chromosomal instability, giving rise to aneuploidy. One consequence of aneuploidy could be the activation of an oncogene by amplification, or loss of a tumour suppressor gene, leading to transformation. To examine the possibility that wild-type LT is able to induce aneuploidy to a greater extent than non-Bub1-binding (dl89-97) LT, it was first decided to test whether karyotype differences could be detected between LT-immortalised REFs that are tumourigenic, and those that are not when injected into rodents. As shown in Chapter 3, wild-type LT is able to both immortalise and transform rat cells, whereas dl89-97 LT is defective for transformation. Since a wild-type LT-immortalised rat cell line which is capable of inducing tumours in irradiated nude mice is a very good model for oncogenic transformation, this cell line (RSV4062), a cell line derived from a tumour induced by RSV4062 (NRSV4062), and two wild-type LT-immortalised rat lines not capable of inducing tumours in mice (RSV4068 and RSV40611) (Jat and Sharp, 1986) were tested initially. The was done to investigate the likelihood of being able to detect karyotype differences between cells expressing wild-type LT (able to transform) and dl89-97 LT (not able to transform) later on.

Metaphase spreads were prepared from each cell line, and stained with Propidium iodide (PI). Several individual metaphase spread images were captured via confocal microscopy to determine the number of chromosomes. The intention was that if a significant difference could be seen between the tumourigenic and non-tumourigenic lines, this would make a large study of metaphase spreads from wild-type and dl89-97 LT cell lines worthwhile.

Of the images of single cell, metaphase spreads captured, ~40 for each cell line were chosen for chromosome counting (images not shown). All images chosen had clearly separated chromosomes, but care was taken not to

choose spreads where the scatter of chromosomes was so great to allow potential "loss" of a chromosome to another part of the slide, so that the karyotype of the cell lines could be investigated with confidence. Figure 5.9 shows histograms for the chromosome counts in each image, for each cell line. A diploid rat cell has a chromosomal count of 42, but none of the cell lines shown in Figure 5.9 appear to have a stable karyotype of 42, with the histograms for all 4 cell lines showing approximately bell-shaped curves for the chromosome counts from ~40 metaphase spreads. The chromosome counts for the RSV4068 metaphase spreads appear to be close to the diploid number of 42, while the counts for RSV40611 are centred at ~43 chromosomes. While the overall karyotype of these two cell lines is not stable, with cells having different apparent degrees of aneuploidy, they are nevertheless very close to diploid. These two cell lines were not able to induce tumours when injected into nude mice (Jat and Sharp, 1986). The chromosome number of RSV4062 and NRSV4062 cells appears to be centred around 45-46 chromosomes per cell, further away from the diploid number of 42 than that seen for RSV4068 and RSV40611 in Figure 5.9. This could be a significant finding, because it was the RSV4062 cell line that was tumourigenic when injected into nude mice, and the NRSV4062 line was derived from one of the resulting tumours.

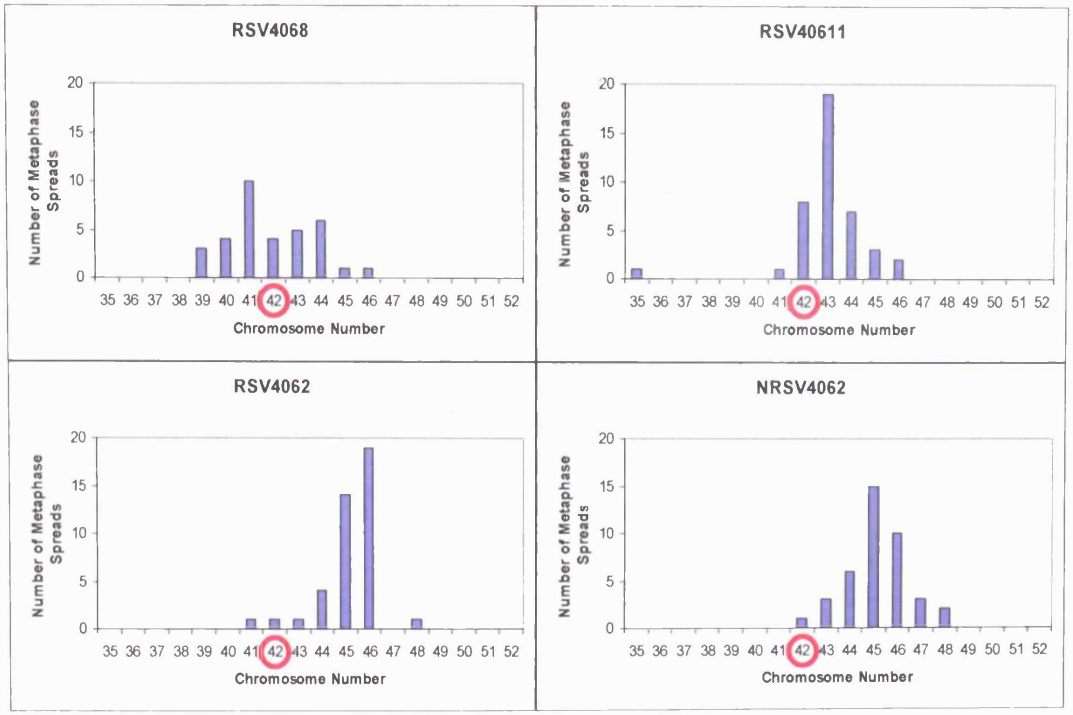

Figure 5.9: Karyotype analysis of REFs immortalised with SV40 large T antigen.

Non-tumourigenic (RSV4068 and RSV40611) and tumourigenic (RSV4062, and NRSV4062, a cell line derived from RSV4062) rat cell lines were karyotyped via metaphase spread. Chromosome numbers are plotted against numbers of cells with that chromosome number. The diploid number for rat is 42, as indicated on the graphs.

5.3.3 *Interaction with Bub1 does not affect the ability of LT to de-regulate the p53-dependent G1/S tetraploidy checkpoint*

As seen in the experiments already detailed in this chapter, when cells are treated with microtubule inhibitors such as nocodazole, the spindle checkpoint is activated, leading to a mitotic arrest prior to anaphase. However, upon prolonged treatment cells are able to adapt and exit mitosis aberrantly, resulting in the occurrence of tetraploid cells in G1. These cells are prevented from proliferating further by activation of a postmitotic, p53-dependent checkpoint in G1, known as the "tetraploidy checkpoint" (reviewed in (Andreassen *et al.*, 2003)). If a cell proceeds past a tetraploid state, genomic instability is inevitable because tetraploidisation caused by spindle checkpoint adaptation results in an alteration of centrosome number (Borel *et al.*, 2002). An increased number of centrosomes will randomly alter the number of spindle poles in the next mitosis, with more than two spindle poles resulting in random chromosome distribution to more than two daughter cells. Therefore, the tetraploidy checkpoint acts as a "fail-safe" mechanism that elicits a durable, cell cycle arrest if the spindle checkpoint has failed to ensure accurate chromosome segregation. It has been suggested that this p53-dependent checkpoint may also be able to impose G1 arrest in cells that become aneuploid via mitotic errors (Margolis *et al.*, 2003), although this has yet to be proven.

The tetraploid arrest in G1 is dependent on the presence of functional p53 and $p21^{WAF1}$ (Andreassen *et al.*, 2001a). It has previously been shown that SV40 LT-expressing cells are not able to arrest at the p53-dependent, G1 tetraploidy checkpoint in response to cleavage failure induced by the drug dihydrocytochalasin B (DCB). Instead, these cells progress to higher ploidy, presumably due to inhibition of p53 by LT (Andreassen *et al.*, 2001b). Following release from DCB-induced arrest, LT-expressing cells were shown to proceed through the cell cycle and become highly aneuploid.

Bypass of the spindle checkpoint in the presence of nocodazole should be accompanied by endoreduplication (accumulation of cells with DNA content greater than 4N), indicative of failure to maintain mitotic arrest in response to spindle damage, and cell cycle progression (Taylor and McKeon, 1997). Data have already been published that show that U20S cells expressing wild-type LT undergo enhanced endoreduplication in response to nocodazole treatment, whereas cells expressing non-Bub1-binding (dl89-97) LT, or untransfected cells, do not (Cotsiki *et al.*, 2004). It was therefore necessary to test that the dl89-97 LT mutant is still able to functionally abrogate the p53-dependent tetraploidy checkpoint pathway, otherwise this could provide an alternate explanation for its failure to induce endoreduplication in response to nocodazole. To rule out this possibility, untransfected (control) NIH 3T3 cells, and NIH 3T3 cells expressing wild-type LT or dl89-97 LT were treated for 24 hours with 12μM of dihydrocytochalasin B (DCB), an inhibitor of actin assembly that is required for cytokinesis (Aubin *et al.*, 1981; Martineau *et al.*, 1995), triggering exclusively the p53-dependent tetraploidy checkpoint, and not the spindle checkpoint. Following the 24 hour DCB treatment, cells were released from the drug into fresh medium. Samples from each cell line were collected for PI FACS analysis at the time when the DCB was added (no drug, zero time control), following the 24 hour DCB treatment, and following 24 hour, 48 hour and 5 day release from the drug. PI FACS cell cycle analysis was then carried out at the FACS laboratory, Cancer Research UK (Lincoln's Inn Fields, London), in collaboration with Dr Derek Davies, as shown in Figure 5.10.

A: No drug, zero time control

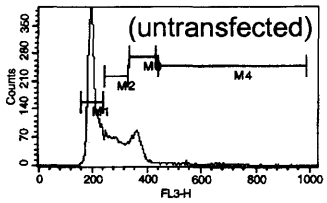

Marker	% Gated
All	100.00
M1	55.47
M2	23.32
M3	16.29
M4	2.44

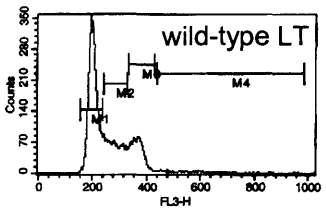

Marker	% Gated
All	100.00
M1	53.34
M2	24.02
M3	18.81
M4	1.37

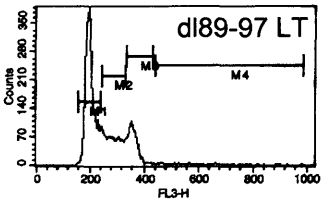

Marker	% Gated
All	100.00
M1	55.02
M2	24.67
M3	16.03
M4	1.65

B: 12μM DCB for 24 hours

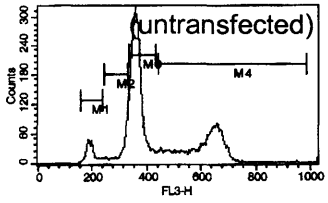

Marker	% Gated
All	100.00
M1	5.39
M2	6.25
M3	51.73
M4	33.76

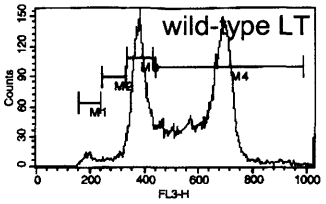

Marker	% Gated
All	100.00
M1	1.58
M2	2.02
M3	30.31
M4	64.17

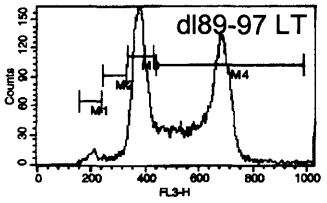

Marker	% Gated
All	100.00
M1	1.64
M2	2.08
M3	35.51
M4	58.66

C: 24 hour release from DCB

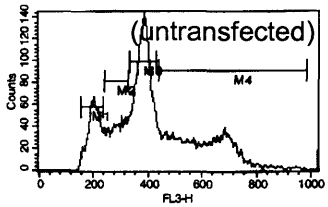

Marker	% Gated
All	100.00
M1	12.94
M2	13.84
M3	37.17
M4	32.77

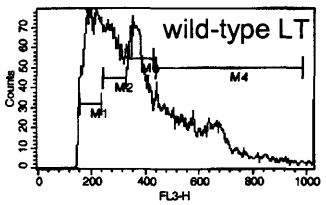

Marker	% Gated
All	100.00
M1	24.08
M2	24.07
M3	21.43
M4	26.20

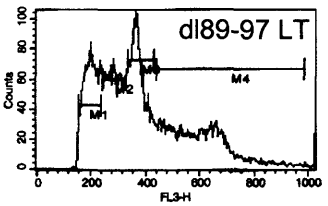

Marker	% Gated
All	100.00
M1	21.20
M2	22.02
M3	25.45
M4	27.38

D: 48 hour release from DCB

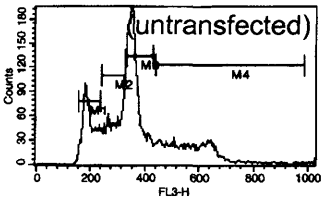

Marker	% Gated
All	100.00
M1	17.98
M2	20.82
M3	35.55
M4	21.15

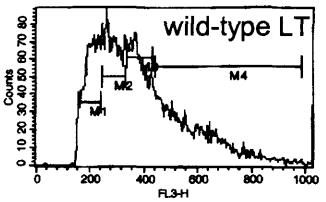

Marker	% Gated
All	100.00
M1	20.10
M2	25.67
M3	23.37
M4	26.42

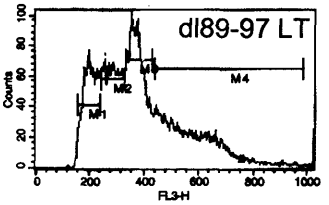

Marker	% Gated
All	100.00
M1	18.99
M2	23.79
M3	27.60
M4	25.82

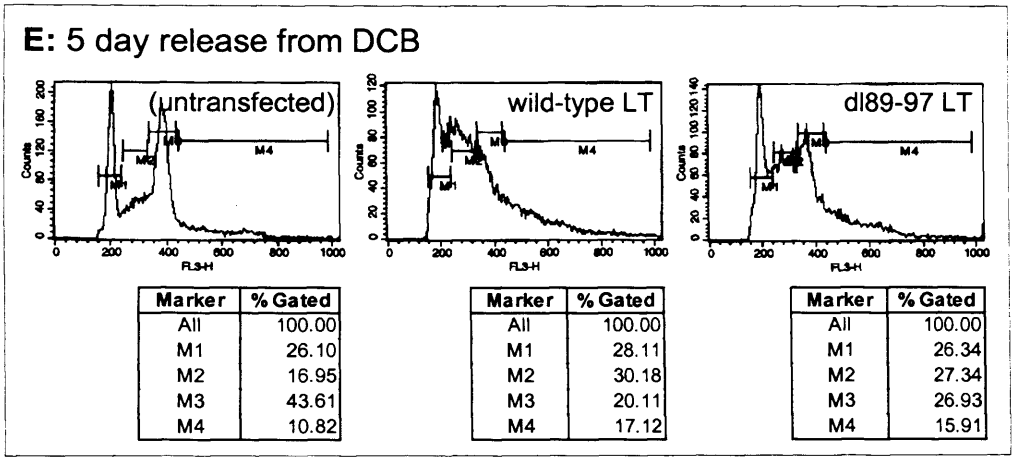

Marker	% Gated
All	100.00
M1	26.10
M2	16.95
M3	43.61
M4	10.82

Marker	% Gated
All	100.00
M1	28.11
M2	30.18
M3	20.11
M4	17.12

Marker	% Gated
All	100.00
M1	26.34
M2	27.34
M3	26.93
M4	15.91

Figure 5.10: Deletion of residues 89-97 of LT does not affect its ability to de-regulate the G1/S tetraploidy checkpoint.

Control (untransfected) NIH 3T3 cells, NIH 3T3 cells expressing wild-type LT or dl89-97 (non-Bub1-binding) LT were treated with the cytokinesis inhibitor dihydrocytochalasin B (DCB) to activate the p53-dependent, G1/S tetraploidy checkpoint. Cells were analysed via PI FACS for DNA content at the time of drug addition (A), following 24 hours of DCB treatment (B), and following 24 hour (C), 48 hour (D), and 5 day (E) release from the drug. Profiles are gated to show percentage of cells with different DNA contents: M1 = 2N (G1 phase) cells, M2 = 2N-4N (S phase) cells, M3 = 4N (G2/M phase, or tetraploid) cells, M4 = >4N (polyploid) cells.

Untransfected NIH 3T3 cells respond to DCB by arresting cells with 4N DNA content, at the tetraploidy checkpoint, whereas both NIH 3T3(wild-type LT) and NIH 3T3(dl89-97 LT) cells are defective for the p53-dependent, tetraploidy arrest, with many cells proceeding to >4N DNA content following DCB treatment, and progression to higher aneuploidy following release from the drug.

Panel A of Figure 5.10 shows that the cell cycle profiles (and DNA contents) of each cell line were very similar at the time of drug addition, with the majority of cells with 2N DNA content (gate M1), and the remainder with between 2N and 4N content (gates M2 and M3). It is important to note that this suggests that the LT constructs have little or no apparent effect on normal cell cycle phase progression in NIH 3T3 cells. Figure 5.10 panel B shows the DNA profiles following 24 hour treatment with 12μM DCB. Control (untransfected) NIH 3T3 cells responded as expected to the drug, the majority of cells (51.73%) arresting with tetraploid, 4N DNA content. However, both wild-type LT and dl89-97 LT-expressing cells were unable to maintain a stable tetraploidy checkpoint arrest, with a peak of 8N DNA content cells of almost the same size as the 4N peak, indicating that many cells are progressing to the next cell cycle even in the presence of the drug. Following a 24 hour release from DCB treatment (see Figure 5.10, panel C), the 2N peak (G1 phase cells, M1 gate) has begun to recover in the untransfected NIH 3T3 cells, indicating that the 2N cells that were present at the time of drug treatment have now come round at least a full cell cycle, and are proliferating well. The 4N (gate M3) peak remains high in these untransfected NIH 3T3 cells following 24 hours (panel C), 48 hours (panel D) and even 5 days (panel E) of release from DCB, indicative of no recovery of the 4N cells that were arrested by the tetraploidy checkpoint. These cells remain indefinitely arrested due to the tetraploidy checkpoint, and thus do not contribute to the recovery population (Andreassen *et al.*, 2001b). By the 5 day release (panel E), the untransfected NIH 3T3 cells have almost recovered to a normal, (as untreated) cell cycle profile, apart form the slightly high 4N population, due to representation of the permanently arrested tetraploid cells. In contrast, the NIH 3T3(wild-type LT) and NIH 3T3(dl89-97 LT) cells appear to never fully recover from the DCB treatment, accumulating more and more aneuploidy, as can be seen by the lack of clear 2N and 4N peaks in panels C-E of Figure 5.10, and the accumulation of many cells with >4N content (gate M4), in comparison to the proportion of these cells seen for the untransfected NIH

3T3 line. Also, the profiles of the NIH 3T3(wild-type LT) and NIH 3T3(dl89-97 LT) cells are very similar. In an independent repeat of this experiment, results identical to those in Figure 5.10 were observed.

This experiment has shown that the ability of dl89-97 LT to abrogate the p53-dependent tetraploidy checkpoint is not diminished in comparison to wild-type LT, and thus the differences observed in endoreduplication in response to nocodazole between cells expressing the different LT proteins is due to a spindle checkpoint defect, and not merely due to failure of the tetraploidy checkpoint following spindle checkpoint arrest. This experiment was carried out in parallel by Tom Roberts' laboratory in U20S cells, giving results that are in agreement with the NIH 3T3 experiment (personal communication).

5.4 SUMMARY & DISCUSSION

An important aim of the project was to demonstrate a spindle checkpoint defect in cells expressing wild-type LT, and to show that interaction of LT with Bub1 is crucial for this compromise of checkpoint function. The results described in this chapter clearly demonstrate that LT is compromising spindle checkpoint function via its interaction with Bub1, and begin to examine the mechanism by which this spindle checkpoint defect is achieved.

Many attempts were made to demonstrate the spindle checkpoint defect caused by LT interaction with Bub1 in NIH 3T3 cells, using both FACS analysis and western blotting. Unfortunately no such defect could be detected in this cell type with the methods used. Lessons learnt during the course of these experiments have suggested that the spindle checkpoint in NIH 3T3 cells may not be as robust as the checkpoint of U20S cells, perhaps preventing detection of a spindle checkpoint defect in the NIH 3T3(wild-type LT) cells. It is possible that inability to detect a difference in the proportion of 4N cells between the wild-type LT versus dl89-97 LT-expressing (or untransfected)

cells treated with nocodazole via FACS could be due to cytokinesis failure in nocodazole treated cells. It has been suggested that a properly formed spindle is required for cytokinesis to occur (Maddox and Oegema, 2003). This could suggest that the 4N population observed by FACS following nocodazole treatment of wild-type LT-expressing cells could contain some tetraploid cells which have escaped a spindle checkpoint arrest (and therefore have lowered securin levels), but have not segregated their chromosomes into two daughter cells. Using FACS analysis, these cells would not have been distinguishable from 4N cells arrested at the spindle checkpoint.

However, with adjustment of nocodazole treatment times in U20S cells, it was possible to demonstrate a spindle checkpoint defect caused by LT interaction with Bub1 in U20S cells via western blotting, using both synchronised cells and asynchronous cultures.

Treatment of asynchronous U20S cells (untransfected, or expressing either wild-type or dl89-97 LT) with 0-400ng/ml nocodazole for 15 hours followed by western blotting of the resulting lysates for securin, Cyclin B (and Mad2) levels clearly demonstrated that LT compromises spindle checkpoint function in these cells, and that interaction with Bub1 is required for this function of LT (see Figure 5.3). These proteins were observed to accumulate in lysates of U20S and U20S(dl89-97 LT) cells in response to increasing nocodazole treatment, indicative of spindle checkpoint arrest prior to anaphase, and therefore no proteolytic destruction of securin and Cyclin B. Mad2 levels have previously been shown to be cell cycle regulated in human cells, peaking at G2/M (Hernando *et al.*, 2004), consistent with the Mad2 levels seen in Figure 5.3. Lack of accumulation of securin, Cyclin B and Mad2 in response to increasing nocodazole in the U20S(wild-type LT) cells indicates that they are not able to arrest at the spindle checkpoint in mitosis, with many cells instead progressing further through the cell cycle even in the presence of a damaged mitotic spindle. Interestingly, Hernando *et al.* also report that when the pRB pathway is inactivated, high Mad2 levels are observed throughout the cell cycle. However, contradictory to this, low (but

fairly constant) levels of Mad2 were observed throughout the cell cycle in U20S(wild-type LT) cells in the experiments described in this chapter, even though pRB is inactivated by wild-type LT (Hernando *et al.*, 2004). Comparison of the securin and Mad2 protein levels (among others) in the soluble and insoluble lysis fractions in Figure 5.5 confirmed that the checkpoint defect observed in U20S(wild-type LT) cells when challenged with nocodazole was real, and not an artefact of a change in subcellular localisation of the proteins in this cell line. Although the spindle checkpoint defect induced by LT via its interaction with Bub1 has already been published (Cotsiki *et al.*, 2004), demonstration of a different response of the U20S cell lines to increasing nocodazole via western blotting has allowed examination of levels of checkpoint proteins and protein complexes in these cell lines under the same conditions, to aid in understanding the mechanism of checkpoint inhibition by LT.

Western blotting of lysates from U20S, U20S(wild-type LT) and U20S(dl89-97) following 15 hour treatment with 0-100ng/ml nocodazole was used to investigate the protein levels of Bub1, LT, Bub3 and $Cdc20^{p55Cdc}$ in the different cell lines in response to spindle checkpoint activation (see Figure 5.4). Other checkpoint proteins were not investigated due to lack of availability of suitable antibodies for western blotting.

Bub1 appeared to accumulate with increasing nocodazole concentration in all three cell lines, as would be expected due to the cell cycle regulation of this protein, peaking at G2/M (Davenport *et al.*, 1999; Taylor *et al.*, 2001). In accordance with the securin, Cyclin B and Mad2 levels in response to nocodazole treatment, Bub1 did not accumulate as much in the U20S(wild-type LT) cells as in the untransfected U20S cells. Multiple Bub1 bands were present in the western blot at all nocodazole concentrations, possibly the result of phosphorylation. However, Bub1 is thought to only be phosphorylated in response to checkpoint activation, and not in a normal mitosis (Chen, 2004; Taylor *et al.*, 2001), suggesting that multiple Bub1 bands should not be observed in the untreated lysates. Further investigation would be required to

determine the cause of the different migrating forms of Bub1 observed in these experiments, although they do not appear to be related to the presence or absence of LT in the cells, because they are observed in all three cell lines. Therefore, level of Bub1 expression and Bub1 cell cycle regulation do not appear to be directly affected by LT. However it is possible that LT is affecting the modification of Bub1, perhaps altering the number of forms of Bub1 present in the cell, under normal conditions or with spindle damage. This would not be surprising since members of Tom Roberts' laboratory have established that the auto-kinase activity of Bub1 is upregulated by the presence of LT (personal communication).

Levels of expression of wild-type and dl89-97 LT do not appear to be cell cycle regulated, staying at the same level in response to increasing nocodazole concentration. An observation made throughout this project has been that wild-type LT is consistently expressed at a higher level than dl89-97 LT in all cell lines, both in single cell clones and mixed populations of cells. Perhaps interaction of LT with Bub1 could be important for the stability of the LT protein in some way, or alternatively the dl89-97 LT protein could be lethal to the cells if expressed at a high level.

Bub3 is also not cell cycle regulated in either yeast or mammalian cells (Brady and Hardwick, 2000; Fraschini *et al.*, 2001; Martinez-Exposito *et al.*, 1999), and consistent with this, the level of Bub3 expression remains constant in all three cell lines in Figure 5.4, at all nocodazole concentrations. Bub3 expression is therefore not affected by the presence of LT.

$Cdc20^{p55Cdc}$ is known to accumulate in M phase in normal cells (Fraschini *et al.*, 2001; Weinstein, 1997), and this is also shown to be the case in U20S cells treated with increasing doses of nocodazole in Figure 5.4. In agreement with the lack of accumulation of securin, Cyclin B, Mad2 and Bub1 in response to spindle damage, p55Cdc levels do not accumulate in U20S(wild-type LT) cells, indicative of a spindle checkpoint defect. However, it was noted that p55Cdc levels are high in U20S(dl89-97 LT) cells at all nocodazole concentrations, even when no nocodazole was added. This is

curious, because none of the other checkpoint proteins investigated behaved differently in the U20S(dl89-97 LT) cell line than in the untransfected U20S cells. Further investigation to confirm this is required, although it is possible that LT could modulate spindle checkpoint function independently of its interaction with Bub1. However, the non-Bub1-binding (dl89-97) LT has not shown any checkpoint defect to date, with a spindle checkpoint as robust as that in cells that do not express LT.

An investigation of the protein complexes present under conditions of increasing spindle damage was carried out in the U20S, U20S(wild-type LT) and U20S(dl89-97 LT) cells (see Figure 5.6). Bub1 immunoprecipitates from the lysates prepared from each cell type with increasing nocodazole treatment showed accumulation of the Bub1 protein with spindle checkpoint activation in all three cell lines (Figure 5.6B), as also seen in the straight western blot for these lysates. However, when the Bub1 immunoprecipitates were blotted for LT, the amount of wild-type LT co-immunprecipitating with Bub1 did not increase with nocodazole dose as might have been expected, perhaps indicating that not all of the LT in the cell is in complex with Bub1. This would not be surprising considering the very high level of expression of LT in the cells. Alternatively, it could equally be the case that not all of the Bub1 in the cell is in a conformation that can be recognised and bound by LT, resulting in a LT-free pool of Bub1 in the cell.

It has previously been shown that Bub1 does not associate with Mad2 in normal mammalian cells (Skoufias *et al.*, 2001). However this did not rule out the possibility that Mad2 and Bub1 could be associating in cells that express LT. Figure 5.6C revealed some very interesting and novel interactions. The first novel finding was that Bub1 was able to associate with Mad2, but surprisingly this interaction was only observed in cells expressing non-Bub1 binding LT, and not in untransfected U20S cells, even though the two cell lines express similar levels of the two proteins in response to nocodazole treatment, and arrest in response to nocodazole in a similar way. The observation that untransfected U20S cells do not show a Bub1-Mad2

interaction under any of the nocodazole treatment conditions, was in agreement with previous studies in the literature. The clear Mad2-Bub1 interaction observed in U20S(dl89-97 LT) cells was only seen when cells were treated with the relatively high nocodazole dose of 100ng/ml, a concentration which results in noticeable securin and Cyclin B accumulation, indicative of cell cycle arrest at the spindle checkpoint. Therefore the presence of LT in the U20S cell lines, albeit without the ability to interact with Bub1, is resulting in an aberrant spindle checkpoint complex, the presence of which does not appear to affect the ability of the cells to arrest at the spindle checkpoint in response to spindle damage. An extremely weak Mad2-Bub1 interaction may be present in the U20S(wild-type LT) cells treated with 100ng/ml nocodazole also, although it is not clear if the reason for the reduced levels of this complex observed in comparison to in the U20S(dl89-97 LT) cells is simply due to the lower levels of Mad2 in this cell line under this condition (see Figure 5.6A Mad2 blot). It is therefore possible that LT can induce the aberrant formation of a Mad2-Bub1 complex in U20S cells upon spindle damage, and that this ability is independent of the interaction between residues 89-97 of LT and Bub1. It remains a possibility however that Mad2 interaction with Bub1 in the U20S(dl89-97 LT) cells could be via LT, but via a different region of the LT protein, for example via the p53-binding region, which may also be involved in Bub1 binding (Personal communication: Dr O. Gjoerup, Dana-Farber Cancer Institute, Boston, MA). However, the aberrant Mad2-Bub1 interaction observed in U20S(dl89-97 LT) cells treated with nocodazole cannot be explained by any of the current models for spindle checkpoint activation because these cells appeared to have a robust spindle checkpoint function.

Further novel findings were revealed when the Mad2 immunoprecipitations in Figure 5.6C were western blotted for LT. First of all, this experiment demonstrated a novel interaction between Mad2 and LT. Mad2 and wild-type LT appeared to interact even in the absence of spindle damage, but the amount of Mad2-LT complex present increased with

increasing nocodazole. This was surprising because the amount of Bub1-LT complex did not increase with increasing spindle damage in Figure 5.6B, the amount of co-immunoprecipitating LT staying constant even when Bub1 levels were increased by increasing the nocodazole dose. In addition, the amount of LT co-immunoprecipitating with Mad2 appears to increase with spindle damage to a much greater extent than could be expected if it were simply due to increasing Mad2, because Mad2 hardly accumulates with nocodazole at all in the western blot of this cell line in Figure 5.6A. Interaction of LT with Mad2 could provide a further explanation, in addition to the presence of the LT-Bub1 interaction, for why wild-type LT is able to compromise spindle checkpoint function. However, this theory cannot hold because the dl89-97 LT, which does not adversely affect spindle checkpoint function in U20S cells, was also able to interact with the Mad2 protein, although strong co-immunoprecipitation of dl89-97 LT with Mad2 is only observed in cells treated with 100ng/ml nocodazole, with lower doses of the drug resulting in virtually no Mad2-dl89-97 LT complex formation. Many efforts have been made to fit these observations into a model which might explain the spindle checkpoint compromise observed in cells expressing wild-type LT, but not in cells expressing non-Bub1 binding (dl89-97 LT), but no simple model can be drawn based on the current information. One attempt has been made to repeat these results without success, although the conditions were changed slightly in an attempt to harvest more lysate for use in future experiments. Further investigations using the original conditions would be needed to confirm that the interactions observed are real. If the results can be repeated then they are very important and novel, and it could be the case that LT induces spindle checkpoint proteins to complex in an aberrant way, and this ability is not limited to the wild-type, Bub1-binding LT. However, the full concert of proteins and protein complexes (including other spindle checkpoint components such as Mad1 and BubR1) present under the different spindle damage conditions in the presence of wild-type and dl89-97 LT needs further investigation to dissect the mechanism by which LT exerts its spindle

checkpoint effects. It is possible that LT could be sequestering functional Mad2 in the cell, as the amount of LT interacting with Mad2 appeared to increase with nocodazole concentration, i.e. under conditions of increasing spindle damage. Perhaps LT compromises the spindle checkpoint by reducing levels of functional Mad2, and thus preventing formation of active MCC. This compromise may not be fully dependent on Bub1 interaction with LT, which may instead act to bring LT into proximity with Mad2. These possibilities could be addressed in the future by co-immunoprecipitation and immunofluorescence studies of the checkpoint components and LT under conditions of spindle damage. It would be important to determine if formation of Mad2-containing protein complexes such as the MCC is altered either temporally or spatially under these conditions in cells which express LT (wild-type and dl89-97 LT). The relevance of the Bub1-LT interaction for the checkpoint compromise and the Mad2-LT interaction could be investigated by conducting similar experiments in cells where Bub1 levels have been significantly reduced via RNAi.

Time lapse movies of REF(wild-type LT) and REF(dl89-97 LT) cells treated with 15ng/ml nocodazole also revealed a different response to spindle checkpoint activation by the two cell lines (See Figures 5.7 and 5.8, and the supplemental CD that accompanies this thesis). REF(wild-type LT) cells formed dumb bell-like shapes (perhaps indicating an attempt at chromosome segregation), whereas REF(dl89-97 LT) cells remained in a perfectly rounded, arrested conformation, prior to adaptation to the spindle checkpoint. It has been shown that when administered at micromolar concentrations, nocodazole rapidly depolymerises microtubules, causing cells to arrest in mitosis (De Brabander *et al.*, 1976). 1μM nocodazole (FW = 301.3) is equivalent to ~300ng/ml, the approximate amount of nocodazole treatment that resulted in observation of significant differences in the amount of securin in the cell population (and hence spindle checkpoint arrest) between wild-type LT and dl89-97 LT-expressing cells (see Figure 5.3). However, when treated with nanomolar concentrations of nocodazole, as in the time lapse experiment

shown here (15ng/ml nocodazole is equivalent to ~50nM), cells are still arrested in mitosis by the drug, but without significant changes in microtubule polymer level (Jordan *et al.*, 1992). A study of mitotic checkpoint control in HeLa cells has been published in which the authors used 50nM nocodazole (equivalent to 15ng/ml) to clearly arrest cells at the spindle checkpoint, suggesting that this nocodazole concentration should also be sufficient to activate the spindle checkpoint in REFs (Wang *et al.*, 2002). Low (nanomolar) concentrations of nocodazole have been shown to result in an overall decrease in microtubule turnover in the cells, and it has been suggested that the cell cycle block observed is due to microtubule stabilisation (Vasquez *et al.*, 1997). Therefore, it seems likely that the formation of dumb bells in the REF(wild-type LT) cells treated with 15ng/ml nocodazole could be indicative of an attempt to override the spindle checkpoint arrest induced by the drug in these cells. The time lapse experiment was repeated twice with similar results, but although dumb-bells were seen in the REF(wild-type LT) cells, no cells succeeded in completing cytokinesis in the presence of the drug. It has been proposed that cytokinesis requires overlapping microtubules from the two spindle poles for recruitment of the component(s) necessary for cleavage, (Maddox and Oegema, 2003), suggesting that the REFs treated with 15ng/ml nocodazole failed to undergo cytokinesis due to absence of a properly formed anaphase spindle, even when the spindle checkpoint is compromised (for example, by SV40 LT). In contrast, the REF(dl89-97 LT) cells treated with 15ng/ml nocodazole appeared to stably arrest at the spindle checkpoint, with no formation of dumb bells indicating that the cells make no obvious attempt to segregate their chromosomes. This might suggest that cells expressing non-Bub1-binding (dl89-97) LT are able to maintain a "more stable" arrest in response to low doses of nocodazole, in accordance with their seemingly uncompromised spindle checkpoint in response to high nocodazole doses (see Figure 5.3). Importantly, the observation that the REF(wild-type LT) cells attempt chromosome segregation even in the absence of a properly formed spindle (due to nocodazole) suggests that in a normal mitosis (without

nocodazole), aberrant segregation of any sister chromatids that have not formed a bipolar attachment may occur in these cells, and be followed by cytokinesis, resulting in aneuploidy. It would have been interesting to examine the response of REFs to 15ng/ml nocodazole in the absence of LT, but unfortunately REFs senesce in the absence of an immortalising gene such as LT, and the use of spontaneous immortal rat cell lines would have the disadvantage of not knowing the identity of the immortalising agent. However it might be possible to examine the response of early passage primary REFs to nocodazole treatment via time lapse microscopy to determine if they have the same response to nocodazole as the REF(dl89-97 LT) cells. In addition it would be informative to repeat the time lapse analysis further and attempt to quantify the observed behaviour of the different cell lines to nocodazole treatment over time.

The chromosome count study of tumourigenic versus non-tumourigenic rat cell lines indicated that while the non-tumourigenic lines were near diploid, the counts from the tumourigenic cell lines were slightly further removed from a diploid phenotype (See Figure 5.9). This might suggest that wild-type LT could produce "more aneuploidy" in cells than the transformation-defective, dl89-97 LT mutant. However, all cell lines tested in Figure 5.9 showed some variability of karyotype. Human mammary epithelial cells immortalised in the laboratory with a combination of hTERT (the catalytic sub-unit of telomerase) and either Bub1-binding or non-Bub1-binding (dl89-97) LT have recently been karyotyped, to determine if interaction of LT with Bub1 results in aneuploidy in the immortalised cells. As predicted, the cells immortalised with dl89-97 LT (and hTERT) were near-diploid, whereas the cells immortalised with Bub1-binding LT (and hTERT) were noticeably aneuploid (Prof. P.S. Jat, personal communication). The same results were also obtained using human mammary fibroblasts. This finding demonstrates that the interaction of LT with Bub1 not only results in a compromise of spindle checkpoint function, causing a failure to arrest in

response to microtubule poisons, but also that this checkpoint defect results in aneuploidy, as expected.

Following prolonged treatment with nocodazole cells eventually adapt to the spindle checkpoint arrest, exiting mitosis aberrantly without sister chromatid segregation and cytokinesis, resulting in a tetraploid, 4N DNA content. The lack of securin and Cyclin B accumulation in wild-type LT but not in dl89-97 LT-expressing or untransfected cells following 15 hours of nocodazole treatment (see Figure 5.3), taken to indicate a spindle checkpoint defect in the wild-type LT-expressing cells, was tested to confirm that it was not simply the result of a difference in the rate of adaptation of the cells. However, at no time point leading up to 15 hours of nocodazole treatment was a high level of securin or Cyclin B accumulation observed in the wild-type LT cells, suggesting that they were bypassing the spindle checkpoint and not simply adapting to the nocodazole arrest faster than the untransfected or dl89-97 LT-expressing cells.

In normal cells, following spindle checkpoint adaptation the resulting tetraploid cells are prevented from proliferating by induction of the p53-dependent tetraploidy checkpoint in G1, a more permanent cell cycle arrest. SV40 large T antigen inhibits p53, thus disrupting the G1 tetraploidy checkpoint arrest, leading to endoreduplication and genomic instability. (A very recent study has argued that mammalian cells do not possess a "tetraploidy checkpoint" because when low doses of DCB are used to block cleavage, binucleate cells are able to undergo DNA synthesis and proceed to mitosis (Uetake and Sluder, 2004). However it was confirmed that high doses of DCB (similar to those used here) do cause binucleate cells to arrest in G1, although no mechanism was proposed for why this occurs). It had already been shown that cells expressing wild-type LT undergo endoreduplication in the presence of nocodazole, indicative of bypass of the spindle checkpoint, whereas cells expressing dl89-97 LT did not endoreduplicate in response to nocodazole (Cotsiki *et al.*, 2004). Therefore it was necessary to confirm that the failure of the dl89-97 LT-expressing cells to endoreduplicate was purely

due to the presence of a robust spindle checkpoint, and not simply due to inability of dl89-97 LT to abrogate the G1 tetraploidy checkpoint. To test this hypothesis, untransfected NIH 3T3 cells, and NIH 3T3 cells expressing wild-type or dl89-97 LT were treated with the drug dihydrocytochalasin B (DCB) to specifically activate the G1 tetraploidy checkpoint. As expected, dl89-97 LT was just as defective for the p53-dependent G1 tetraploidy checkpoint as wild-type LT, with DCB treatment resulting in accumulation of polyploid cells (See Figure 5.10). This not only shows that the 89-97 region of LT is crucial for the spindle checkpoint defect of cells expressing LT, but also shows that the dl89-97 LT mutant is still capable of abrogating p53 checkpoint function.

6. Summary and Final Discussion

Accurate transmission of genetic information is absolutely critical for both cell and organism survival. This is regulated by intrinsic properties of the cell cycle, which ensure that appropriate events occur at the correct time and in the correct order. A further level of control is provided by checkpoints that prevent cell cycle progression in the presence of any errors that may threaten the fidelity of cell division. Mitosis is considered to be the most dramatic and potentially dangerous event in the cell cycle because sister chromatids are irreversibly segregated to daughter cells. Correct assembly and positioning of the mitotic spindle are critical for accurate chromosome segregation. The checkpoint that monitors this process is the spindle checkpoint. It ensures that one chromosome of each pair of chromatids is segregated to each daughter cell, and is able to detect even a single unattached chromosome and in response generate a "wait signal" until all chromosomes are attached and aligned correctly. Defects in the spindle checkpoint can lead to chromosomal instability (CIN) and cancer.

SV40 large T antigen (LT) is a viral oncoprotein known to induce chromosome aberrations leading to aneuploidy in its cellular host. An interaction between LT and the spindle checkpoint protein Bub1 was identified in the Jat laboratory. It was proposed that LT might be compromising the spindle checkpoint function of Bub1 via this interaction. If this were the case, it seemed reasonable to suggest that LT overrides the spindle checkpoint to allow accumulation of mitotic errors in its host cells, potentially leading to aneuploidy and a transformed phenotype. The aim of the research described in this thesis has been to attempt to answer these questions. Progress has been made in elucidating the function of LT-Bub1 interaction and some of the data presented in this thesis is now published (Cotsiki *et al.*, 2004).

6.1 SUMMARY OF RESULTS

The interaction site of Bub1 on LT was initially mapped to residues 89-97 of LT using co-immunoprecipitation experiments in lysates from cells expressing different LT mutants. The site was then finer mapped using single amino acid mutations to alanine. The results suggested that three tryptophan residues in the 89-97 region that are conserved between large T antigens from several different viruses were the most critical for Bub1 interaction. The importance of Bub1 interaction for the immortalisation and transformation functions of LT were next examined. While LT was able to efficiently immortalise primary rat cells in the absence of Bub1 interaction, the Bub1-binding residues of LT were shown to be critical for the transformation activities of the viral protein.

To aid subsequent experiments, three highly specific monoclonal antibodies were generated against the mouse Bub1 protein. While verifying the specificity of the new antibodies to the Bub1 protein, the migration of Bub1 on SDS-PAGE was confirmed to be at ~150kDa, higher that the predicted molecular weight for the protein of ~120kDa. The mBub1 monoclonal antibodies were used for immunofluorescence studies of mouse cells expressing wild-type LT. Bub1 localisation in these cells did not appear to differ from that previously reported in normal mammalian cells under the conditions tested.

It was clearly demonstrated that LT compromises the ability of the spindle checkpoint to arrest cells in response to nocodazole-induced spindle damage. Wild-type LT prevented cell cycle arrest in nocodazole treated cells, as observed by inappropriate destruction of securin in the absence of a properly formed spindle. Time lapse experiments also suggested that wild-type LT-expressing cells attempt to segregate their chromosomes inappropriately even in the presence of nocodazole. This checkpoint abrogation by LT was dependent on LT-Bub1 interaction, as shown by evidence of robust spindle checkpoint function in dl89-97 LT-expressing cells.

Initial attempts to examine the mechanism by which LT is affecting the spindle checkpoint provided a hint that the Mad2 checkpoint protein may also be involved.

Tumourigenic and non-tumourigenic rat cells were karyotyped to help determine if the transformation (and therefore perhaps the Bub1-binding) functions of LT could be related to chromosomal instability. Initial results suggested that this might be the case. In addition, karyotyping of primary human cells immortalised with hTERT and either wild-type or dl89-97 LT has also linked the LT-Bub1 interaction to aneuploidy. Furthermore, experimental evidence suggests that LT may be inhibiting spindle checkpoint function via Bub1 to produce chromosome aberrations which can then go undetected at later checkpoints that are independently abrogated by LT. In agreement with this, FACS analysis of cells treated with dihydrocytochalasin B (DCB) (a drug that specifically activates the tetraploidy checkpoint) showed that in cells expressing dl89-97 LT the p53-dependent tetraploidy checkpoint is de-regulated to the same extent as in cells expressing wild-type LT.

6.2 FUTURE DIRECTIONS

It would be interesting to further investigate the nature of the LT-Bub1 interaction. The importance of residues 89-97 of LT (and especially the conserved tryptophan residues in this region) has already been highlighted, but this does not rule out the possibility that the interaction site of Bub1 on LT may extend further. It has been suggested by Dr Ole Gjoerup that residues 98-102 of LT may also play a role in Bub1 binding (personal communication). These residues were recently implicated in binding of LT with Cul7, a member of the cullin family involved in forming the scaffold for multi-subunit complexes that target proteins for ubiquitination (Ali *et al.*, 2004). Like the Bub1-binding region of LT, the Cul7-binding region was shown to be important for the transformation functions of LT, but not for the immortalisation activities. However, while the Bub1 interaction site of LT is

critical for viral DNA replication, Cul7 binding is not required for this function of LT. Therefore it would be important to determine if the 89-97 region of LT is involved in both Cul7 and Bub1 binding. This would help to determine if dissociation of immortalisation and transformation activities seen in the dl89-97 LT mutant involves simply Bub1, or if it involves both Bub1 and Cul7 proteins. The possibility also remains that LT-Bub1 interaction is not direct, and could in fact involve the Cul7 protein. Bub3 could also act as a bridging protein for the LT-Bub1 interaction, as it was found in the same complex (Cotsiki *et al.*, 2004). However, it has been reported that a GLEBS-like (GLE2p-Binding Sequence) motif located at residues 249-264 of hBub1 is sufficient for Bub3 binding (Wang *et al.*, 2001b). It therefore seems less likely (although not impossible) that endogenous yeast Bub3 could have been acting as a bridging protein for LT-Bub1 interaction, since only amino acids 600-1085 of hBub1 were encoded by the cDNA that was identified in the original yeast two-hybrid screen. *In vitro* binding assays could be used to confirm whether or not the LT-Bub1 interaction is direct.

Closer mapping of the LT interaction site within residues 600-1085 of Bub1 would also be useful. This information could provide clues to how LT is compromising Bub1 functions. It is known that Bub1 kinase activity is modulated by LT (personal communication, Dr Ole Gjoerup), and it would be interesting to find out if LT directly binds to the Bub1 carboxy-terminal kinase domain. A Bub1 mutant defective for LT interaction could be ectopically expressed in cells in which levels of the endogenous Bub1 have been significantly reduced via immunodepletion or RNAi. This would allow examination of the activities of a non-LT-binding Bub1 in both the spindle checkpoint and chromosome segregation. The Bub1 kinase activity and downstream targets of the Bub1 kinase in cells expressing wild-type or dl89-97 LT could also be further examined, both with and without nocodazole treatment. It has recently been demonstrated that Bub1 directly phosphorylates Cdc20 and inhibits APC/C^{Cdc20} activity in a catalytic manner (Tang *et al.*, 2004). Bub1-mediated phosphorylation of Cdc20 was necessary for proper

checkpoint signalling, further highlighting the importance of investigating the kinase activity of Bub1 in the presence of LT.

The mBub1 monoclonal antibodies generated could be used for more in-depth immunofluorescence studies in cells expressing wild-type or dl89-97 LT, as well as in untransfected cells. Co-localisation of checkpoint proteins with the kinetochore (and with LT) could be compared in both cycling and nocodazole-arrested cells. FRAP (fluorescence recovery after photobleaching) experiments would also allow analysis of the dynamics of the spindle checkpoint proteins at kinetochores in these cells. hBub1 monoclonal antibodies are now being generated in the laboratory, and may provide a further useful tool for these studies.

As a direct continuation of the work begun in this thesis, an important next step would be to follow up investigation of checkpoint proteins and complexes present in cells expressing wild-type or dl89-97 LT under conditions of spindle damage. Co-immunoprecipitation experiments similar to those reported here would be used. This could later be followed by proteomic approaches such as 2-Dimensional SDS-PAGE and mass spectrometry to positively identify proteins that are complexed or modified differently in the presence of wild-type versus dl89-97 LT.

A separation-of-function allele of Bub1 has recently been identified in fission yeast, demonstrating that the spindle checkpoint role of Bub1 is separate from the chromosome segregation role of the protein (Vanoosthuyse *et al.*, 2004). An amino-terminal domain of Bub1, required for targeting of Bub1, Bub3 and Mad3 to kinetochores and spindle checkpoint function, was not required for the role of Bub1 in chromosome congression, which was dependent on the carboxy-terminal region of Bub1 that includes the kinase domain. LT compromises the spindle checkpoint function of Bub1, but observations of lagging chromosomes and other segregation defects in wild-type LT (unpublished observations: Dr Ole Gjoerup) might suggest that the other functions of Bub1 may also be perturbed by LT interaction with the carboxy-terminal region of the protein. Therefore if Bub1 kinetochore

localisation functions remain intact in LT-expressing cells, it would be interesting to determine how LT is achieving the observed spindle checkpoint perturbation.

One possible reason for why wild-type but not dl89-97 LT can induce cell transformation might be that LT induces genetic instability via interaction with Bub1. This would then increase the likelihood of acquiring a second event that can give rise to cell transformation. There is some evidence in the literature to link Bub1 inhibition to aneuploidy in cancer cells (Cahill *et al.*, 1998), but it is still not clear if this is a causal relationship because others have reported different observations. A robust spindle checkpoint has been observed in aneuploid cells (Tighe *et al.*, 2001), and two colorectal cancer lines with mutations in Bub1 were shown to be tetraploid, a less severe karyotype defect than that normally observed with chromosomal instability (Grigorova *et al.*, 2004). However, preliminary studies have shown that primary human cells immortalised with hTERT and wild-type LT have an aneuploid karyotype, whereas the karyotype of cell lines generated using non-Bub1-binding dl89-97 LT is near diploid. These studies need to be extended to give statistically meaningful data. It would then be important to analyse these cell lines for both focus formation and anchorage-independent growth in soft agar, to determine if genetic instability in any way correlates with transformation phenotype. The robustness of the spindle checkpoint could then be compared in transformed versus non-transformed cultures generated from these assays.

It has been suggested that interaction of LT with Ran (a small GTPase that is involved in mitotic spindle organisation among other functions) could be one mechanism by which LT causes genomic instability (De Luca *et al.*, 2003). Modulation of levels of Ran's exchange factor, RCC1, have also been shown to abrogate the spindle checkpoint (Arnaoutov and Dasso, 2003). This suggests that the spindle checkpoint is directly responsive to levels of Ran-GTP in the cell, and could therefore lead to the possibility that SV40 LT interaction with Ran might affect the spindle checkpoint directly. It is not

known which residues of LT are involved in binding to Ran, but this would be interesting to investigate as it would provide further insight into the mechanisms by which LT is inducing genomic instability and perturbing spindle checkpoint function.

6.3 FINAL REMARKS

In conclusion, the results presented in this thesis have suggested a possible mechanism by which LT can transform cells to tumourigenicity. By understanding how this viral oncoprotein carries out its transforming functions it may be possible to gain greater insight into the cellular processes that lead to cancer. Examination of the mechanism by which LT perturbs the spindle checkpoint function of Bub1 may serve as a new direction from which to approach analysis of the spindle checkpoint pathway in normal cells. In addition, use of the dl89-97 LT mutant for generation of cell lines to study the basis of human diseases will provide a very useful tool if it eliminates problems associated with induction of aneuploidy during immortalisation by LT.

7. References

Abrieu, A., Kahana, J. A., Wood, K. W., and Cleveland, D. W. (2000). CENP-E as an essential component of the mitotic checkpoint in vitro. *Cell* **102,** 817-26.

Abrieu, A., Magnaghi-Jaulin, L., Kahana, J. A., Peter, M., Castro, A., Vigneron, S., Lorca, T., Cleveland, D. W., and Labbe, J. C. (2001). Mps1 is a kinetochore-associated kinase essential for the vertebrate mitotic checkpoint. *Cell* **106,** 83-93.

Acquaviva, C., Herzog, F., Kraft, C., and Pines, J. (2004). The anaphase promoting complex/cyclosome is recruited to centromeres by the spindle assembly checkpoint. *Nat Cell Biol* **6,** 892-8.

Adams, P. D. (2001). Regulation of the retinoblastoma tumor suppressor protein by cyclin/cdks. *Biochim Biophys Acta* **1471,** M123-33.

Ali, S. H., and DeCaprio, J. A. (2001). Cellular transformation by SV40 large T antigen: interaction with host proteins. *Semin Cancer Biol* **11,** 15-23.

Ali, S. H., Kasper, J. S., Arai, T., and DeCaprio, J. A. (2004). Cul7/p185/p193 binding to simian virus 40 large T antigen has a role in cellular transformation. *J Virol* **78,** 2749-57.

Alwine, J. C., Reed, S. I., and Stark, G. R. (1977). Characterization of the autoregulation of simian virus 40 gene A. *J Virol* **24,** 22-7.

Anand, S., Penrhyn-Lowe, S., and Venkitaraman, A. R. (2003). AURORA-A amplification overrides the mitotic spindle assembly checkpoint, inducing resistance to Taxol. *Cancer Cell* **3,** 51-62.

Andreassen, P. R., Lacroix, F. B., Lohez, O. D., and Margolis, R. L. (2001a). Neither p21WAF1 nor 14-3-3sigma prevents G2 progression to mitotic catastrophe in human colon carcinoma cells after DNA damage, but p21WAF1 induces stable G1 arrest in resulting tetraploid cells. *Cancer Res* **61,** 7660-8.

Andreassen, P. R., Lohez, O. D., Lacroix, F. B., and Margolis, R. L. (2001b). Tetraploid state induces p53-dependent arrest of nontransformed mammalian cells in G1. *Mol Biol Cell* **12,** 1315-28.

Andreassen, P. R., Lohez, O. D., and Margolis, R. L. (2003). G2 and spindle assembly checkpoint adaptation, and tetraploidy arrest: implications for intrinsic and chemically induced genomic instability. *Mutat Res* **532,** 245-53.

Andreassen, P. R., Martineau, S. N., and Margolis, R. L. (1996). Chemical induction of mitotic checkpoint override in mammalian cells results in aneuploidy following a transient tetraploid state. *Mutat Res* **372,** 181-94.

Appella, E., and Anderson, C. W. (2001). Post-translational modifications and activation of p53 by genotoxic stresses. *Eur J Biochem* **268,** 2764-72.

Arnaoutov, A., and Dasso, M. (2003). The Ran GTPase regulates kinetochore function. *Dev Cell* **5,** 99-111.

Aubin, J. E., Osborn, M., and Weber, K. (1981). Inhibition of cytokinesis and altered contractile ring morphology induced by cytochalasins in synchronized PtK2 cells. *Exp Cell Res* **136,** 63-79.

Avantaggiati, M. L., Carbone, M., Graessmann, A., Nakatani, Y., Howard, B., and Levine, A. S. (1996). The SV40 large T antigen and adenovirus E1a oncoproteins interact with distinct isoforms of the transcriptional co-activator, p300. *Embo J* **15,** 2236-48.

Avantaggiati, M. L., Ogryzko, V., Gardner, K., Giordano, A., Levine, A. S., and Kelly, K. (1997). Recruitment of p300/CBP in p53-dependent signal pathways. *Cell* **89,** 1175-84.

Babu, J. R., Jeganathan, K. B., Baker, D. J., Wu, X., Kang-Decker, N., and van Deursen, J. M. (2003). Rae1 is an essential mitotic checkpoint regulator that cooperates with Bub3 to prevent chromosome missegregation. *J Cell Biol* **160,** 341-53.

Baker, D. J., Jeganathan, K. B., Cameron, J. D., Thompson, M., Juneja, S., Kopecka, A., Kumar, R., Jenkins, R. B., de Groen, P. C., Roche, P., and van Deursen, J. M. (2004). BubR1 insufficiency causes early onset of aging-associated phenotypes and infertility in mice. *Nat Genet* **36,** 744-9.

Bartek, J., Bartkova, J., and Lukas, J. (1996). The retinoblastoma protein pathway and the restriction point. *Curr Opin Cell Biol* **8,** 805-14.

Basu, J., Logarinho, E., Herrmann, S., Bousbaa, H., Li, Z., Chan, G. K., Yen, T. J., Sunkel, C. E., and Goldberg, M. L. (1998). Localization of the Drosophila checkpoint control protein Bub3 to the kinetochore requires Bub1 but not Zw10 or Rod. *Chromosoma* **107,** 376-85.

Bernard, P., Maure, J. F., and Javerzat, J. P. (2001). Fission yeast Bub1 is essential in setting up the meiotic pattern of chromosome segregation. *Nat Cell Biol* **3,** 522-6.

Bharadwaj, R., and Yu, H. (2004). The spindle checkpoint, aneuploidy, and cancer. *Oncogene* **23,** 2016-27.

Bischoff, J. R., Casso, D., and Beach, D. (1992). Human p53 inhibits growth in Schizosaccharomyces pombe. *Mol Cell Biol* **12,** 1405-11.

Bodnar, A. G., Ouellette, M., Frolkis, M., Holt, S. E., Chiu, C. P., Morin, G. B., Harley, C. B., Shay, J. W., Lichtsteiner, S., and Wright, W. E. (1998). Extension of life-span by introduction of telomerase into normal human cells. *Science* **279,** 349-52.

Borel, F., Lohez, O. D., Lacroix, F. B., and Margolis, R. L. (2002). Multiple centrosomes arise from tetraploidy checkpoint failure and mitotic centrosome clusters in p53 and RB pocket protein-compromised cells. *Proc Natl Acad Sci U S A* **99,** 9819-24.

Bradford, M. M. (1976). A rapid and sensitive method for the quantitation of microgram quantities of protein utilizing the principle of protein-dye binding. *Anal Biochem* **72,** 248-54.

Brady, D. M., and Hardwick, K. G. (2000). Complex formation between Mad1p, Bub1p and Bub3p is crucial for spindle checkpoint function. *Curr Biol* **10,** 675-8.

Brown, D. R., Deb, S., Munoz, R. M., Subler, M. A., and Deb, S. P. (1993). The tumor suppressor p53 and the oncoprotein simian virus 40 T antigen bind to overlapping domains on the MDM2 protein. *Mol Cell Biol* **13,** 6849-57.

Brown, K. D., Coulson, R. M., Yen, T. J., and Cleveland, D. W. (1994). Cyclin-like accumulation and loss of the putative kinetochore motor CENP-E results from coupling continuous synthesis with specific degradation at the end of mitosis. *J Cell Biol* **125,** 1303-12.

Brummelkamp, T. R., Bernards, R., and Agami, R. (2002). A system for stable expression of short interfering RNAs in mammalian cells. *Science* **296,** 550-3.

Buvelot, S., Tatsutani, S. Y., Vermaak, D., and Biggins, S. (2003). The budding yeast Ipl1/Aurora protein kinase regulates mitotic spindle disassembly. *J Cell Biol* **160,** 329-39.

Cahill, D. P., da Costa, L. T., Carson-Walter, E. B., Kinzler, K. W., Vogelstein, B., and Lengauer, C. (1999). Characterization of MAD2B and other mitotic spindle checkpoint genes. *Genomics* **58,** 181-7.

Cahill, D. P., Lengauer, C., Yu, J., Riggins, G. J., Willson, J. K., Markowitz, S. D., Kinzler, K. W., and Vogelstein, B. (1998). Mutations of mitotic checkpoint genes in human cancers. *Nature* **392,** 300-3.

Campbell, L., and Hardwick, K. G. (2003). Analysis of Bub3 spindle checkpoint function in Xenopus egg extracts. *J Cell Sci* **116,** 617-28.

Carey Hanly, W., Artwohl, J. E., and Taylor Bennett, B. (1995). Adjuvants and Antibody Production: Review of Polyclonal Antibody Production Procedures in Mammals and Poultry. *ILAR Journal* **37,** http://dels.nas.edu/ilar/jour_online/37_3/37_3Polyclonal.asp.

Carroll, R. B., Hager, L., and Dulbecco, R. (1974). Simian virus 40 T antigen binds to DNA. *Proc Natl Acad Sci U S A* **71,** 3754-7.

Carroll, R. B., Samad, A., Mann, A., Harper, J., and Anderson, C. W. (1988). RNA is covalently linked to SV40 large T antigen. *Oncogene* **2,** 437-44.

Chan, G. K., Jablonski, S. A., Sudakin, V., Hittle, J. C., and Yen, T. J. (1999). Human BUBR1 is a mitotic checkpoint kinase that monitors CENP-E functions at kinetochores and binds the cyclosome/APC. *J Cell Biol* **146,** 941-54.

Chan, G. K., Schaar, B. T., and Yen, T. J. (1998). Characterization of the kinetochore binding domain of CENP-E reveals interactions with the kinetochore proteins CENP-F and hBUBR1. *J Cell Biol* **143,** 49-63.

Chang, T. H., Ray, F. A., Thompson, D. A., and Schlegel, R. (1997). Disregulation of mitotic checkpoints and regulatory proteins following acute expression of SV40 large T antigen in diploid human cells. *Oncogene* **14,** 2383-93.

Chang, T. H., and Schlegel, R. (1996). SV40 T antigen increases the expression and activities of p34cdc2, cyclin A, and cyclin B prior to immortalization of human diploid fibroblasts. *J Cell Biochem* **60,** 161-72.

Chen, J., and Fang, G. (2001). MAD2B is an inhibitor of the anaphase-promoting complex. *Genes Dev* **15,** 1765-70.

Chen, R. H. (2002). BubR1 is essential for kinetochore localization of other spindle checkpoint proteins and its phosphorylation requires Mad1. *J Cell Biol* **158,** 487-96.

Chen, R. H. (2004). Phosphorylation and activation of Bub1 on unattached chromosomes facilitate the spindle checkpoint. *Embo J* **23,** 3113-21.

Chen, R. H., Brady, D. M., Smith, D., Murray, A. W., and Hardwick, K. G. (1999). The spindle checkpoint of budding yeast depends on a tight complex between the Mad1 and Mad2 proteins. *Mol Biol Cell* **10,** 2607-18.

Chen, R. H., Shevchenko, A., Mann, M., and Murray, A. W. (1998). Spindle checkpoint protein Xmad1 recruits Xmad2 to unattached kinetochores. *J Cell Biol* **143,** 283-95.

Chen, R. H., Waters, J. C., Salmon, E. D., and Murray, A. W. (1996). Association of spindle assembly checkpoint component XMAD2 with unattached kinetochores. *Science* **274,** 242-6.

Chung, E., and Chen, R. H. (2002). Spindle checkpoint requires Mad1-bound and Mad1-free Mad2. *Mol Biol Cell* **13,** 1501-11.

Ciosk, R., Zachariae, W., Michaelis, C., Shevchenko, A., Mann, M., and Nasmyth, K. (1998). An ESP1/PDS1 complex regulates loss of sister chromatid cohesion at the metaphase to anaphase transition in yeast. *Cell* **93,** 1067-76.

Classon, M., and Dyson, N. (2001). p107 and p130: versatile proteins with interesting pockets. *Exp Cell Res* **264,** 135-47.

Cole, C. N. (1996). *In* "Polyomaviridae: the viruses and their replication" (B. N. Fields, Knipe, D. M., Howley, P. M., Ed.), pp. p.1997-2043. Lippincott-Raven Publishers, Philadelphia, Pa.

Conzen, S. D., and Cole, C. N. (1995). The three transforming regions of SV40 T antigen are required for immortalization of primary mouse embryo fibroblasts. *Oncogene* **11,** 2295-302.

Cotsiki, M., Lock, R. L., Cheng, Y., Williams, G. L., Zhao, J., Perera, D., Freire, R., Entwistle, A., Golemis, E. A., Roberts, T. M., Jat, P. S., and Gjoerup, O. V. (2004). Simian virus 40 large T antigen targets the spindle assembly checkpoint protein Bub1. *Proc Natl Acad Sci U S A* **101,** 947-52.

Counter, C. M., Meyerson, M., Eaton, E. N., Ellisen, L. W., Caddle, S. D., Haber, D. A., and Weinberg, R. A. (1998). Telomerase activity is restored in human cells by ectopic expression of hTERT (hEST2), the catalytic subunit of telomerase. *Oncogene* **16,** 1217-22.

Dai, W., Wang, Q., Liu, T., Swamy, M., Fang, Y., Xie, S., Mahmood, R., Yang, Y. M., Xu, M., and Rao, C. V. (2004). Slippage of mitotic arrest and enhanced tumor development in mice with BubR1 haploinsufficiency. *Cancer Res* **64,** 440-5.

D'Angiolella, V., Mari, C., Nocera, D., Rametti, L., and Grieco, D. (2003). The spindle checkpoint requires cyclin-dependent kinase activity. *Genes Dev* **17,** 2520-5.

Daum, J. R., Tugendreich, S., Topper, L. M., Jorgensen, P. M., Hoog, C., Hieter, P., and Gorbsky, G. J. (2000). The 3F3/2 anti-phosphoepitope antibody binds the mitotically phosphorylated anaphase-promoting complex/cyclosome. *Curr Biol* **10,** R850-2.

Davenport, J. W., Fernandes, E. R., Harris, L. D., Neale, G. A., and Goorha, R. (1999). The mouse mitotic checkpoint gene bub1b, a novel bub1 family member, is expressed in a cell cycle-dependent manner. *Genomics* **55,** 113-7.

De Brabander, M. J., Van de Veire, R. M., Aerts, F. E., Borgers, M., and Janssen, P. A. (1976). The effects of methyl (5-(2-thienylcarbonyl)-1H-benzimidazol-2-yl) carbamate, (R 17934; NSC 238159), a new synthetic antitumoral drug interfering with microtubules, on mammalian cells cultured in vitro. *Cancer Res* **36,** 905-16.

De Luca, A., Mangiacasale, R., Severino, A., Malquori, L., Baldi, A., Palena, A., Mileo, A. M., Lavia, P., and Paggi, M. G. (2003). E1A deregulates the centrosome cycle in a Ran GTPase-dependent manner. *Cancer Res* **63,** 1430-7.

DeCaprio, J. A., Ludlow, J. W., Figge, J., Shew, J. Y., Huang, C. M., Lee, W. H., Marsilio, E., Paucha, E., and Livingston, D. M. (1988). SV40 large tumor antigen forms a specific complex with the product of the retinoblastoma susceptibility gene. *Cell* **54,** 275-83.

Deming, P. B., Cistulli, C. A., Zhao, H., Graves, P. R., Piwnica-Worms, H., Paules, R. S., Downes, C. S., and Kaufmann, W. K. (2001). The human decatenation checkpoint. *Proc Natl Acad Sci U S A* **98,** 12044-9.

Deppert, W., Haug, M., and Steinmayer, T. (1987). Modulation of p53 protein expression during cellular transformation with simian virus 40. *Mol Cell Biol* **7,** 4453-63.

Dewar, H., Tanaka, K., Nasmyth, K., and Tanaka, T. U. (2004). Tension between two kinetochores suffices for their bi-orientation on the mitotic spindle. *Nature* **428,** 93-7.

Ditchfield, C., Johnson, V. L., Tighe, A., Ellston, R., Haworth, C., Johnson, T., Mortlock, A., Keen, N., and Taylor, S. S. (2003). Aurora B couples

chromosome alignment with anaphase by targeting BubR1, Mad2, and Cenp-E to kinetochores. *J Cell Biol* **161,** 267-80.

Dobles, M., Liberal, V., Scott, M. L., Benezra, R., and Sorger, P. K. (2000). Chromosome missegregation and apoptosis in mice lacking the mitotic checkpoint protein Mad2. *Cell* **101,** 635-45.

Doree, M., and Hunt, T. (2002). From Cdc2 to Cdk1: when did the cell cycle kinase join its cyclin partner? *J Cell Sci* **115,** 2461-4.

Draviam, V. M., Xie, S., and Sorger, P. K. (2004). Chromosome segregation and genomic stability. *Curr Opin Genet Dev* **14,** 120-5.

Dyson, N., Buchkovich, K., Whyte, P., and Harlow, E. (1989). The cellular 107K protein that binds to adenovirus E1A also associates with the large T antigens of SV40 and JC virus. *Cell* **58,** 249-55.

Eckner, R., Ludlow, J. W., Lill, N. L., Oldread, E., Arany, Z., Modjtahedi, N., DeCaprio, J. A., Livingston, D. M., and Morgan, J. A. (1996). Association of p300 and CBP with simian virus 40 large T antigen. *Mol Cell Biol* **16,** 3454-64.

Evans, T., Rosenthal, E. T., Youngblom, J., Distel, D., and Hunt, T. (1983). Cyclin: a protein specified by maternal mRNA in sea urchin eggs that is destroyed at each cleavage division. *Cell* **33,** 389-96.

Ewen, M. E., Ludlow, J. W., Marsilio, E., DeCaprio, J. A., Millikan, R. C., Cheng, S. H., Paucha, E., and Livingston, D. M. (1989). An N-terminal transformation-governing sequence of SV40 large T antigen contributes to the binding of both p110Rb and a second cellular protein, p120. *Cell* **58,** 257-67.

Fang, G. (2002). Checkpoint protein BubR1 acts synergistically with Mad2 to inhibit anaphase-promoting complex. *Mol Biol Cell* **13,** 755-66.

Fang, G., Yu, H., and Kirschner, M. W. (1998). The checkpoint protein MAD2 and the mitotic regulator CDC20 form a ternary complex with the anaphase-promoting complex to control anaphase initiation. *Genes Dev* **12,** 1871-83.

Fanning, E. (1992). Simian virus 40 large T antigen: the puzzle, the pieces, and the emerging picture. *J Virol* **66,** 1289-93.

Fishkind, D. J., and Wang, Y. L. (1993). Orientation and three-dimensional organization of actin filaments in dividing cultured cells. *J Cell Biol* **123,** 837-48.

Fisk, H. A., and Winey, M. (2001). The mouse Mps1p-like kinase regulates centrosome duplication. *Cell* **106,** 95-104.

Fraschini, R., Beretta, A., Sironi, L., Musacchio, A., Lucchini, G., and Piatti, S. (2001). Bub3 interaction with Mad2, Mad3 and Cdc20 is mediated by WD40 repeats and does not require intact kinetochores. *Embo J* **20,** 6648-59.

Gachet, Y., Tournier, S., Millar, J. B., and Hyams, J. S. (2001). A MAP kinase-dependent actin checkpoint ensures proper spindle orientation in fission yeast. *Nature* **412,** 352-5.

Gardner, R. D., and Burke, D. J. (2000). The spindle checkpoint: two transitions, two pathways. *Trends Cell Biol* **10,** 154-8.

Garner, M., van Kreeveld, S., and Su, T. T. (2001). mei-41 and bub1 block mitosis at two distinct steps in response to incomplete DNA replication in Drosophila embryos. *Curr Biol* **11,** 1595-9.

Gayther, S. A., Batley, S. J., Linger, L., Bannister, A., Thorpe, K., Chin, S. F., Daigo, Y., Russell, P., Wilson, A., Sowter, H. M., Delhanty, J. D., Ponder, B. A., Kouzarides, T., and Caldas, C. (2000). Mutations truncating the EP300 acetylase in human cancers. *Nat Genet* **24,** 300-3.

Gilinger, G., and Alwine, J. C. (1993). Transcriptional activation by simian virus 40 large T antigen: requirements for simple promoter structures containing either TATA or initiator elements with variable upstream factor binding sites. *J Virol* **67,** 6682-8.

Gillett, E. S., Espelin, C. W., and Sorger, P. K. (2004). Spindle checkpoint proteins and chromosome-microtubule attachment in budding yeast. *J Cell Biol* **164,** 535-46.

Ginsberg, D., Mechta, F., Yaniv, M., and Oren, M. (1991). Wild-type p53 can down-modulate the activity of various promoters. *Proc Natl Acad Sci U S A* **88,** 9979-83.

Gire, V., and Wynford-Thomas, D. (1998). Reinitiation of DNA synthesis and cell division in senescent human fibroblasts by microinjection of anti-p53 antibodies. *Mol Cell Biol* **18,** 1611-21.

Gjorup, O. V., Rose, P. E., Holman, P. S., Bockus, B. J., and Schaffhausen, B. S. (1994). Protein domains connect cell cycle stimulation directly to initiation of DNA replication. *Proc Natl Acad Sci U S A* **91,** 12125-9.

Gonos, E. S., Burns, J. S., Mazars, G. R., Kobrna, A., Riley, T. E., Barnett, S. C., Zafarana, G., Ludwig, R. L., Ikram, Z., Powell, A. J., and Jat, P. S. (1996). Rat embryo fibroblasts immortalized with simian virus 40 large T antigen undergo senescence upon its inactivation. *Mol Cell Biol* **16,** 5127-38.

Goodman, R. H., and Smolik, S. (2000). CBP/p300 in cell growth, transformation, and development. *Genes Dev* **14,** 1553-77.

Gorbsky, G. J., Chen, R. H., and Murray, A. W. (1998). Microinjection of antibody to Mad2 protein into mammalian cells in mitosis induces premature anaphase. *J Cell Biol* **141,** 1193-205.

Grabsch, H. I., Askham, J. M., Morrison, E. E., Pomjanski, N., Lickvers, K., Parsons, W. J., Boecking, A., Gabbert, H. E., and Mueller, W. (2004). Expression of BUB1 protein in gastric cancer correlates with the histological subtype, but not with DNA ploidy or microsatellite instability. *J Pathol* **202,** 208-14.

Grand, R. J., Turnell, A. S., Mason, G. G., Wang, W., Milner, A. E., Mymryk, J. S., Rookes, S. M., Rivett, A. J., and Gallimore, P. H. (1999). Adenovirus early region 1A protein binds to mammalian SUG1-a regulatory component of the proteasome. *Oncogene* **18,** 449-58.

Grand, R. J. A. (2001). Viruses, Cell Transformation and Cancer. *In* "Perspectives in Medical Virology" (A. J. Zuckerman, Mushahwar, I., Ed.), Vol. 5. Elsevier.

Green, R. A., and Kaplan, K. B. (2003). Chromosome instability in colorectal tumor cells is associated with defects in microtubule plus-end attachments caused by a dominant mutation in APC. *J Cell Biol* **163,** 949-61.

Grigorova, M., Staines, J. M., Ozdag, H., Caldas, C., and Edwards, P. A. (2004). Possible causes of chromosome instability: comparison of chromosomal abnormalities in cancer cell lines with mutations in BRCA1, BRCA2, CHK2 and BUB1. *Cytogenet Genome Res* **104,** 333-40.

Grossman, S. R., Perez, M., Kung, A. L., Joseph, M., Mansur, C., Xiao, Z. X., Kumar, S., Howley, P. M., and Livingston, D. M. (1998). p300/MDM2 complexes participate in MDM2-mediated p53 degradation. *Mol Cell* **2,** 405-15.

Gruda, M. C., Zabolotny, J. M., Xiao, J. H., Davidson, I., and Alwine, J. C. (1993). Transcriptional activation by simian virus 40 large T antigen: interactions

with multiple components of the transcription complex. *Mol Cell Biol* **13,** 961-9.

Habu, T., Kim, S. H., Weinstein, J., and Matsumoto, T. (2002). Identification of a MAD2-binding protein, CMT2, and its role in mitosis. *Embo J* **21,** 6419-28.

Hagting, A., Den Elzen, N., Vodermaier, H. C., Waizenegger, I. C., Peters, J. M., and Pines, J. (2002). Human securin proteolysis is controlled by the spindle checkpoint and reveals when the APC/C switches from activation by Cdc20 to Cdh1. *J Cell Biol* **157,** 1125-37.

Hahn, W. C., Counter, C. M., Lundberg, A. S., Beijersbergen, R. L., Brooks, M. W., and Weinberg, R. A. (1999). Creation of human tumour cells with defined genetic elements. *Nature* **400,** 464-8.

Hanahan, D. (1985). Heritable formation of pancreatic beta-cell tumours in transgenic mice expressing recombinant insulin/simian virus 40 oncogenes. *Nature* **315,** 115-22.

Hanks, S., Coleman, K., Reid, S., Plaja, A., Firth, H., Fitzpatrick, D., Kidd, A., Mehes, K., Nash, R., Robin, N., Shannon, N., Tolmie, J., Swansbury, J., Irrthum, A., Douglas, J., and Rahman, N. (2004). Constitutional aneuploidy and cancer predisposition caused by biallelic mutations in BUB1B. *Nat Genet* **36,** 1159-61.

Hannon, G. J., Demetrick, D., and Beach, D. (1993). Isolation of the Rb-related p130 through its interaction with CDK2 and cyclins. *Genes Dev* **7,** 2378-91.

Hansen, U., Tenen, D. G., Livingston, D. M., and Sharp, P. A. (1981). T antigen repression of SV40 early transcription from two promoters. *Cell* **27,** 603-13.

Hardwick, K. G., Johnston, R. C., Smith, D. L., and Murray, A. W. (2000). MAD3 encodes a novel component of the spindle checkpoint which interacts with Bub3p, Cdc20p, and Mad2p. *J Cell Biol* **148,** 871-82.

Hardwick, K. G., and Murray, A. W. (1995). Mad1p, a phosphoprotein component of the spindle assembly checkpoint in budding yeast. *J Cell Biol* **131,** 709-20.

Hardwick, K. G., Weiss, E., Luca, F. C., Winey, M., and Murray, A. W. (1996). Activation of the budding yeast spindle assembly checkpoint without mitotic spindle disruption. *Science* **273,** 953-6.

Hartwell, L. (1992). Defects in a cell cycle checkpoint may be responsible for the genomic instability of cancer cells. *Cell* **71,** 543-6.

Hartwell, L. H., and Weinert, T. A. (1989). Checkpoints: controls that ensure the order of cell cycle events. *Science* **246,** 629-34.

Hassold, T., and Hunt, P. (2001). To err (meiotically) is human: the genesis of human aneuploidy. *Nat Rev Genet* **2,** 280-91.

Hauf, S., Cole, R. W., LaTerra, S., Zimmer, C., Schnapp, G., Walter, R., Heckel, A., van Meel, J., Rieder, C. L., and Peters, J. M. (2003). The small molecule Hesperadin reveals a role for Aurora B in correcting kinetochore-microtubule attachment and in maintaining the spindle assembly checkpoint. *J Cell Biol* **161,** 281-94.

Hayflick, L., Moorhead, P.S. (1961). The serial cultivation of human diploid cell strains. *Exp Cell Res* **25,** 585-621.

Hempen, P. M., Kurpad, H., Calhoun, E. S., Abraham, S., and Kern, S. E. (2003). A double missense variation of the BUB1 gene and a defective mitotic spindle checkpoint in the pancreatic cancer cell line Hs766T. *Hum Mutat* **21,** 445.

Henning, W., Rohaly, G., Kolzau, T., Knippschild, U., Maacke, H., and Deppert, W. (1997). MDM2 is a target of simian virus 40 in cellular transformation and during lytic infection. *J Virol* **71,** 7609-18.

Hernando, E., Nahle, Z., Juan, G., Diaz-Rodriguez, E., Alaminos, M., Hemann, M., Michel, L., Mittal, V., Gerald, W., Benezra, R., Lowe, S. W., and Cordon-Cardo, C. (2004). Rb inactivation promotes genomic instability by uncoupling cell cycle progression from mitotic control. *Nature* **430,** 797-802.

Hilioti, Z., Chung, Y. S., Mochizuki, Y., Hardy, C. F., and Cohen-Fix, O. (2001). The anaphase inhibitor Pds1 binds to the APC/C-associated protein Cdc20 in a destruction box-dependent manner. *Curr Biol* **11,** 1347-52.

Hilleman, M. R. (1998). Discovery of simian virus 40 (SV40) and its relationship to poliomyelitis virus vaccines. *Dev Biol Stand* **94,** 183-90.

Hoffmann, I., Clarke, P. R., Marcote, M. J., Karsenti, E., and Draetta, G. (1993). Phosphorylation and activation of human cdc25-C by cdc2--cyclin B and its involvement in the self-amplification of MPF at mitosis. *Embo J* **12,** 53-63.

Hollstein, M., Rice, K., Greenblatt, M. S., Soussi, T., Fuchs, R., Sorlie, T., Hovig, E., Smith-Sorensen, B., Montesano, R., and Harris, C. C. (1994). Database of p53 gene somatic mutations in human tumors and cell lines. *Nucleic Acids Res* **22,** 3551-5.

Hottiger, M. O., and Nabel, G. J. (2000). Viral replication and the coactivators p300 and CBP. *Trends Microbiol* **8,** 560-5.

Howell, B. J., Hoffman, D. B., Fang, G., Murray, A. W., and Salmon, E. D. (2000). Visualization of Mad2 dynamics at kinetochores, along spindle fibers, and at spindle poles in living cells. *J Cell Biol* **150,** 1233-50.

Howell, B. J., McEwen, B. F., Canman, J. C., Hoffman, D. B., Farrar, E. M., Rieder, C. L., and Salmon, E. D. (2001). Cytoplasmic dynein/dynactin drives kinetochore protein transport to the spindle poles and has a role in mitotic spindle checkpoint inactivation. *J Cell Biol* **155,** 1159-72.

Howell, B. J., Moree, B., Farrar, E. M., Stewart, S., Fang, G., and Salmon, E. D. (2004). Spindle checkpoint protein dynamics at kinetochores in living cells. *Curr Biol* **14,** 953-64.

Hoyt, M. A., Totis, L., and Roberts, B. T. (1991). S. cerevisiae genes required for cell cycle arrest in response to loss of microtubule function. *Cell* **66,** 507-17.

Hu, Q. J., Dyson, N., and Harlow, E. (1990). The regions of the retinoblastoma protein needed for binding to adenovirus E1A or SV40 large T antigen are common sites for mutations. *Embo J* **9,** 1147-55.

Huang, J. Y., and Raff, J. W. (2002). The dynamic localisation of the Drosophila APC/C: evidence for the existence of multiple complexes that perform distinct functions and are differentially localised. *J Cell Sci* **115,** 2847-56.

Huang, S., Wang, N. P., Tseng, B. Y., Lee, W. H., and Lee, E. H. (1990). Two distinct and frequently mutated regions of retinoblastoma protein are required for binding to SV40 T antigen. *Embo J* **9,** 1815-22.

Hughes, T. A., and Cook, P. R. (1996). Mimosine arrests the cell cycle after cells enter S-phase. *Exp Cell Res* **222,** 275-80.

Hwang, L. H., Lau, L. F., Smith, D. L., Mistrot, C. A., Hardwick, K. G., Hwang, E. S., Amon, A., and Murray, A. W. (1998). Budding yeast Cdc20: a target of the spindle checkpoint. *Science* **279,** 1041-4.

Ikram, Z., Norton, T., and Jat, P. S. (1994). The biological clock that measures the mitotic life-span of mouse embryo fibroblasts continues to function in the presence of simian virus 40 large tumor antigen. *Proc Natl Acad Sci U S A* **91,** 6448-52.

Itahana, K., Campisi, J., and Dimri, G. P. (2004). Mechanisms of cellular senescence in human and mouse cells. *Biogerontology* **5,** 1-10.

Iwanaga, Y., and Jeang, K. T. (2002). Expression of mitotic spindle checkpoint protein hsMAD1 correlates with cellular proliferation and is activated by a gain-of-function p53 mutant. *Cancer Res* **62,** 2618-24.

Jablonski, S. A., Chan, G. K., Cooke, C. A., Earnshaw, W. C., and Yen, T. J. (1998). The hBUB1 and hBUBR1 kinases sequentially assemble onto kinetochores during prophase with hBUBR1 concentrating at the kinetochore plates in mitosis. *Chromosoma* **107,** 386-96.

Jallepalli, P. V., and Lengauer, C. (2001). Chromosome segregation and cancer: cutting through the mystery. *Nat Rev Cancer* **1,** 109-17.

Jallepalli, P. V., Waizenegger, I. C., Bunz, F., Langer, S., Speicher, M. R., Peters, J. M., Kinzler, K. W., Vogelstein, B., and Lengauer, C. (2001). Securin is required for chromosomal stability in human cells. *Cell* **105,** 445-57.

Janknecht, R. (2002). The versatile functions of the transcriptional coactivators p300 and CBP and their roles in disease. *Histol Histopathol* **17,** 657-68.

Jat, P. S., and Sharp, P. A. (1986). Large T antigens of simian virus 40 and polyomavirus efficiently establish primary fibroblasts. *J Virol* **59,** 746-50.

Jat, P. S., and Sharp, P. A. (1989). Cell lines established by a temperature-sensitive simian virus 40 large-T-antigen gene are growth restricted at the nonpermissive temperature. *Mol Cell Biol* **9,** 1672-81.

Jay, G., Nomura, S., Anderson, C. W., and Khoury, G. (1981). Identification of the SV40 agnogene product: a DNA binding protein. *Nature* **291,** 346-9.

Jiang, Y., Zhang, Y., Lees, E., and Seghezzi, W. (2003). AuroraA overexpression overrides the mitotic spindle checkpoint triggered by nocodazole, a microtubule destabilizer. *Oncogene* **22,** 8293-301.

Jin, D. Y., Spencer, F., and Jeang, K. T. (1998). Human T cell leukemia virus type 1 oncoprotein Tax targets the human mitotic checkpoint protein MAD1. *Cell* **93,** 81-91.

Johnson, V. L., Scott, M. I., Holt, S. V., Hussein, D., and Taylor, S. S. (2004). Bub1 is required for kinetochore localization of BubR1, Cenp-E, Cenp-F and Mad2, and chromosome congression. *J Cell Sci* **117,** 1577-89.

Jones, J. T., Myers, J. W., Ferrell, J. E., and Meyer, T. (2004). Probing the precision of the mitotic clock with a live-cell fluorescent biosensor. *Nat Biotechnol* **22,** 306-12.

Jordan, M. A., Thrower, D., and Wilson, L. (1992). Effects of vinblastine, podophyllotoxin and nocodazole on mitotic spindles. Implications for the role of microtubule dynamics in mitosis. *J Cell Sci* **102 (Pt 3),** 401-16.

Jorgensen, P. M., Brundell, E., Starborg, M., and Hoog, C. (1998). A subunit of the anaphase-promoting complex is a centromere-associated protein in mammalian cells. *Mol Cell Biol* **18,** 468-76.

Kalderon, D., Richardson, W. D., Markham, A. F., and Smith, A. E. (1984). Sequence requirements for nuclear location of simian virus 40 large-T antigen. *Nature* **311,** 33-8.

Kalitsis, P., Earle, E., Fowler, K. J., and Choo, K. H. (2000). Bub3 gene disruption in mice reveals essential mitotic spindle checkpoint function during early embryogenesis. *Genes Dev* **14,** 2277-82.

Kallio, M., Weinstein, J., Daum, J. R., Burke, D. J., and Gorbsky, G. J. (1998). Mammalian p55CDC mediates association of the spindle checkpoint protein Mad2 with the cyclosome/anaphase-promoting complex, and is involved in regulating anaphase onset and late mitotic events. *J Cell Biol* **141,** 1393-406.

Kallio, M. J., Beardmore, V. A., Weinstein, J., and Gorbsky, G. J. (2002a). Rapid microtubule-independent dynamics of Cdc20 at kinetochores and centrosomes in mammalian cells. *J Cell Biol* **158,** 841-7.

Kallio, M. J., McCleland, M. L., Stukenberg, P. T., and Gorbsky, G. J. (2002b). Inhibition of aurora B kinase blocks chromosome segregation, overrides the spindle checkpoint, and perturbs microtubule dynamics in mitosis. *Curr Biol* **12,** 900-5.

Kaplan, K. B., Burds, A. A., Swedlow, J. R., Bekir, S. S., Sorger, P. K., and Nathke, I. S. (2001). A role for the Adenomatous Polyposis Coli protein in chromosome segregation. *Nat Cell Biol* **3,** 429-32.

Kapoor, T. M., Mayer, T. U., Coughlin, M. L., and Mitchison, T. J. (2000). Probing spindle assembly mechanisms with monastrol, a small molecule inhibitor of the mitotic kinesin, Eg5. *J Cell Biol* **150,** 975-88.

Kastan, M. B., Onyekwere, O., Sidransky, D., Vogelstein, B., and Craig, R. W. (1991). Participation of p53 protein in the cellular response to DNA damage. *Cancer Res* **51,** 6304-11.

Katakura, Y., Alam, S., and Shirahata, S. (1998). Immortalization by gene transfection. *Methods Cell Biol* **57,** 69-91.

Kaufmann, W. K., Levedakou, E. N., Grady, H. L., Paules, R. S., and Stein, G. H. (1995). Attenuation of G2 checkpoint function precedes human cell immortalization. *Cancer Res* **55,** 7-11.

Kim, S. H., Lin, D. P., Matsumoto, S., Kitazono, A., and Matsumoto, T. (1998). Fission yeast Slp1: an effector of the Mad2-dependent spindle checkpoint. *Science* **279,** 1045-7.

Kitagawa, K., Abdulle, R., Bansal, P. K., Cagney, G., Fields, S., and Hieter, P. (2003). Requirement of Skp1-Bub1 interaction for kinetochore-mediated activation of the spindle checkpoint. *Mol Cell* **11,** 1201-13.

Kitajima, T. S., Kawashima, S. A., and Watanabe, Y. (2004). The conserved kinetochore protein shugoshin protects centromeric cohesion during meiosis. *Nature* **427,** 510-7.

Kiyono, T., Foster, S. A., Koop, J. I., McDougall, J. K., Galloway, D. A., and Klingelhutz, A. J. (1998). Both Rb/p16INK4a inactivation and telomerase activity are required to immortalize human epithelial cells. *Nature* **396,** 84-8.

Koerte, A., Chong, T., Li, X., Wahane, K., and Cai, M. (1995). Suppression of the yeast mutation rft1-1 by human p53. *J Biol Chem* **270,** 22556-64.

Kohrman, D. C., and Imperiale, M. J. (1992). Simian virus 40 large T antigen stably complexes with a 185-kilodalton host protein. *J Virol* **66,** 1752-60.

Kops, G. J., Foltz, D. R., and Cleveland, D. W. (2004). Lethality to human cancer cells through massive chromosome loss by inhibition of the mitotic checkpoint. *Proc Natl Acad Sci U S A* **101,** 8699-704.

Kramer, E. R., Scheuringer, N., Podtelejnikov, A. V., Mann, M., and Peters, J. M. (2000). Mitotic regulation of the APC activator proteins CDC20 and CDH1. *Mol Biol Cell* **11,** 1555-69.

Kuerbitz, S. J., Plunkett, B. S., Walsh, W. V., and Kastan, M. B. (1992). Wild-type p53 is a cell cycle checkpoint determinant following irradiation. *Proc Natl Acad Sci U S A* **89,** 7491-5.

Kussie, P. H., Gorina, S., Marechal, V., Elenbaas, B., Moreau, J., Levine, A. J., and Pavletich, N. P. (1996). Structure of the MDM2 oncoprotein bound to the p53 tumor suppressor transactivation domain. *Science* **274,** 948-53.

Lane, D. P. (1992). Cancer. p53, guardian of the genome. *Nature* **358,** 15-6.

Lane, D. P., and Crawford, L. V. (1979). T antigen is bound to a host protein in SV40-transformed cells. *Nature* **278,** 261-3.

Lanni, J. S., and Jacks, T. (1998). Characterization of the p53-dependent postmitotic checkpoint following spindle disruption. *Mol Cell Biol* **18,** 1055-64.

Lee, J. O., Russo, A. A., and Pavletich, N. P. (1998). Structure of the retinoblastoma tumour-suppressor pocket domain bound to a peptide from HPV E7. *Nature* **391,** 859-65.

Lee, M. H., and Yang, H. Y. (2001). Negative regulators of cyclin-dependent kinases and their roles in cancers. *Cell Mol Life Sci* **58,** 1907-22.

Lee, M. S., and Spencer, F. A. (2004). Bipolar orientation of chromosomes in Saccharomyces cerevisiae is monitored by Mad1 and Mad2, but not by Mad3. *Proc Natl Acad Sci U S A* **101,** 10655-60.

Lens, S. M., Wolthuis, R. M., Klompmaker, R., Kauw, J., Agami, R., Brummelkamp, T., Kops, G., and Medema, R. H. (2003). Survivin is required for a sustained spindle checkpoint arrest in response to lack of tension. *Embo J* **22,** 2934-47.

Li, R., and Murray, A. W. (1991). Feedback control of mitosis in budding yeast. *Cell* **66,** 519-31.

Li, W., Lan, Z., Wu, H., Wu, S., Meadows, J., Chen, J., Zhu, V., and Dai, W. (1999). BUBR1 phosphorylation is regulated during mitotic checkpoint activation. *Cell Growth Differ* **10,** 769-75.

Li, X., and Nicklas, R. B. (1995). Mitotic forces control a cell-cycle checkpoint. *Nature* **373,** 630-2.

Li, X., and Nicklas, R. B. (1997). Tension-sensitive kinetochore phosphorylation and the chromosome distribution checkpoint in praying mantid spermatocytes. *J Cell Sci* **110 (Pt 5),** 537-45.

Li, Y., and Benezra, R. (1996). Identification of a human mitotic checkpoint gene: hsMAD2. *Science* **274,** 246-8.

Li, Y., Gorbea, C., Mahaffey, D., Rechsteiner, M., and Benezra, R. (1997). MAD2 associates with the cyclosome/anaphase-promoting complex and inhibits its activity. *Proc Natl Acad Sci U S A* **94,** 12431-6.

Lill, N. L., Grossman, S. R., Ginsberg, D., DeCaprio, J., and Livingston, D. M. (1997a). Binding and modulation of p53 by p300/CBP coactivators. *Nature* **387,** 823-7.

Lill, N. L., Tevethia, M. J., Eckner, R., Livingston, D. M., and Modjtahedi, N. (1997b). p300 family members associate with the carboxyl terminus of simian virus 40 large tumor antigen. *J Virol* **71,** 129-37.

Linzer, D. I., and Levine, A. J. (1979). Characterization of a 54K dalton cellular SV40 tumor antigen present in SV40-transformed cells and uninfected embryonal carcinoma cells. *Cell* **17,** 43-52.

Liu, S. T., Chan, G. K., Hittle, J. C., Fujii, G., Lees, E., and Yen, T. J. (2003). Human MPS1 kinase is required for mitotic arrest induced by the loss of CENP-E from kinetochores. *Mol Biol Cell* **14,** 1638-51.

Lock, R. L., Benvenuti, S., and Jat, P. S. (2004). Chapter 14: Immortalization by SV40 Large T antigen. *In* "Cell Cycle and Growth Control: Biomolecular Regulation and Cancer, Second Edition" (G. S. Stein and A. B. Pardee, Eds.), pp. 467-495. John Wiley & Sons, Inc., Hoboken, New Jersey.

Loeb, L. A. (1991). Mutator phenotype may be required for multistage carcinogenesis. *Cancer Res* **51,** 3075-9.

Logarinho, E., Bousbaa, H., Dias, J. M., Lopes, C., Amorim, I., Antunes-Martins, A., and Sunkel, C. E. (2004). Different spindle checkpoint proteins monitor microtubule attachment and tension at kinetochores in Drosophila cells. *J Cell Sci* **117,** 1757-71.

Ludlow, J. W., DeCaprio, J. A., Huang, C. M., Lee, W. H., Paucha, E., and Livingston, D. M. (1989). SV40 large T antigen binds preferentially to an underphosphorylated member of the retinoblastoma susceptibility gene product family. *Cell* **56,** 57-65.

Ludlow, J. W., Shon, J., Pipas, J. M., Livingston, D. M., and DeCaprio, J. A. (1990). The retinoblastoma susceptibility gene product undergoes cell cycle-dependent dephosphorylation and binding to and release from SV40 large T. *Cell* **60,** 387-96.

Luo, X., Tang, Z., Rizo, J., and Yu, H. (2002). The Mad2 spindle checkpoint protein undergoes similar major conformational changes upon binding to either Mad1 or Cdc20. *Mol Cell* **9,** 59-71.

Maddox, A. S., and Oegema, K. (2003). Deconstructing cytokinesis. *Nat Cell Biol* **5,** 773-6.

Maltzman, W., and Czyzyk, L. (1984). UV irradiation stimulates levels of p53 cellular tumor antigen in nontransformed mouse cells. *Mol Cell Biol* **4,** 1689-94.

Malumbres, M., and Barbacid, M. (2001). To cycle or not to cycle: a critical decision in cancer. *Nat Rev Cancer* **1,** 222-31.

Manos, M. M., and Gluzman, Y. (1984). Simian virus 40 large T-antigen point mutants that are defective in viral DNA replication but competent in oncogenic transformation. *Mol Cell Biol* **4,** 1125-33.

Mao, Y., Abrieu, A., and Cleveland, D. W. (2003). Activating and silencing the mitotic checkpoint through CENP-E-dependent activation/inactivation of BubR1. *Cell* **114,** 87-98.

Margolis, R. L., Lohez, O. D., and Andreassen, P. R. (2003). G1 tetraploidy checkpoint and the suppression of tumorigenesis. *J Cell Biochem* **88,** 673-83.

Martin, D. W., Subler, M. A., Munoz, R. M., Brown, D. R., Deb, S. P., and Deb, S. (1993). p53 and SV40 T antigen bind to the same region overlapping the conserved domain of the TATA-binding protein. *Biochem Biophys Res Commun* **195,** 428-34.

Martineau, S. N., Andreassen, P. R., and Margolis, R. L. (1995). Delay of HeLa cell cleavage into interphase using dihydrocytochalasin B: retention of a postmitotic spindle and telophase disc correlates with synchronous cleavage recovery. *J Cell Biol* **131,** 191-205.

Martinez-Exposito, M. J., Kaplan, K. B., Copeland, J., and Sorger, P. K. (1999). Retention of the BUB3 checkpoint protein on lagging chromosomes. *Proc Natl Acad Sci U S A* **96,** 8493-8.

Martin-Lluesma, S., Stucke, V. M., and Nigg, E. A. (2002). Role of Hec1 in spindle checkpoint signaling and kinetochore recruitment of Mad1/Mad2. *Science* **297,** 2267-70.

Mayer, G. (2000). Immunology - Chapter Three: Antigens. *In* "Microbiology and Immunology On-line", pp. http://www.med.sc.edu:85/mayer/antigens2000.htm. University of South Carolina, School of Medicine.

Mayer, T. U., Kapoor, T. M., Haggarty, S. J., King, R. W., Schreiber, S. L., and Mitchison, T. J. (1999). Small molecule inhibitor of mitotic spindle bipolarity identified in a phenotype-based screen. *Science* **286,** 971-4.

Mazia, D. (1961). Mitosis and physiology of cell division. *In* "The Cell, Biochemistry, Physiology, Morphology." (J. Brachet, Mirsky, A., Ed.), pp. p. 77-412. Academic Press, New York.

McCarthy, S. A., Symonds, H. S., and Van Dyke, T. (1994). Regulation of apoptosis in transgenic mice by simian virus 40 T antigen-mediated inactivation of p53. *Proc Natl Acad Sci U S A* **91,** 3979-83.

Meraldi, P., Draviam, V. M., and Sorger, P. K. (2004a). Timing and checkpoints in the regulation of mitotic progression. *Dev Cell* **7,** 45-60.

Meraldi, P., Honda, R., and Nigg, E. A. (2004b). Aurora kinases link chromosome segregation and cell division to cancer susceptibility. *Curr Opin Genet Dev* **14,** 29-36.

Mercer, W. E. (1998). Checking on the cell cycle. *J Cell Biochem Suppl* **30-31,** 50-4.

Mercer, W. E., Shields, M. T., Lin, D., Appella, E., and Ullrich, S. J. (1991). Growth suppression induced by wild-type p53 protein is accompanied by selective down-regulation of proliferating-cell nuclear antigen expression. *Proc Natl Acad Sci U S A* **88,** 1958-62.

Michael-Michalovitz, D., Yehiely, F., Gottlieb, E., and Oren, M. (1991). Simian virus 40 can overcome the antiproliferative effect of wild-type p53 in the absence of stable large T antigen-p53 binding. *J Virol* **65,** 4160-8.

Michel, L., Diaz-Rodriguez, E., Narayan, G., Hernando, E., Murty, V. V., and Benezra, R. (2004). Complete loss of the tumor suppressor MAD2 causes premature cyclin B degradation and mitotic failure in human somatic cells. *Proc Natl Acad Sci U S A* **101,** 4459-64.

Michel, L. S., Liberal, V., Chatterjee, A., Kirchwegger, R., Pasche, B., Gerald, W., Dobles, M., Sorger, P. K., Murty, V. V., and Benezra, R. (2001). MAD2 haplo-insufficiency causes premature anaphase and chromosome instability in mammalian cells. *Nature* **409,** 355-9.

Mikhailov, A., Cole, R. W., and Rieder, C. L. (2002). DNA damage during mitosis in human cells delays the metaphase/anaphase transition via the spindle-assembly checkpoint. *Curr Biol* **12,** 1797-806.

Millband, D. N., and Hardwick, K. G. (2002). Fission yeast Mad3p is required for Mad2p to inhibit the anaphase-promoting complex and localizes to kinetochores in a Bub1p-, Bub3p-, and Mph1p-dependent manner. *Mol Cell Biol* **22,** 2728-42.

Mills, G. B., Schmandt, R., McGill, M., Amendola, A., Hill, M., Jacobs, K., May, C., Rodricks, A. M., Campbell, S., and Hogg, D. (1992). Expression of TTK, a novel human protein kinase, is associated with cell proliferation. *J Biol Chem* **267,** 16000-6.

Minn, A. J., Boise, L. H., and Thompson, C. B. (1996). Expression of Bcl-xL and loss of p53 can cooperate to overcome a cell cycle checkpoint induced by mitotic spindle damage. *Genes Dev* **10,** 2621-31.

Mitchell, P. J., Wang, C., and Tjian, R. (1987). Positive and negative regulation of transcription in vitro: enhancer-binding protein AP-2 is inhibited by SV40 T antigen. *Cell* **50,** 847-61.

Miyashita, T., Krajewski, S., Krajewska, M., Wang, H. G., Lin, H. K., Liebermann, D. A., Hoffman, B., and Reed, J. C. (1994). Tumor suppressor p53 is a regulator of bcl-2 and bax gene expression in vitro and in vivo. *Oncogene* **9,** 1799-805.

Miyoshi, Y., Iwao, K., Egawa, C., and Noguchi, S. (2001). Association of centrosomal kinase STK15/BTAK mRNA expression with chromosomal instability in human breast cancers. *Int J Cancer* **92,** 370-3.

Moberg, K. H., Tyndall, W. A., and Hall, D. J. (1992). Wild-type murine p53 represses transcription from the murine c-myc promoter in a human glial cell line. *J Cell Biochem* **49,** 208-15.

Momand, J., Wu, H. H., and Dasgupta, G. (2000). MDM2--master regulator of the p53 tumor suppressor protein. *Gene* **242,** 15-29.

Moran, E. (1988). A region of SV40 large T antigen can substitute for a transforming domain of the adenovirus E1A products. *Nature* **334,** 168-70.

Morgenstern, J. P., and Land, H. (1990). Advanced mammalian gene transfer: high titre retroviral vectors with multiple drug selection markers and a complementary helper-free packaging cell line. *Nucleic Acids Res* **18,** 3587-96.

Motoyama, N., and Naka, K. (2004). DNA damage tumor suppressor genes and genomic instability. *Curr Opin Genet Dev* **14,** 11-6.

Munger, K., Werness, B. A., Dyson, N., Phelps, W. C., Harlow, E., and Howley, P. M. (1989). Complex formation of human papillomavirus E7 proteins with the retinoblastoma tumor suppressor gene product. *Embo J* **8,** 4099-105.

Muraoka, M., Konishi, M., Kikuchi-Yanoshita, R., Tanaka, K., Shitara, N., Chong, J. M., Iwama, T., and Miyaki, M. (1996). p300 gene alterations in colorectal and gastric carcinomas. *Oncogene* **12,** 1565-9.

Murata-Hori, M., and Wang, Y. L. (2002). The kinase activity of aurora B is required for kinetochore-microtubule interactions during mitosis. *Curr Biol* **12,** 894-9.

Murray, A. W. (2004). Recycling the cell cycle: cyclins revisited. *Cell* **116,** 221-34.

Musio, A., Montagna, C., Zambroni, D., Indino, E., Barbieri, O., Citti, L., Villa, A., Ried, T., and Vezzoni, P. (2003). Inhibition of BUB1 results in genomic instability and anchorage-independent growth of normal human fibroblasts. *Cancer Res* **63,** 2855-63.

Nagele, R., Freeman, T., McMorrow, L., and Lee, H. Y. (1995). Precise spatial positioning of chromosomes during prometaphase: evidence for chromosomal order. *Science* **270,** 1831-5.

Napolitano, E. W., Pachter, J. S., and Liem, R. K. (1987). Intracellular distribution of mammalian stress proteins. Effects of cytoskeletal-specific agents. *J Biol Chem* **262,** 1493-504.

Nigg, E. A. (2001). Mitotic kinases as regulators of cell division and its checkpoints. *Nat Rev Mol Cell Biol* **2,** 21-32.

Nigro, J. M., Sikorski, R., Reed, S. I., and Vogelstein, B. (1992). Human p53 and CDC2Hs genes combine to inhibit the proliferation of Saccharomyces cerevisiae. *Mol Cell Biol* **12,** 1357-65.

O'Connell, C. B., and Wang, Y. L. (2000). Mammalian spindle orientation and position respond to changes in cell shape in a dynein-dependent fashion. *Mol Biol Cell* **11,** 1765-74.

Oegema, K., and Mitchison, T. J. (1997). Rappaport rules: cleavage furrow induction in animal cells. *Proc Natl Acad Sci U S A* **94,** 4817-20.

O'Hare, M. J., Bond, J., Clarke, C., Takeuchi, Y., Atherton, A. J., Berry, C., Moody, J., Silver, A. R., Davies, D. C., Alsop, A. E., Neville, A. M., and Jat, P. S. (2001). Conditional immortalization of freshly isolated human mammary fibroblasts and endothelial cells. *Proc Natl Acad Sci U S A* **98,** 646-51.

Oliferenko, S., and Balasubramanian, M. K. (2002). Astral microtubules monitor metaphase spindle alignment in fission yeast. *Nat Cell Biol* **4,** 816-20.

Oren, M., Maltzman, W., and Levine, A. J. (1981). Post-translational regulation of the 54K cellular tumor antigen in normal and transformed cells. *Mol Cell Biol* **1,** 101-10.

Ouellette, M. M., Liao, M., Herbert, B. S., Johnson, M., Holt, S. E., Liss, H. S., Shay, J. W., and Wright, W. E. (2000). Subsenescent telomere lengths in fibroblasts immortalized by limiting amounts of telomerase. *J Biol Chem* **275,** 10072-6.

Ouyang, B., Lan, Z., Meadows, J., Pan, H., Fukasawa, K., Li, W., and Dai, W. (1998). Human Bub1: a putative spindle checkpoint kinase closely linked to cell proliferation. *Cell Growth Differ* **9,** 877-85.

Pardee, A. B. (1989). G1 events and regulation of cell proliferation. *Science* **246,** 603-8.

Pardee, A. B. (2004). Chapter 1: Cell Fates. *In* "Cell Cycle and Growth Control: Biomolecular Regulation and Cancer, Second Edition" (G. S. Stein and A. B. Pardee, Eds.), pp. 3-13. John Wiley & Sons, Inc., Hoboken, New Jersey.

Pear, W. S., Nolan, G. P., Scott, M. L., and Baltimore, D. (1993). Production of high-titer helper-free retroviruses by transient transfection. *Proc Natl Acad Sci U S A* **90,** 8392-6.

Peden, K. W., Spence, S. L., Tack, L. C., Cartwright, C. A., Srinivasan, A., and Pipas, J. M. (1990). A DNA replication-positive mutant of simian virus 40 that is defective for transformation and the production of infectious virions. *J Virol* **64,** 2912-21.

Peters, J. M. (1999). Subunits and substrates of the anaphase-promoting complex. *Exp Cell Res* **248,** 339-49.

Peterson, J. R., and Mitchison, T. J. (2002). Small molecules, big impact: a history of chemical inhibitors and the cytoskeleton. *Chem Biol* **9,** 1275-85.

Pfleger, C. M., and Kirschner, M. W. (2000). The KEN box: an APC recognition signal distinct from the D box targeted by Cdh1. *Genes Dev* **14,** 655-65.

Pfleger, C. M., Lee, E., and Kirschner, M. W. (2001a). Substrate recognition by the Cdc20 and Cdh1 components of the anaphase-promoting complex. *Genes Dev* **15,** 2396-407.

Pfleger, C. M., Salic, A., Lee, E., and Kirschner, M. W. (2001b). Inhibition of Cdh1-APC by the MAD2-related protein MAD2L2: a novel mechanism for regulating Cdh1. *Genes Dev* **15,** 1759-64.

Polyak, K., Xia, Y., Zweier, J. L., Kinzler, K. W., and Vogelstein, B. (1997). A model for p53-induced apoptosis. *Nature* **389,** 300-5.

Powell, A. J., Darmon, A. J., Gonos, E. S., Lam, E. W., Peden, K. W., and Jat, P. S. (1999). Different functions are required for initiation and maintenance of immortalization of rat embryo fibroblasts by SV40 large T antigen. *Oncogene* **18,** 7343-50.

Prinz, S., Hwang, E. S., Visintin, R., and Amon, A. (1998). The regulation of Cdc20 proteolysis reveals a role for APC components Cdc23 and Cdc27 during S phase and early mitosis. *Curr Biol* **8,** 750-60.

Putkey, F. R., Cramer, T., Morphew, M. K., Silk, A. D., Johnson, R. S., McIntosh, J. R., and Cleveland, D. W. (2002). Unstable kinetochore-microtubule capture and chromosomal instability following deletion of CENP-E. *Dev Cell* **3,** 351-65.

Quartin, R. S., Cole, C. N., Pipas, J. M., and Levine, A. J. (1994). The amino-terminal functions of the simian virus 40 large T antigen are required to overcome wild-type p53-mediated growth arrest of cells. *J Virol* **68,** 1334-41.

Ramos-Morales, F., Dominguez, A., Romero, F., Luna, R., Multon, M. C., Pintor-Toro, J. A., and Tortolero, M. (2000). Cell cycle regulated expression and phosphorylation of hpttg proto-oncogene product. *Oncogene* **19,** 403-9.

Rappaport, R. (1969). Aster-equatorial surface relations and furrow establishment. *J Exp Zool* **171,** 59-68.

Ray, F. A., Peabody, D. S., Cooper, J. L., Cram, L. S., and Kraemer, P. M. (1990). SV40 T antigen alone drives karyotype instability that precedes neoplastic transformation of human diploid fibroblasts. *J Cell Biochem* **42,** 13-31.

Reshetnikova, G., Barkan, R., Popov, B., Nikolsky, N., and Chang, L. S. (2000). Disruption of the actin cytoskeleton leads to inhibition of mitogen-induced cyclin E expression, Cdk2 phosphorylation, and nuclear accumulation of the retinoblastoma protein-related p107 protein. *Exp Cell Res* **259,** 35-53.

Rice, P. W., and Cole, C. N. (1993). Efficient transcriptional activation of many simple modular promoters by simian virus 40 large T antigen. *J Virol* **67,** 6689-97.

Richter, J. D., Slavicek, J. M., Schneider, J. F., and Jones, N. C. (1988). Heterogeneity of adenovirus type 5 E1A proteins: multiple serine phosphorylations induce slow-migrating electrophoretic variants but do not

affect E1A-induced transcriptional activation or transformation. *J Virol* **62,** 1948-55.

Rieder, C. L. (1990). Formation of the astral mitotic spindle: ultrastructural basis for the centrosome-kinetochore interaction. *Electron Microsc Rev* **3,** 269-300.

Rieder, C. L., and Salmon, E. D. (1998). The vertebrate cell kinetochore and its roles during mitosis. *Trends Cell Biol* **8,** 310-8.

Rieder, C. L., Schultz, A., Cole, R., and Sluder, G. (1994). Anaphase onset in vertebrate somatic cells is controlled by a checkpoint that monitors sister kinetochore attachment to the spindle. *J Cell Biol* **127,** 1301-10.

Roberts, B. T., Farr, K. A., and Hoyt, M. A. (1994). The Saccharomyces cerevisiae checkpoint gene BUB1 encodes a novel protein kinase. *Mol Cell Biol* **14,** 8282-91.

Romero, F., Multon, M. C., Ramos-Morales, F., Dominguez, A., Bernal, J. A., Pintor-Toro, J. A., and Tortolero, M. (2001). Human securin, hPTTG, is associated with Ku heterodimer, the regulatory subunit of the DNA-dependent protein kinase. *Nucleic Acids Res* **29,** 1300-7.

Roy, R., Trowbridge, P., Yang, Z., Champoux, J. J., and Simmons, D. T. (2003). The cap region of topoisomerase I binds to sites near both ends of simian virus 40 T antigen. *J Virol* **77,** 9809-16.

Ru, H. Y., Chen, R. L., Lu, W. C., and Chen, J. H. (2002). hBUB1 defects in leukemia and lymphoma cells. *Oncogene* **21,** 4673-9.

Rushton, J. J., Jiang, D., Srinivasan, A., Pipas, J. M., and Robbins, P. D. (1997). Simian virus 40 T antigen can regulate p53-mediated transcription independent of binding p53. *J Virol* **71,** 5620-3.

Sablina, A. A., Ilyinskaya, G. V., Rubtsova, S. N., Agapova, L. S., Chumakov, P. M., and Kopnin, B. P. (1998). Activation of p53-mediated cell cycle checkpoint in response to micronuclei formation. *J Cell Sci* **111 (Pt 7),** 977-84.

Saffer, J. D., Jackson, S. P., and Thurston, S. J. (1990). SV40 stimulates expression of the transacting factor Sp1 at the mRNA level. *Genes Dev* **4,** 659-66.

Salmon, E. D. (1989). Cytokinesis in animal cells. *Curr Opin Cell Biol* **1,** 541-7.

Sancar, A., Lindsey-Boltz, L. A., Unsal-Kacmaz, K., and Linn, S. (2004). Molecular mechanisms of mammalian DNA repair and the DNA damage checkpoints. *Annu Rev Biochem* **73,** 39-85.

Sanchez, Y., Bachant, J., Wang, H., Hu, F., Liu, D., Tetzlaff, M., and Elledge, S. J. (1999). Control of the DNA damage checkpoint by chk1 and rad53 protein kinases through distinct mechanisms. *Science* **286,** 1166-71.

Santos, M., and Butel, J. S. (1982). Association of SV40 large tumor antigen and cellular proteins on the surface of SV40-transformed mouse cells. *Virology* **120,** 1-17.

Saraga, E., Bautista, D., Dorta, G., Chaubert, P., Martin, P., Sordat, B., Protiva, P., Blum, A., Bosman, F., and Benhattar, J. (1997). Genetic heterogeneity in sporadic colorectal adenomas. *J Pathol* **181,** 281-6.

Sawai, E. T., and Butel, J. S. (1989). Association of a cellular heat shock protein with simian virus 40 large T antigen in transformed cells. *J Virol* **63,** 3961-73.

Scheffner, M., Knippers, R., and Stahl, H. (1989). RNA unwinding activity of SV40 large T antigen. *Cell* **57,** 955-63.

Sedivy, J. M. (1998). Can ends justify the means?: telomeres and the mechanisms of replicative senescence and immortalization in mammalian cells. *Proc Natl Acad Sci U S A* **95,** 9078-81.

Sedivy, J. M., Capone, J. P., RajBhandary, U. L., and Sharp, P. A. (1987). An inducible mammalian amber suppressor: propagation of a poliovirus mutant. *Cell* **50,** 379-89.

Seeley, T. W., Wang, L., and Zhen, J. Y. (1999). Phosphorylation of human MAD1 by the BUB1 kinase in vitro. *Biochem Biophys Res Commun* **257,** 589-95.

Sekine, Y., Okada, Y., Noda, Y., Kondo, S., Aizawa, H., Takemura, R., and Hirokawa, N. (1994). A novel microtubule-based motor protein (KIF4) for organelle transports, whose expression is regulated developmentally. *J Cell Biol* **127,** 187-201.

Shah, J. V., Botvinick, E., Bonday, Z., Furnari, F., Berns, M., and Cleveland, D. W. (2004). Dynamics of centromere and kinetochore proteins; implications for checkpoint signaling and silencing. *Curr Biol* **14,** 942-52.

Shapiro, P. S., Vaisberg, E., Hunt, A. J., Tolwinski, N. S., Whalen, A. M., McIntosh, J. R., and Ahn, N. G. (1998). Activation of the MKK/ERK pathway during somatic cell mitosis: direct interactions of active ERK with kinetochores and regulation of the mitotic 3F3/2 phosphoantigen. *J Cell Biol* **142,** 1533-45.

Sharp, P. A. (1999). RNAi and double-strand RNA. *Genes Dev* **13,** 139-41.

Sharp-Baker, H., and Chen, R. H. (2001). Spindle checkpoint protein Bub1 is required for kinetochore localization of Mad1, Mad2, Bub3, and CENP-E, independently of its kinase activity. *J Cell Biol* **153,** 1239-50.

Shay, J. W., Wright, W. E., and Werbin, H. (1991). Defining the molecular mechanisms of human cell immortalization. *Biochim Biophys Acta* **1072,** 1-7.

Shichiri, M., Yoshinaga, K., Hisatomi, H., Sugihara, K., and Hirata, Y. (2002). Genetic and epigenetic inactivation of mitotic checkpoint genes hBUB1 and hBUBR1 and their relationship to survival. *Cancer Res* **62,** 13-7.

Shiio, Y., Yamamoto, T., and Yamaguchi, N. (1992). Negative regulation of Rb expression by the p53 gene product. *Proc Natl Acad Sci U S A* **89,** 5206-10.

Shin, H. J., Baek, K. H., Jeon, A. H., Park, M. T., Lee, S. J., Kang, C. M., Lee, H. S., Yoo, S. H., Chung, D. H., Sung, Y. C., McKeon, F., and Lee, C. W. (2003). Dual roles of human BubR1, a mitotic checkpoint kinase, in the monitoring of chromosomal instability. *Cancer Cell* **4,** 483-97.

Shirayama, M., Zachariae, W., Ciosk, R., and Nasmyth, K. (1998). The Polo-like kinase Cdc5p and the WD-repeat protein Cdc20p/fizzy are regulators and substrates of the anaphase promoting complex in Saccharomyces cerevisiae. *Embo J* **17,** 1336-49.

Simmons, D. T. (2000). SV40 large T antigen functions in DNA replication and transformation. *Adv Virus Res* **55,** 75-134.

Simmons, D. T., Gai, D., Parsons, R., Debes, A., and Roy, R. (2004). Assembly of the replication initiation complex on SV40 origin DNA. *Nucleic Acids Res* **32,** 1103-12.

Sironi, L., Melixetian, M., Faretta, M., Prosperini, E., Helin, K., and Musacchio, A. (2001). Mad2 binding to Mad1 and Cdc20, rather than oligomerization, is required for the spindle checkpoint. *Embo J* **20,** 6371-82.

Skoufias, D. A., Andreassen, P. R., Lacroix, F. B., Wilson, L., and Margolis, R. L. (2001). Mammalian mad2 and bub1/bubR1 recognize distinct spindle-attachment and kinetochore-tension checkpoints. *Proc Natl Acad Sci U S A* **98,** 4492-7.

Sluder, G., Hinchcliffe, E. H., and Rieder, C. L. (2004). Chapter 6: The Progression and Regulation of Mitotic Events. *In* "Cell Cycle and Growth Control: Biomolecular Regulation and Cancer, Second Edition" (G. S. Stein and A. B. Pardee, Eds.), pp. 201-235. John Wiley & Sons, Inc, Hoboken, New Jersey.

Smale, S. T., and Tjian, R. (1986). T-antigen-DNA polymerase alpha complex implicated in simian virus 40 DNA replication. *Mol Cell Biol* **6,** 4077-87.

Smith, T. F., Gaitatzes, C., Saxena, K., and Neer, E. J. (1999). The WD repeat: a common architecture for diverse functions. *Trends Biochem Sci* **24,** 181-5.

Sompayrac, L., and Danna, K. J. (1991). The amino-terminal 147 amino acids of SV40 large T antigen transform secondary rat embryo fibroblasts. *Virology* **181,** 412-5.

Soule, H. R., and Butel, J. S. (1979). Subcellular Localization of simian virus 40 large tumor antigen. *J Virol* **30,** 523-32.

Srinivasan, A., McClellan, A. J., Vartikar, J., Marks, I., Cantalupo, P., Li, Y., Whyte, P., Rundell, K., Brodsky, J. L., and Pipas, J. M. (1997). The amino-terminal transforming region of simian virus 40 large T and small t antigens functions as a J domain. *Mol Cell Biol* **17,** 4761-73.

Stern, B. M., and Murray, A. W. (2001). Lack of tension at kinetochores activates the spindle checkpoint in budding yeast. *Curr Biol* **11,** 1462-7.

Stewart, N., and Bacchetti, S. (1991). Expression of SV40 large T antigen, but not small t antigen, is required for the induction of chromosomal aberrations in transformed human cells. *Virology* **180,** 49-57.

Stringer, J. R. (1982). Mutant of simian virus 40 large T-antigen that is defective for viral DNA synthesis, but competent for transformation of cultured rat cells. *J Virol* **42,** 854-64.

Struhl, K. (1998). Histone acetylation and transcriptional regulatory mechanisms. *Genes Dev* **12,** 599-606.

Stubdal, H., Zalvide, J., and DeCaprio, J. A. (1996). Simian virus 40 large T antigen alters the phosphorylation state of the RB-related proteins p130 and p107. *J Virol* **70,** 2781-8.

Stucke, V. M., Sillje, H. H., Arnaud, L., and Nigg, E. A. (2002). Human Mps1 kinase is required for the spindle assembly checkpoint but not for centrosome duplication. *Embo J* **21,** 1723-32.

Sudakin, V., Chan, G. K., and Yen, T. J. (2001). Checkpoint inhibition of the APC/C in HeLa cells is mediated by a complex of BUBR1, BUB3, CDC20, and MAD2. *J Cell Biol* **154,** 925-36.

Sullivan, C. S., and Pipas, J. M. (2002). T antigens of simian virus 40: molecular chaperones for viral replication and tumorigenesis. *Microbiol Mol Biol Rev* **66,** 179-202.

Swedlow, J. R., and Hirano, T. (2003). The making of the mitotic chromosome: modern insights into classical questions. *Mol Cell* **11,** 557-69.

Tanaka, T. U., Rachidi, N., Janke, C., Pereira, G., Galova, M., Schiebel, E., Stark, M. J., and Nasmyth, K. (2002). Evidence that the Ipl1-Sli15 (Aurora kinase-INCENP) complex promotes chromosome bi-orientation by altering kinetochore-spindle pole connections. *Cell* **108,** 317-29.

Tang, Z., Bharadwaj, R., Li, B., and Yu, H. (2001). Mad2-Independent inhibition of APCCdc20 by the mitotic checkpoint protein BubR1. *Dev Cell* **1,** 227-37.

Tang, Z., Shu, H., Oncel, D., Chen, S., and Yu, H. (2004). Phosphorylation of Cdc20 by Bub1 Provides a Catalytic Mechanism for APC/C Inhibition by the Spindle Checkpoint. *Mol Cell* **16,** 387-97.

Tarunina, M., Alger, L., Chu, G., Munger, K., Gudkov, A., and Jat, P. S. (2004). A functional genetic screen for genes involved in senescence: Role of Tid1, a homologue of the Drosophila tumor suppressor l(2)tid, in senescence and cell survival. *Mol Cell Biol* **24.**

Taylor, S. S., Ha, E., and McKeon, F. (1998). The human homologue of Bub3 is required for kinetochore localization of Bub1 and a Mad3/Bub1-related protein kinase. *J Cell Biol* **142,** 1-11.

Taylor, S. S., Hussein, D., Wang, Y., Elderkin, S., and Morrow, C. J. (2001). Kinetochore localisation and phosphorylation of the mitotic checkpoint components Bub1 and BubR1 are differentially regulated by spindle events in human cells. *J Cell Sci* **114,** 4385-95.

Taylor, S. S., and McKeon, F. (1997). Kinetochore localization of murine Bub1 is required for normal mitotic timing and checkpoint response to spindle damage. *Cell* **89,** 727-35.

Tessema, M., Lehmann, U., and Kreipe, H. (2004). Cell cycle and no end. *Virchows Arch* **444,** 313-23.

Tevethia, M. J., Pipas, J. M., Kierstead, T., and Cole, C. (1988). Requirements for immortalization of primary mouse embryo fibroblasts probed with mutants bearing deletions in the 3' end of SV40 gene A. *Virology* **162,** 76-89.

Thomas, N. S., Ennis, S., Sharp, A. J., Durkie, M., Hassold, T. J., Collins, A. R., and Jacobs, P. A. (2001). Maternal sex chromosome non-disjunction: evidence for X chromosome-specific risk factors. *Hum Mol Genet* **10,** 243-50.

Tibbetts, R. S., Brumbaugh, K. M., Williams, J. M., Sarkaria, J. N., Cliby, W. A., Shieh, S. Y., Taya, Y., Prives, C., and Abraham, R. T. (1999). A role for ATR in the DNA damage-induced phosphorylation of p53. *Genes Dev* **13,** 152-7.

Tighe, A., Johnson, V. L., Albertella, M., and Taylor, S. S. (2001). Aneuploid colon cancer cells have a robust spindle checkpoint. *EMBO Rep* **2,** 609-14.

Tjian, R., and Robbins, A. (1979). Enzymatic activities associated with a purified simian virus 40 T antigen-related protein. *Proc Natl Acad Sci U S A* **76,** 610-4.

Tooze, J. (1981). Molecular biology of tumor viruses: DNA tumor viruses. *NY: Cold Spring Harbor Laboratory.*

Topper, L. M., Campbell, M. S., Tugendreich, S., Daum, J. R., Burke, D. J., Hieter, P., and Gorbsky, G. J. (2002). The dephosphorylated form of the anaphase-promoting complex protein Cdc27/Apc3 concentrates on kinetochores and chromosome arms in mitosis. *Cell Cycle* **1,** 282-92.

Tugendreich, S., Tomkiel, J., Earnshaw, W., and Hieter, P. (1995). CDC27Hs colocalizes with CDC16Hs to the centrosome and mitotic spindle and is essential for the metaphase to anaphase transition. *Cell* **81,** 261-8.

Turenne, G. A., Paul, P., Laflair, L., and Price, B. D. (2001). Activation of p53 transcriptional activity requires ATM's kinase domain and multiple N-terminal serine residues of p53. *Oncogene* **20,** 5100-10.

Tutt, A., Gabriel, A., Bertwistle, D., Connor, F., Paterson, H., Peacock, J., Ross, G., and Ashworth, A. (1999). Absence of Brca2 causes genome instability by chromosome breakage and loss associated with centrosome amplification. *Curr Biol* **9,** 1107-10.

Uetake, Y., and Sluder, G. (2004). Cell cycle progression after cleavage failure: mammalian somatic cells do not possess a "tetraploidy checkpoint". *J Cell Biol* **165,** 609-15.

Uhlmann, F., Lottspeich, F., and Nasmyth, K. (1999). Sister-chromatid separation at anaphase onset is promoted by cleavage of the cohesin subunit Scc1. *Nature* **400,** 37-42.

Uhlmann, F., Wernic, D., Poupart, M. A., Koonin, E. V., and Nasmyth, K. (2000). Cleavage of cohesin by the CD clan protease separin triggers anaphase in yeast. *Cell* **103,** 375-86.

Vanoosthuyse, V., Valsdottir, R., Javerzat, J. P., and Hardwick, K. G. (2004). Kinetochore targeting of fission yeast mad and bub proteins is essential for spindle checkpoint function but not for all chromosome segregation roles of bub1p. *Mol Cell Biol* **24,** 9786-801.

Vasquez, R. J., Howell, B., Yvon, A. M., Wadsworth, P., and Cassimeris, L. (1997). Nanomolar concentrations of nocodazole alter microtubule dynamic instability in vivo and in vitro. *Mol Biol Cell* **8,** 973-85.

Vaziri, H., and Benchimol, S. (1998). Reconstitution of telomerase activity in normal human cells leads to elongation of telomeres and extended replicative life span. *Curr Biol* **8,** 279-82.

Vigneron, S., Prieto, S., Bernis, C., Labbe, J. C., Castro, A., and Lorca, T. (2004). Kinetochore localization of spindle checkpoint proteins: who controls whom? *Mol Biol Cell* **15,** 4584-96.

Visintin, R., Prinz, S., and Amon, A. (1997). CDC20 and CDH1: a family of substrate-specific activators of APC-dependent proteolysis. *Science* **278,** 460-3.

Vodermaier, H. C. (2001). Cell cycle: Waiters serving the Destruction machinery. *Curr Biol* **11,** R834-7.

Vogel, C., Kienitz, A., Hofmann, I., Muller, R., and Bastians, H. (2004). Crosstalk of the mitotic spindle assembly checkpoint with p53 to prevent polyploidy. *Oncogene* **23,** 6845-53.

Wang, H., Liu, D., Wang, Y., Qin, J., and Elledge, S. J. (2001a). Pds1 phosphorylation in response to DNA damage is essential for its DNA damage checkpoint function. *Genes Dev* **15,** 1361-72.

Wang, X., Babu, J. R., Harden, J. M., Jablonski, S. A., Gazi, M. H., Lingle, W. L., de Groen, P. C., Yen, T. J., and van Deursen, J. M. (2001b). The mitotic checkpoint protein hBUB3 and the mRNA export factor hRAE1 interact with GLE2p-binding sequence (GLEBS)-containing proteins. *J Biol Chem* **276,** 26559-67.

Wang, X., Jin, D. Y., Ng, R. W., Feng, H., Wong, Y. C., Cheung, A. L., and Tsao, S. W. (2002). Significance of MAD2 expression to mitotic checkpoint control in ovarian cancer cells. *Cancer Res* **62,** 1662-8.

Wang, X., Jin, D. Y., Wong, Y. C., Cheung, A. L., Chun, A. C., Lo, A. K., Liu, Y., and Tsao, S. W. (2000). Correlation of defective mitotic checkpoint with aberrantly reduced expression of MAD2 protein in nasopharyngeal carcinoma cells. *Carcinogenesis* **21,** 2293-7.

Warren, C. D., Brady, D. M., Johnston, R. C., Hanna, J. S., Hardwick, K. G., and Spencer, F. A. (2002). Distinct chromosome segregation roles for spindle checkpoint proteins. *Mol Biol Cell* **13,** 3029-41.

Wasch, R., and Cross, F. R. (2002). APC-dependent proteolysis of the mitotic cyclin Clb2 is essential for mitotic exit. *Nature* **418,** 556-62.

Wassmann, K., and Benezra, R. (1998). Mad2 transiently associates with an APC/p55Cdc complex during mitosis. *Proc Natl Acad Sci U S A* **95,** 11193-8.

Wassmann, K., Liberal, V., and Benezra, R. (2003). Mad2 phosphorylation regulates its association with Mad1 and the APC/C. *Embo J* **22,** 797-806.

Waters, J. C., Chen, R. H., Murray, A. W., Gorbsky, G. J., Salmon, E. D., and Nicklas, R. B. (1999). Mad2 binding by phosphorylated kinetochores links error detection and checkpoint action in mitosis. *Curr Biol* **9,** 649-52.

Waters, J. C., Chen, R. H., Murray, A. W., and Salmon, E. D. (1998). Localization of Mad2 to kinetochores depends on microtubule attachment, not tension. *J Cell Biol* **141,** 1181-91.

Weaver, B. A., Bonday, Z. Q., Putkey, F. R., Kops, G. J., Silk, A. D., and Cleveland, D. W. (2003). Centromere-associated protein-E is essential for the mammalian mitotic checkpoint to prevent aneuploidy due to single chromosome loss. *J Cell Biol* **162,** 551-63.

Weinberg, R. A. (1995). The retinoblastoma protein and cell cycle control. *Cell* **81,** 323-30.

Weinstein, J. (1997). Cell cycle-regulated expression, phosphorylation, and degradation of p55Cdc. A mammalian homolog of CDC20/Fizzy/slp1. *J Biol Chem* **272,** 28501-11.

Weinstein, J., Jacobsen, F. W., Hsu-Chen, J., Wu, T., and Baum, L. G. (1994). A novel mammalian protein, p55CDC, present in dividing cells is associated with protein kinase activity and has homology to the Saccharomyces

cerevisiae cell division cycle proteins Cdc20 and Cdc4. *Mol Cell Biol* **14,** 3350-63.

Weiss, E., and Winey, M. (1996). The Saccharomyces cerevisiae spindle pole body duplication gene MPS1 is part of a mitotic checkpoint. *J Cell Biol* **132,** 111-23.

White, J. G., and Borisy, G. G. (1983). On the mechanisms of cytokinesis in animal cells. *J Theor Biol* **101,** 289-316.

Winey, M., Goetsch, L., Baum, P., and Byers, B. (1991). MPS1 and MPS2: novel yeast genes defining distinct steps of spindle pole body duplication. *J Cell Biol* **114,** 745-54.

Wojcik, E., Basto, R., Serr, M., Scaerou, F., Karess, R., and Hays, T. (2001). Kinetochore dynein: its dynamics and role in the transport of the Rough deal checkpoint protein. *Nat Cell Biol* **3,** 1001-7.

Wood, K. W., Sakowicz, R., Goldstein, L. S., and Cleveland, D. W. (1997). CENP-E is a plus end-directed kinetochore motor required for metaphase chromosome alignment. *Cell* **91,** 357-66.

Woods, C., LeFeuvre, C., Stewart, N., and Bacchetti, S. (1994). Induction of genomic instability in SV40 transformed human cells: sufficiency of the N-terminal 147 amino acids of large T antigen and role of pRB and p53. *Oncogene* **9,** 2943-50.

Wright, W. E., Pereira-Smith, O. M., and Shay, J. W. (1989). Reversible cellular senescence: implications for immortalization of normal human diploid fibroblasts. *Mol Cell Biol* **9,** 3088-92.

Wu, H., Lan, Z., Li, W., Wu, S., Weinstein, J., Sakamoto, K. M., and Dai, W. (2000). p55CDC/hCDC20 is associated with BUBR1 and may be a downstream target of the spindle checkpoint kinase. *Oncogene* **19,** 4557-62.

Wu, X., Avni, D., Chiba, T., Yan, F., Zhao, Q., Lin, Y., Heng, H., and Livingston, D. (2004). SV40 T antigen interacts with Nbs1 to disrupt DNA replication control. *Genes Dev* **18,** 1305-16.

Xia, G., Luo, X., Habu, T., Rizo, J., Matsumoto, T., and Yu, H. (2004). Conformation-specific binding of p31(comet) antagonizes the function of Mad2 in the spindle checkpoint. *Embo J* **23,** 3133-43.

Yamaguchi, S., Decottignies, A., and Nurse, P. (2003). Function of Cdc2p-dependent Bub1p phosphorylation and Bub1p kinase activity in the mitotic and meiotic spindle checkpoint. *Embo J* **22,** 1075-87.

Yamamoto, A., Guacci, V., and Koshland, D. (1996a). Pds1p is required for faithful execution of anaphase in the yeast, Saccharomyces cerevisiae. *J Cell Biol* **133,** 85-97.

Yamamoto, A., Guacci, V., and Koshland, D. (1996b). Pds1p, an inhibitor of anaphase in budding yeast, plays a critical role in the APC and checkpoint pathway(s). *J Cell Biol* **133,** 99-110.

Yanai, N., and Obinata, M. (1994). Apoptosis is induced at nonpermissive temperature by a transient increase in p53 in cell lines immortalized with temperature-sensitive SV40 large T-antigen gene. *Exp Cell Res* **211,** 296-300.

Yang, J., Chang, E., Cherry, A. M., Bangs, C. D., Oei, Y., Bodnar, A., Bronstein, A., Chiu, C. P., and Herron, G. S. (1999). Human endothelial cell life extension by telomerase expression. *J Biol Chem* **274,** 26141-8.

Yao, X., Abrieu, A., Zheng, Y., Sullivan, K. F., and Cleveland, D. W. (2000). CENP-E forms a link between attachment of spindle microtubules to kinetochores and the mitotic checkpoint. *Nat Cell Biol* **2,** 484-91.

Yen, T. J., Li, G., Schaar, B. T., Szilak, I., and Cleveland, D. W. (1992). CENP-E is a putative kinetochore motor that accumulates just before mitosis. *Nature* **359,** 536-9.

Yeong, F. M., Lim, H. H., Padmashree, C. G., and Surana, U. (2000). Exit from mitosis in budding yeast: biphasic inactivation of the Cdc28-Clb2 mitotic kinase and the role of Cdc20. *Mol Cell* **5,** 501-11.

Yu, H. (2002). Regulation of APC-Cdc20 by the spindle checkpoint. *Curr Opin Cell Biol* **14,** 706-14.

Zalvide, J., Stubdal, H., and DeCaprio, J. A. (1998). The J domain of simian virus 40 large T antigen is required to functionally inactivate RB family proteins. *Mol Cell Biol* **18,** 1408-15.

Zecevic, M., Catling, A. D., Eblen, S. T., Renzi, L., Hittle, J. C., Yen, T. J., Gorbsky, G. J., and Weber, M. J. (1998). Active MAP kinase in mitosis: localization at kinetochores and association with the motor protein CENP-E. *J Cell Biol* **142,** 1547-58.

Zhou, Y., Mehta, K. R., Choi, A. P., Scolavino, S., and Zhang, X. (2003). DNA damage-induced inhibition of securin expression is mediated by p53. *J Biol Chem* **278,** 462-70.

Zhu, J. Y., Rice, P. W., Chamberlain, M., and Cole, C. N. (1991). Mapping the transcriptional transactivation function of simian virus 40 large T antigen. *J Virol* **65,** 2778-90.

Zou, H., McGarry, T. J., Bernal, T., and Kirschner, M. W. (1999). Identification of a vertebrate sister-chromatid separation inhibitor involved in transformation and tumorigenesis. *Science* **285,** 418-22.

Zur, A., and Brandeis, M. (2001). Securin degradation is mediated by fzy and fzr, and is required for complete chromatid separation but not for cytokinesis. *Embo J* **20,** 792-801.

Appendix I

pcDNA3.1 Vectors

Map of pcDNA3.1(+) and pcDNA3.1(-)

The figure below summarizes the features of the pcDNA3.1(+) and pcDNA3.1(-) vectors. **The complete sequences for pcDNA3.1(+) and pcDNA3.1(-) are available for downloading from our World Wide Web site (www.invitrogen.com) or from Technical Service (see page 13).** Details of the multiple cloning sites are shown on page 3 for pcDNA3.1(+) and page 4 for pcDNA3.1(-).

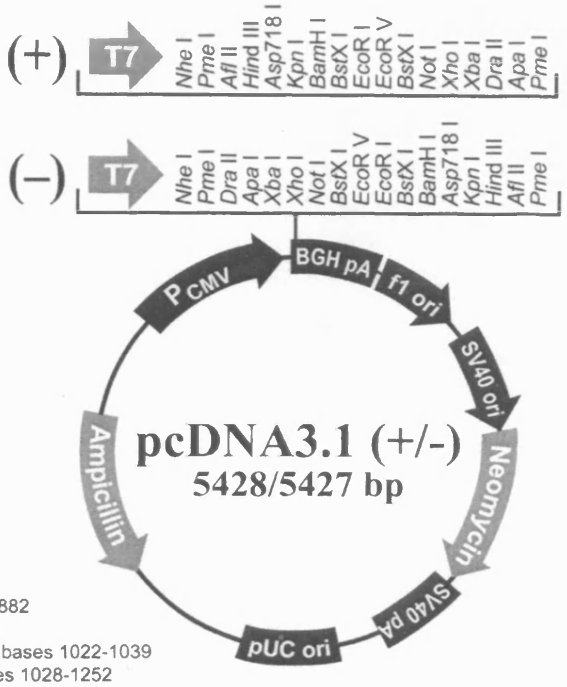

Comments for pcDNA3.1 (+)
5428 nucleotides

CMV promoter: bases 232-819
T7 promoter/priming site: bases 863-882
Multiple cloning site: bases 895-1010
pcDNA3.1/BGH reverse priming site: bases 1022-1039
BGH polyadenylation sequence: bases 1028-1252
f1 origin: bases 1298-1726
SV40 early promoter and origin: bases 1731-2074
Neomycin resistance gene (ORF): bases 2136-2930
SV40 early polyadenylation signal: bases 3104-3234
pUC origin: bases 3617-4287 (complementary strand)
Ampicillin resistance gene (*bla*): bases 4432-5428 (complementary strand)
ORF: bases 4432-5292 (complementary strand)
Ribosome binding site: bases 5300-5304 (complementary strand)
bla promoter (P3): bases 5327-5333 (complementary strand)

(reproduced from website: www.invitrogen.com)

Appendix II

pSUPERretro vector map (RNAi system from OligoEngine):

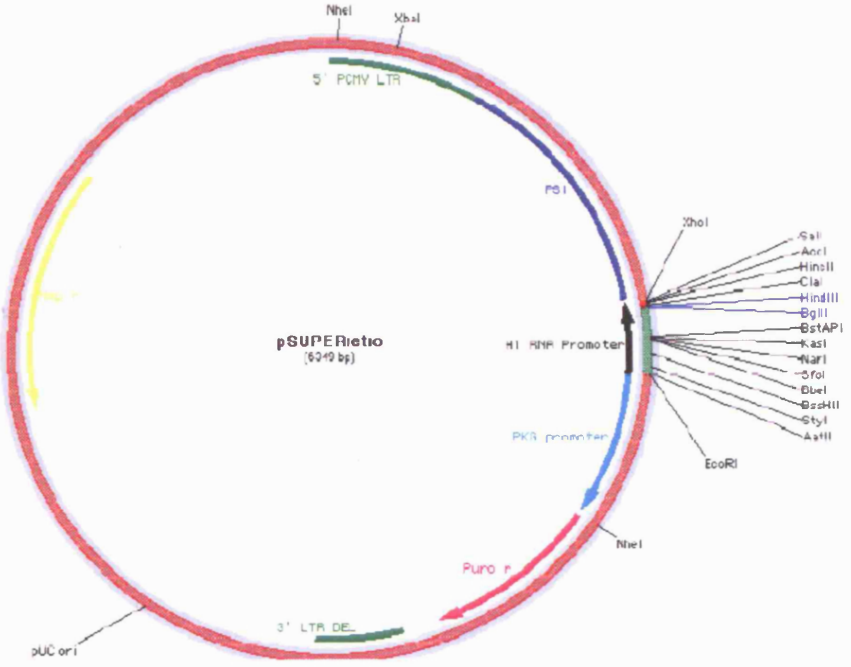

(reproduced from website: www.oligoengine.com)

Appendix III

U20S growth rate data:

Table 1: raw data and normalised average values (used to plot graph in Figure 5.2):

U20S				
Hours after plating @ 3x10^5/plate:	**20**	**41**	**66**	**90**
Cell counts(plate1) (10^4)	37	41	94	215
	27	59	117	205
	29	45	89	175
	28	58	73	180
Cell counts(plate2) (10^4)	24	35	79	199
	36	52	68	188
	25	57	76	172
	24	37	63	159
Average Plate 1 count	30.25	50.75	93.25	193.75
Average Plate 2 count	27.25	45.25	71.5	179.5
Overall Average	28.75	48	82.375	186.625
Average Value, Normalised	**1.000**	**1.670**	**2.865**	**6.491**

U20S(wild-type LT)				
Hours after plating @ 3x10^5/plate:	**20**	**41**	**66**	**90**
Cell counts(plate1) (10^4)	42	61	91	338
	37	74	118	288
	33	69	109	297
	43	45	124	286
Cell counts(plate2) (10^4)	56	67	148	313
	56	50	156	297
	52	51	147	242
	40	102	183	242
Average Plate 1 count	38.75	62.25	110.5	302.25
Average Plate 2 count	51	67.5	158.5	273.5
Overall Average	44.875	64.875	134.5	287.875
Average Value, Normalised	**1.000**	**1.446**	**2.997**	**6.415**

U20S(dl89-97 LT) clone #2				
Hours after plating @ 3x10^5/plate:	**20**	**41**	**66**	**90**
Cell counts(plate1) (10^4)	44	73	176	357
	47	67	172	452
	44	79	160	352
	40	86	140	352
Cell counts(plate2) (10^4)	45	91	150	405
	49	70	172	392
	37	94	162	333
	35	69	154	358
Average Plate 1 count	43.75	76.25	162	378.25
Average Plate 2 count	41.5	81	159.5	372
Overall Average	42.625	78.625	160.75	375.125
Average Value, Normalised	**1.000**	**1.845**	**3.771**	**8.801**

U20S(dl89-97 LT) clone #4				
Hours after plating @ 3x10^5/plate:	**20**	**41**	**66**	**90**
Cell counts(plate1) (10^4)	37	52	134	285
	35	54	141	288
	42	49	132	299
	28	47	131	276
Cell counts(piate2) (10^4)	21	59	139	287
	31	62	132	247
	40	65	130	265
	37	54	127	258
Average Plate 1 count	35.5	50.5	134.5	287
Average Plate 2 count	32.25	60	132	264.25
Overall Average	33.875	55.25	133.25	275.625
Average Value, Normalised	**1.000**	**1.631**	**3.934**	**8.137**

Average Value, Normalised
= Overall Average/(Overall Average at 20 hours)

Appendix III (continued)

U20S growth rate data, normalised,
showing 95% confidence interval calculations (see Figure 5.2):

Table 2: normalised data and 95% confidence intervals:

U20S				
Hours after plating @ 3x10^5/plate:	**20**	**41**	**66**	**90**
Normalised counts (plate1)	1.287	1.426	3.270	7.478
	0.939	2.052	4.070	7.130
	1.009	1.565	3.096	6.087
	0.974	2.017	2.539	6.261
Normalised counts (plate2)	0.835	1.217	2.748	6.922
	1.252	1.809	2.365	6.539
	0.870	1.983	2.643	5.983
	0.835	1.287	2.191	5.530
Average Value, Normalised	**1.000**	**1.670**	**2.865**	**6.491**
Standard Deviation (S.D.), Normalised	0.178	0.339	0.602	0.651
1.96 x S.D. (95% confidence interval) = +/-	0.349	0.665	1.181	1.276

U20S(wild-type LT)				
Hours after plating @ 3x10^5/plate:	**20**	**41**	**66**	**90**
Normalised counts (plate1)	0.936	1.359	2.028	7.532
	0.825	1.649	2.630	6.418
	0.735	1.538	2.429	6.618
	0.958	1.003	2.763	6.373
Normalised counts (plate2)	1.248	1.493	3.298	6.975
	1.248	1.114	3.476	6.618
	1.159	1.136	3.276	5.393
	0.891	2.273	4.078	5.393
Average Value, Normalised	**1.000**	**1.446**	**2.997**	**6.415**
Standard Deviation (S.D.), Normalised	0.195	0.405	0.657	0.731
1.96 x S.D. (95% confidence interval) = +/-	0.383	0.793	1.287	1.432

U20S(dl89-97 LT) clone #2				
Hours after plating @ 3x10^5/plate:	**20**	**41**	**66**	**90**
Normalised counts (plate1)	1.032	1.713	4.129	8.375
	1.103	1.572	4.035	10.604
	1.032	1.853	3.754	8.258
	0.938	2.018	3.284	8.258
Normalised counts (plate2)	1.056	2.135	3.519	9.501
	1.150	1.642	4.035	9.196
	0.868	2.205	3.801	7.812
	0.821	1.619	3.613	8.399
Average Value, Normalised	**1.000**	**1.845**	**3.771**	**8.801**
Standard Deviation (S.D.), Normalised	0.114	0.247	0.291	0.911
1.96 x S.D. (95% confidence interval) = +/-	0.224	0.485	0.571	1.785

U20S(dl89-97 LT) clone #4				
Hours after plating @ 3x10^5/plate:	**20**	**41**	**66**	**90**
Normalised counts (plate1)	1.092	1.535	3.956	8.413
	1.033	1.594	4.162	8.502
	1.240	1.446	3.897	8.827
	0.827	1.387	3.867	8.148
Normalised counts (plate2)	0.620	1.742	4.103	8.472
	0.915	1.830	3.897	7.292
	1.181	1.919	3.838	7.823
	1.092	1.594	3.749	7.616
Average Value, Normalised	**1.000**	**1.631**	**3.934**	**8.137**
Standard Deviation (S.D.), Normalised	0.204	0.185	0.137	0.519
1.96 x S.D. (95% confidence interval) = +/-	0.399	0.363	0.269	1.016

All counts in Table 1 (Appendix III) were normalised, to allow calculation of the standard deviation (S.D.), using Microsoft Excel.

Normalised count = count/(overall average at 20 hours)

N.B. the "Average Value, Normalised" for each cell line, at each time point shown in this table is the same as that calculated using the raw data, shown in Table 1.

95% confidence interval = +/- (1.96 x S.D.)